



European Organization for Experimental Photogrammetric Research

November 2001

OEEPE workshop on
Airborne Laserscanning and
Interferometric SAR for Detailed
Digital Elevation Models

1 - 3 March, 2001

Edited by Kennert Torlegård and Jonas Nelson

The present publication is the exclusive property of the
European Organization for Experimental Photogrammetric Research

All rights of translation and reproduction are reserved on behalf of the OEEPE.
Published by the Bundesamt für Kartographie und Geodäsie, Frankfurt am Main

EUROPEAN ORGANIZATION
for
EXPERIMENTAL PHOTOGRAMMETRIC RESEARCH

STEERING COMMITTEE

(composed of Representatives of the Governments of the Member Countries)

President:	Prof. Ø. ANDERSEN Norges Landbrukshøgskole Institutt for Kartfag P. O. Box 5034 N-1432 Ås	Norway
Members:	Dipl.-Ing. M. FRANZEN Bundesamt für Eich- und Vermessungswesen Krotenthallergasse 3 A-1080 Wien	Austria
	Mr. J. VANOMMESLAEGHE Dept. of Photogrammetry Institut Géographique National 13, Abbaye de la Cambre B-1000 Bruxelles	Belgium
	Mr. C. ZENONOS Department of Lands & Surveys Ministry of Interior Demofontos and Alasias corner Nicosia	Cyprus
	Mr. M. SAVVIDES Department of Lands & Surveys Ministry of Interior Demofontos and Alasias corner Nicosia	
	Prof. Dr. J. HÖHLE Dept. of Development and Planning Aalborg University Fibigerstraede 11 DK-9220 Aalborg	Denmark
	Mr. L.T. JØRGENSEN Kort & Matrikelstyrelsen Rentemestervej 8 DK-2400 København NV	
	Prof. Dr. R. KUITTINEN Director General Finnish Geodetic Institut Geodeetinrinne 2 SF-02430 Masala	Finland
	Mr. J. VILHOMAA National Land Survey of Finland Aerial Image Centre P.O. Box 84 Opastinsilta 12C SF-00521 Helsinki	
	Dr. J.-P. LAGRANGE Directeur des activités internationales et européennes Institut Géographique National 2 Avenue Pasteur F-94165 Saint-Mande Cedex	France

Mr. C. VALORGE
Centre National
d'Etudes Spatiales
18, Avenue Belin
F-31401 Toulouse Cedex

Germany

Prof. Dr. D. FRITSCH
Institut für Photogrammetrie
Universität Stuttgart
Geschwister-Scholl-Straße 24
D-70174 Stuttgart

Prof. Dr. D. GRÜNREICH
Präsident des Bundesamts für
Kartographie und Geodäsie
Richard-Strauss-Allee 11
D-60598 Frankfurt am Main

Prof. G. NAGEL
Präsident
Bayerisches Landesvermessungsamt
Alexandrastraße 4
D-80538 München

Mr. C. BRAY
Dpt. Data Collection
Ordnance Survey Ireland
Phoenix Park
Dublin 1

Ireland

Mr. K. MOONEY
Department of Geomatics
Dublin Institute of Technology
Bolton Street
Dublin 1

Eng. C. CANNAFOGLIA
Ministry of Finance
Agenzia per il Territorio
Largo Leopardi 5
Roma

Italy

Prof. R. GALETTO
University of Pavia
Via Ferrata 1
I-27100 Pavia

Prof. Dr. Ir. M. MOLENAAR
Rector
International Institute für Aerospace
Survey and Earth Sciences
P.O. Box 6
NL-7500 AA Enschede

Netherlands

Dr. M. GROTHE
Survey Department of the Rijkswaterstaat
Postbus 5023
NL-2600 GA Delft

Mrs. T. I. KRISTIANSEN
Land Division
Norwegian Mapping Authority
N-3511 Hønefoss

Norway

Mrs. E. MALANOWICZ
Head Office of Geodesy and Cartography
Department of Cartography and Photogrammetry
ul. Wspólna 2
PL-00-926 Warszawa

Poland

<p>Mr. F. PAPI Instituto Geographico Nacional General Ibáñez de Ibero 3 E-28003 Madrid</p>	Spain
<p>Mr. J. HERMOSILLA Instituto Geografico Nacional General Ibáñez de Ibero 3 E-28003 Madrid</p>	
<p>Mr. S. Jönsson National Land Survey of Sweden S-80182 Gävle</p>	Sweden
<p>Prof. Dr. A. ÖSTMAN Luleå Technical University Geographical Information Technology S-97187 Luleå</p>	
<p>Prof. Dr. O. KÖLBL Institut de Photogrammétrie, EPFL GR-Ecublens CH-1015 Lausanne</p>	Switzerland
<p>Mr. C. EIDENBENZ Bundesamt für Landestopographie Seftigenstrasse 264 CH-3084 Wabern</p>	
<p>Dr. Eng. Col. M. ÖNDER Ministry of National Defence General Command of Mapping MSB Harita Genel Komutanligi Dikimevi TR-06100 Ankara</p>	Turkey
<p>Dipl. Eng Lt. Col. O. AKSU Ministry of National Defence General Command of Mapping MSB Harita Genel Komutanligi Dikimevi TR-06100 Ankara</p>	
<p>Mr. K. J. MURRAY Ordnance Survey Romsey Road Maybush Southampton SO16 4GU</p>	United Kingdom
<p>Prof. Dr. I. J. DOWMAN Dept. of Photogrammetry and Surveying University College London Gower Street 6 London WC 1E 6BT</p>	

SCIENCE COMMITTEE

Prof. Dr. Ir. M. MOLENAAR
 International Institute für Aerospace
 Survey and Earth Sciences
 P.O. Box 6
 NL-7500 AA Enschede

EXECUTIVE BUREAU

Mr. C. M. PARESI
Secretary General of the OEEPE
International Institute for Aerospace Survey
and Earth Sciences
350 Boulevard 1945, P. O. Box 6
NL-7500 AA Enschede (Netherlands)

Mr. E. HOLLAND
International Institute for
Aerospace Survey and Earth Sciences
P.O. Box 6
NL-7500 AA Enschede

OFFICE OF PUBLICATIONS

Prof. Dr. B.-S. SCHULZ
Bundesamt für Kartographie und Geodäsie
Richard-Strauss-Allee 11
D-60598 Frankfurt am Main

SCIENTIFIC COMMISSIONS

Commission 1:

Sensors, primary data acquisition and geo-referencing

President: Prof. Ø. ANDERSEN
Norges Landbrukshøgskole
Institutt for Kartfag
P.O. Box 5034
N-1432 Ås

Commission 2:

Image analysis and information extraction

President: Prof. Dr.-Ing. C. HEIPKE
Institute of Photogrammetry and
Engineering Surveys
Universität Hannover
Nienburger Str. 1
D-30167 Hannover

Commission 3:

Production systems and processes

President: Dr.-Ing. E. Gülch
Docent Advanced Technologies
INPHO GmbH
Smaragdweg 1
D-70174 Stuttgart

Commission 4:

Core geospatial data

President: Mr. K. J. MURRAY
Ordnance Survey
Romsay Road
Maybush
Southampton SO164GU

Commission 5:

Integration and delivery of data and services

President: Mr. P. WOODSFORD
Deputy Chairman
Laser-Scan Ltd.
101 Science Park
Milton Road
Cambridge CB4 0FY



**Proceedings of OEEPE workshop on
Airborne Laserscanning and
Interferometric SAR
for Detailed Digital Elevation Models
1-3 March 2001**

**Editor: Kennert Torlegård
Co-editor: Jonas Nelson**

September 2001

Contents

Summary

Ian Dowman

The use of airborne IfSAR for topographic mapping: Executive summary of the Stockholm meeting

Papers

Ian Dowman

Airborne Interferometric SAR – A Review of the State of the Art and of OEEPE Activities

Antonio Ruiz, Manuel Castillo, Román Arbiol and José L. Colomer

ISAR DEM Data Processing for Contours Generation

Dave Barker

The DERA ESR Radar: Overview and Initial Interferometric SAR Results

Alexander V Ksendzuk

Increasing resolution of SAR images

Toni Schenk

Modeling and Recovering Systematic Errors in Airborne Laser Scanners

Norbert Pfeifer, Philipp Stadler and Christian Briese

Derivation of Digital Elevation Models in the SCOP++ Environment

George Vosselman and Hans-Gerd Maas

Adjustment and Filtering of Raw Laser Altimetry Data

Magnus Elmqvist

Ground Estimation of Laser Radar Data using Active Shape Models

Jochen Schiewe

Region-based Information Extraction from Laser Scanner Data and Optical Imagery

Eberhard Steinle, John Kiema, Johannes Leebemann and Hans-Peter Bähr

Laserscanning for Analysis of Damages Caused by Earthquake Hazards

Maurizio Barbarella and Carmine Fazio

Surveying of Zones at Risk of Landslide by Laser Scanning.
Repeatability and Accuracy Analysis

Gottfried Mandlbürger and Herbert Brockmann

Modelling a Watercourse DTM Based on airborne Laser-Scanner Data – using the Example of the River Oder along the German/Polish Border

Sergio Dequal, Andrea Lingua and Fulvio Rinaudo

Laser Scanner Data for True Digital Orthoprojection

Marco Roggero

Dense DTM from Laser Scanner Data

Peter Reiss

Topographical Survey using Laserscanning at the State Surveying & Mapping Authority of Bavaria

Karl-Heinz Thiel and Aloysius Wehr

Operational Production of DTMs Using ScaLARS

Regine Brügelmann and Remko de Lange

Airborne Laserscanning versus Airborne InSAR – A Quality Comparison of DTMs

Ian Dowman and Peggy Fischer

A comparison of airborne IfSAR and LIDAR data over the Vaihingen test site

Borislav Marinov

Building Detection and Excluding in Digital Terrain Modelling

Viewgraph presentations

Peter Axelsson

Laser Scanning – an Overview

Peter Axelsson

Ground Estimation of Laser Scanner Data using Adaptive TIN Models

Pål Herman Sund

Presentation of Fotonor

Markus Rombach

Airborne Laserscanning and Interferometric SAR for Detailed Digital Elevation Models

Eberhard Gülch

Aspects of Modern Digital Elevation Models

The use of airborne IfSAR for topographic mapping: Executive summary of the Stockholm meeting

Ian Dowman
University College London

The OEEPE Workshop on Airborne Laserscanning and Interferometric SAR for detailed Digital Elevation Models was organised by the OEEPE Working groups on Laserscanning and on Interferometric SAR. The IfSAR working group had already held a meeting in London in March 2000 and had recommended that a joint meeting be held to exploit the complementarity between Laserscanning and IfSAR. The majority of the papers at the Stockholm workshop concerned Laserscanning (this term is used synonymously with the term LIDAR) and it is possible to form a useful comparison between the two techniques and to see where common algorithms and approaches could be used to process the data. This report deals with the IfSAR aspects of the workshop and makes comparisons between IfSAR and LIDAR. The conclusions include those brought forward from the London workshop.

The meeting started with an overview of airborne IfSAR from Dowman and this was followed by a session on IfSAR in which papers by Barker and Rombach described the DERA and Aerosensing Radarsysteme systems. Ruiz described a method of processing IfSAR DEMs for contour generation for a project that mapped 267,000 km² in Venezuela. Shigeko described an application of IfSAR to flood plain mapping for insurance purposes. Later in the programme Wehr described the ScaLARS system and Mercer presented the Intermap Technologies system. Dowman and Brügge Imann both presented work that compared IfSAR and Laserscanning data for DEM generation.

In other papers a number of general points were made which relate to both technologies. Filtering techniques used for LIDAR can be applied to IfSAR as well. Of particular note is the work of Pfeiffer who uses a weighting approach, Vosselman who uses mathematical morphology and Schiewe who uses a multi-sensor approach with the eCognition software. Axelsson presented an active/iterative method of formation of a DEM from a TIN and analyses the angles in the vertical plane to determine break lines. Elmquist uses snakes to estimate ground surface beneath wooded areas. Work needs to be done to test whether these algorithms can be used on both LIDAR and IfSAR data.

Schenk described a model for LIDAR and in the discussion there was a general feeling that this is essential and that a similar model should be considered for IfSAR. Because of the generally narrow strips in laserscanning, a block adjustment is often necessary, this is necessary but less significant in IfSAR because of the wider coverage. Vosselman noted the problems caused by occlusions in Laserscanning, clearly also a major problem with IfSAR if only one pass is made. Several speakers made the point that there were aspects of data capture from these systems which introduced errors which were difficult to quantify. LIDAR and SAR are both based on integration over a footprint, this is used to form a point DEM, but actually a DEM defines a surface. The scan angle has an effect that is largely unquantified. The footprint changes from a circle to an ellipse and this effect is exaggerated on slopes, especially sloping roofs. Multipath effects will also effect the quality of the data. A

different approach to the provision of ground control points was noted. LIDAR does not generally make use of GCPs but they are necessary for high resolution IfSAR work. The point was made that all data needs control for validation.

Gülch gave a useful summary of both technologies. His most important points were that more work needs to be done on comparative investigations and on developing theory. He also noted that there should be more dissemination of information on the two technologies and that potential users need to be educated.

The main conclusions relating to IfSAR which come from the Stockholm and London meetings are as follows:

- Airborne IfSAR is a reliable and cost effective way of acquiring data for DEMs.
- Processing of single pass data is robust.
- Accuracy can be selected to suit the application. This ranges from 5cm to several metres.
- Accuracy is dependent on the type of terrain and land cover and the DEM produced will be of the surface features.
- Gaps may occur in hilly terrain where Radar shadow occurs, or phase unwrapping was not possible because of coherence problems. Multiple passes can overcome this problem.
- The end user may process the data to generate value added products;
- No special software is required for many applications, where special processing is required tools are already available. New tools such as eCognition show promise.
- IfSAR has been used operationally for a wide range of applications, often by users previously inexperienced in the use of SAR data.
- Users need to gain experience in the operational and interpretation aspects of acquiring and using IfSAR data.

The workshop was extremely useful for obtaining an overview of the operational issues and the potential applications of airborne LIDAR and IfSAR data. The meeting demonstrated that airborne IfSAR and LIDAR are complementary technologies, but which share many features which can be exploited when processing the data. It is apparent that IfSAR can be used for a number of applications but that experience and understanding of the principles is required for effective use. IfSAR is not as complex and difficult to use as is sometimes thought.

Airborne Interferometric SAR

A Review of the State of the Art and of OEEPE activities

Ian Dowman
University College London

1.0 Background

SAR Interferometry (IfSAR) has been used for a number of years now. The technique attained some prominence when it was used to create digital elevation models from satellite data and later when centimetric accuracy was achieved by using differential IfSAR to measuring the displacement after the Landers earthquake. The method was not considered to be accurate enough for national mapping. Although of high theoretical accuracy, many practical problems due to the nature of the terrain and the atmosphere reduced both accuracy and coverage. Some of these problems were solved with the introduction of single pass airborne systems. This technique removed some of the errors matching caused by loss of temporal decorrelation and due to atmospheric effects.

In 1997 recognised the potential of airborne IfSAR and established a working group which was charged with evaluating IfSAR for mapping and particularly for use by National Mapping Agencies (NMAs). The first activity of the group was to carry out a survey, by questionnaire, to assess the interest in this topic. The questionnaire was sent to all European NMAs, using the CERCO mailing list. 13 responses were received. The response indicated a wide range of potential interests which includes map revision, DEM update, change detection and monitoring coastal areas. Response also indicated that some activity was going on at that time.

The second planned activity was to acquire data over test sites in Europe and to carry out an evaluation of the data. However the cost of acquiring data proved to be high and the responses from the NMAs did not indicate that they were prepared to fund an OEEPE test to that extent. As a result of this, other sources of data were sought. These were found from two organisations. Rijkwaterstaat in the Netherlands had carried out a test of IfSAR for their own purposes and were prepared to make the data available to OEEPE. Also Intermap, a Canadian company had acquired data for a large area in UK and were able to make part of this available to OEEPE. Subsequently Intermap has also provided data of the Vaihingen test site in Germany, where Laser data also exists.

The data was made available to interested organisations and these organisations were then invited to attend a workshop in London on 30-31st March 2000, to discuss their experiences with the data and to contribute to a report on the potential of airborne IfSAR.

This report gives background to the data and the workshop and draws conclusions and recommendations on the potential use of airborne IfSAR and reports on subsequent activity.

2.0 Introduction to IfSAR

Interferometric SAR (IfSAR) has been a technique of considerable scientific interest for some years now. This has been particularly so since data became widely available from the microwave sensor on the ERS-1 satellite. Using the phase difference from two SAR images, the range difference can be computed for every common point on the two images. This can then be converted into a digital elevation model. Accuracies a few metres can be achieved by this method. Differential interferometric SAR can detect movement of the ground of a few millimetres from 3 images taken at different times. Research has demonstrated both the accuracy of IfSAR in producing DEMs but also the problems. The problems in using satellite IfSAR arise from there being too long an interval between acquisition of the two images and from errors introduced by atmospheric effects. Steep terrain may also cause problems as well as the land cover and the moisture content of the vegetation and the soil.

Although satellite SAR has created the largest interest, airborne SAR also has a significant potential, and whilst having its own set of problems, also has significant advantages over satellite SAR, including greater accuracy and freedom from the effects of the atmosphere and from effects due to the imagery being taken at different times. Airborne SAR is becoming more accessible because of the greater availability of aircraft equipped with GPS and INS and much more experience in operating these systems.

3.0 Test data

Two data sets were initially made available by OEEPE these are summarised here.

Terschelling

This test site is an island in North West Netherlands, north of IJsselmeer.

The data has been acquired by DLR, Germany and is made available by Rijkwaterstaat and TNO, the Dutch Research Laboratory.

The following SAR products are available:

- Intensity image
- Coherence image derived from the interferometric pair
- DEM derived from the interferometric pair

In addition a DEM derived from Laser Scanning is available and map data provided by Rijkwaterstaat.

West London, UK

This is an urban area with many open spaces (Kew Gardens, River Thames) and a variety of building types.

The data has been acquired by Intermap of Canada.

The following SAR products are available:

DEM with 5m grid spacing
Image data referenced to same system with 5m pixel size.

Ordnance Survey Landline data and DEM is also available.

A third data set has since become available but has not been distributed widely.

Vaihingen

This is a rural area in southern Germany containing a small town, a large river, agricultural areas, forest and a quarry.

The data has been acquired by Intermap of Canada.

The following SAR products are available:

DEM with 5m grid spacing
Image data referenced to same system with 5m pixel size.

Accurate ground control points and profiles are also available, obtained by The University of Stuttgart.

4.0 Report on Workshop

18 people attended the workshop. The objectives of the workshop were as follows:

- To review the present situation regarding the acquisition and use of airborne interferometric SAR
- To assess the potential of such data for mapping, particularly for use by National Mapping Agencies
- To produce a report covering the above two aspects for the OEEPE steering committee and to make recommendations for any further tests or investigations which might increase understanding of IFSAR and promote its use.

The use made of the data is summarised in table 1. Some of the participants at the workshop had used data from other areas, this is also summarised in the table.

Organisation	Area	Reference
Rijkwaterstaat/TNO	Terschelling	Huising et al, 1999. Airborne and spaceborne SAR interferometry. USP-2 report 99-19, Netherlands Remote Sensing Board. 88 pages.
Turkish General Command for Mapping	Terschelling	
UCL	West London	
Ordnance Survey	Intermap data at Marlborough, UK	
Willis	Intermap data of whole of Thames Valley	Paper and brochure at appendix VI
ICC	Venezuela	
Danish National Survey Danish Centre for Remote Sensing	Various using Danish sensor	
Intermap	Various	
Aerosensing Radar-Systeme	Various	

Table 1. Data used by attendees at Workshop.

This section of the report gives brief summary of the presentations.

The first session comprised presentations from the companies which operate data acquisition systems. Intermap and Aerosensing Radar Systeme attended the workshop and presented the work of their companies. Andersen presented some work of from the aircraft operated by the Danish remote sensing Centre. Other organisations which operate an airborne IfSAR are DLR in Germany, DERA in United Kingdom and there is also the Lynx-SAR manufactured by Sandia Laboratories and operated experimentally by various organisations.

Bryan Mercer presented the activities of Intermap. The talk focused firstly on the theory of radar DEM generation and then finished with case studies assessing accuracy with comparisons to LIDAR. Mercer described the Intermap processing strategy which involved the following features:

Initial processing was done in a local SCH co-ordinate system oriented to the flight path and perpendicular to the ellipsoid. Orientation is acquired only from GPS/INS.

Multiple overlapping strips were used.

Statistical analysis over overlapping areas was carried out to indicate errors such as (systematic) range tilts.

32 bit floating point data used in processing (8 bit image & 32 bit coherence).

Conversion to UTM.

Holes are filled, (these are caused by shadow, layover, low S/N ratio), using opposite look direction images and an algorithm involving neighbourhood filtering spline surface fitting in the elevation data.

Data resampled to 5m or 10m.

Merge of elevation data (weighted data).

Tile creation of DEMs (7.5 minutes, similar to USGS DEM grid tiles)

Transform to geoidal datum e.g. NAVD88.

Editing using false stereo (e.g. on SOCET Set workstations). Water areas are given a constant value.

Output product (ascii xyz, geotiff, bmpetc.)

Marcus Schwaebisch described the Aerosensing Radarsysteme GmbH AeS-1 IfSAR system. The end to end processing chain is shown in appendix VI. The talk focused on the applications that Aerosensing have carried out. Case studies looked at horizontal and vertical accuracies with comparisons to LIDAR and GPS / surveyed ground control points, further detail are given below.

In the second session presentations were made by organisations which had made use of airborne IfSAR data either for production use or experimentally. John Walk described the work of Ordnance Survey (Great Britain). OS had tested the IfSAR data for change detection and to infill existing height data from cartographic sources. GCPs had been used in the orthoimage to transform the DEM.

Mustafa Erdogan from the General Command of Mapping, Turkey described the test carried out with the Terschelling data, their main need was for rapid DEMs for orthophoto generation.

Rune C Andersen from the Danish National Survey described work done by Danish Remote Sensing Centre. The main requirement was for topographic mapping and map update and work had been done to develop automatic procedures using the Danish SAR system which included polarimetric capability by SAR.

Ian Dowman and Thongthit Chayakula gave a talk on the processing carried out on the Chiswick data at UCL. A number of algorithms had been tested to extract features and derive cartographic products.

Vincenc Pala of the Cartographic Institute of Catalonia (ICC) described a large project which involved the production of digital radar maps of the states of Bolivar and Amazonas

of the Venezuelan Republic. 1:50000 scale mapping was required for large areas and the project involved a significant effort in data acquisition and processing. The experience illustrated the advantages and problems of using IfSAR for this type of work.

In the next session potential uses were discussed. Nick Holden from the UK Environment Agency described their work done for flood monitoring and mitigation which was largely done with LIDAR data. Although IfSAR was less accurate, it was also less expensive and had an application in some of the mapping done by EA. Holden made a number of important points:

The end user wants to gain information from data and is not interested in the actual numbers.

SAR can detect water and can indicate areas in flood (if flown during flood) and can be used to calibrate flood models.

Accuracy needs to be related to gravity oriented accuracy: geoidal rather than spheroidal and the quoted precision of the geoid in UK of 10cm was a limiting factor.

Hugh Mackay gave a talk in place of Matthew Foote from Willis, who was unfortunately unable to attend at the last minute. Willis is a large insurance company who had used a DEM of the Thames Valley in UK generated from airborne IfSAR, for flood risk mapping. They had generated a DEM and land cover maps and were very satisfied with the result. The point was made that there is a hierarchy of DEM acquisition:

Regional	accuracy to 1m	radar
Detail	20 cm	LIDAR
High detail	<20cm	ground survey

The presentations generated discussion which is summarised under thematic headings in the next section.

5.0 Summary and discussion

Operational aspects

The systems available for data acquisition appear to be suitable for the task although costs are quite high. There was considerable discussion on the comparison with Laser scanning data (LIDAR), and it was established that for large projects the cost of SAR is less than LIDAR. This is because the IfSAR covers larger areas for comparable flying time.

The need for ground control points varied. Intermap uses GCPs only for its GT1 (Vertical RMSE <1 meter) product, in order to remove potential systematic errors. GCPs are not required for coarser product specs. Aerosensing consider them essential as GPS/INS is not accurate enough. Aerosensing use corner reflectors as control and these must be placed so as to be free of contaminants.

The data is subject to fewer problems than repeat pass processing. Weather conditions are not generally a problem but cases were reported of humidity affecting the data quality. Weather (rain, turbulence etc.) can cause problems from an operational point of view.

The problems of phase unwrapping are not completely solved and can still cause problems in areas of high relief, in areas of moderate relief phase unwrapping was considered to be easy. Multiple pass data can be used to improve the reliability of the product. Aerosensing uses a 3rd aerial to ensure robustness. Gaps can be filled at additional cost, i.e. the end user gets what he pays for.

The products from airborne IfSAR are intensity images, coherence images and DEMs, all of these have extensive use in applications.

Reference systems can still cause problems. The standard product tends to be WGS84 and the users must be responsible for transformation to their own datum. Transformations at this stage require ground control.

Conclusions

Airborne IfSAR is a reliable and cost effective way of acquiring data for DEMs.

Processing of single pass data is robust.

Accuracy

The main product from IfSAR is a DEM. The quality and completeness of this will be dependent on the SAR system itself and the position and attitude system and on the nature of the terrain and the land cover. The 'raw' DEM will include features such as buildings and woodland area and in hilly areas will be subject to gaps cause by radar shadow and lack of coherence. The main sources of errors are:

Sensor position and attitude (GPS/INS);
Signal to noise ratio, atmosphere;

Processing and production errors: filtering, thresholding, hole filling and editing.

Target (terrain type, vegetation cover, interaction with buildings);

The final accuracy of the DEM will also be subject to the editing and 'hole filling' which has been necessary.

In order to validate the product a full understanding of the system is necessary, and suitable reference data for validation

The accuracy of the geoid may be a limiting factor, in UK the geoid is only quoted to 10cm.

Some examples of accuracy are given in table 2.

Organisation	Project	Results		Comment	
		Mean	Std deviation		
Intermap	Baden Wurtenburg	Bald earth	-0.47m	0.28m	Forest results shows effect of volume scattering
		Cropland	0.66m	0.34 m	
		Forest	21.04m	2.16m	
	Red River	0.1m	0.6m	Flat river plain	
	Freiburg	Mixed	-1.3m	0.9m	
		Flat	-1.1m	0.7m	
Sloped		-1.4m	1.0m		
	Leetsdale	Building heights app 2m lower than laser derived heights		Study of building heights	
Aerosensing	Indonesia	Horizontal spacing	2.5m	3.0m	
	Brazil	0.5m	0.25m		Hilly area validated with D-GPS
	Venezuela	5m	3.0m		
	Bremerhaven			0.05m	Tidal flats validated with theodolite measurements
	Netherlands			0.22m	LIDAR DEM

Table 2. Accuracy of airborne IfSAR quoted at workshop.

Ordnance Survey had use the IfSAR DEM to geocode the image and found that straight lines did not always appear straight.

A number of established methods are available for validation. These include:

- Use of GCPs
- Use of DEMs of higher accuracy
- GPS transects

Conclusions

Accuracy can be selected to suit the application. This ranges from 5cm to several metres.

Accuracy is dependent on the type of terrain and land cover and the DEM produced will be of the surface features.

Gaps may occur in hilly terrain where Radar shadow occurred, or phase unwrapping was not possible because of coherence problems.

User processing

A user may wish to process or edit the data for their own application. The processes which may be required are:

- Generating a ground surface model;
- Extracting features such as buildings or roads;
- Land cover classification;
- Hydrological modelling;
- Change detection;
- Fusion of IfSAR products with other image data, map data or DEMs;
- Validation.

A number of tools are available within standard software packages. ERDAS and ARC/Info were both used by the participants. Amongst algorithms used those discussed were:

- Smoothing and filtering algorithms to give ground level.
- Polygon overlays to remove features not at ground level such as woodland.
- Segmentation, edge extraction to extract roads, woodland etc.

IfSAR provides intensity images, coherence images and DEMs which may be used for and cover classification (e.g. Willis), image map production (e.g. ICC) or automatic feature extraction (e.g. Denmark)

Conclusions

The end user may process the data to generate value added products;

No special software is required for many applications, where special processing is required tools are already available.

Applications

Many actual and potential applications were described or discussed at the workshop, the major ones are listed in table 3.

Application	Status	Example
Digital Radar maps	Operational	ICC project for Venezuela
DEMs for orthoimages	Operational	Response to Earthquake monitoring in Turkey
Topo mapping 1:10 000	Experimental	Denmark, using automatic techniques
Topo mapping 1:25 000	Experimental	Turkey
Change detection	Experimental	Denmark; Ordnance Survey for rural revision
Flood modelling	Operational	Willis in Thames Valley; Environment Agency (UK) interested as alternative to Lidar
Coastal erosion	Operational	Rijkwaterstaat/TNO; Environment Agency (UK)
DEM generation/infill	Experimental	Denmark; Ordnance Survey; Environment Agency (UK)
3D city models	Operational	Aerosensing (Berlin); Intermap (Leetsdale)
Powerlines	Operational	Aerosensing

Table 3. Applications of airborne IfSAR data

Conclusions

IfSAR has been used operationally for a wide range of applications, often by users previously inexperienced in the use of SAR data.

Users need to gain experience in the operational and interpretation aspects of acquiring and using IfSAR data.

Summary

The workshop was extremely useful for obtaining an overview of the operational issues and the potential applications of airborne IfSAR data. It is apparent that the method can be used for a number of applications but that experience and understanding of the principles is

required for effective use. IfSAR is not a complex and difficult to use as is sometimes thought; ICC, who had previously had limited experience of RADAR successfully carried out a large complex project in Venezuela and Willis in UK has successfully applied IfSAR data to a day to day application.

6.0 Update

Since the workshop airborne IfSAR has continued to be used and at this meeting in Stockholm further applications and research will be presented. It has been recognised that there is much in common in the algorithms required for processing IfSAR and LIDAR and this workshop should provide useful cross fertilisation of ideas.

ISAR DEM Data Processing for Contours Generation

Antonio Ruiz, Manuel Castillo, Román Arbiol and José L. Colomer

Institut Cartogràfic de Catalunya, Parc de Montjuïc. 08038 Barcelona, Spain

E-mail: toni@icc.es

Abstract

This contribution presents the different processes applied to a wide area DEM (Digital Elevations Model) in a region in the South of Venezuela, that was obtained by means of single-pass airborne SAR interferometry. Taking into account the well-known SAR technology limitations, the applied SAR interferometric processing as well as the flight mission constraints, different filtering and mosaic techniques have been applied to compute the DEM contour maps.

Keywords: DEM, SAR interferometry, altimetry, mapping, contour.

Introduction

The Institut Cartogràfic de Catalunya under contract with the Servicio Autónomo de Geografía y Cartografía Nacional de Venezuela has performed the mapping of a vast region between the Orinoco River and the Brazilian border. The project covered a region of 266616 square km in the South of Venezuela. This remote region of Venezuela has a warm and humid climate, with almost permanent cloud cover. The topography is hilly, with few flat areas and very abrupt elevations emerging from the plain ("tepuis"). The land is mostly covered by rainforest, with trees reaching 40 meters in height. The project consisted in producing 5 meter pixel digital orthoimages and DEM, and orthoimage maps at 1:50,000 scale with 40 meter contours derived from a ground DEM. The whole project involved 536 map sheets.

SAR mapping was selected to perform the project because this technology provides at the same time the image data and the altimetric data required for producing the orthoimages. Moreover, the data can be obtained and the final product delivered in a predictable period of time, regardless of the weather conditions and abundant cloud cover.

The accuracy and pixel size specifications excluded the use of SAR satellite systems. Therefore, the AeS-1 single-pass airborne cross-track interferometric SAR from AeroSensing Radarsysteme GmbH. (Moreira, 1996) was proposed and selected for the project. It operates in X-band with an interferometric baseline of 0.59 m and a viewing angle ranging from 20° to 67°. It was flown at 26,000 feet. The orientation and positional data required to process the SAR data was acquired by means of differential GPS and an on-board INS (Applanix).

After a preliminary ground survey campaign and the preparation of the logistics, the flight mission begun on October 20, 1998 and it ended successfully on February 5, 1999. During the whole year 1999 the SAR interferometric data was processed and a

first version of all the maps was produced, but a new edition of the DEM and the revision took more than expected. A shaded representation of the final DEM is shown in image 1. More details about the logistic of the mission and the processing of the radar data can be found in Arbiol and González, 2000.

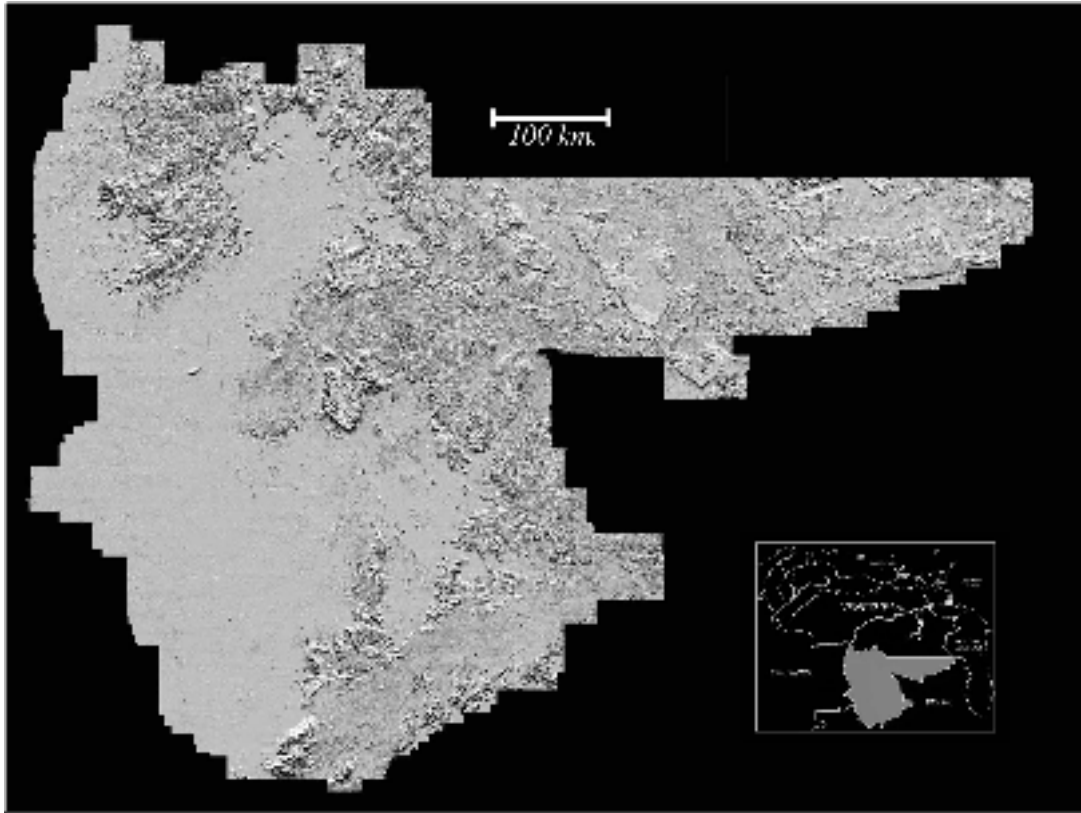


Image 1: DEM produced by the ICC interferometric SAR mission covering 266616 square km in the South of Venezuela.

SAR technology constraints

Several well-known SAR technology limitations exist for the operational use of SAR data. Mainly, they are related to the performance of the SAR in tropical rainforest areas.

The first limitation is the microwave wavelength. The used wavelength (X-Band) can not penetrate the canopy. It is a critical problem when the interest is focussed on the ground altimetry. However, it is not an inconvenient for orthoimage generation.

Another important constraint is that all of the SAR systems, as range sensors, present the following characteristic geometric effects of foreshortening, layover and shadowing. All these effects cause information loss or degradation (low coherence), mainly in high relief areas. Their impact can be reduced by flying in different directions to illuminate the slopes from different angles. Thus, the flights were performed from west to east and vice versa. Note that as in any range sensor, the resolution at near distance is different

from far distance. A fifty per cent overlapping between parallel tracks guarantees good resolution data for all the interest area.

Also severe atmospheric phenomena (heavy storms, etc) can degrade the signal leading to very low coherence. Using overlapping tracks this problem can be mostly reduced or avoided.

More than fifty per cent of the map sheets show calm water river networks. Calm water areas have a very low backscattering and, as a consequence, they present very low coherence. It is especially problematic during the SAR interferometric processing, because in the phase reconstruction these calm water areas produce “islands” (isolated zones) where the coherence is high but can not be reconstructed. A more sophisticated phase reconstruction, sometimes requiring user interaction, must be used to fix this problem.

SAR data processing constraints

The complete SAR processing workflow consist of three separated steps: SAR focussing, interferometric processing and cartographic processing.

The raw data recorded on-board must be processed into an imaging product suitable for SAR interferometry. This is done by means of the SAR focussing. This process uses the navigation and attitude data derived from the differential GPS and the INS. The main characteristic of a SAR processor is its ability to process accurately the phase that must be preserved during the processing because it has a direct impact on the quality of the output DEM. This is only guaranteed when the flight squint angle is small so this constraint must be taken into account during the data acquisition. Also problems with the accurate determination of flight position and attitude can critically affect the SAR processor performance due to communication problems with the differential GPS reference station.

The second step is the interferometric processing of the data that ends in the generation of the DEM. Due to the constraints associated to the low coherence areas, phase unwrapping can be difficult, especially when isolated areas exist. In this case, the solution consists of a manual reconstruction or editing of the phase. After the reconstruction of the phase, the unwrapped relative phases must be transformed to absolute values in order to generate a geocoded DEM. The absolute phase offsets were calculated by adjusting its values between different pairs of tracks. The offset adjustment between pairs of tracks can propagate RMS error from track to track. In our opinion, it would have been better to use a block type of adjustment. In order to avoid such problems, some of the tracks had to be reprocessed until a consistent set of absolute offsets was found.

In the cartographic processing, the DEMs and the corresponding orthorectified SAR images are mosaicked to generate the final data for each map sheet. Tracks flown in parallel and opposite directions covering the same area are mosaicked selecting the best coherence data to fill the low coherence gaps. In case of high coherence data but different resolution, the best resolution data is chosen. Where the resolution is similar, a mean value was computed in the overlapping areas. Despite of this procedure, DEM

gaps remain. For example, in high slope regions, when one track is affected by shadowing, the track flown in opposite direction might be affected by layover. In these cases the mosaicking process generates a gap.

Flight mission constraints

Before starting operations, the SAR system basic configuration parameters were accurately calibrated using corner reflectors as ground control points. This calibration was performed twice more during the mission. However, an accuracy degradation of the system during the flight campaign was observed when the data was processed. Different tracks showed orientation problems that affected the final DEM accuracy. A re-calibration was performed after flight campaign to compensate for the observed drifts.

Another problem associated to the acquisition of the data was the difficulty to follow the flight plan. The flight must be extremely precise to facilitate as much as possible the focussing and the interferometric processing of the data. The flown trajectory must be very close to the planned trajectory in order to assure the required overlapping. Unfortunately, despite the efforts of the flight crew, some tracks presented high squint angles and some data gaps appeared.

ISAR DEM

The ISAR DEMs resulting from the above described processing workflow have a pixel of 5 by 5 meters and are very smooth. They were processed into sheets according to the geodetic tiling of the country. Due to the constraints mentioned before, the DEMs have different unavoidable artefacts. The most important identified artefacts are gaps, stripping, mosaic problems and granulation.

Gaps. The DEM is obtained mosaicking tracks flown in opposite directions. Even so some gaps remain in regions of high slope or due to the presence of water. In water covered regions the backscattering is very low because water is calm and we have mirror reflection of the radar signal. Close to the gaps the signal coherence is low and the noise is higher. In this project the coherence threshold for accepting the data has ranged between 0.3 and 0.5. The lower the threshold is, the smaller the gaps without information are but, in return, the noisier this information is. This threshold has been chosen because we gave more priority to the image. Image quality is less sensitive to the coherence than the DEM. Close to the water gaps the z values of the DEM take random values that in some places range some hundreds of meters. The DEM generated by the AeroSensing software is smooth due to the applied filtering, so removing the noise is even more difficult. (image 2).

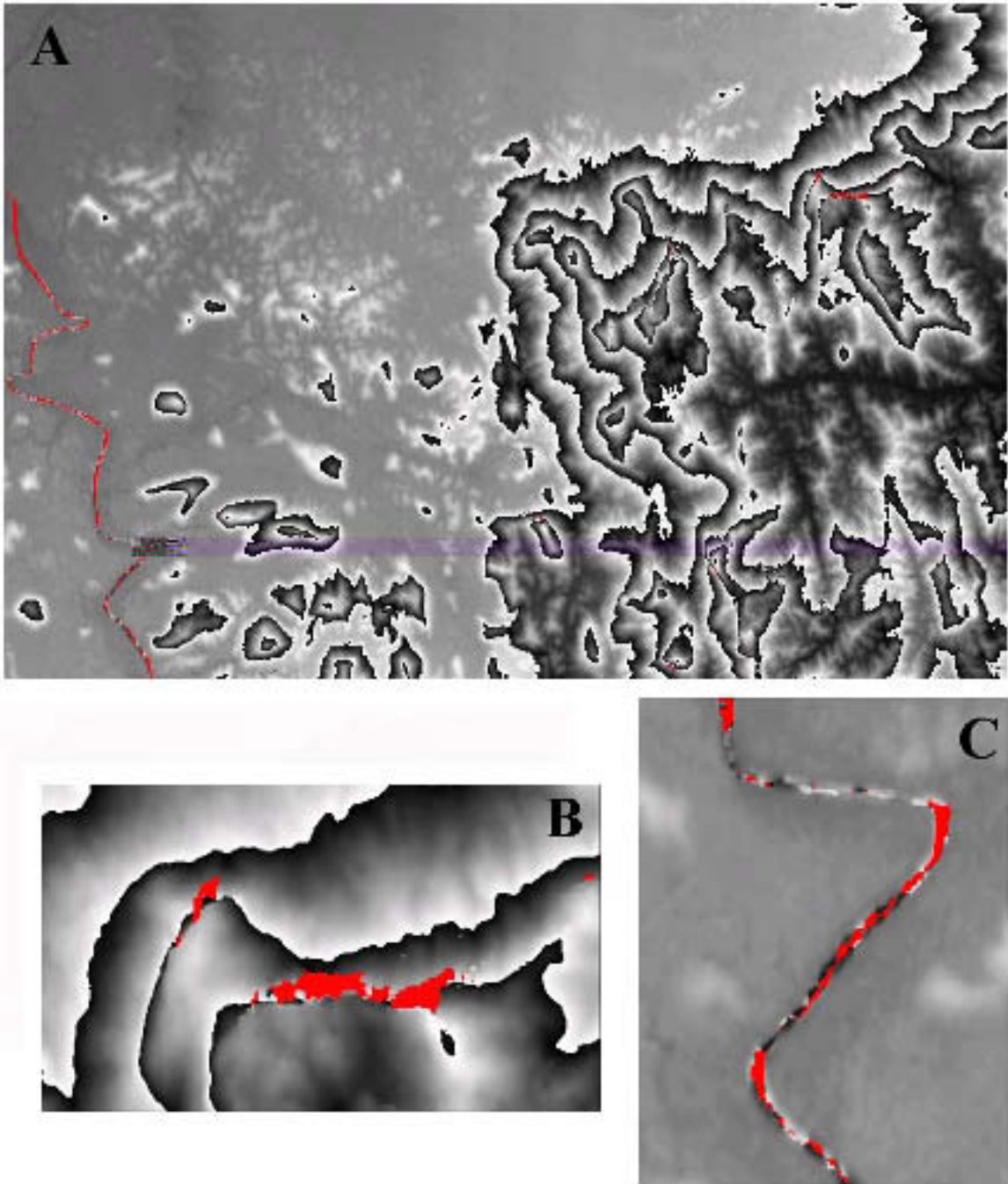


Image 2: Gaps detected in map sheet 7021ii: A: Full map; B: Detail of gaps associated to high slopes; C: Detail of gaps associated to water bodies.

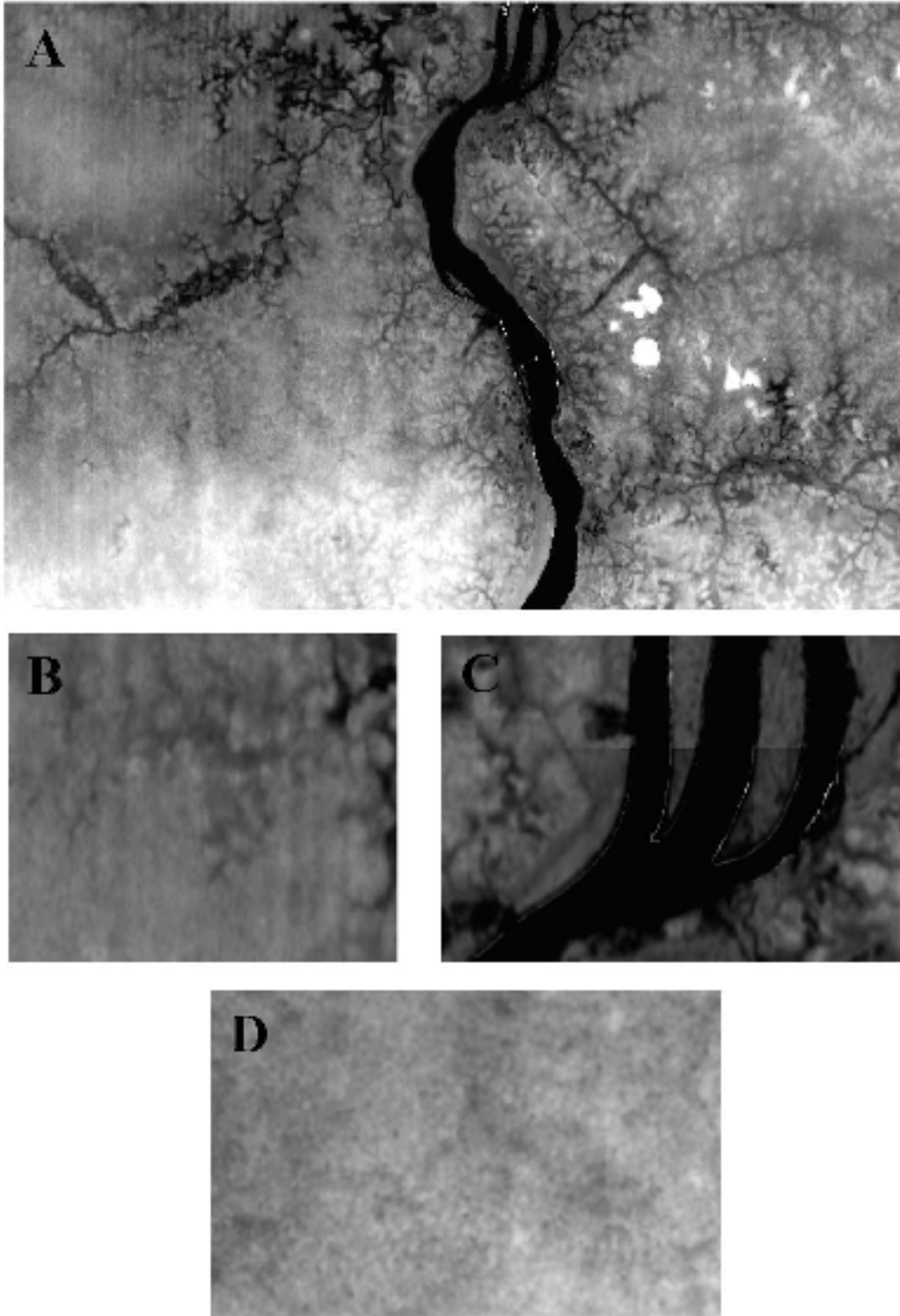


Image 3: Artefacts observed on map sheet 6819iv: A: Full map; B: Stripping artefact detail; C: Mosaic Artefact detail; D: Granulation artefact detail.

Stripping. This artefact appears when flight parameters exceed some specific values. For example, the reconstruction of the signal algorithm performs better if the images are taken at small squint angles. In flat regions the DEM may show this residual stripping that is very apparent in hypsometric representations of the flat terrain due to the low range in elevations. Anyway, the height error is in the range of acceptable tolerances (Image 3-B).

Mosaic problems. Due to the adjustment of the absolute phase offset between pairs of tracks, a residual offset error remains, even if the adjustment is within the range of acceptable tolerances. This residual can generate a very apparent mosaic artefact between tracks in flat areas. This kind of artefact can be fixed by readjusting the offset with its neighbour tracks (Image 3-C).

Granulation. Ground DEM resolution (5 m) is enough to resolve the individual trees in rainforest. The canopy is the main contribution to the DEM in low relief regions (Image 3-D).

DEM Post-processing

In order to remove or reduce as possible the described artefacts different procedures were applied to the ISAR DEMs.

DEM editing

The processing applied fulfilled the following objectives:

- Remove gross errors
- Filter artefacts
- Fill the gaps originating from shadows, occlusions and low coherence areas

It was decided not to interpolate and fill the gaps in water areas with the values of the borders because of the artefacts that could be introduced.

We wanted to remove noise as far as possible but without affecting the model details. To do so a filtered DEM is generated with a grid size of 15 m to which a median filter of size 7x7 is applied. Then the original 5x5 m DEM and the smoothed one are compared. Null values are assigned to the original DEM points where the difference between both models is larger than 40 m. (In order to compare both models the smoothed one is re-sampled to 5 m by bilinear interpolation) (image 4).

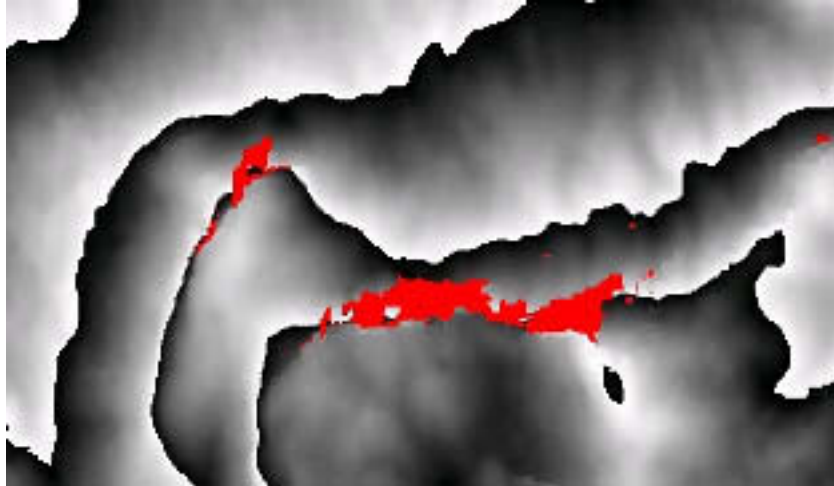


Image 4: Sub-scene of the map sheet 7021ii (Image 2-B) after cleaning of noise.

The remaining noise is removed by manual editing with the help of a hypsometric representation of the terrain. Only null values are assigned during these editions. The editing process increases the number and the area of the original gaps.

Automatic filling of gaps

An automatic filling process has been developed and applied to the 15 m DEMs and the resulting values are transferred to the original 5 m DEM after bilinear interpolation.

The filling technique applied is different depending on the size of the gap. Gaps larger than 10 pixels are filled with the help of a triangular irregular network (TIN) model. For gaps smaller than 10 pixels a 3x3 binomial (gaussian) filter is applied iteratively to the values in the boundary until no null values remain. Only null values are modified during these iterations.

The TIN based gap filling procedure works as follows. First, the masks of null value regions are expanded by one pixel and then a TIN is interpolated over the null values from pixels of the border. With this TIN model we obtained a reasonable height for the pixels in the gaps with Akima's quintic interpolation (Akima, 78). This interpolation is very smooth (it is C^1 and visually C^2) (Images 5 and 6).

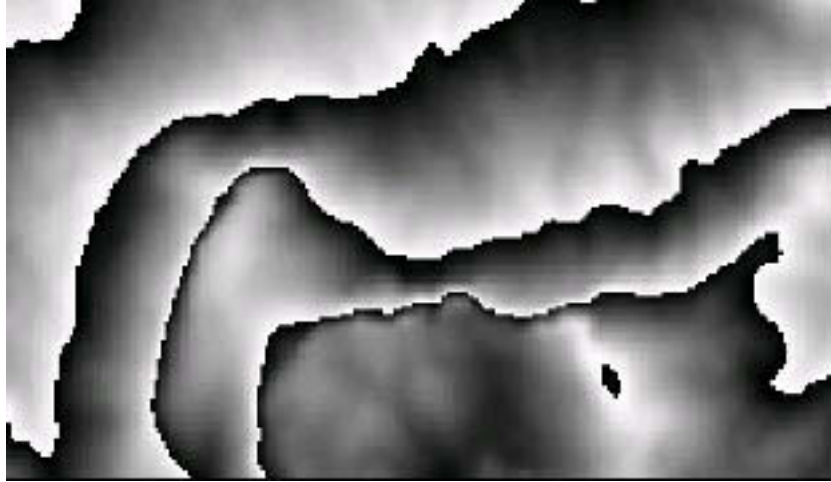


Image 5: Sub-scene of the map sheet 7021ii without holes.

Generation of Contour lines

The contour lines are generated from the filled and filtered DEMs described so far but resampled at 15 m. DEMs are 500 m larger than required by each side (image 6). To ensure the continuity between neighbouring DEMs, up to eight neighbours are mosaicked and averaged with weights computed with the help of Hermite polynomials in the overlapping areas.

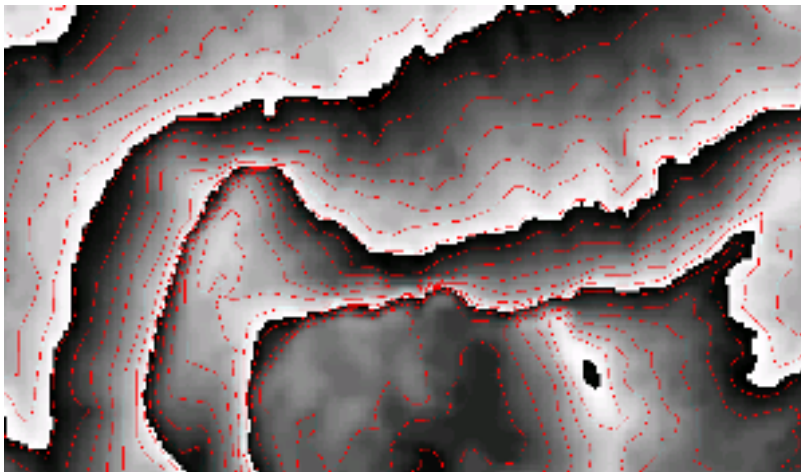


Image 6: Sub-scene of the map sheet 7021ii with the interpolated contours.

In order to account for the height of the canopy, classified cloud free Landsat images with a pixel of 25 m are generated. For some regions without Landsat coverage, texture synthetic bands derived from the radar images are used in image classification (Otazu and Arbiol, 2000). The height profiles are analysed on class boundaries and a least squares estimation of height differences between classes is performed. A procedure has been designed in order to assign a height to each multispectral class using non-vegetated areas as reference values (image 7).

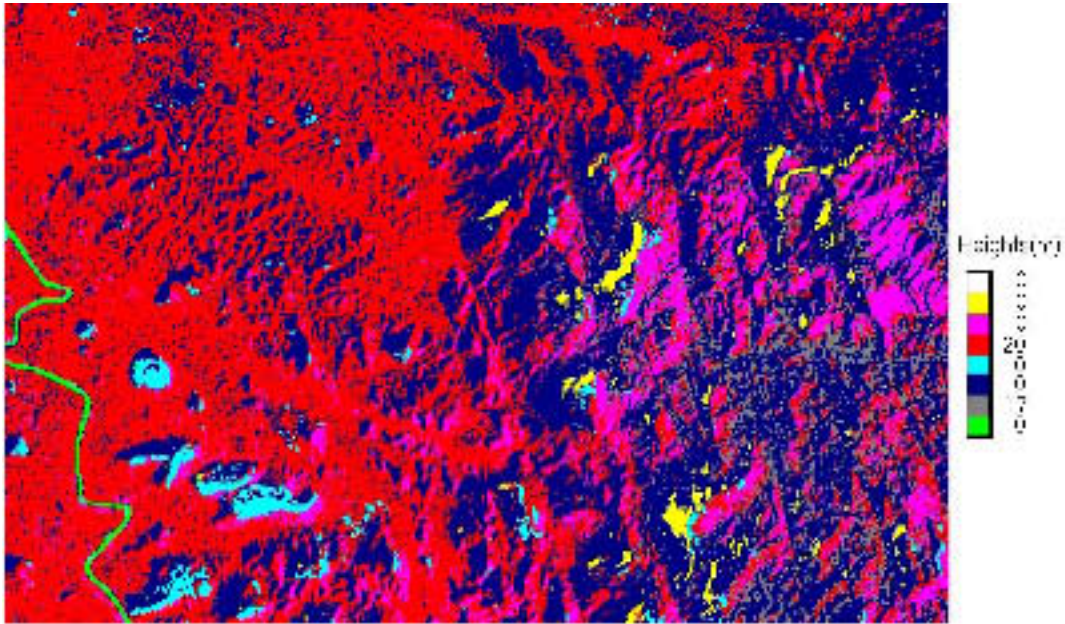


Image 7: Landsat image classification of map sheet 7021ii.

Some mismatches between Landsat and radar images have been observed due to different epoch acquisition and registration errors. The effect on the DEM is the creation of spurious local minima and maxima in the border of vegetation areas. They are reduced by filtering with a binomial filter of 5x5 pixel size. Then local minima are filled and local maxima with height smaller than 40 m are removed. The filling of local minima is justified because depressions are very rare in natural landscapes. The removal of small local maxima helps to eliminate the small contours originated by the vegetation residuals.

In areas with slope larger than 160% only the master contours (200 m) are drawn in the map. The selection is automatic. After mask generation for the steep regions, small sized masks are removed and the remaining are simplified. These masks are used to reclassify the inner contours and to remove the inner contour labels.

Too small contours (perimeter < 700 m) are removed and when the contour corresponded to a peak, it is substituted by a spot height. We consider that the spot height corresponds to a peak when it is closed by a contour and there is nothing else in the area delimited by this contour.

Some spot heights are generated randomly in flat regions with a homogeneous distribution. To perform this step, a grid of 6 by 6 sq. km cell size is analysed. Taking into account the maximum and minimum height in each cell we check if there is a contour in the cell. If there isn't any, a spot height is generated by interpolation in the DEM.

Contours are snapped to neighbouring map sheets and snap mistakes are detected. Due to the simplification of the contour lines it is possible that intersections between contours occur in steep regions. These contour problems are automatically detected and corrected by hand.

Other corrections performed by hand are the edition of the contours in water covered regions and in steep regions, and the improvement of the contour label placement. In mountainous regions only master contours are labelled. After all these editing procedures, the final map sheet contours are generated (image 8).

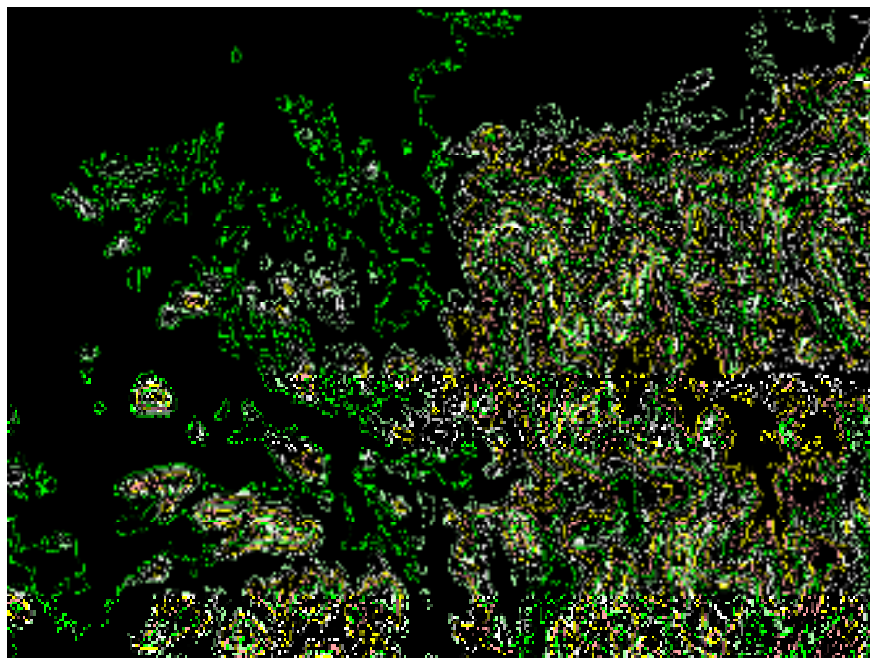


Image 8: Final Map sheet 7021ii contours.

Programming

The SAR focussing and the ISAR processing were done by using the AeroSensing software. Additional image processing was performed by means of the ICC software coded in Fortran and running on Compaq Open VMS. Almost all of the DEM post-processing and the contour generation programming was done in AML, the programming language of Arc/Info.

Conclusions

In this contribution, an operational application of airborne SAR interferometry has been shown. The obtained results indicate that this technique is able to generate high density and high precision DEMs in large areas at low cost and with very satisfactory performances. However, the limitations of the SAR technology, the present state-of-art of the SAR data processing, together with the difficulties associated to the flight mission, impact directly on the quality of the data. Usually, data acquired in extreme conditions, such high relief areas, low coherence areas, non-precise flight performances, etc., are highly degraded. Only a low percentage of the covered area present degradation but these areas are particularly problematic. To mitigate as possible its effects, the standard procedures required to generate map products must be modified. In this contribution, the methods developed to generate contour lines in presence of low quality data, have been shown and discussed. The obtained contour maps are within the range

of acceptable tolerances. This is very encouraging because the implemented procedures overcome very well some of the described system constraints. Nevertheless, an improvement of the limiting elements, related to the system, the processing or the mission, seem to be essential to carry out projects with more demanding requirements and performances.

Acknowledgements

A lot of people worked hard to achieve the goals of this project. Among them, we want to acknowledge the work of: Carolina Martínez, Xesca Serra, Fernando Pérez, Anna Tardà and Sergio Anguita for the ISAR and the DEM processing, Carles Serra for the contouring programs, Gemma Cuatrecasas, Antonio López and the other operators for the editing of the DEMs, Xavier Otazu for the classification programs, Francesc Sánchez for his help in AML programming, and Monica Velilla, Vicenç Palà, Assumpta Lleonart, Lluïsa Colomer, Inma Menacho, Antonio Ramos and Anna Lleopard for essential complementary tasks related to the project .

References

Akima, H., 1978. A method of bivariate interpolation and smooth surface fitting for irregularly distributed data points, *ACM Transactions on Mathematical Software*, vol. 4(2): 148-159.

Arbiol, R., González, G., 2000. Map production in Venezuela using airborne InSAR. *International Archives of Photogrammetry and Remote Sensing*, vol. 33(B1): 24-28. Amsterdam.

Moreira, J., 1996. Airborne SAR: image generation and height precision DEM generation. *International Archives of Photogrammetry and Remote Sensing*, vol. 31(B2): 256-260. Vienna.

Otazu, X. and Arbiol, R., 2000. Land use map production by fusion of multispectral classification of LANDSAT images and texture analysis of high resolution images. *International Archives of Photogrammetry and Remote Sensing*, vol. 33. Amsterdam.

The DERA ESR Radar: Overview and initial interferometric SAR results

Dave Barker
Radar Signal Processing Group
R117, DERA Malvern
St Andrew's Rd
Malvern
Worcs
WR14 3PS
e-mail: daveb@sar.dera.gov.uk

Abstract

The Defence Evaluation and Research Agency (DERA) commissioned a new experimental radar, the Enhanced Surveillance Radar (ESR) in September 2000. This is a versatile, high performance synthetic aperture radar (SAR) and moving target indication (MTI) radar that is used to support MOD sponsored defence research. It is widely applicable to a variety of commercial applications such as terrain mapping, digital elevation model (DEM) production, flood warning and monitoring. The radar is fully polarimetric and operates in both strip and spotlight SAR modes. An overview of the radar and off-line processing techniques is given followed by initial results obtained from the interferometric SAR (InSAR) modes.

Introduction

The DERA ESR radar is a versatile radar platform which supports a variety of research programmes, in the fields of SAR imaging techniques, polarimetry, automatic target detection/recognition and interferometric SAR (InSAR) as well as moving target indication, detection and imaging. The radar has been in development for several years and was finally commissioned in September 2000.

The radar is mounted in a BAC 1-11, series 500 (ZH763) aircraft which is shown in figure 1.



Figure 1: The DERA Enhanced Surveillance Radar

The main antenna is a 360° scanning antenna, space stabilised in azimuth and elevation, mounted underneath

the fuselage, as can clearly be seen above. This can transmit in either vertical (V), horizontal (H) or circular polarisation and simultaneously receive in V and H. Sum and difference channels can be recorded to provide MTI monopulse functionality. Two auxiliary horns, whose along-track spacing can be varied up to 2m apart, are mounted to starboard about 3m vertically above the main antenna to provide clutter-cancelling displaced phase centre (DPCA) MTI, along-track interferometry and a high performance InSAR capability.

A system overview of the ESR is given followed by details of off-line processing. This is followed by an example of initial results from InSAR processing of the data.

System overview of the ESR radar

The important system parameters of the ESR are listed in table 1. The radar operates at X-band between 9.45 and 9.95 GHz, with a peak power of 15 kW. The instantaneous bandwidth is up to 500 MHz with selectable filters to limit receiver bandwidth (20, 125, 250 and 500 MHz) for narrower band signals. Range resolution is at least 0.5 m at the highest bandwidth with range sidelobes better than -30 dB. Azimuth resolution is a nominal 0.65 m in stripmap mode as determined by the antenna length. In spotlight mode a resolution of better than 0.3 m has been achieved.

Operating frequency	9.45 to 9.95 GHz
Power	15 kW peak
Bandwidth	500 MHz (with selectable filters of 20, 125, 250 MHz)
Range resolution	>0.5 m with -30 dB sidelobes
Main antenna length	1.3 m
Frequency agility	Programmable pulse-to-pulse, coherent
PRF	300 Hz - 17.5 KHz, fixed or spatial sampling mode
Pulse length	Fully programmable up to 20 us
Waveform	Fully programmable, pulse-to-pulse.
Tx Polarisation	V/H pulse-to-pulse and circular
Rx	Simultaneous V and H on main antenna, V or H on auxiliary.
Main antenna beamwidth	1.3° azimuth 10.7° elevation
Auxiliary horns	2 15dB horns, with up to 2m along-track spatial separation
Depression angles	0 to 75°
Motion sensors	IMU, INU, GPS - pcode
Other main sensors	Baro altimeter, air data, ground speed

Table 1: ESR system parameters

The design philosophy of the ESR was based on providing versatility and full programmability, in terms of waveforms, frequency agility, burst lengths and available pulse lengths. Thus ESR can mimic a variety of radar operating conditions including spaceborne SAR and specialised MTI modes.

The main antenna is fully space stabilised in elevation and azimuth and is capable of sector scanning, spotlighting or 360° scanning at up to 500°/sec. A wide range of antenna depression angles is possible.

Fig 2 shows a schematic of the ESR data and signal paths. Two channels can be recorded simultaneously onto an Ampex DCRSi recorder for off-line processing. In addition a processor can be mounted in the radar for real-time SAR or MTI display.

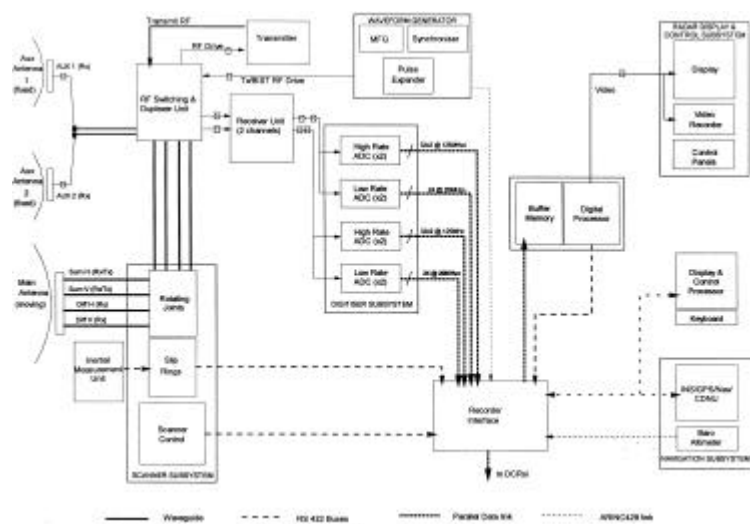


Figure 2: Block diagram of ESR radar

The PRF can be fixed or linked to the aircraft speed for constant spatial sampling mode. Again this is fully programmable, dependant on aircraft ground speed, recorder bandwidth and Nyquist sampling considerations.

The motion sensor suite includes a Litton LR86 inertial navigation unit (INU) strapped to the main antenna, Litton LN-93 inertial navigation unit and p-code GPS receiver as well as air data and other sensors. The IMU provides motion data, to precisely stabilise the antenna in azimuth and elevation. The motion sensor data is recorded onto tape for off-line processing. This data is used as input to a sophisticated Kalman-filter based motion compensation (MOCO) system.

Interferometric SAR

Introduction

For this application the fore auxiliary is set in a central position, directly above the main antenna. The nominal baseline is around 3.5m and baseline angle 65°, dependant on the main and auxiliary antenna depression angles. The ESR has a much higher power and about twice the baseline of the now decommissioned DERA C-Band radar [1] and consequently should have much better single pass InSAR performance. Additionally, the MOCO system will facilitate dual-pass InSAR.

Off-line SAR Processing

The raw SAR data is processed using a flexible, modular, parallelized, fully-pipelined, processor, capable of simultaneously processing multiple data channels. Radar data (RDM) and processing (RPM) modules are selectable and configurable for a variety of SAR and MTI modes for ESR data. In addition data from other platforms such as the (2GHz bandwidth) Helicopter SAR and the decommissioned DERA C-Band and X-band Canberra SARs can be processed.

Figure 3 shows the RDM configuration window. Data input and synchronisation is followed by motion compensation and then the data is decoded into the 2 channels: main and auxiliary. The MOCO generates phase corrections and displacements which enable the raw SAR data to be corrected to a straight and level reference track.

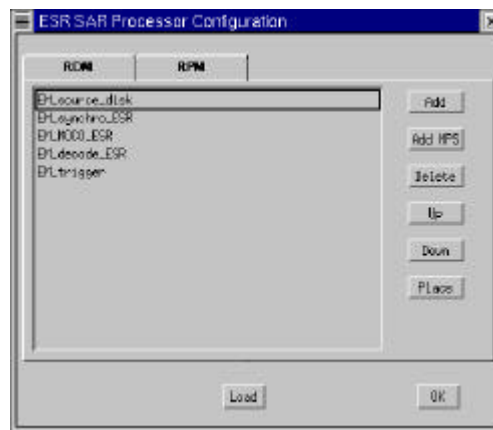


Fig 3: ESR Processor configuration of RDM modules

Figure 4 shows the ESR processor RPM configuration window. Bias compensation, azimuth presuming, range compression, phase compensation and range wander correction take place followed by azimuth compression, display and data grabbing (latter not shown).

Range curvature correction and autofocussing, using either multi-look registration or contrast optimisation, can also easily be selected in the RPM chain as well as optional diagnostic displays. Parameters are modified in individual module parameter windows. Both

configuration and parameters are stored in associated files. The processing chain for processing of spotlight SAR data is similar but due to its intensive nature, uses multi-port (multiple inputs and outputs) modules.

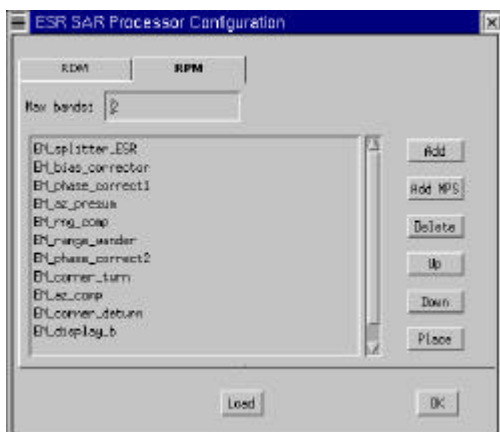


Figure 4: ESR Processor configuration of RPM modules

InSAR processing

The steps in formation of InSAR digital elevation maps (DEMs) are as follows. The main and auxiliary images are registered to sub-pixel accuracy (specified by an oversampling factor) using a stand-alone correlation-based registration program. This is followed by interferogram formation, flat earth correction, roll correction, phase unwrapping and phase-to-height mapping. As explained in [2], roll is the dominant aircraft motion, which must be corrected for. Several techniques have been developed which deduce sensor motions from the data itself. The first method derives roll phase corrections from the image shifts outputted from the correlation-registering step, relating the shifts to the relative cross-track motion (and consequential change in baseline angle) between the two antennas. Another method uses the phase differences between 2 or more multi-looks to derive the necessary phase corrections [3]. These methods are necessary for platforms that do not have sophisticated motion sensors. With ESR InSAR data the roll information from the auxiliary radar information is used to derive the phase corrections.

Theoretical performance of ESR for InSAR applications

The accuracy of determination of interferometric phase is limited primarily by the signal to noise ratio of the processed SAR imagery. Figure 5 shows thermal noise limited height accuracy errors for terrain (distributed target) mapping. The parameters specified were a radar bandwidth of 250MHz, 2 us pulse, an azimuth resolution of 0.7m with a clutter reflectivity (σ_0) of $-14 \text{ dBm}^2/\text{m}^2$. This figure is of course degraded by geometrical inaccuracies and baseline decorrelation. Geometrical inaccuracies include errors in estimation of platform height, baseline angle, target range and baseline separation. Baseline decorrelation, which is due to the spectral shift between the 2 slightly different

interferometric imaging angles can be reduced (albeit at the expense of range resolution) by range spectral filtering. Future work will quantify the phase errors realised in ESR SAR for both single and multiple-pass InSAR. However, initial results for single pass InSAR are consistent with theoretical predictions as given below.

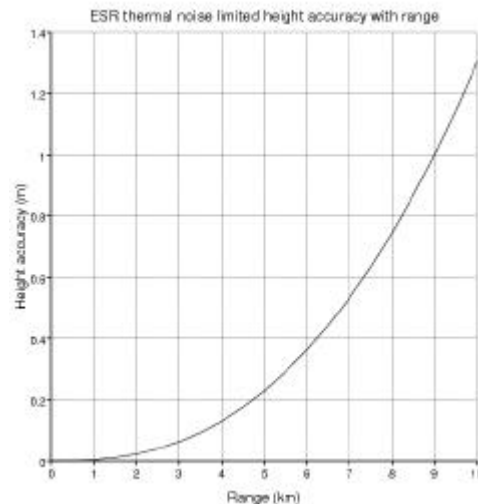


Figure 5: ESR thermal noise limited height accuracy with range

Initial results for single-pass InSAR

SAR imagery of the Isle of Wight has been collected in October 2000 under internal funding, in order to demonstrate a capability for commercial applications of ESR and for initial performance assessment. Figure 6 is an example SAR image of part of Totland Bay, to the west of the Isle of Wight. The data was collected at a resolution of around 1m in azimuth and range at a short stand-off range of around 2 km. Azimuth direction is along the horizontal and near range is at the bottom of the image.

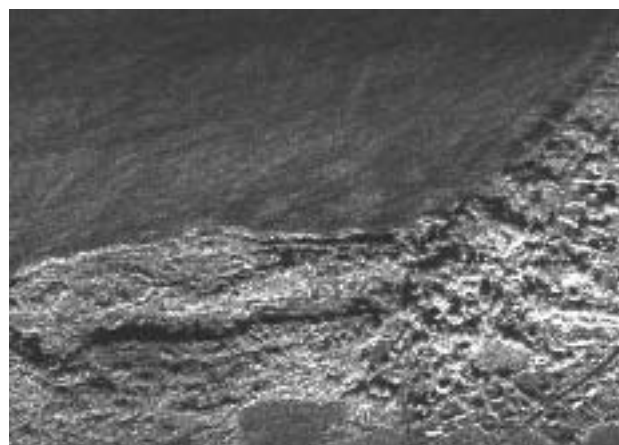


Figure 6: SAR image of Totland Bay, Isle of Wight

Figure 7 is the raw interferogram produced from registered main and auxiliary channel SAR images. The presence of roll can clearly be seen which manifests itself as a sinusoidal disturbance of the phase in the

azimuth direction. Figure 8 is the roll corrected interferogram which is phase unwrapped and geo-referenced to produce the SAR DEM of figure 9. The SAR DEM has an rms error of around 3 m in comparison with the OS (landform) DEM, which is a promising initial result. The difference can be accounted for by the culture (building, vegetation, trees) which are imaged by SAR.

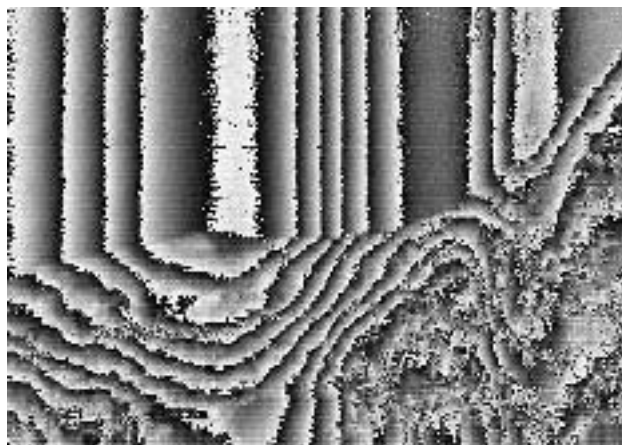


Figure 7: Uncorrected Interferogram

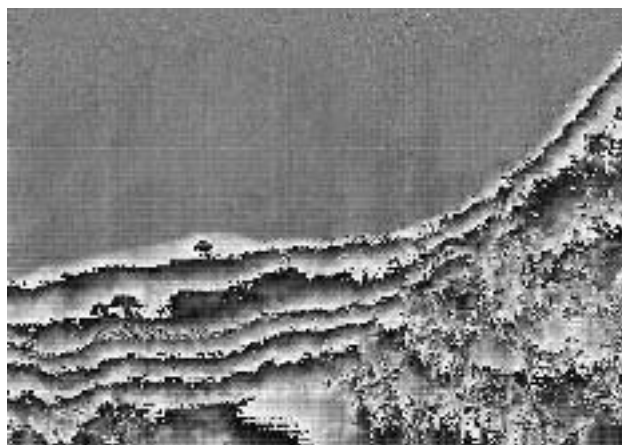


Figure 8: Corrected Interferogram

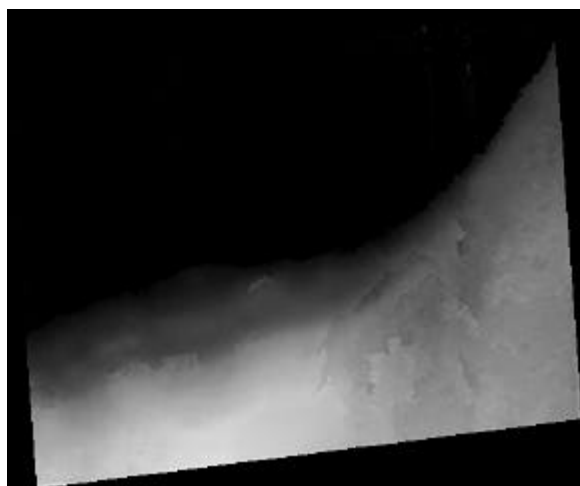


Figure 9: Geo-registered SAR DEM of Totland Bay

Summary and Conclusions

A system overview of the DERA ESR has been presented, along with a description of off-line processing techniques for general SAR and InSAR image formation. Initial results from ESR for height mapping are promising with rms height errors within predicted bounds. Future work will analyse and quantify these errors for both single and multiple-pass InSAR modes.

References

- [1] "The DRA C Band SAR", D Barker et al, Microwaves 94 Conference Proceeding, pp. 53-61.
- [2] "Single and multiple pass height finding interferometry from an airborne platform", A Currie et al, IEE Radar 97 Conf., pp. 114-118.
- [3] "Estimation and correction of roll errors in dual antenna interferometric SAR", R J Bullock et al, IEE Radar 97 Conf., pp. 253-257.

© British Crown Copyright 2001. Published with the permission of the Defence Evaluation and Research Agency on behalf of the Controller HMSO

Alexander V Ksendzuk

Increasing resolution of SAR Images

Abstract.

Synthetic aperture radar (SAR) provides good resolution of images, but sometimes desired resolution is much more higher. Common methods such as changing signal parameters, using complicated antenna arrays provides higher resolution, but expensive. In this paper presented method of increasing resolution due to advanced processing technique without changing SAR parameters. Space resolution, which is determines by space ambiguity function of signal (image of SAR is a convolution of real image and space ambiguity function), was considered as a resolution-quality appraisalment. Of course, higher resolution provides higher quality of image and allow recognize objects more accurately and detect small targets. By using de-correlation of the input signal width of space ambiguity function (for both coordinates of a surface) may be decreased – this results in higher resolution in space. In this paper derived optimal algorithm for processing with de-correlation for producing high-resolution image and for accurate parameter estimation, shown space ambiguity functions for standard optimal processing and optimal processing with de-correlation. With quite small signal-to noise ratio (20), resolution increases more than 4 times. Higher signal-to-noise ratios provide more higher resolution

Modeling and Recovering Systematic Errors in Airborne Laser Scanners

T. Schenk

Department of Civil and Environmental Engineering and Geodetic Science
The Ohio State University
2070 Neil Ave., Columbus, OH 43210
schenk.2@osu.edu

1 Introduction

Laser altimetry is a new technology for rapidly capturing data on physical surfaces. It offers many advantages, including the high precision of the laser points. It appears at the outset that the elevation accuracy is limited by the range accuracy which is assumed to be better than one decimeter. Planimetric errors are often disregarded with the argument that they do not matter on flat surfaces. This view is too simple—the error budget of laser points is far more complex. It is important to distinguish between the accuracy potential and the actual results achieved with today's systems.

Several papers report about errors encountered in laser points or surfaces derived from laser points. In The Netherlands, for example, airborne laser altimetry has been extensively used on a nation-wide scale for establishing DEMs and for monitoring coastal erosion. *Huis-ing and Gomes Pereira* (1998) identified elevation errors in overlapping strips on the order of a few decimeters and planimetric errors of more than one meter. Often the problems encountered cannot be satisfactorily explained and the authors suggest to improve the error models and to define more realistic accuracy requirements. Similar elevation errors are also reported in *Crombaghs et al.* (2000). The authors also describe an adjustment procedure to eliminate systematic errors. The discrepancy between the accuracy potential and actual accuracy achieved with today's laser altimeter systems permits the following conclusions:

lack of adequate error model: errors encountered in airborne laser altimetry cannot be sufficiently explained. Often, the lack of plausible explanations results in lack of confidence, which may be a bigger concern than the magnitude of errors. *Gardner* (1992) provides a detailed account on spaceborne laser altimetry systems and error sources. Similarly, *Lemmens* (1997) list and quantify systematic and random error sources but does not provide an error model.

lack of adequate calibration procedure: the errors reported are encountered in calibrated systems. The purpose of calibration is to determine systematic errors and to provide means to correct them. State-of-the-art calibration procedures of laser altimeter systems are not adequate, not transparent, often times ad-hoc, and lack objective quality control measures.

detection and correction of systematic errors: is a tedious post processing step that reduces the degree of automation, causes delays in delivering results, and lowers the overall performance. Errors are quantified but not modeled. The lack of an error model casts doubts on the validity of the proposed correction methods.

The purpose of this paper is to develop a first order error model of airborne laser scanning systems that is based on imperfections of the system components. The general laser equation presented in the first section describes an ideal system. Based on this, an error model for the laser scanner, and the INS and GPS units is developed. The result is a modified laser equation that contains all errors introduced. The following section presents an analysis of the error model based on the example of scan angle errors. Finally, the last section deals with the recoverability of the errors. Several systematic errors can be determined independently from

each other if certain flight configurations are followed. We conclude that these errors are not correlated within the proposed calibration geometry. It also follows that all parameters introduced in the error model can be determined.

2 General Laser Equation

The three sub-systems that make up an ALS are schematically depicted in Fig. 1 together with their reference frames. The general laser equation 1 establishes relationships among the measuring sub-systems of an ALS. The derivation is similar to *Lindenberger* (1993). First, the laser coordinate system is transformed to the local INS system. The origin of the laser coordinate system is at the laser's firing point. The x -axis points toward the flight direction and the z -axis is identical to the zero position of the laser system. With local INS system we refer to a coordinate system that is centered at the INS system and oriented according to the INS reference frame, as installed on the platform. Like in the laser coordinate system, the x -axis is in the flight direction and the z -axis is vertical. That is, the x -, y - plane is kept horizontal during the installation.

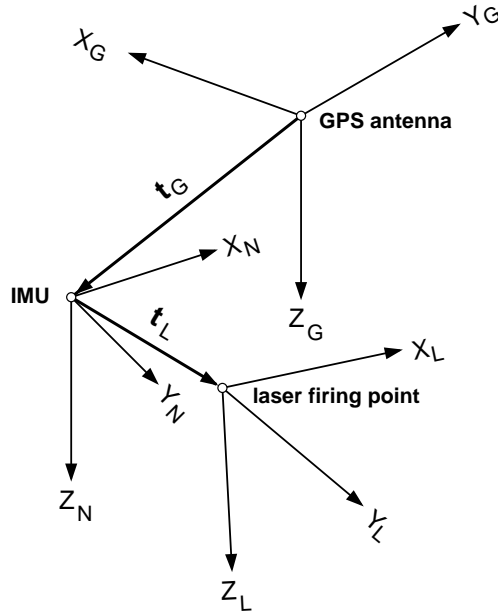


Figure 1: Reference frames of ALS sub-systems.

The transformation of the LS system to the INS system involves the rotation matrix \mathbf{R}_M and the translation vector \mathbf{t}_L . Next, the INS system is transformed to the local north-oriented system centered at the GPS Antenna. This is accomplished by \mathbf{R}_N and \mathbf{t}_L . The final step is concerned with the transformation of the local north-oriented system to WGS-84 coordinate system.

$$\mathbf{p}_W = \mathbf{R}_W \mathbf{R}_G \mathbf{R}_N (\mathbf{R}_M \mathbf{R}_L \mathbf{r} + \mathbf{t}_L + \mathbf{t}_G) + \mathbf{t}_{GPS} \quad (1)$$

$\mathbf{R}_W, \mathbf{R}_G, \mathbf{t}_{GPS}$ are functions of the current position of the platform
 $\mathbf{R}_N, \mathbf{R}_L, \mathbf{r}$ are measured or interpolated at the time of ranging
 $\mathbf{R}_M, \mathbf{t}_L, \mathbf{t}_G$ are the mounting parameters (constants)

This general laser equation transforms the measurements of the ALS into WGS-84 coordinates. This is often followed by an additional transformation, for example to a national system or to a local system centered in the project area.

3 Error Models

Eq. 1 describes an errorless system. We ought to consider the impact of systematic errors that occur within the ALS' sub-systems and between them. In this section we analyze the effect of these errors on the laser footprint position. A better understanding of the nature of systematic errors and their influence on the footprint will help in devising more transparent calibration procedures to eliminate these errors. Emphasis is placed on physical error modeling. Errors introduced describe imperfections of real systems.

3.1 Laser Scanning System

The laser scanning system measures the range and the spatial direction of the laser beam with respect to the laser coordinate system. We now consider systematic errors of these measured quantities.

3.1.1 Range Error

Various factors contribute to the range error. It is often difficult to distinguish between systematic and random errors. For simplicity we assume that there is a constant systematic range error of 5 cm for flat surfaces. This range bias Δr may considerably increase, depending on the local surface properties within the footprint area.

3.1.2 Scan Angle Errors

Another measured quantity is the instantaneous scan angle τ_i . Two errors may occur as Fig. 2 illustrates

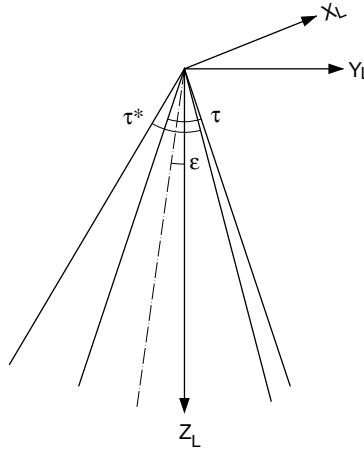


Figure 2: Illustration of scan angle errors. The ideal system is symmetric to the z -axis with a swath angle τ . The real scanning system is rotated by the index error ϵ and the scan angle is τ^* .

index error ϵ the "0" direction and the z -axis may not coincide. This amounts to adding a constant angle ϵ to τ_i .

swath angle error $\Delta\tau$ an inaccurate swath angle affects τ_i linearly.

scan plane error expresses that the scan plane and the x -axis are not perpendicular. The offset is described by the two small angular errors $\Delta\varphi$, $\Delta\kappa$.

Considering the index and scan angle error, the instantaneous scan angle becomes

$$\tau_i^* = \frac{\tau + \Delta\tau}{2} - i \frac{\tau + \Delta\tau}{n-1} + \epsilon \quad (2)$$

The difference between wrong scan angle τ^* and the correct one is the scan angle error $\Delta\tau_i$.

$$\Delta\tau_i = \tau_i^* - \tau = \epsilon + \frac{\Delta\tau}{2} - \frac{\Delta\tau}{n-1}i \quad (3)$$

The scan angle error $\Delta\tau$ causes a small rotation about the x -axis of the laser coordinate system. Additionally, the scan plane errors $\Delta\varphi$ and $\Delta\kappa$ take into account that the scan plane is not perfectly perpendicular to the x -axis. With these three small rotation angles we determine the rotation matrix $\Delta\mathbf{R}_L$ which rotates the true vector \mathbf{p}_L into a wrong position \mathbf{p}_L^* .

$$\Delta\mathbf{R}_L = \begin{vmatrix} 1 & -\Delta\kappa & \Delta\varphi \\ \Delta\kappa & 1 & -\Delta\tau_i \\ -\Delta\varphi & \Delta\tau_i & 1 \end{vmatrix} \quad (4)$$

Note that the scan angle error $\Delta\tau_i$ changes with the scan angle according to Eq. 3. The other two angles are constants. Not much is known about these errors. Let us derive an error magnitude by the following consideration. Suppose, in a laboratory calibration, the position of the laser beam in its zero position ($\tau = 0$) is measured 1 meter away from the firing point. Then, a measurement error of 0.1 mm will cause an angular error of 0.006° . With a maximum error that is three times larger, we have $\epsilon \approx 0.02^\circ$ as an estimate for the index error. Similar considerations lead to an estimated swath angle error of $\Delta\tau = 0.03^\circ$.

For the misalignment of the scanning plane we assume an error of 0.03° for the angles $\Delta\varphi$ and $\Delta\kappa$. The errorless equation is now modified as follows

$$\mathbf{p}_L^* = \Delta\mathbf{R}_L \mathbf{R}_L (\mathbf{r} + \Delta\mathbf{r}) \quad (5)$$

3.2 Mounting Errors

3.2.1 LS Mounting Errors

The transformation of the laser coordinate system to the local INS system involves the mounting rotation matrix \mathbf{R}_M and the translation vector \mathbf{t}_L . These quantities are determined after installation. It is quite obvious that the angular relationship, that is \mathbf{R}_M , cannot be determined well because it is difficult to physically represent the INS and the LS coordinate systems. Therefore, the mounting parameters must be determined more precisely during an in-flight calibration procedure.

The magnitude of the translation vector (distance between LS and INS origins) can be measured quite accurately. As outlined above, errors in the orientation are considerably larger and thus the components of the vector are not as accurate as its magnitude. In the attempt of deriving a general laser equation, we consider a systematic translation error $\Delta\mathbf{t}_L$, although it is usually neglected.

Remaining angular errors, referred to as *mounting bias*, affect the position of the footprint proportional to the flying height. The mounting errors define the rotation matrix $\Delta\mathbf{R}_M$.

There is no standard procedure for calibrating the mounting angles and information about accuracies achieved is difficult to interpret because it depends on the procedure and is often times convoluted with other system errors. After in-flight calibration we assume an error of 0.01° in all three mounting angles α , β , γ , resulting in

$$\Delta\mathbf{R}_M = \begin{vmatrix} 1 & -\Delta\gamma & \Delta\beta \\ \Delta\gamma & 1 & -\Delta\alpha \\ -\Delta\beta & \Delta\alpha & 1 \end{vmatrix} \quad (6)$$

After installation, but before in-flight calibration, the mounting errors are much larger. As indicated, this may cause component errors in the off-set vectors \mathbf{t}_L and \mathbf{t}_G .

3.2.2 GPS Mounting Errors

The problem of accurately measuring the translation vector \mathbf{t}_G between the INS coordinate system and the center the GPS antenna is related to the difficulty of establishing a physical representation of the INS coordinate system in order to determine the components of the vector. The orientation may be expressed by the mounting angles of the INS. Now, the mounting parameters of the INS are determined after installation on the ground. In contrast to the LS mounting parameters, they are hardly ever calibrated in-flight. Therefore, larger error quantities must be expected. Assuming an error of 0.3° and a distance between the origin and the GPS antenna of 5 m we have a component error of approximately 3 cm.

3.3 INS Errors

Initialization errors, misalignment, and gyro drifts are contributing to a systematic INS errors. Modeling these errors and estimating error quantities is a controversial subject. We model it here as a constant error, although there is indication that the error is time dependent and perhaps also dependent on the flight direction.

With the assumed errors in heading, pitch, and roll, the rotation matrix $\Delta\mathbf{R}_N$ is formed

$$\Delta\mathbf{R}_N = \begin{vmatrix} 1 & -\Delta h & \Delta p \\ \Delta h & 1 & -\Delta r \\ -\Delta p & \Delta r & 1 \end{vmatrix} \quad (7)$$

This matrix affects the position of the laser footprint as it rotates the vector \mathbf{p}_W in Eq. 1 into a wrong position.

3.4 Systematic GPS Error

Differential troposphere and ionosphere and multipath are among factors that cause a systematic GPS error. For a reasonably size project area we assume a constant error $\Delta\mathbf{t}_{GPS} = 10$ cm.

3.5 Error in Geoid Normal

The transformation from the local INS system to the WGS84 requires the angle between ellipsoid normal and geoid normal (local vertical). If the latter is not well known in the project area, an angular error may occur, resulting in $\Delta\mathbf{R}_G$.

Information about the geoid in the project area is available. The geoid error may vary within the project area, especially in the presence of large mass differences. Errors may reach 0.017° .

3.6 Summary

Considering the errors discussed in this section we now modify the ideal laser equation 1 as follows

$$\mathbf{p}_W^* = \mathbf{R}_W \Delta\mathbf{R}_G \mathbf{R}_G \Delta\mathbf{R}_N \mathbf{R}_N (\Delta\mathbf{R}_M \mathbf{R}_M \Delta\mathbf{R}_L \mathbf{R}_L (\mathbf{r} + \Delta\mathbf{r}) + \mathbf{t}_L + \Delta\mathbf{t}_L + \mathbf{t}_G + \Delta\mathbf{t}_G) + \mathbf{t}_{GPS} + \Delta\mathbf{t}_{GPS} + \Delta\mathbf{t}_{TB}$$

Adding the mounting translation vectors $\mathbf{t}_G + \mathbf{t}_L = \mathbf{t}_{GL}$ and their errors $\Delta\mathbf{t}_G + \Delta\mathbf{t}_L = \Delta\mathbf{t}_{GL}$ simplifies above equation. Eq. 8 is used in the following section for error analysis.

$$\mathbf{p}_W^* = \mathbf{R}_W \Delta\mathbf{R}_G \mathbf{R}_G \Delta\mathbf{R}_N \mathbf{R}_N (\Delta\mathbf{R}_M \mathbf{R}_M \Delta\mathbf{R}_L \mathbf{R}_L (\mathbf{r} + \Delta\mathbf{r}) + \mathbf{t}_{LG} + \Delta\mathbf{t}_{LG}) + \mathbf{t}_{GPS} + \Delta\mathbf{t}_{GPS} + \Delta\mathbf{t}_{TB} \quad (8)$$

Table 1 lists the systematic errors and estimated error bounds, including brief comments.

Table 1: Summary of systematic errors and error bounds.

error	typical values	comments
$\Delta \mathbf{R}_G$	0.017^0	max. deflection of vertical
$\Delta \mathbf{R}_N$	0.01^0	INS + time bias
$\Delta \mathbf{R}_M$	$0.3^0/0.01^0$	before/after in-flight calibration
$\Delta \mathbf{R}_L$	$\epsilon = 0.02^0, \Delta\tau = 0.03^3$	index error and scan angle error
$\Delta \mathbf{r}$	5–10 cm	
$\Delta \mathbf{t}_L$	3 cm	computed with $\Delta \mathbf{R}_M$
$\Delta \mathbf{t}_G$	3 cm	before in-flight calibration
$\Delta \mathbf{t}_{GPS}$	10 cm	
$\Delta \mathbf{t}_{TB}$	1 cm	if synchronization $< 10^{-4}$ sec

4 Error Analysis and Error Recovery

The general laser equation 1 determines the coordinates of a laser point assuming that all quantities are errorless. In contrast, Eq. 8 computes the laser points considering a variety of systematic errors. In order to study the effect of errors, individually or in groups, we simply take the difference

$$\mathbf{e} = \mathbf{p}_W^* - \mathbf{p}_W \quad (9)$$

We present an analysis of the scan angle error in the following section. For an analysis of the other errors, the interested reader is referred to *Schenk* (2001).

4.1 Scan Angle Errors

The scan angle errors determine $\Delta \mathbf{R}_L$. Neglecting all other errors in Eq. 8 we find

$$\mathbf{p}_W^{\Delta R_L} = \mathbf{R}_W \mathbf{R}_G (\mathbf{R}_N \mathbf{R}_M \Delta \mathbf{R}_L \mathbf{R}_L \mathbf{r} + \mathbf{t}_{LG}) + \mathbf{t}_{GPS} \quad (10)$$

To determine the influence of errors in the scan angles on the position of laser points, we subtract from above equation the errorless Eq. 1.

$$\mathbf{e}_W^{\Delta R_L} = \mathbf{R}_W \mathbf{R}_G \mathbf{R}_N \mathbf{R}_M (\Delta \mathbf{R}_L \mathbf{R}_L \mathbf{r} - \mathbf{R}_L \mathbf{r}) \quad (11)$$

Following the approach of analyzing the range error we now examine the effect of scan angle errors for a normalized scan line where all quantities are constants, except \mathbf{R}_L and the measured range r_i . Thus Eq. 11 is modified as follows

$$\mathbf{e}_i^{\Delta R_L} \approx (\Delta \mathbf{R}_L - \mathbf{I}) \mathbf{R}_L \mathbf{r} \quad (12)$$

With Eqs. 4 we obtain

$$\Delta \mathbf{R}_L \mathbf{R}_L - \mathbf{R}_L = \begin{vmatrix} 0 & \Delta\varphi \sin \tau_i - \Delta\kappa \cos \tau_i & \Delta\kappa \sin \tau_i + \Delta\varphi \cos \tau_i \\ \Delta\kappa & -\Delta\tau_i \sin \tau_i & -\Delta\tau_i \cos \tau_i \\ -\Delta\varphi & \Delta\tau_i \cos \tau_i & -\Delta\tau_i \sin \tau_i \end{vmatrix} \quad (13)$$

with τ_i the instantaneous scan angle. With $\mathbf{r} = [0, 0, r_i]^T$ (r_i = measured range), the following error components are now explicitly determined as a function of range and scan angle

Table 2: Positional errors introduced by scan angle errors.

	$\tau_i = 15^0$	$\tau_i = 0^0$	$\tau_i = -15^0$
e_x	0.66	0.52	0.38
e_y	-0.61	-0.35	-0.09
e_z	-0.16	0.00	0.02

$$\mathbf{e}^{\Delta R_L} = r_i \begin{bmatrix} (\Delta\kappa \sin \tau_i + \Delta\varphi \cos \tau_i) \\ -\Delta\tau_i \cos \tau_i \\ -\Delta\tau_i \sin \tau_i \end{bmatrix} \quad (14)$$

In case of a horizontal surface the measured range can be expressed as a function of the flying height H and the instantaneous scan angle τ_i . With $r_i = H / \cos \tau_i$, above equation becomes

$$\mathbf{e}^{\Delta R_L} = H \begin{bmatrix} (\Delta\kappa \tan \tau_i + \Delta\varphi) \\ -\Delta\tau_i \\ -\Delta\tau_i \tan \tau_i \end{bmatrix} \quad (15)$$

Assume a swath angle $\tau = 30^0$, flying height $H = 1000$ m, a swath angle error $\Delta\tau = 0.03^0$, an index error $\epsilon = 0.02^0$, and a scanning plane that is not perpendicular to the x -axis by $\Delta\varphi = \Delta\kappa = 0.03^0$. With Eqs. 3, 15, the error components are computed for $t_i = 15^0, 0^0, -15^0$. The values are listed in Table 2.

From analyzing Eq. 15 and the numbers listed in Table 2 we realize that scan angle errors substantially affect the position of laser points. The x - and y -components are non-linear, resulting in a distorted laser surface. The error component in x is independent of the scan angle errors $\Delta\tau$ and ϵ ; it is caused by a scanning plane that is not perpendicular to the x -axis of the laser coordinate system.

The elevation errors are different at the swath ends. The difference Δz can be determined from Eq. 15

$$\Delta z = -\Delta\tau_{\tau/2} \tan(\tau/2) - (-\Delta\tau_{-\tau/2} \tan(-\tau/2)) \quad (16)$$

The elevation difference causes a horizontal plane to be tilted. The tilt angle, ρ , is

$$\rho = \frac{\Delta z}{2 \cdot H \tan(\tau/2)} = \epsilon \quad (17)$$

A horizontal plane will be tilted by an angle equal the index error ϵ (misalignment of the zero position and the z -axis). This result can be verified with the numbers listed in the third row of Table 2. The swath width in the example used is 536 m.

Fig. 3 illustrates the effect of the scan angle error $\Delta\tau_i$ which is caused by the index error ϵ and a wrong swath angle $\tau^* = \tau + \Delta\tau$.

For non-horizontal surfaces, the range r_i in Eq. 14 can be computed from the following equation

$$r_i = H \frac{\cos \delta}{\cos(\delta + \tau_i)} \quad (18)$$

with δ the slope angle and H the flying height.

4.2 Recovering Systematic Errors

In this section we determine the systematic errors directly. As shown in detail in *Schenk* (2001), some of the errors can be recovered individually while others are not separable and

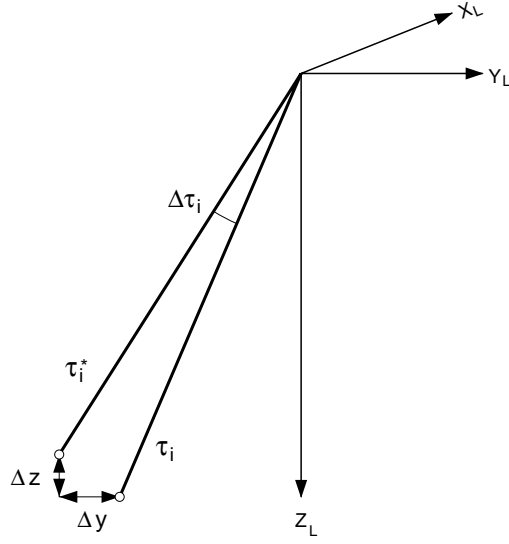


Figure 3: Influence of a scan error $\Delta\tau_i$ on the y - and z -coordinates of laser points.

must be determined as groups. The direct determination provides insight into the correlation of systematic errors. The results achieved in this section let us predict the success or failure to determine the systematic errors in a simultaneous adjustment. Moreover, it will lay the foundation for understanding specific flight patterns and calibration test sites to optimally recover the calibration parameters.

As an example we show now how a constant INS error can be determined directly. Analyzing Eq. 8 reveals that all planimetric errors, $[e_x, e_y]^T$, are multiplied by \mathbf{R}_N , except the INS error $\Delta\mathbf{R}_N$ which is assumed to be a constant for the project area. This has a most interesting consequence for meandering flight patterns. The planimetric components of the INS error will remain constant, while all the other planimetric error components have opposite sign and cancel! Thus, analyzing the error components e_x, e_y allows the determination of the INS error.

Roll, pitch, and heading errors of the INS cause small planimetric displacements. From these displacements one can determine the three angular errors directly. Fig. 4(a) depicts the roll error $\Delta\omega$. It causes a y -displacement that can be used to recover $\Delta\omega$. Similarly, the pitch error $\Delta\varphi$ causes an x -displacement. Fig. 4(c) shows the effect of the heading error $\Delta\kappa$. Here, we need the x -coordinate differences at the swath ends to recover the error. The following equations are adequate approximations for recovering the angular INS errors (in radians):

$$\Delta\omega = \frac{C_y^F - C_y^B}{H} \quad (19)$$

$$\Delta\varphi = \frac{C_x^F - C_x^B}{H} \quad (20)$$

$$\Delta\kappa = \frac{(L_x^F - R_x^F) - (R_x^B + L_x^B)}{S} \quad (21)$$

with L and R the left and right swath end, and C the vertical laser position. Superindices F and B indicate forward and backward flight direction. S is the swath width.

5 Concluding Remarks

The error modeling presented in this paper is based on an assessment of the deficiencies of a real system and differences between ideal and real environment (e.g. atmosphere). The error

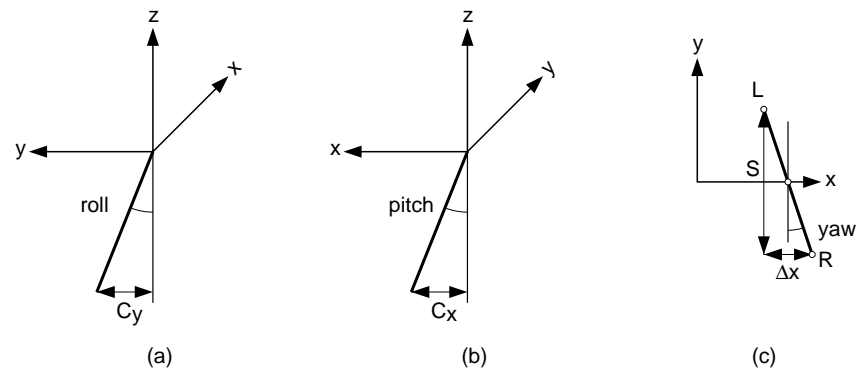


Figure 4: Recovering INS errors from determining the displacements they cause. In (a), the roll error $\Delta\omega$ causes the displacement C_y that is perpendicular to the flight direction. In (b), the pitch error $\Delta\varphi$ causes the C_x displacement in flight direction. Finally, the heading error $\Delta\kappa$ in (c) causes x -displacements at the swath ends L and R .

model permits to predict the errors of the laser points. Comparing simulated errors with observed errors in real data sets allows plausible explanations if the errors are modeled on the basis of system imperfections.

The systematic errors examined distort the position of laser points considerably. Planimetric distortions usually exceed elevation errors. The errors are a function of the exterior orientation of the aircraft, the instantaneous scan angle, and the topography of the surface. These factors change from point to point and so do the error vectors. As a consequence, the error vectors are extremely heterogeneous in terms of their orientation and magnitude. This makes it impossible to correct the errors from analyzing individual error vectors without an error model.

The compelling conclusion from the error analysis is that for calibration purposes and error removal it is imperative to consider how laser points are computed from original measurements. It does not suffice to work with the point coordinates only. The answer to the determination and subsequent correction of systematic errors cannot be found in the data—a model that takes system imperfections into account is needed.

References

- Crombaghs, M.J.E., R. Brügelmann, and E.J. de Min, (2000). On the adjustment of overlapping strips of laseraltimeter height data. In *International Archives of Photogrammetry and Remote Sensing*, 33(B3/1), 230–237.
- Gardner, C.S. (1992). Ranging Performance of Satellite Laser Altimeters. *IEEE Transactions on Geoscience and remote Sensing*, 30(5), 1061–1072.
- Huising, E.J. and L.M. Gomes Pereira, (1998). Errors and accuracy estimates of laser data acquired by various laser scanning systems for topographic applications. *ISPRS Journal of Photogrammetry & Remote Sensing*, 53(1998),245–261.
- Lemmens, M. (1997). Accurate height information from airborne laser altimetry. *Proc. IGARS '97*, 222–243.
- Lindenberger, J. (1993). *Laser-Profilmessungen zur topographischen Geländeaufnahme*. DGK, Nr. 400, 131 pages.
- Schenk, T. (2001). *Modeling and Analyzing Systematic Errors in Airborne Laser Scanners*. Technical Notes in Photogrammetry, No. 19, Dept. of Civil and Environmental Eng., OSU, 42 p.

DERIVATION OF DIGITAL TERRAIN MODELS IN THE SCOP++ ENVIRONMENT

Norbert PFEIFER, Philipp STADLER and Christian BRIESE

Institute of Photogrammetry and Remote Sensing
Vienna University of Technology
np@ipf.tuwien.ac.at

KEY WORDS: DTM, laser scanning, filtering, classification, SCOP

ABSTRACT

Airborne laser scanning is widely used for the derivation of terrain information in wooded or open areas but also for the production of building models in cities. For this, the generation of a digital terrain model (DTM) is also required. In this paper the filtering and classification of laser scanner data with iterative robust linear prediction in a hierarchical fashion using data pyramids is described. The coarse-to-fine approach is advantageous because it strengthens the robustness of the method and makes it faster. The results for test data sets of the OEEPE are presented.

1 INTRODUCTION

Airborne laser scanning has become a widely used technique for the derivation of topographic data. The high degree of automation in both, capturing the data and processing the data, contributed to its fast spread. Currently, the main application for laser scanner data is the production of digital terrain models (DTM), whereas the fully automatic derivation of building models ((Wang and Schenk, 2000), (Morgan and Tempfli, 2000), (Brenner, 2000)) is not as operational yet. The automatic derivation of tree height and extraction of other forest stand parameters is investigated (Kraus and Rieger, 1999), as well as the automatic derivation of break lines in the laser data ((Brügelmann, 2000), (Wild and Krzystek, 1996)).

This paper will focus on the filtering of laser scanner data for obtaining elevation information in wooded as well as in built-up areas. The DTM is necessary for all the applications described in the previous paragraph. In the next section a short presentation of the algorithm developed at the Institute of Photogrammetry and Remote Sensing of the Vienna University of Technology (I.P.F.) will be given, especially the extension to the hierarchical approach will be treated. The following section will treat the user interface for the filtering program. The OEEPE test data are investigated in section 4. We are mainly concerned with the filtering and the accuracy determination.

2 ALGORITHM

The algorithm for filtering the laser scanner data was originally designed for laser data in wooded areas. Altering the values of some parameters and the application of a hierarchical approach made it possible to apply it also to city areas. In order to describe these extensions completely, a brief review of the algorithm will be given first. For a comprehensive description see (Kraus and Pfeifer, 1998) and (Pfeifer et al., 1999). Other filter algorithms based on mathematical morphology are described e.g. in (Vosselman, 2000), different approaches can be found in (Hansen and Vögtle, 1999) or (Axelsson, 2000). Unfortunately, the term *to filter* can have various meanings. On one hand it can mean the filtering (smoothing) of random measurement errors, on the other hand it stands for the filtering (elimination) of gross errors, which is also a classification. Unless stated otherwise we will always use the term in its second meaning.

In our algorithm — the iterative robust interpolation — a rough approximation of the surface is computed first. Next, the residuals, i.e. the oriented distances from the surface to the measured points, are computed. Each (z -)measurement is given a weight according to its distance value, which is the parameter of a *weight function*. The surface is then recomputed under the consideration of the weights. A point with a high weight will attract the surface, resulting in a small residual at this point, whereas a point that has been assigned a low weight will have little influence on the run of the surface. During these iterations a classification is performed, too. If an oriented distance is above or below certain values, the point is classified as off-terrain point and eliminated completely from this surface interpolation. This process of weight iteration is perpetuated until all gross errors are eliminated (a stable situation) or a maximum number of iterations is reached.

There are two important entities in this algorithm. On one hand, the stochastic model, which is defined by the weight function, on the other hand, the functional model, which describes the way the surface is interpolated. Obviously, the

weight function must assign high values (close to 1) to ground points, which are below or on the averaging surface, and low values (weights close to 0) to the vegetation points which are above (or on) the averaging surface. The standard weight function of robust adjustment (used for example in bundle block triangulation) can be adapted to suit the needs for the interpolation and classification of laser scanner data. The function we use is not symmetrical, allowing a sharper decline for values above its origin (residuals belonging to vegetation points), and a slower decline — or no decline at all — for the ground point residuals. The graph of the weight function can be seen in fig. 1. Furthermore, the weight function does not need to be centered on the zero-point of the real axis. It can be shifted to the left (into the negative) for the interpolation of laser scanner data. What is more, the shift of the origin can be determined automatically, depending on the given data itself.

The interpolation method itself (functional model) is restricted to those methods which can consider the stochastic model described in the previous paragraph. This is possible for moving least squares ((Lancaster and Salkauskas, 1986)), kriging and linear prediction. These methods have in common that the surface is described as a sum of basis functions which are centered on the data points. However, the basis functions could also be arranged over a regular grid as e.g. in B-spline surface approximation (used for laser scanner data in (Kilian et al., 1996)). The basis functions themselves influence the rigidity of the surface. We use linear prediction which is very similar to kriging ((Kraus, 1998)). The covariance function (i.e. the basis function, corresponding to the variogram of kriging) is determined automatically, depending on the data itself.

What has been described so far is the core of the algorithm. Classification and DTM generation are performed in one step, there is no assumption that the terrain is horizontal. It is applied patch wise to the data, which results in an adaptive setting of the shift of the origin of the weight function. Furthermore, the basis functions are determined for each patch separately, too. However, in its present implementation the algorithm relies on a ‘good mixture’ of ground and off-terrain (vegetation) points, which can also be seen as a high frequency of change from ground to vegetation points. This is necessary for a reliable determination of the shift value for the origin of the weight function. What can be done if this high frequency is not given? One method is to extend the way the shift value is computed, the other is to provide the input data (points) in a suitable form. Because it is comparatively easy to establish these conditions (the suitable form) we chose to follow the second method, which will be explained in the following section.

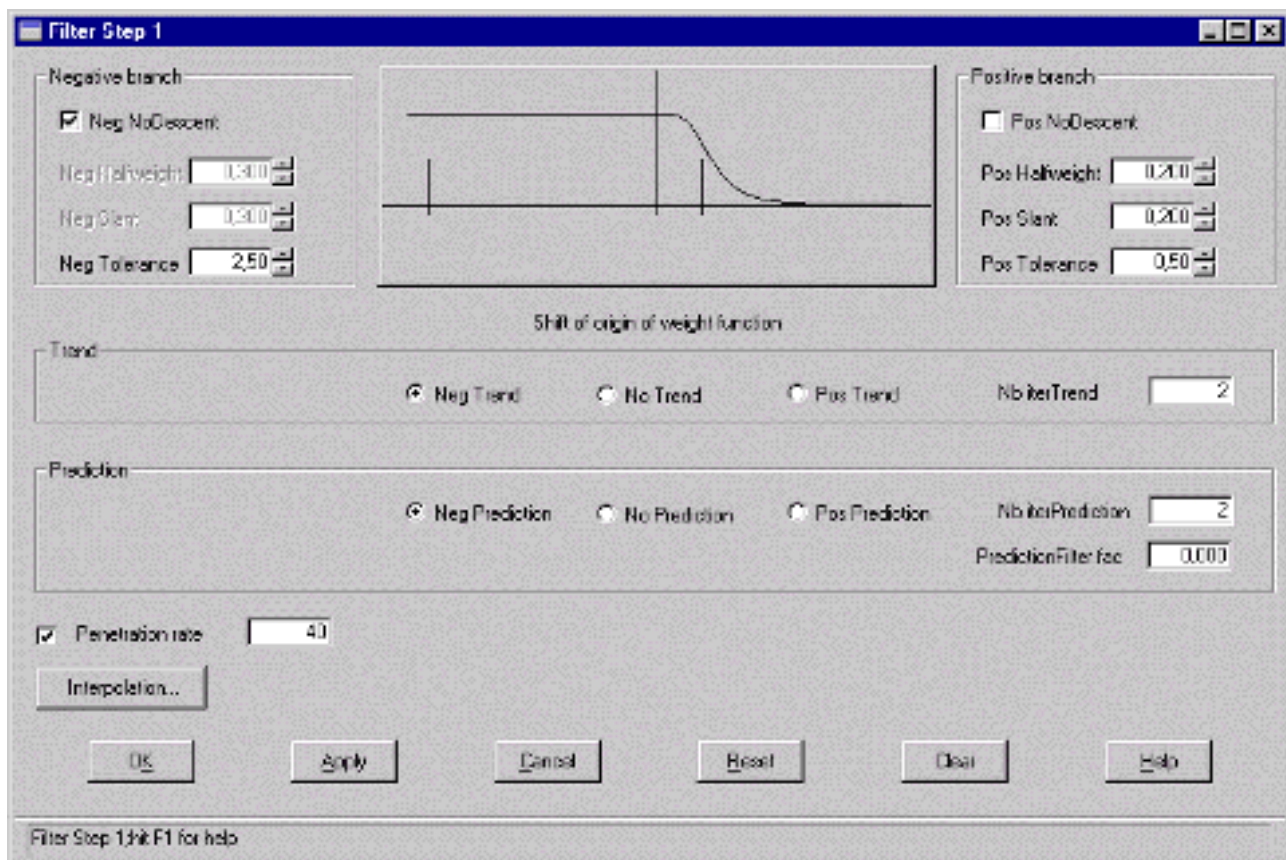


Figure 1: User interface for the determination of the filter parameters. In the upper part the parameters of the weight function are defined, whereas the lower part is for the iteration control. Below the text ‘Shift of origin of weight function’, the user can decide whether to search for the shift value in the negative, the positive, or not at all. This can be done for the trend (plane) and the predicted surface.

2.1 Hierarchical approach

Our approach is comparable to a hierarchical setup using image pyramids, in our case data pyramids. The structure of these pyramids is regular (as in image processing) and typically two or three levels are sufficient. However, in comparison to image analysis, the reduction function operates on point data, not on pixels. (If the laser scanner data is provided as a digital geo-coded image where the grey values represent the terrain heights, the pyramids would indeed be image pyramids.) The method proceeds as follows:

1. Create the data sets with the lower resolutions,
2. filter the data and generate a DTM,
3. compare the DTM to the data of higher resolution and take points within a certain interval.

This process (steps 2 and 3) are repeated for each level, schematically it is shown in fig. 2 for two levels (level 0 and 1). Though this procedure can be applied to any data set of laser scanner data, or other data with gross errors, its advantages become important for dense data sets (0.5 point/m² or more). The method speeds up the filter process, enforces the elimination of houses and dense vegetation and makes the process more robust.

There are many possibilities to generate a coarser resolution (higher levels) of the given data (lower level, level 0 is the original data), the most straightforward techniques are to place a square grid (or any other tessellation) over the data and compute for each cell one point (regular pyramid). There are different methods to compute this point which are applicable for filtering of laser scanner data:

- Take the mean point in each cell.
- Take the lowest point in each cell.
- Take the point closest to the center in each cell.

Only the first of these reduction functions is linear (fast to compute), whereas the others are nonlinear. More complex methods can be performed by analyzing a histogram of the heights in each cell, but the methods described above are sufficient for our needs. Even more simple methods can be used. One possibility is to take every n-th point, which — under the pre-condition that the points have not been sorted after the measurement — maintains the ratios of point densities, though these data pyramids are not regular anymore. However, this method and the third method of the list, do not change the penetration rate of the data set. As the point density itself is diminished in this step we call it a *thin out*.

The second method speeds up the filtering, but there is the danger of taking a point which is a large (or small!) negative blunder. The third method provides a more regular structure of the generated point set. The choice of method can also be made depending on the kind of data (penetration rate, city or wooded area, ...). A thin out of the data has two advantages:

1. The regular structure of laser scanner data in built up areas (long sequences of points on the ground, on the roof, resp.) is broken apart.
2. The classification and filtering is accelerated, because a smaller data set is handled.

With the coarser data set a filtering is performed and a DTM is generated. Of course, embankments, break lines and other features are represented less distinctively than in the original data, but this is due to the coarser level of data, not due to the filtering. Therefore, for performing the filtering on the next lower level, the original point data (or the data of the corresponding pyramid level) and the DTM of the coarser level have to be combined to generate the data for the lower (finer) level. The original points and their distances to the DTM at the current resolution are analyzed. If they are within a certain interval they are accepted, otherwise they are rejected (sorted out). Thus, this step is called *sort out*. For laser scanner data the lower bound of this interval is negative (e.g. -1m) and the upper bound is positive (e.g. 1m). With this data set the next filter step can be performed. The choice of the intervals is not as critical as one might expect first, which is due to the filter step that is performed afterwards. Some vegetation points are included in the data set because they are relatively low to the ground, but they can be filtered in the next step.

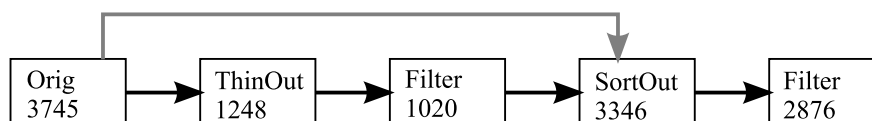


Figure 2: Schema of the hierarchical approach. The numbers below the names of the steps (taken from the Vaihingen data) represent: number of given points (Orig), reduced point number (ThinOut), ground points after filtering (Filter), number of points within a certain distance to the DTM (SortOut). The original data is used twice: first for the Thin Out, and later (after Filter, grey line) for the Sort Out.

3 LASER SCANNING WITHIN SCOP++

The algorithm described above is included in the program package SCOP (SCOP-WWW, 2001) for the derivation, application and presentation of DTMs. This set of programs is in use and applied in different environments (public authorities, universities, private companies). With the transition to SCOP++ (Dorffner et al., 1999) many new features have been introduced, amongst others:

- a graphical user interface (GUI) including project management,
- support for different data formats (Winput, DXF, ArcInfo, TIFF, JPEG, PDF, ...),
- mixing of raster graphics (also of different resolutions and areas covered).

The extension for laser scanner data filtering will be available in the Extended Data Acquisition package of SCOP++. Fig. 3 shows the main window with the data of the eastern part of the Vaihingen example during an iteration step at the very beginning.

In the GUI-version of the laser data filtering, the user can, after project definition and data import, decide which strategy to use for the classification and filtering of the laser scanner measurements ('Strategy window'). These strategies distinguish themselves in the order of the particular steps ('thin out', application of filter algorithm, 'sort out') and the values for the

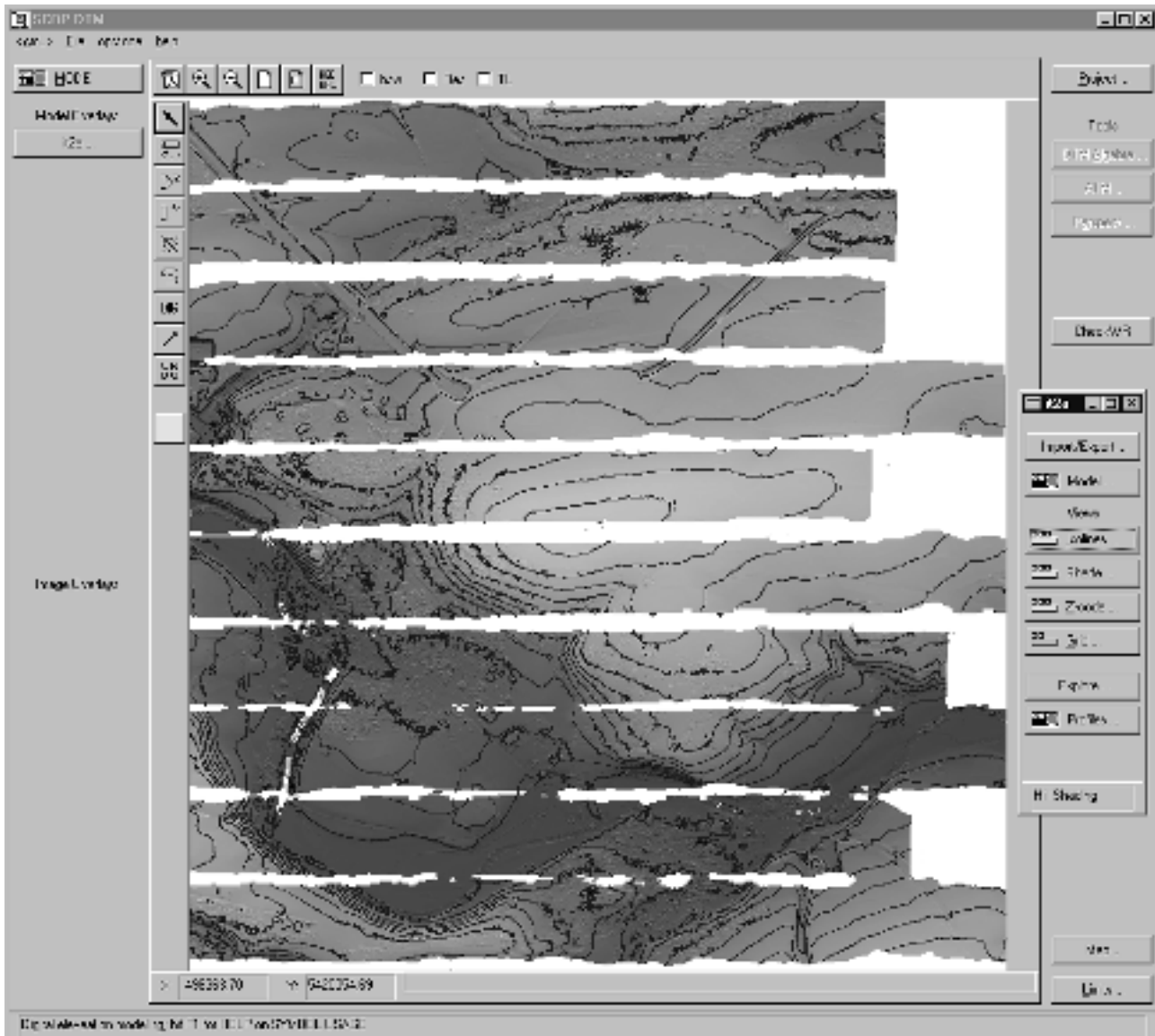


Figure 3: Main graphics window, showing a surface model in a combination of shading (from the north) and color coding (black to white) and the contour lines.

parameters for these steps. However, the user can also create and apply a new strategy and save it for later re-use. Different strategies are predefined for laser scanner data in city areas and wooded areas, but of course this list can be enlarged. As there is no perfect all-purpose filter algorithm, the purpose of the DTM could play a role here, too. Depending on the application, it may be worse to miss small dikes (e.g. flood simulation) whereas for other applications the correct representation of trenches may be more important.

In fig. 1 the window for the filter parameters is shown. In the upper middle is the graph of the weight function, to its left and right, are the settings for the negative and positive branch. Below the weight function the iteration control is situated. The first few numbers of iterations are normally performed with the trend (a tilted plane), which describes the surface sufficiently detailed, if the patches are small. Otherwise the number of iterations with the trend should be set to zero. The next iterations are performed with the predicted surface. For both kinds of iterations the shift of the origin of the weight function can be influenced. As mentioned above, it is set automatically, but the user can decide whether it should be searched in the negative, the positive, or not at all. A rough estimate of the penetration rate can be used to search for this shift value, too. The other parameters of the elevation model (accuracy of the points, size of patches, ...) can be defined under the 'Interpolation' button, which opens a window. The parameters in this window are necessary for all terrain models, not only for those derived with the iterative robust filtering.

4 OEEPE TEST

The Stuttgart data set and the Vaihingen data set provided by Fotonor have been used for the OEEPE laser scanning test. The data are in UTM32, based on the WGS84 co-ordinate system. First and last pulse and the intensities have been recorded simultaneously with an Optech laser scanner. The results for the TopoSys data set over Stuttgart (also available within the OEEPE test), captured with the TopoSys I laser scanner, are not included in this paper. Instead, the results of a vertical accuracy determination for this scanner in Vienna will be presented briefly.

The data sets have been processed with the hierarchical approach of the filter algorithm described above. Default values have been used for the parameters of the filter and no manual editing was performed. Tuning the parameters might have improved the result slightly but at the expense of more time spent. The processing of the data will be described in more detail for the Vaihingen data set, the filter results will be presented for both data sets. The vertical accuracy is determined with ground points for Vaihingen. For the Vaihingen and Stuttgart data sets small studies and preliminary results on the first-and-last pulse data and the intensities will be presented.

4.1 Vaihingen

First, all strips were combined to one file. We used the Fotonor-'all'-data set, which contains the last recorded echo (pulse), because our aim was to filter the vegetation and houses and obtain a ground model. For practical reasons we split the data of the Vaihingen example in an eastern and a western part along the north-south line with easting 3495950m. Under our present working conditions (esp. computing environment) we process data sets of up to 4 mio. points as one unit. The eastern part will be treated in more detail. The size of this area is 25.27km². As it can be seen in the upper part of fig. 4 (a small part of the whole area, which can be seen in fig. 3) there are houses, vegetation and negative gross errors which have to be eliminated from the data set. The average point density is 0.23 points/m².

4.1.1 Data processing The relevant parameters for the filtering (including the hierarchical setup) can be found in tab. 1. The process is also shown in fig. 2. The first step is to thin out the data. As the data is sufficiently isotropically distributed every third point was taken to generate the coarser representation of the original point cloud. The minimum and maximum height in this area are 225.8m, 878.8m, respectively, but these elevations belong to gross error measurements.

The purpose of the second iteration (It.=2) is to eliminate negative blunders. Of course, also vegetation points above the terrain are eliminated during this step. After the first 5 iterations (maximum number of iterations at level 1, representing

It.	surface	pts. 10 ³	patch	tol+	tol-	HW+	HW-	pen.	off-terrain.
1	plane	1248	40x40m ²	3m	—	20cm	-∞	50%	5.2%
2	plane	1184	15x15m ²	2.5m	-2.5m	20cm	-∞	50%	2.9%
3-5	pred.	1149	45x45m ²	0.3m	-3m	20cm	-∞	80%	11.2%
'sort out'		3745	—	2m	-2m				10.6%
6-8	pred.	3346	12x12m ²	0.1m	-0.3m	20cm	-∞	85%	13.1%

Table 1: Parameters for the filtering of the Vaihingen example. The meaning of the columns is: number of iteration (It. 1-5 $\hat{=}$ level 1); type of computed surface (pred. $\hat{=}$ linear prediction); number of points on input; patch size; upper/lower bound for classification; positive/negative half-width value of weight function; penetration rate parameter; portion of points classified as off-terrain points.

the first filter step in fig. 2), the 'sort out' is performed. The interval values of $\pm 2\text{m}$ may seem very high, but the purpose of the previous iterations is mainly to eliminate the buildings and contiguous clusters of vegetation points without ground points in between. Additionally, these values ensure, that all points belonging to an embankment are in the new data set. In the following, a maximum number of 3 iteration steps (at level 0) are performed to eliminate the near ground vegetation and remaining building points.

In fig. 3 the elevation model after the second iteration (It.=2) is shown. A substantial part of the houses has already been eliminated. The wrinkles of the contour lines indicate, that the vegetation is not eliminated completely at this state. In fig. 4 a comparison between the original data and the filtered data after the last iteration step can be seen. Only a small part of the size of $0,82\text{km}^2$ of the complete eastern part of the Vaihingen data set is shown here. No manual intervention was performed during the iteration, the parameters used are default parameters and have not been adapted to this special data set, no manual deletion or inclusion of points was performed.

4.1.2 Result of Filtering The patches for the DTM computation were smaller for the original data. Thus, the void spaces in the upper half of the fig. 4 follow the strip more closely. The negative blunders have been eliminated completely. Also the houses are eliminated, but there remains a kind of ridge east of the middle. This appears to be a large but low building which could not be eliminated completely. The embankments have been preserved, though one of them (in the western part, running north-west in the lower strip) lost some of its sharpness. The vegetation has been eliminated completely. The remaining building could have been removed with a different set of parameters, but this would have eliminated more of the embankments.

The western part of this example has roughly the same dimensions as the eastern part and has been processed in exactly the same manner. The results are similar (see fig. 5). Negative blunders occurred in the western half as well, though none of them is shown in the figure.

As it can be seen, not all the houses have been eliminated completely. This is a consequence of the parameters and

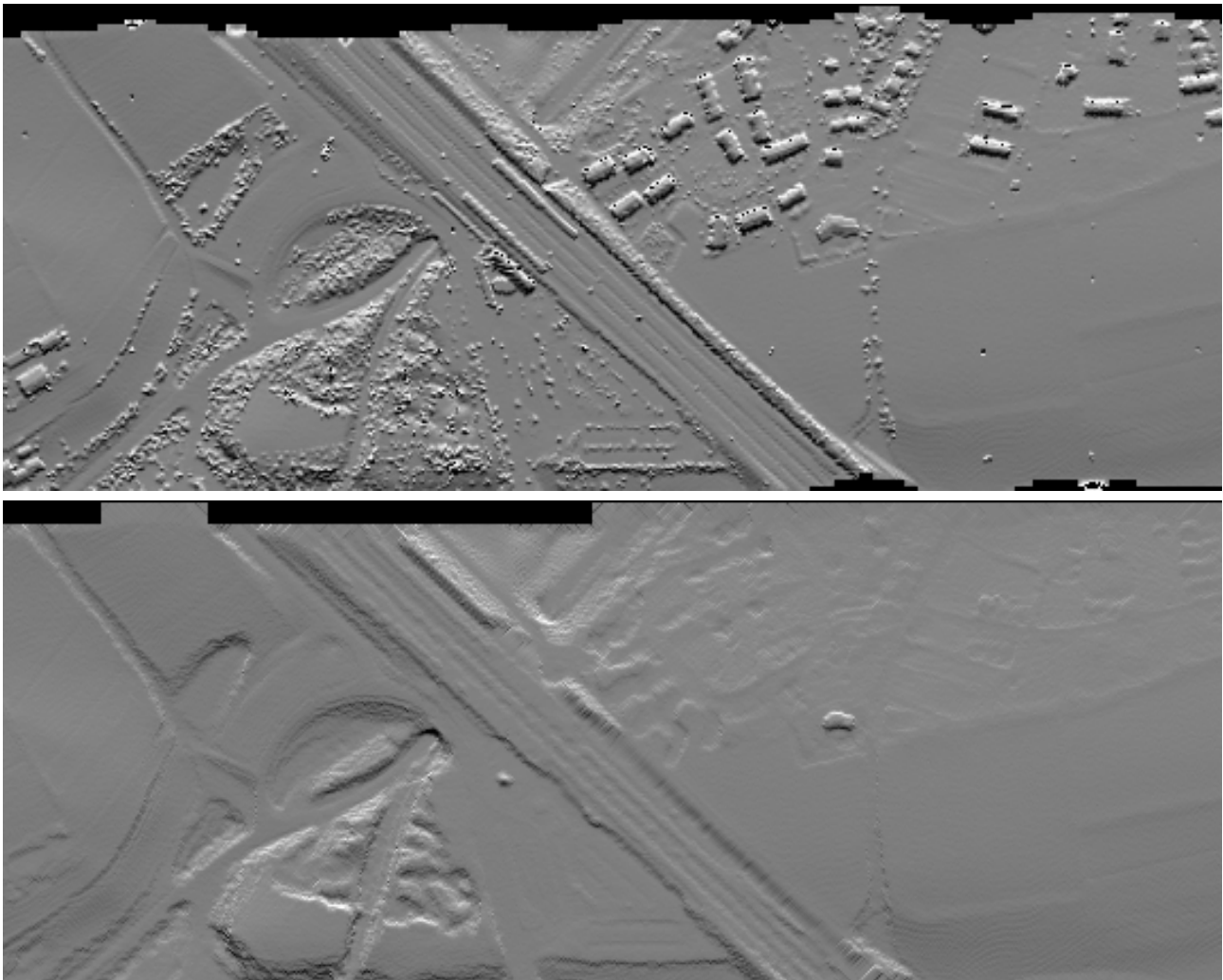


Figure 4: Vaihingen, original vs. filtered data in a shading, area: [(3496480, 5421370), (3497620, 5421806)]

iteration settings, which are set for the removal of vegetation. A portion of the data holes have been closed, but of course, the terrain height in these areas is questionable, although the terrain height is interpolated — more or less — linearly between the two sides. The diagonal pattern in the eastern part of the closed holes is a consequence of the (imperfect) interpolation (over point-less terrain) applied there.¹ In the selected area shown, north-west of the middle (at co-ordinates 3493791, 5419797), a structure can be seen which is presumably a natural, vegetated bump. It has been made smaller during the filtering, but equally it could have been a manmade structure. Again, the purpose the DTM is derived for, could solve the question whether to keep such structures or not. The setting of parameters will be affected by such a predetermination, too.

4.1.3 Accuracy determination For the area of Vaihingen the Institut for Photogrammetry at Stuttgart University measured ground points with a Leica Wild GPS System 200 using a reference and a rover station. All together 4 areas with different terrain characteristics have been measured. Unfortunately, in 3 of these areas not all the points could be used, because of the lack of ground coverage from the laser scanner measurements. Furthermore, the Insitute for Photogrammetry observed a systematic vertical shift in the laser scanner data and determined it to be 0.35m. This shift was taken into account.

The vertical accuracies have been determined by means of an elevation model. The vertical distances from the check points to the elevation models were computed. For 3 of the 4 areas we used the terrain model derived as described in the previous subsections. However, as the filter algorithm could have eroded the railway ramps we computed an elevation

¹For an easier interpretation of such artifacts we suggest the use of a quality layer (supplied with the DTM). It shows the reliability (average filter values, distance to nearest given point, ...) of the interpolation for a certain area.

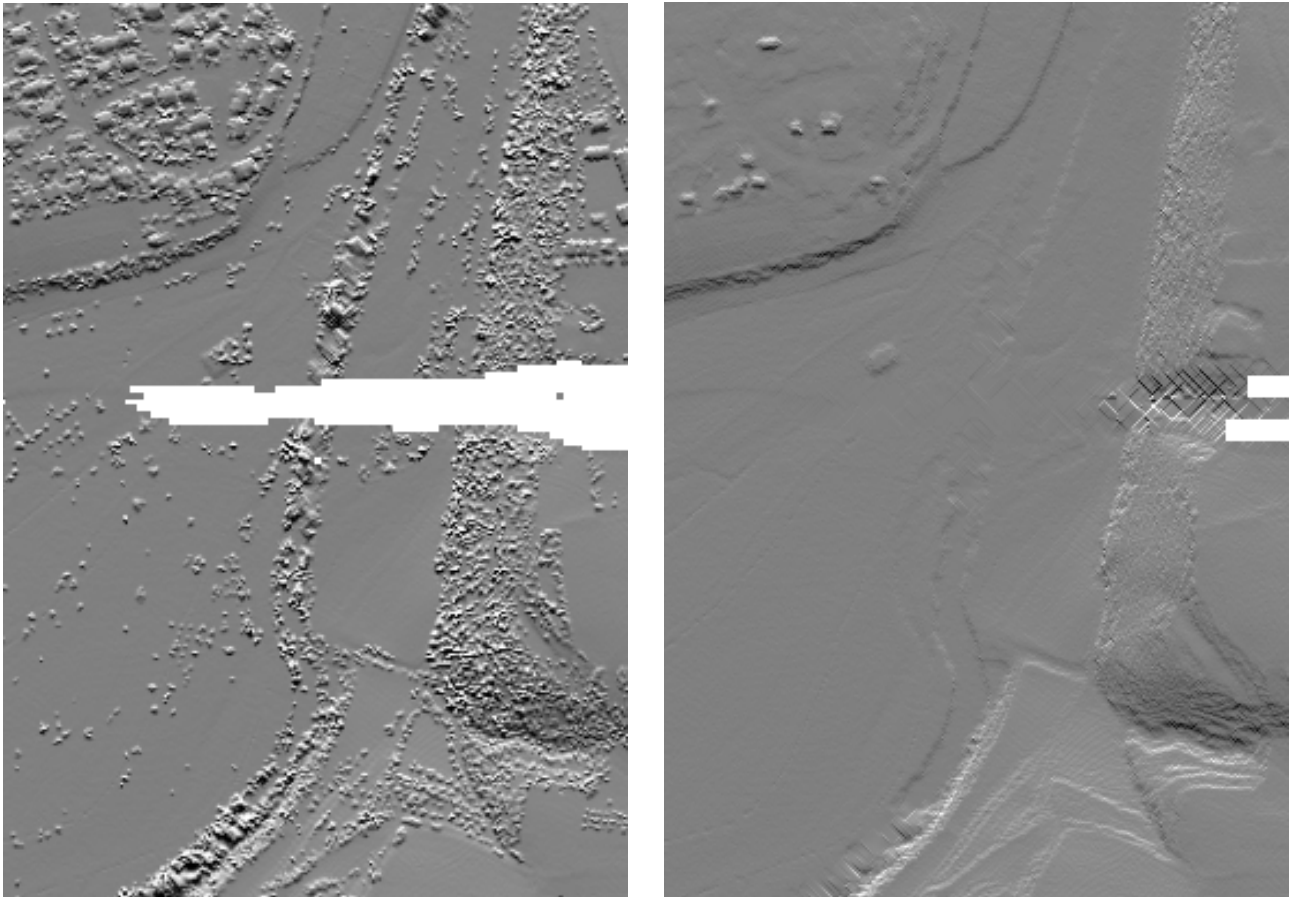


Figure 5: Original vs. filtered data in a shading, area: [(3493590, 5419300), (3494160, 5420120)], extension: 0.47km²

area	r.m.s.	mean	max	point num.	characteristics
Grassland	0.11	+0.08	0.73	1368	different slope, smooth
Sport ground Vaihingen	0.08	+0.06	0.30	77	flat
Sport ground Illingen	0.08	+0.07	0.17	102	flat
Railway station	0.48	+0.39	1.46	210	railway ramp

Table 2: Accuracies for the test areas in Vaihingen. The last line has to be inspected carefully (see text). The unit for the accuracies is meter.

model without filtering for this area. The vertical accuracies (under the assumption of error free check points) are shown in table 2. For the first 3 areas there is still a systematic shift of about 7cm. This shows that the accuracy of a single laser measurement is even higher, but uncertainties in the determination of the transformation parameters and the modelling of the flight path and orientation will always remain. The area ‘Grassland’, which is not flat has a lower accuracy than the 2 flat sport grounds. This is an indication for a (systematic) horizontal shift. For the first 3 areas the r.m.s. error is 10.7cm. The errors for the railway ramp are higher. This is a consequence of the structure of the elevation model we used. As described above, we use a grid based model with a grid point distance of 1m, which is less than the point distance in the laser scanner data set. Because of the grid structure of the elevation model and because of the random point sampling of the laser scanner the edges are not represented correctly, break lines would be necessary for this. However, visual inspection of the co-ordinate values of the laser points and the check points showed, that the accuracies are similar to those of the other three examples. This means, that the accuracy of the laser scanner data for the railway ramp is better than what the table indicates on first sight.

4.1.4 First and last pulse data The question arises, whether the first and last pulse data can be used to simplify or improve the filter process in wooded areas. Therefore, 6 rectangular areas of the Vaihingen data set were selected, all lying completely in wooded areas. The areas all together have an extension of 0.58km². The characteristics can be seen in the left part of tab. 3. It is notable that the point density of 0.20 points/m² over the wooded areas is smaller than the average point density, which is 0.23 points/m².

First, the distances between the first and the last reflected pulse for each measurement were computed. When we speak of measurement we mean the position and intensity of the first and the last pulse (8 values). A histogram of the distribution of these distances can be seen in fig. 6, left side. For 19.7% the distances are smaller than 1m. These points are not necessarily ground points. It is also possible that the laser beam is reflected twice in the canopy or in medium layers of the trees. As it can be seen, the pulses are either very close to each other (within 1m), or more than 4m apart. The first–last distances go up to 40m, which also includes a few gross errors. The points were separated in two groups, the ones which are close to each other and the ones which have a higher distance (The threshold was 4m, but it could have been 1m as well, as it can be seen in the histogram.) These 2 groups have been compared to the ground model which was derived as described in section 4.1.1. For the time being, we assumed that the filtering worked 100% correct. Additionally, it can be assumed, that if the filtering is not completely correct, the errors occur only locally, for specific positions like peaks or steep descents. Thus, the errors — if any — induced by filtering errors are small in number.

The distances from the last pulse points to the ground model can be seen in the right part of fig. 6. The last pulse points range from 5m below the terrain to 36m above the terrain. For the measurements where the first and the last pulse are

area	num.pt.	size	pt/m ²	low distance				high distance			
				num.	r.m.s.	mean	max	num.	r.m.s.	mean	max
1A	3135	0.015	0.207	617	6.97	3.89	25.67	2518	2.10	1.10	16.10
1B	12072	0.061	0.199	1058	4.35	1.26	32.70	11014	2.17	0.52	27.81
3	52152	0.251	0.208	12217	7.99	4.14	35.90	39935	3.02	0.93	30.76
4	12906	0.080	0.187	2468	8.14	3.97	30.83	12438	2.22	0.81	25.57
5	10601	0.049	0.214	2451	3.82	1.77	33.17	8150	2.58	0.87	26.85
10	25999	0.129	0.202	4676	4.77	1.75	28.92	21323	2.07	0.71	24.44
overall	118865	0.585	0.204	23487	6.95	3.26	—	95378	2.58	0.82	—

Table 3: Distances of last pulse points over wooded terrain. In the left part the number of points in each sample, the area size (km²) and the density are shown. The middle part shows the distance to the terrain for those points, where the first and the last pulse are very similar. The same is shown for those points with large distances between first and last pulse in the right part. All the error measures (r.m.s., mean and max error) are in unit m.

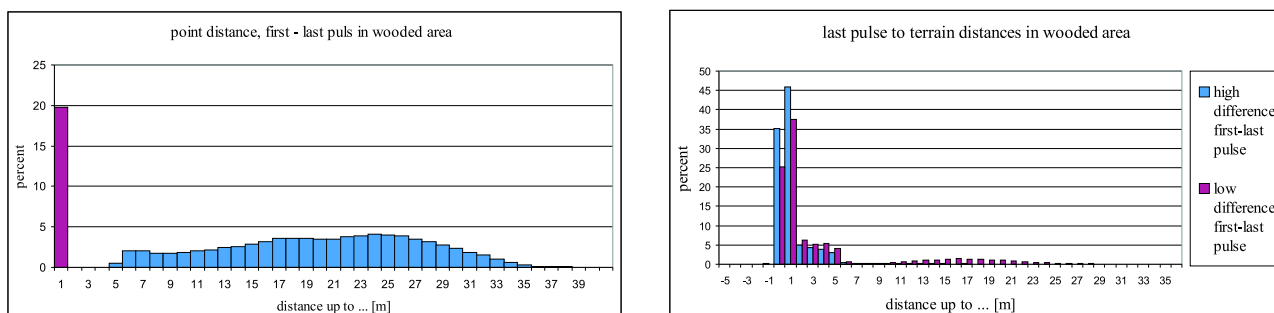


Figure 6: Laser scanner data over wooded terrain. *Left*: histogram of first–last pulse distances. *Right*: histogram of last pulse to terrain distances

close to each other, 62.8% of the last pulse points lie within $\pm 1\text{m}$ terrain distance, whereas for the points which have a higher difference between first and last pulse this number is 81.0%. Furthermore, 16% of the last pulse points lie between 10m and 30m above the terrain.

The penetration rate for this data set is about 77% (points within $\pm 1\text{m}$ terrain distance). The chances that a last pulse point is a ground point are higher, if the distance between the first and the last pulse point is large, than if the distance is small. However, the differences are not too big. Furthermore, no strong correlation between the intensities over the forested areas and the distance from the last pulse to the filtered terrain could be proven. (The first intensity is usually low (dark), whereas the second is larger (bright).) The development and application of filter algorithms will stay important.

4.2 Stuttgart

As mentioned above, the Fotonor data set of Stuttgart is given in UTM32, based on WGS84. The point density for this data is higher than for Vaihingen, it is 0.81 points/m^2 . The original data can be seen in the upper part of fig. 7.

4.2.1 Processing and Filtering the data For Stuttgart, too, we used the Fotonor data set. Again the last pulse data was used in order to filter the vegetation and the houses. Again, because of the size of the test area, the data set was split

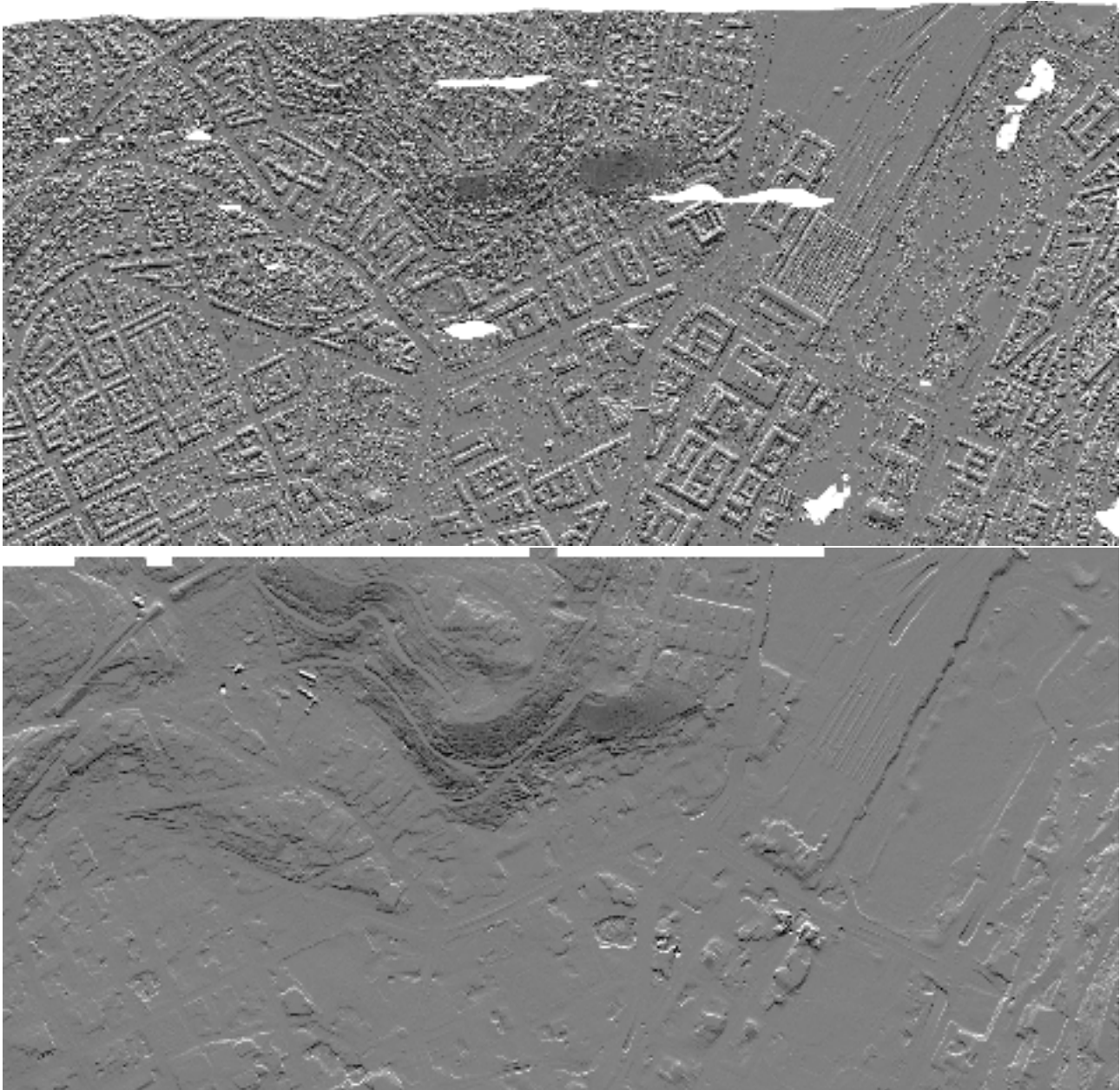


Figure 7: Northern part of Stuttgart, original data vs. ground model. A small number of buildings (e.g. the train station) were not eliminated.

into 2 parts at the east-west line with northing 5402900m. Thus, the norther part has an extension of 2500m by 1220m (3.05km^2 , 2472834 points).

The processing of the data, the filtering of the houses and the vegetation, ran in the same way as the Vaihingen example, but the parameters were slightly different. First, the thin out was performed over a regular grid of 5m by 5m, choosing always the lowest point in each cell. While this speeded up the filtering, it also favored negative blunders. Apart from the patch sizes, which were slightly larger in this example, the parameters are the same as in tab. 1.

Fig. 7 shows the original data vs. the filtered data. Almost all houses were eliminated, only the biggest ones (the train station) remained. In the north-western part a few artifacts remained, also a big hole in the ground. This is, because we could not eliminate all negative blunders correctly in the automatic procedure. With minimal human intervention these errors were corrected.

4.2.2 First and last pulse and intensities Like in Vaihingen, a histogram was computed which shows the distances between the first and the last pulse points. For 84.7% the distance is smaller than 25cm (fig. 8, left side). To record two distinctive echoes they must originate from surfaces which have a certain distance, which is at least half of the length of the wave package (pulse duration \times speed of light). As it can be seen in the histogram the first and last pulse points are either more than 4m apart or identical.² There are point distances larger than 35m. To some extent these measurements may be due to high buildings which have been partially hit by the laser beam whilst the other part was reflected on the ground, but most of these measurements originate in gross errors. This is either a first pulse point which is much too high or a last pulse point which is below the terrain level. Both situations occur in the Stuttgart data set.

On the right hand side of fig. 8 the distribution of the intensity values of the first recorded pulse can be seen. The histogram for the second intensities looks similar, but with less entries below the intensity value 50 and more above this value. Furthermore, different methods have been performed to compute an ortho image with the recorded intensities which can be seen in fig. 9. The intensities from 0 to 250 have been assigned to the identical grey values, larger intensities were set to grey value 255. The images on the left hand side were generated using a 2 by 2m² raster. The intensities of all points falling in such a cell (which is determined with the x and y co-ordinate of the point) are averaged. The upper image shows this for the first intensities, the lower one for the last intensities. The choice of the cell size is critical. If it is too small, to many cells (pixels) obtain no value and the visual impression is unappealingly. In the upper left image 0.2% of the pixel represent no intensity value. If the cell size is too big, then image detail is lost. Therefore, the cell size has to be in the order of the average point distance. This problem can be avoided by interpolating a functional model (like an elevation model) with the intensity values as the observed function values and the x and y co-ordinates as the locations in the parameter domain (upper right image). This avoids the question of the cell size, only the grid size has to be chosen, which is much less critical. If it is too small, the processing time may increase, but no holes appear. For the upper right image a grid length of 1.5m has been chosen, thus the image is sharper. Here, also the first intensities were used.

The lower right image of fig. 9 shows a difference image of the first and last pulse image on the left side. The palette has been linearly scaled to cover the whole range. Single trees can be detected: in the first pulse data they appear black, in the last pulse data they have higher intensities.

²There is a small number of point pairs which is about 1 to 2m apart, preliminary inexplicable to us .

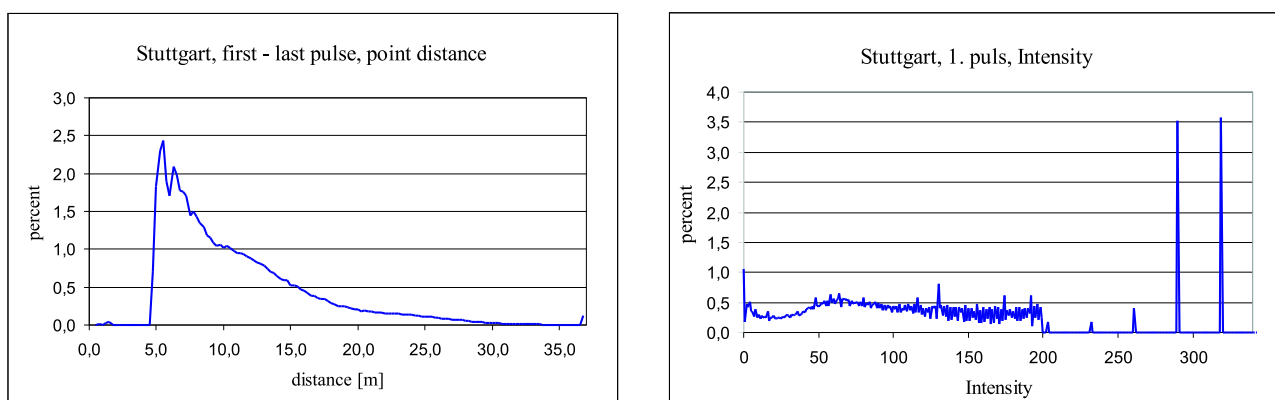


Figure 8: First and last pulse and intensity measurements of the Stuttgart data set (7,948,617 points). *Left*: Histogram of the distances between the first and last recorded echo for each emitted laser beam. For 85% the first and last pulse are identical (not shown in the histogram). *Right*: Distribution of the intensity values of the first pulse, 75% of the values are below 200, but the values go up to 5000 with gaps in between as on the right hand side.

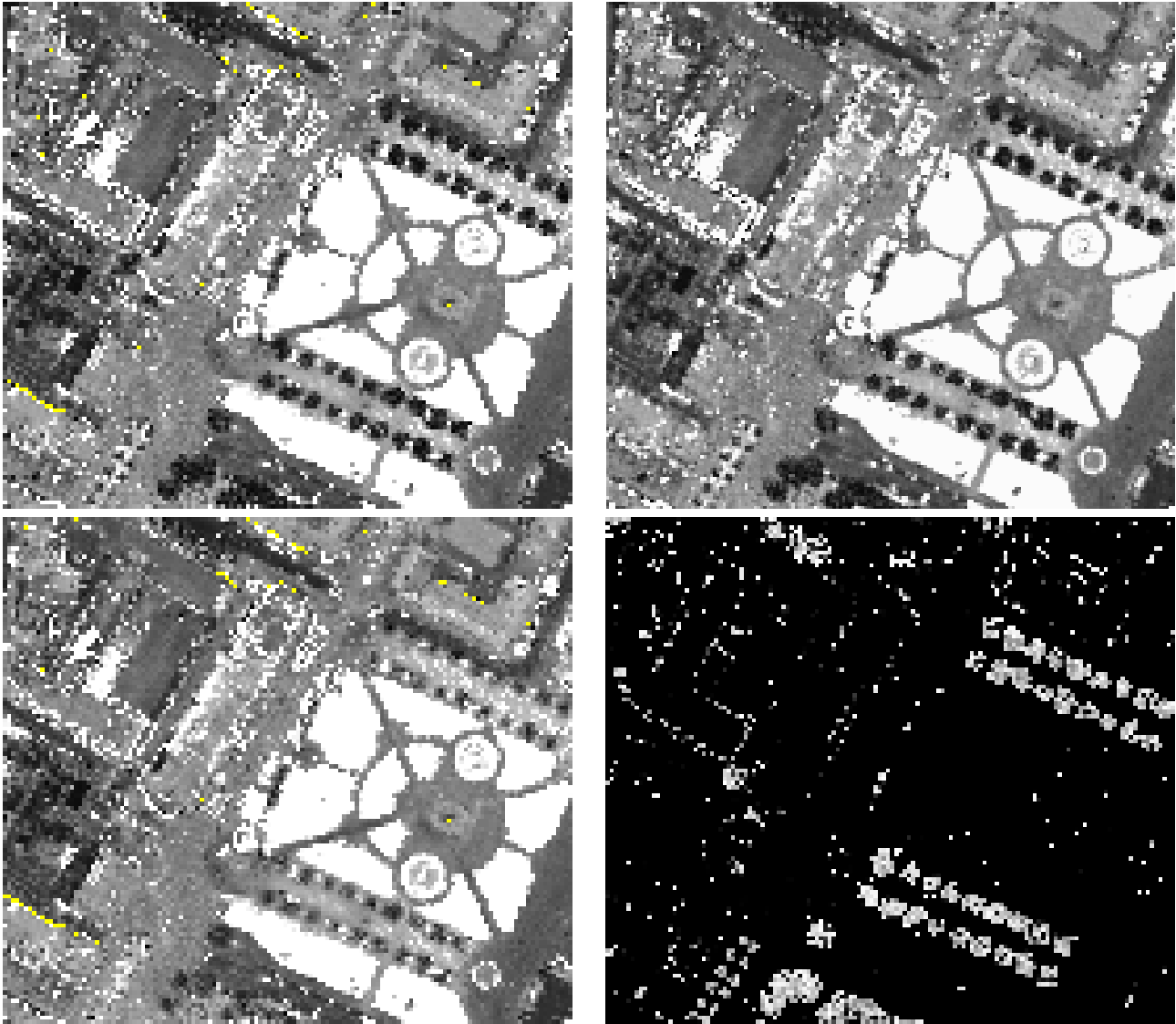


Figure 9: Ortho images from intensities. *Upper left*: regular 2 by 2m² grid, averaging of intensities in a cell, first intensities. *Lower left*: like upper image, second intensities. *Lower right*: difference image of first and second intensities, the histogram has been scaled. *Upper right*: image generated by interpolating intensities over a regular 1.5 by 1.5m² grid.

4.3 Vienna

For the City of Vienna our institute performed a laser scanner data examination with data of the TopoSys I scanner. The aim was to filter the vegetation and the houses and to determine the accuracy of the data. The test was carried out in 2000, initiated by the Vienna Municipal Department 41 – Surveyors. The test area had a size of 2.5km². On the ground 816 check points were measured manually to determine the accuracy of the DTM (Briese et al., 2001). The results are shown in tab. 4. Partly the accuracies are better than the accuracy of a single laser measurement (± 10 cm), but for well defined, only slightly curved areas linear prediction produces an elevation model which is substantially more accurate than a single point measurement (Kraus, 2000). However, these accuracy values (r.m.s.) agree to those derived in section 4.1.3 for the Vaihingen data set.

description of region	r.m.s.	std.dev.
overall area	± 10.5 cm	± 7.1 cm
park, densed stock of trees	± 14.5 cm	± 11.1 cm
park, light stock of trees	± 11.4 cm	± 7.8 cm
park, open area	± 8.6 cm	± 4.5 cm
street, with parking cars	± 9.2 cm	± 3.7 cm
street, without cars	± 2.4 cm	± 1.0 cm

Table 4: Accuracies (r.m.s. of the residuals and standard deviation of the distribution of the residuals) of laser scanner derived DTM in a city.

5 CONCLUSIONS

In this paper we presented the iterative robust interpolation (using linear prediction) which has been embedded in a hierarchical approach. This improves the filter result and speeds up the computation. The software used is SCOP++, a GUI-version of the laser scanner extension will be available, too. With the OEEPE test data sets the suitability of the algorithm has been demonstrated.

The quality of laser scanner derived DTMs is very high. However, improvements can come from various sources. Especially the automatic detection of break lines in the laser data itself, or the utilization of extern data (e.g. digital maps) are important.

As the penetration rate can vary strongly in laser scanner data sets, a laser scanner DTM should be supplied together with a reliability and/or accuracy layer, indicating the quality of the model for a certain area. Furthermore, the purpose the DTM is used for plays a role during the filter process. For our algorithm this corresponds to different sets of parameters during the filter steps.

The simultaneous recording of first and last pulse and the intensities offers the possibility to obtain an ortho-image. The interpolation of the intensities is a suitable method to generate such images. Trees appear darker in a first intensities image and brighter in a last intensities image. For the area of Stuttgart we observed that 85% of the first and last pulses are identical (no difference in position), whereas for the wooded areas of the Vaihingen example this is only valid for 20%. Although more information is available with first and last pulse and intensity data, filtering still remains an important task.

Acknowledgements

This research has been supported by the Austrian Science Foundation (FWF) under Project No. P14083-MAT.

REFERENCES

- Axelsson, P. (2000). DEM generation from laser scanner data using adaptive tin models. In *International Archives of Photogrammetry and Remote Sensing, Vol. XXXIII, Part B4*, pages 111–118, Amsterdam, Netherlands.
- Brenner, C. (2000). Towards fully automatic generation of city models. In *International Archives of Photogrammetry and Remote Sensing, Vol. XXXIII, Part B3*, pages 85–92, Amsterdam, Netherlands.
- Briese, C., Kraus, K., Mandelburger, G., and Pfeifer, N. (2001). Einsatzmöglichkeiten der flugzeuggetragenen Laser-Scanner. In *Tagungsband der 11. Internationalen Geodätischen Woche in Oberurgl*. In print.
- Brügelmann, R. (2000). Automatic breakline detection from airborne laser range data. In *International Archives of Photogrammetry and Remote Sensing, Vol. XXXIII, Part B3*, pages 109–115, Amsterdam, Netherlands.

- Dorffner, L., Mandelburger, G., Molnar, L., Wintner, J., and Wöhner, B. (1999). Geländemodelltechnologien - Forschung und Weiterentwicklung am I.P.F. In *Tagungsband der 10. Internationale Geodätische Woche in Obergurgl*, pages 31–44.
- Hansen, W. and Vögtle, T. (1999). Extraktion der Geländeoberfläche aus flugzeuggetragenen Laserscanner-Aufnahmen. *Photogrammetrie Fernerkundung Geoinformation*, pages 229–236.
- Kilian, J., Haala, N., and Englich, M. (1996). Capture and evaluation of airborne laser scanner data. In *International Archives of Photogrammetry and Remote Sensing, Vol. XXXI, Part B3*, pages 383–388, Vienna, Austria.
- Kraus, K. (1998). Interpolation nach kleinsten Quadraten versus Krige-Schätzer. *Österreichische Zeitschrift für Vermessung & Geoinformation*, 1.
- Kraus, K. (2000). *Photogrammetrie, Band 3, Topographische Informationssysteme*. Dümmler.
- Kraus, K. and Pfeifer, N. (1998). Determination of terrain models in wooded areas with airborne laser scanner data. *ISPRS Journal of Photogrammetry and Remote Sensing*, 53:193–203.
- Kraus, K. and Rieger, W. (1999). Processing of laser scanning data for wooded areas. In Fritsch and Spiller, editors, *Photogrammetric Week '99*, pages 221–231, Stuttgart, Germany. Wichmann Verlag.
- Lancaster, P. and Salkauskas, K. (1986). *Curve and surface fitting, An Introduction*. Academic Press.
- Morgan, M. and Tempfli, K. (2000). Automatic building extraction from airborne laser scanning data. In *International Archives of Photogrammetry and Remote Sensing, Vol. XXXIII, Part B3*, pages 616–623, Amsterdam, Netherlands.
- Pfeifer, N., Köstli, A., and Kraus, K. (1999). Restitution of airborne laser scanner data in wooded area. *GIS Geo-Information-Systems*, 12:18–21.
- SCOP-WWW (2001). http://www.ipf.tuwien.ac.at/produktinfo/scop/scop_dtm_sheet.htm. Institut of Photogrammetry and Remote Sensing, Vienna University of Technology.
- Vosselman, G. (2000). Slope based filtering of laser altimetry data. In *International Archives of Photogrammetry and Remote Sensing, Vol. XXXIII, Part B3*, pages 935–942, Amsterdam, Netherlands.
- Wang, Z. and Schenk, T. (2000). Building extraction and reconstruction from lidar data. In *International Archives of Photogrammetry and Remote Sensing, Vol. XXXIII, Part B4*, pages 958–964, Amsterdam, Netherlands.
- Wild, D. and Krzystek, P. (1996). Automated breakline detection using an edge preserving filter. In *International Archives of Photogrammetry and Remote Sensing, Vol. XXXI, Part B3*, pages 946–952, Vienna, Austria.

ADJUSTMENT AND FILTERING OF RAW LASER ALTIMETRY DATA

George VOSSelman¹ and Hans-Gerd MAAS²

¹ Department of Geodesy, Faculty of Civil Engineering and Geosciences
Delft University of Technology, The Netherlands
g.vosselman@geo.tudelft.nl

² Institute of Photogrammetry and Remote Sensing
Dresden University of Technology, Germany
hmaas@rcs1.urz.tu-dresden.de

KEY WORDS: Laser altimetry, DEM, adjustment, filtering

ABSTRACT

Although laser altimetry has been used for the production of digital elevation models in different countries for several years, the completely automatic derivation of a DEM from the raw laser altimetry measurements is not yet mature. The two major problems are the detection of and correction for systematic errors in the laserscanner data and the separation of ground points from points resulting from reflections on buildings, vegetation or other objects above ground. This paper discusses strategies for dealing with these two steps in the production of a DEM from raw laser altimetry data. Results are shown of experiments with different data sets.

1 INTRODUCTION

In the last few years airborne laser altimetry has become the prime method for the acquisition of digital elevation models in several countries. The reduction of costs for DEM production and the increase of reliability, precision and completeness will have played a major role in preferring laser altimetry as the acquisition method above analytical or digital photogrammetry. Whereas laser altimetry also has some other advantages over photogrammetry (e.g. the penetration in forested areas), the evaluation of DEM's derived from laser altimetry data shows that the production process of these DEM's is not yet mature [Huising and Gomes Pereira, 1998]. Most errors in these DEM's can be attributed to two problems: (1) the detection and elimination of systematic errors in the acquired GPS, INS, laser ranging, and calibration data and (2) the elimination of points caused by reflections of laser pulses on vegetation and buildings. Both subjects will be addressed in this paper.

Kilian et al. [1996] noted the systematic errors in the laser data and introduced the concept of strip adjustment in analogy to the independent model adjustment in photogrammetry. The independent model adjustment transforms points from a model coordinate system to the terrain coordinate system by a 3D similarity transform. In a strip adjustment, the transformation from a strip coordinate system to the terrain coordinate system also needs to compensate for systematic deformations of a strip. Different geometric models have been proposed for these transformation. Kilian et al [1996] used twelve offset and drift parameters for position and orientation of a strip. Crombaghs et al. [2000] described the use of three parameter transformation which compensates for an offset in height and tilts in flight direction and perpendicular to the flight direction. In both cases tie points were created by measuring corresponding points in overlapping strips. In the next section we discuss the need to explicitly model the error sources in the transformation from a strip coordinate system to the terrain coordinate system. Furthermore, we show that tie points need to be selected with care, since matching algorithms may very well produce biased estimates. Preliminary results of a strip adjustment will be presented.

The elimination of points caused by reflections of laser pulses on vegetation and buildings is usually referred to as filtering. Several filters have been proposed based on auto-regressive processes [Lindenberger, 1993], mathematical morphology [Kilian et al., 1996], least squares interpolation [Pfeifer et al., 1998] and slope thresholding in a TIN [Axelsson, 2000, Vosselman, 2000]. In section three, the performance of slope based filtering is discussed. Most filter algorithms are known to fail in case of larger buildings. A heuristic to eliminate these buildings is introduced. Results are shown for parts of the OEEPE test data sets of Vaihingen and Stuttgart.

All algorithms described in this paper operate on the original irregularly distributed laser points. Most algorithms will be faster and much easier to implement when using laser data in a grid. Producing such a grid, however, requires interpolation. Many interpolated points will be mixtures of ground points and points on vegetation or buildings. This complicates the filtering of the data and may also lead to biases in the estimation of tie points for strip adjustment. We therefore prefer to work with the original irregularly distributed laser data points. TIN's are used to establish the neighbourhood relationships between the points.

Both process steps, strip adjustment and filtering, are required to create a seamless digital elevation model. They may, however, also interfere with each other. In section four suggestions are made on how to combine strip adjustment and filtering in the production processes of digital elevation models.

2 STRIP ADJUSTMENT

Airborne laser scanner data of larger areas is usually acquired in a strip wise manner. In typical applications with the goal of digital terrain model generation the strip width is in the order of 500 to 800 meter. Modern systems with high pulse rates and large range capabilities allow for the acquisition of strips with widths in the order of 1000 meter or more. Larger blocks are flown strip wise, with an overlap of 50 to 100 meter between neighbouring strips. Due to systematic and random errors of both the laser scanner system and the GPS/INS unit, errors will occur in the ground point data. These errors become obvious from ground control points and as discrepancies in the overlap region between neighbouring strips.

Depending on their source, these errors can be distinguished into strip wise errors and local errors. Strip wise errors are caused by imperfections of the GPS/INS system, such as GPS cycle slips, by misalignments between GPS/INS system and laser scanner measurement head or by INS drift effects. They affect a whole strip or multiple strips. Local errors include the noise of the laser distance measurement unit, affecting single points, as well as the GPS noise, affecting several neighbouring scan lines. Strip wise errors have a systematic effect and become obvious from ground control point differences or discrepancies in the overlap region between neighbouring or crossing strips. Local errors of the laser distance measurement unit may become obvious from the analysis of neighbouring points on an object surface with known geometric properties, but will often remain undetected. Local errors caused by noise of the GPS coordinate determination may become obvious as local discrepancies in strip overlap regions, if tie points can be measured reliably with high density.

Basically, both strip wise and local effects have an influence on all three ground point coordinates. With GPS noise often being the primary error source, the effect in height direction will usually be larger than the effect in planimetry. In traditional DEM applications of laser altimetry with average point distances in the order of 3-4 meter over terrain of limited steepness, only the effect in height direction will be relevant. In modern applications such as 3-D building reconstruction based on laser scanner data with a density of several points per square meter [e.g. Maas and Vosselman, 1999], both effects in height and planimetry become equally relevant.

As the strip wise errors do often show a clearly systematic behaviour, they can be modelled and corrected for in a laser scanner strip adjustment procedure. In [Crombaghs et al., 2000], systematic errors in the height component have been shown, and a model for strip adjustment limited to the height coordinates, has been discussed. In the following, we will show a model for strip adjustment including height and planimetry components.

The strip adjustment procedure includes the following components:

- A mathematical model for the deformation of strips.
- A stochastic model (least squares adjustment, Gauss-Markov model).
- Ground control points.
- A method for measurement of tie points, defined as discrepancies detected in overlap regions between laser scanner data strips.

Due to the effort of providing reference values of ground control points, it is intended to reduce their necessity to a minimum. In an ideal case, four ground control points in the corners of a large region acquired by laser scanning should be sufficient.

In the following, the mathematical model used for strip adjustment in planimetry and height is formulated, and least squares matching applied to laser scanner data points in a TIN structure is discussed as a tool for the provision of tie point measurements.

2.1 Mathematical model

While a simple linear mathematical model for laser scanner strip adjustment restricted to the height component can be limited to three parameters [Crombaghs et al., 2000], the inclusion of planimetric effects requires significantly more parameters. [Kilian et al., 1996] used a twelve parameter model, including three offsets and three rotations of a strip, plus linear drifts of these parameters over time. Due to strong correlations between strip rotations and offset drifts, the number of parameters may be reduced to nine (eq.1). The errors are modelled in a strip coordinate system (x, y, z) which has its origin in the centre of the strip and an x -axis which is approximately aligned to the flight direction.

$$\begin{pmatrix} X \\ Y \\ Z \end{pmatrix} = R_{strip_to_ref} \cdot (R_e + xR_{et}) \begin{bmatrix} \begin{pmatrix} x \\ y \\ z \end{pmatrix} + \begin{pmatrix} e_x \\ e_y \\ e_z \end{pmatrix} \end{bmatrix} + \begin{pmatrix} X_{strip\ center} \\ Y_{strip\ center} \\ Z_{strip\ center} \end{pmatrix} \quad (1)$$

$$\text{with } R_e = \begin{pmatrix} 1 & -\kappa & \varphi \\ \kappa & 1 & -\omega \\ -\varphi & \omega & 1 \end{pmatrix} \quad \text{and} \quad R_{et} = \begin{pmatrix} 0 & -\dot{\kappa} & \dot{\varphi} \\ \dot{\kappa} & 0 & -\dot{\omega} \\ -\dot{\varphi} & \dot{\omega} & 0 \end{pmatrix}$$

In this formulation $R_{strip_to_ref}$, $X_{strip\ center}$, $Y_{strip\ center}$, and $Z_{strip\ center}$ define the transformation between the reference coordinate system (X, Y, Z) and the ideal (e.g. error free) strip coordinate system (x, y, z) . The deviations from the ideal strip coordinate system are modelled by three offsets (e_x, e_y, e_z), three rotations (ω, φ, κ) and three time-dependent rotations ($\dot{\omega}, \dot{\varphi}, \dot{\kappa}$). It has to be noted that this model does only correct for systematic errors, which cause linear deformations of strips. Local effects, especially those caused by the limited precision of GPS, are not covered by this model and will be more difficult to deal with.

2.2 Measurement of tie points

Due to the aspired limitation of control points to a minimum, the major observations as input into the strip adjustment procedure are tie points in the overlap region between neighbouring or crossing strips. In the presence of systematic strip errors, these tie points will show discrepancies in their coordinates. Obviously, due to the scan pattern of laser scanner systems, datasets representing two strips of laser scanner data will not contain identical points. Therefore, points have to be interpolated. [Crombaghs et al., 2000] chose height tie points by interactively selecting flat areas in strip overlap regions and calculating the differences of the average heights of points within a certain radius in both strips. If strip adjustment shall be extended to planimetry, both height and planimetric tie point discrepancies have to be determined. A simple way to provide these measurements is the interpolation of laser scanner data of both strips to raster height images, allowing for the application of standard image matching tools [Kilian et al., 1996]. Suitable locations for matching with the aim of determining strip discrepancies must contain gradients in three non-coplanar directions. In many regions, such patches are only provided by buildings with according roof shapes. It can be shown that in such cases, matching applied to interpolated height images may lead to a strong bias in the determined shift parameters as a consequence of points in occlusion regions [Maas, 2000].

A solution for this problem is provided by the formulation of least squares matching (LSM) for irregularly distributed points in a TIN structure [Maas, 2000]. This formulation allows for extensions to exclude points in occlusion regions and to restrict matching to planar patches visible in both datasets, resulting in unbiased estimates for all three tie point coordinate discrepancies. Besides these three shift parameters, LSM does also provide estimates for the precision of the estimated parameters. The design matrix in LSM is derived from observations with stochastic properties; in combination with the noise properties of laser scanner data, this causes the values in the covariance matrix to be too large and thus the estimated shift parameter standard deviations to be too optimistic. This applies especially for high density laser scanner data and may have severe consequences for the analysis of the determinability of parameters. Methods to overcome this problem and to obtain realistic figures on precision and determinability of tie point shift parameters are also discussed in [Maas, 2000].

Applied to laser scanner data with moderate point density (1.8 meter average point spacing), standard deviations in the order of one decimetre for the two planimetric shift components ($1/20$ point spacing) and one centimetre for the height discrepancies could be achieved [Maas, 2000]. The standard deviations of matching should be used as weight for observations in strip adjustment. In the same experiments, planimetric discrepancies of up to 40 cm and height discrepancies in the order of 10 cm could be detected. These shifts are significant.

While flat regions for determining height discrepancies are easy to find, the requirement for patches with gradients in three non-coplanar directions restricts the choice of suitable patches considerably. One consequence of this restriction should be the implementation of adaptive matching, reducing the number of parameters automatically in the case of non-determinability of some parameters. Another solution is provided by using reflectance data, which are provided by most laser scanner systems, for determining horizontal shifts as suggested by [Burman, 2000] and [Maas, 2000]. A matching strategy for automatically finding suitable regions for matching might be based on an interest operator implemented on irregularly distributed points in a TIN structure. As an alternative, available GIS data may indicate buildings, or buildings may be detected in the laser scanner data automatically, as shown in [Oude Elberink and Maas, 2000].

2.3 Adjustment results

The mathematical model described in 2.1 and the tie point measurement method described in 2.2 have been applied to two small data sets. Both data sets contained buildings that could be used for tie point measurements. No ground control points were available for these data sets. Therefore, a minimum number of control points was assumed, such that they did not deform the strips. The four strips of the Eelde test site are shown in figure 1. The two North-South strips cross the two East-West strips.

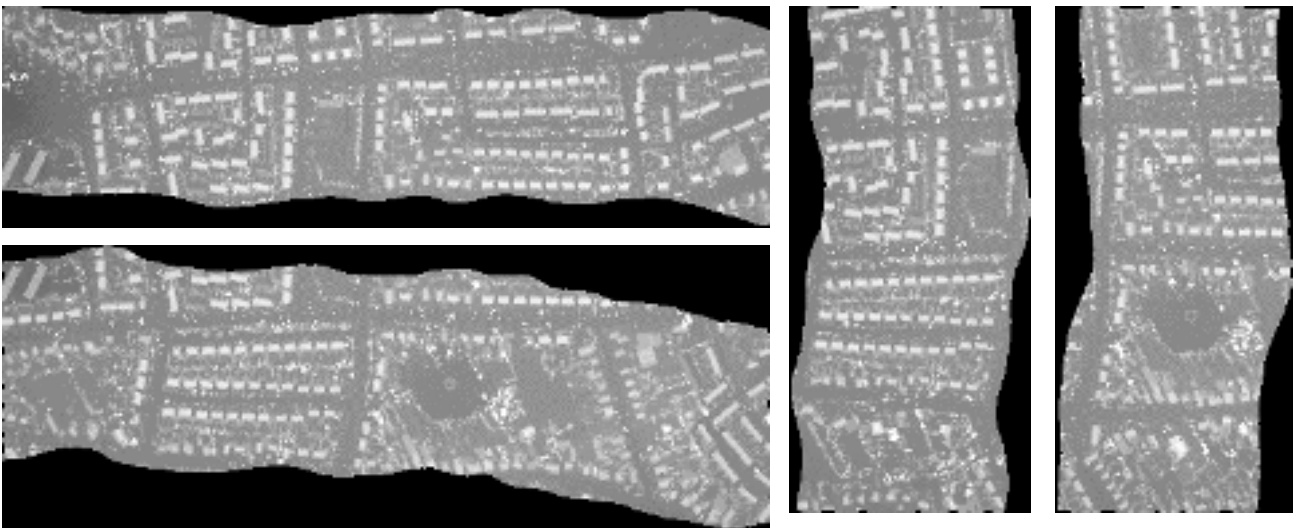


Figure 1. Four strips of the Eelde test site.

The preliminary adjustment results are summarised in table 1. Standard deviations were estimated from the residuals before and after the strip adjustment.

Sensor	FLI-MAP			ALTM1020		
Test site	IJsselstreek (NL)			Eelde (NL)		
Point density (pts/m ²)	5-6			0.3		
Flying height (m)	110			500		
Number of strips	2			4		
Number of tie points	75			46		
σ_0 before adjustment (cm)	15.2			35.6		
σ_0 after adjustment (cm)	9.7			20.3		
σ_0 improvement (%)	36			43		
$\sigma_X \sigma_Y \sigma_Z$ before adjustment (cm)	16.4	20.0	5.0	48.6	40.5	11.6
$\sigma_X \sigma_Y \sigma_Z$ after adjustment (cm)	11.2	11.6	4.7	26.0	24.5	8.5
$\sigma_X \sigma_Y \sigma_Z$ improvement (%)	32	42	6	47	40	27

Table 1. Strip adjustment results

In both cases no larger systematic errors were present in the data as was already noted by visual inspection. By the adjustment, the standard deviations of the coordinate differences between the tie points reduced by about 40%. Interestingly, the planimetric precision improved much more than the height precision. For the production of accurate 3D city models strip adjustment may therefore be even more important than for the production of DEM's.

The height precision achieved with the FLI-MAP scanner is quite good and is in agreement with other accuracy analyses [Brügelmann, 2001]. The height standard deviation of the ALTM1020 scanner is also quite acceptable, considering that the estimated standard deviation contains the noise in the heights of two different strips and possibly small biases caused by the tie point transfer.

3 FILTERING VEGETATION AND BUILDINGS

For the production of digital elevation models, the many points that are measured on vegetation, buildings and other objects above the ground surface need to be removed from the data set. Several algorithms have been developed for this purpose [Kilian et al., 1996, Pfeifer et al. 1998, Axelsson, 2000, Vosselman, 2000]. These filter algorithms make assumptions on the spatial distribution of points in the terrain. By verifying these assumptions points are classified as ground point or not. Huising and Pereira [1998] show that filtering becomes difficult when objects to be removed (like buildings) are similar in shape to objects that are part of the terrain (e.g. dikes). Whereas the filters can correctly eliminate most points above the ground, there are many cases left in which the laser data by itself provide insufficient information to reliably classify the points without the usage of additional information. This holds for example for points on low vegetation and points on large buildings.

Parts of the OEEPE data set of Vaihingen and Stuttgart have been processed using the slope based filter described in [Vosselman, 2000]. This filter can be implemented using mathematical morphology. In order to deal with larger buildings without the use of large structure element for the mathematical morphology, a post processing step was performed in which larger higher objects were detected.

3.1 Slope based filtering using mathematical morphology

In contrast to the min/max operators, the slope based filter defines the maximum allowed height difference between two points as function $\Delta h_{\max}(d)$ of the distance d between these points. When this function are known, the DEM points are defined as a subset of all laser points A by

$$DEM = \{p_i \in A \mid \forall p_j \in A : h_{p_i} - h_{p_j} \leq \Delta h_{\max}(d(p_i, p_j))\} \quad (2)$$

It can be shown that this is equivalent to accepting all points below the eroded surface, if the structure element for this erosion is defined by

$$k(\Delta x, \Delta y) = -\Delta h_{\max} \left(\sqrt{\Delta x^2 + \Delta y^2} \right) \quad (3)$$

Hence, for each point, the eroded height at the same (X,Y) location is computed and compared to the original height. If the eroded height is lower, the point is rejected [Vosselman, 2000].

The size of the kernel has a large effect on the computational effort. To reduce this effort heuristics can be applied that produce virtually the same results in only a fraction of the time used for the strict implementation. Depending on the amount of point above the ground surface the filtering speed varies between 2 and 10 million points per hour (on a SGI O2 10k).

Slope based filtering only accepts a point as a ground point if its height is not much above neighbouring points. The discriminative power of the filter therefore depends on the height differences in the terrain and the point density. The higher the point density, the steeper the slopes between ground points and points on nearby buildings and vegetation will be. Therefore filtering results improve with an increasing point density [Vosselman, 2000]. Steep slopes in the terrain clearly deteriorate the filter results. In order to avoid that all points on these terrain slopes are eliminated, one has to accept large height differences between nearby points. Consequently, similar height differences caused by vegetation, cars or lower buildings will also be accepted.

3.2 Removal of buildings

Buildings are not completely eliminated by morphological filters if the kernel size is smaller than half the size of a building. Figure 2 shows the typical pattern of accepted (white) and rejected (black) points for such cases. Points on the roof and near the edge of a building are rejected due to large height differences between these points and ground points. Due to the limited size of the kernel, points in the interior of the roof are only compared to other points on the roof. In case of flat roofs, these points are not eliminated.

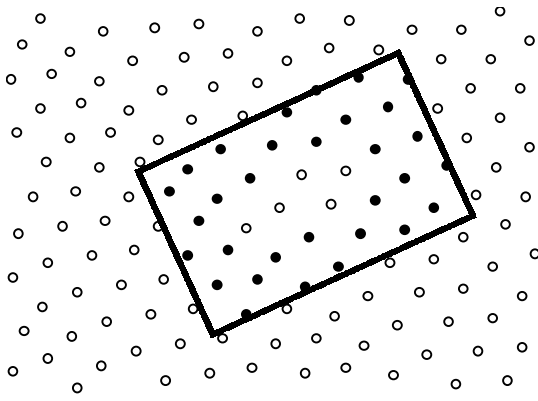


Figure 2. Pattern of accepted (white) and rejected (black) points around a large building.

One way to eliminate the interior roof points is to make use of a GIS. This requires an accurate registration of the laser data to the GIS. Errors in the registration will lead to the removal of ground points if these points fall inside a building contour. The usage of a GIS for this purpose, of course, also relies on the completeness of the GIS.

For processing data with large buildings we use a simple heuristic based on the analysis of heights in the connected components of accepted and rejected points. Patterns as shown in figure 2 are detected in the TIN data structure. They consist of a connected component of accepted points, surrounded by a connected component of rejected points, which on its turn is again surrounded by a connected component of accepted points. These components will be named RI (roof interior), RE (roof edge), respectively G (ground).

If the components RE and RI belong to a building it is expected that the points in RE were rejected because of height differences with points of G, but not because of points in RI. For a building, the heights in RI are expected to be higher or equal to the heights in RE. Furthermore, there should be a significant height difference between the points in RI and the points of G that are near the building. Resulting from these considerations, the heuristic for the removal of buildings is defined as follows. All points of a component RI are rejected if

- all points of RI are higher than the lowest point in RE, and
- the median height of points in RI exceeds the median height of those points of G that are adjacent to RE by some assumed minimum building height (e.g. 2 m).

Using this heuristic most buildings can be removed from the dataset. The weak point of the heuristic lies in the assumption that the component of the interior roof points is separated from the component of the ground points. I.e., there should be no TIN edge that connects a ground point to a roof point that was not eliminated by the morphological filter. Sometimes, however, these components are connected. This is the case if there are some reflections on low vegetation and the wall of a building such that there is a path of points from a ground to a roof point along which there are no steep slopes between the successive points. The occlusion of an area beside a building may have a similar effect. In this case the distance between the roof points and the nearest ground points increases. Consequently, the slope between these points decreases and may fall below the slope threshold. Ground points and roof points are then connected by long TIN edges.

3.3 Processing the OEEPE datasets Vaihingen and Stuttgart

Two parts with buildings and/or vegetation were selected from the OEEPE datasets of Vaihingen and Stuttgart (figure 3). Clearly visible are the effects of a flight planning error: the strips are not, or not completely, overlapping. The

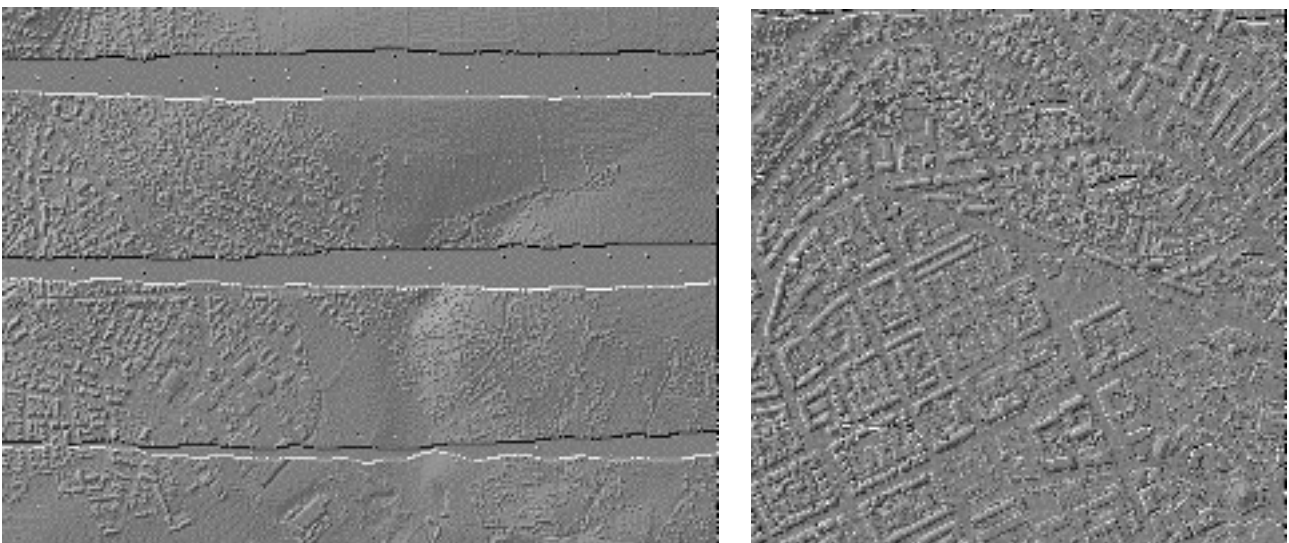


Figure 3. Shaded height images of the selected parts from the datasets Vaihingen (left) and Stuttgart (right).

Vaihingen dataset also shows some large outliers. These points are clearly visible in the gaps between the strips, but are also present within the strips. Outliers above the ground surface will be eliminated by the filtering. Several points, however, are situated below the ground surface. These points need to be removed before the filtering. Otherwise, these low points would lead to the elimination of nearby ground points.

For the elimination of the outliers it was assumed that these points were at least 2 m below the ground surface. The whole dataset was eroded with using the following maximum height difference function:

$$\Delta h_{\max}(d) = \begin{cases} 0 \text{ m} & d = 0 \text{ m} \\ 2 \text{ m} & 0 \text{ m} < d \leq 10 \text{ m} \end{cases} \quad (4)$$

If, for some point, the eroded height equals the original height, this implies that within a distance of 10 m all other points are at least 2 m higher than this point. Those kind of points were classified as outliers. Most of the outliers could be removed this way. At some locations in the dataset, the distance between the outliers was less than 2 m. In those cases only the lowest outlier was removed. The filter was therefore modified such that the number of points within a distance of 10 m that are less than 2 m higher should be above a small number (e.g. 3). Points that do not meet this condition are classified as outliers. In this way, all visible outliers could be eliminated.

Both the Vaihingen and Stuttgart datasets were filtered with a function that assumed a maximum slope of 50%. The size of the erosion kernel was 30 m. The heuristic to remove unfiltered parts of buildings was applied to the results of the slope filter. A minimum building height of 2 m was assumed. The original data and the filtered data before and after the application of the building removal procedure are shown in figures 4 (Vaihingen) and 5 (Stuttgart). In order to create a DEM and visualise it in a grid, points were interpolated up to distances of 50 m. This explains why some but not all the space between strips in the Vaihingen dataset is covered by an interpolated DEM.

In the Vaihingen dataset one can observe that the slope based filter removed the virtually all vegetation. Some of the buildings were not completely eliminated. A few buildings could be removed by the developed heuristic. For those buildings the building points near the roof edges did not separate the accepted building points from the ground points. The gap between the strips also caused this problem. Due to the large distance between points on the building in one strip and points on the ground in another strip, the slope between these points became smaller than 50%. Hence, these building points were not eliminated. In the TIN these building points were connected to ground points. Consequently, they were not detected by the heuristic.

Similar results were obtained for the Stuttgart dataset. A few points on buildings were not eliminated. With a little effort these points can be removed by manual editing. Several building blocks seem to be a bit higher than the street level. This may be caused by reflections on the walls of the buildings or on low vegetation near the buildings that were not removed by the slope based filter.

4 THE COMBINATION OF STRIP ADJUSTMENT AND FILTERING

Strip adjustment and filtering are both essential steps in the production of a DEM from laser altimetry data. The order in which these two steps are combined will influence the quality of the DEM. Two reasons can be given to start with a strip adjustment and then filter the dataset in which the data of all adjusted strips is combined.

- A 3D strip adjustment requires height differences. In particular, sloped areas are required. Slanted building roofs are very valuable for the estimation of planimetric differences between strips. If one would filter before the strip adjustment, the building roofs would not be available for the estimation of tie points.
- Filter algorithms perform better with higher point densities [Vosselman, 2000]. When the data from the strips is combined after the adjustment, the point densities in the overlapping parts will double. In these areas the filters will perform better. Without a preceding strip adjustment such a combination of data from different strips with the purpose of an improved filter performance may even lead to worse results. If two strips show a significant height differences in the overlapping part, a filter may remove ground points from the higher strip!

On the other hand, the measurement of tie points for the strip adjustment is not possible in areas with vegetation. The height texture in these areas is more or less random and differs from strip to strip. Matching between strips will therefore lead to unpredictable results. Hence, in areas with a lot of vegetation, tie points can only be measured after filtering.

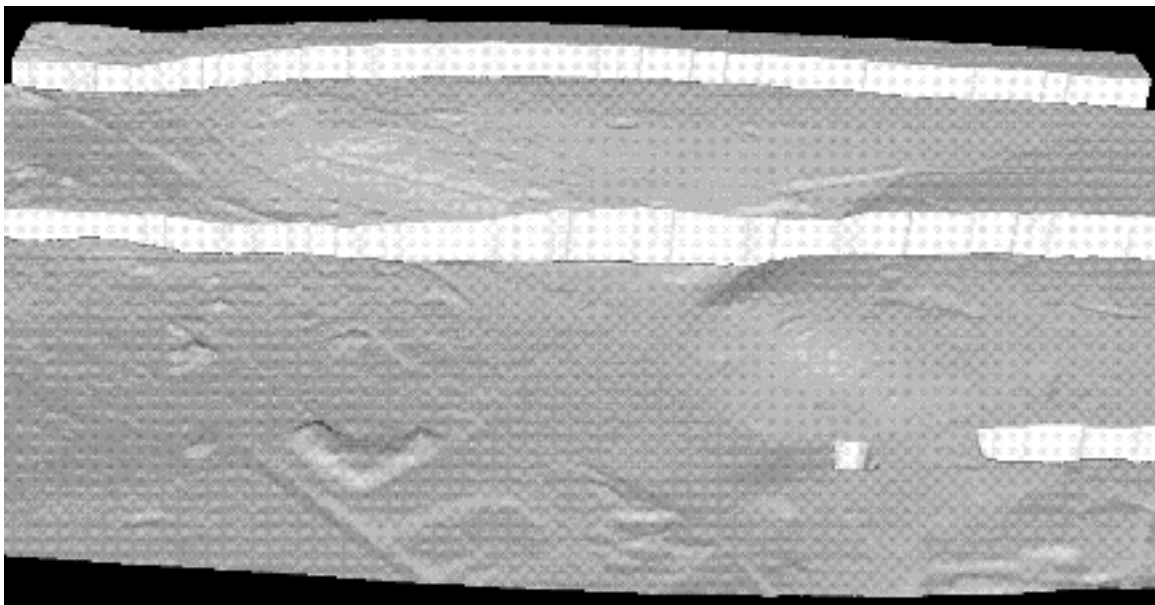
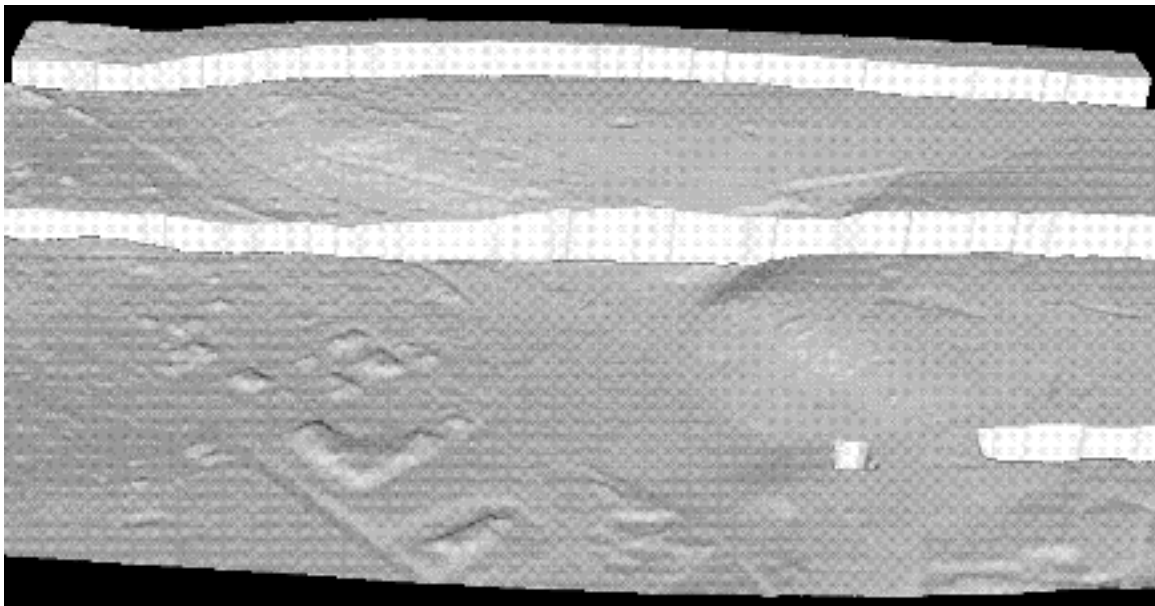
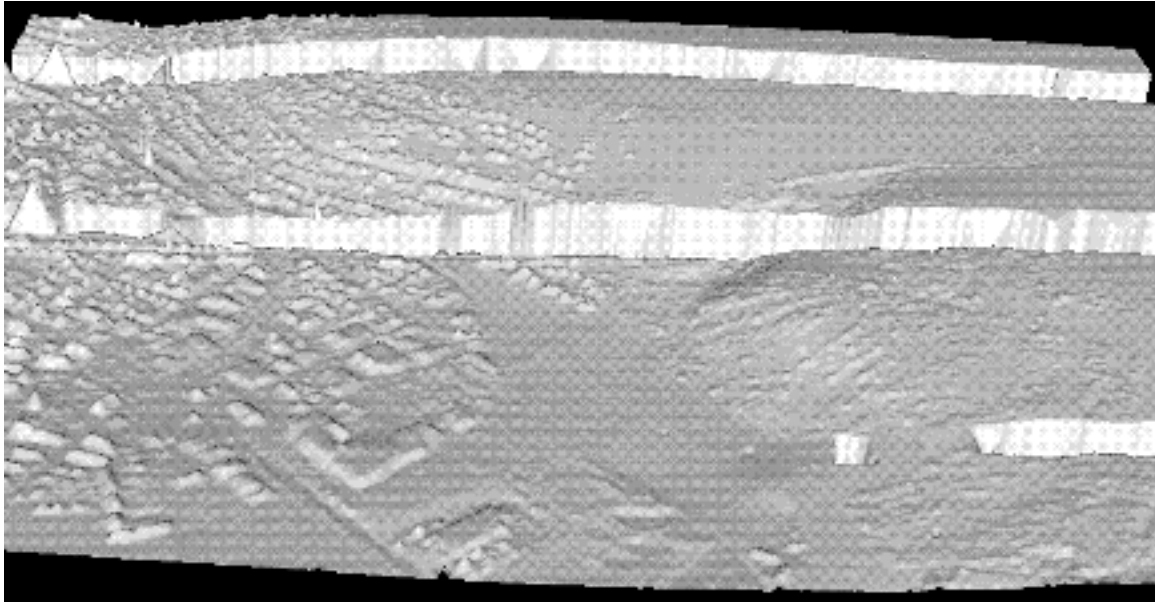


Figure 4. Part of dataset Vaihingen. Top: original data. Middle: after slope based filtering. Bottom: after building removal.

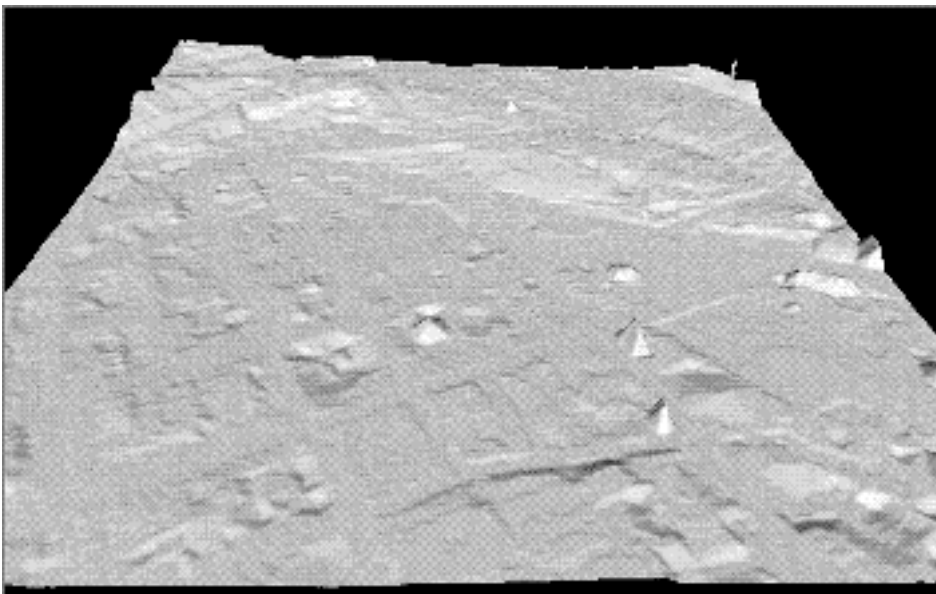
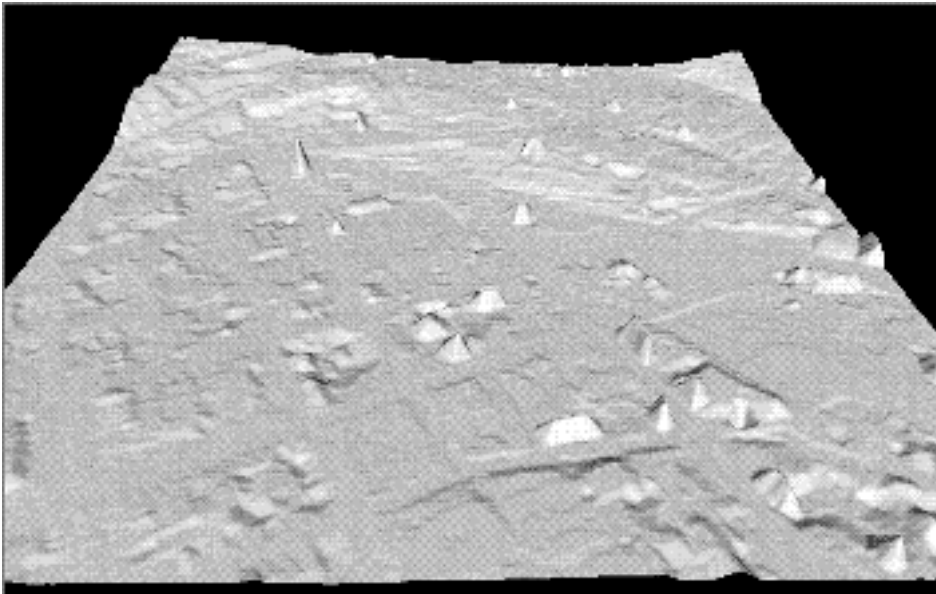
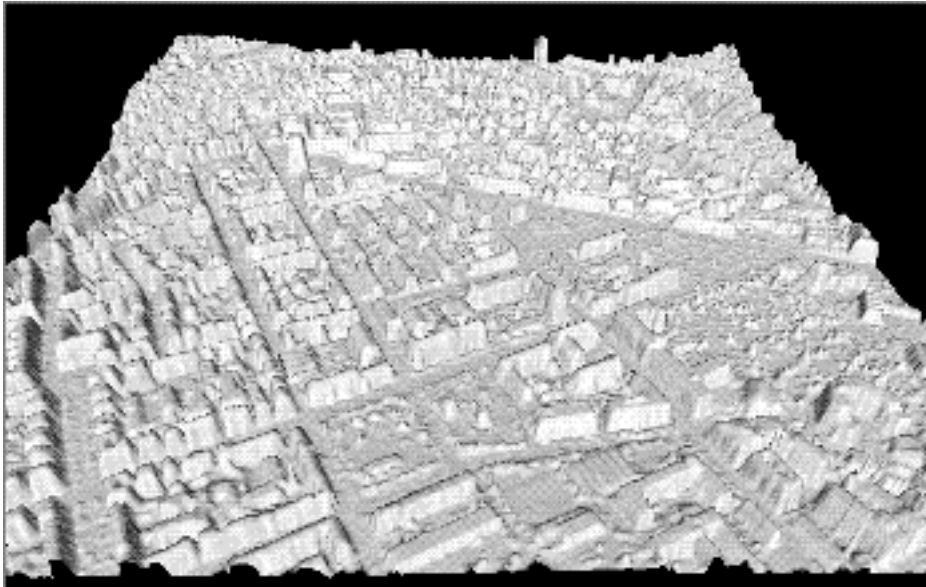


Figure 5. Part of dataset Stuttgart. Top: original data. Middle: after slope based filtering. Bottom: after building removal.

Based on these considerations we suggest to split the filter process in two parts. The procedure for the production of a digital elevation model from raw laser altimetry data would then consist of the following steps:

- Filtering the vegetation while keeping the buildings. This can be achieved using morphological filter with a small kernel. In case of very dense vegetation and a low point density the separation between points on vegetation and points on buildings may, however, become difficult.
- Measurement of tie points and adjustment of the strips. Use can be made of tie points on slanted roofs as well as of tie points on the ground surface of areas with vegetation.
- Merging the data sets from the different strips to one seamless data set.
- Filtering of the buildings. Because of the higher point densities in the overlaps between the strips, some points on low vegetation, that were not removed in the first step, may now be detected and filtered.
- Finally, for many applications a data reduction may be required.

5 DISCUSSION

Although digital elevation models produced by laser altimetry are already successfully used for many applications, processing procedures are not yet standardised. Strip adjustment is often not a part of the procedure used in practice. Software for strip adjustment is not yet commercially available and the mathematical models for the adjustment are still under development. One might argue that strip adjustment will not be necessary in future. Once all laser altimetry surveys are more controlled and routinely calibrated, the acquired laser data may show no or only very small systematic errors. For the time being, however, one can not be sure that systematic errors can be neglected. Performing a strip adjustment is recommended as good practice.

Filtering procedures are used more often in practice, simply because filtering by hand is just too labour-intensive. Several algorithms have been proposed that use quite different concepts. For the further development of the filtering procedures it would be interesting to compare these filters on different types of terrain.

Both the selection of good tie points and the filtering become easier if the point density increases. With the increasing pulse rates of airborne laser scanners, the obtainable point densities can be much higher than the densities that are usually required for the resulting digital elevation models. To improve the processing results one should therefore consider to scan the terrain with higher point densities than strictly required for the DEM production. The higher costs for the acquisition of the raw laser data may very well be offset by the better possibilities to automatically process these data.

ACKNOWLEDGMENTS

The laser altimetry data used for the research in this paper was kindly provided by the Survey Department of the Ministry of Transport, Public Works and Water Management (Delft/NL) and by Geodelta B.V. (Delft/NL) and Fotonor (Sandefjord/N).

REFERENCES

Axelsson, P., 2000. DEM Generation from Laser Scanner Data Using Adaptive TIN Models. In: International Archives of Photogrammetry and Remote Sensing, vol. 33, part B4/1, pp. 110-117.

Brügelmann, R. and R. de Lange, 2001. Airborne laserscanning versus airborne INSAR - a quality comparison of DEM's. OEEPE workshop on LaserScanning and Interferometric SAR for Detailed Digital Elevation Models.

Burman, H., 2000. Adjustment of laser scanner data for correction of orientation errors. In: International Archives of Photogrammetry and Remote Sensing, vol. 33, part B3/1, pp. 119-126.

Crombaghs, M.J.E., R. Brügelmann, E.J. de Min, 2000. On the adjustment of overlapping strips of laseraltimeter height data. In: International Archives of Photogrammetry and Remote Sensing, vol. 33, part B3/1, pp. 224-231.

Huising, E.J., Gomes Pereira, L.M., 1998. Errors and accuracy estimates of laser data acquired by various laser scanning systems for topographic applications. ISPRS Journal of Photogrammetry and Remote Sensing, Vol. 53, No. 5, pp. 245-261.

- Kilian, J., Haala, N., Englich, M., 1996. Capture and evaluation of airborne laser scanner data. In: International Archives of Photogrammetry and Remote Sensing, Vol. XXXI, Part B3, Vienna, pp. 383-388.
- Lindenberger, J., 1993. Laser-Profilmessungen zur topographischen Geländeaufnahme. Deutsche Geodätische Kommission, Series C, No. 400, Munich.
- Maas, H.-G., 2000. Least squares matching with airborne laserscanning data in a TIN structure. In: International Archives of Photogrammetry and Remote Sensing, vol. 33, part B3/1, pp. 548-555.
- Maas, H.-G. and Vosselman, G., 1999. Two algorithms for extracting building models from raw laser altimetry data. ISPRS Journal of Photogrammetry and Remote Sensing, vol. 54, no. 2/3, pp. 153-163.
- Pfeifer, N. Köstli, A., Kraus, K., 1998. Interpolation and filtering of laser scanner data - implementation and first results. In: International Archives of Photogrammetry and Remote Sensing, vol. 32, part 3/1, Columbus, pp 153-159.
- Oude Elberink, S., Maas, H-G., 2000. The use of anisotropic height texture measures for the segmentation of airborne laserscanner data. In: International Archives of Photogrammetry and Remote Sensing, vol. 33, part B3/2, pp. 678-684.
- Vosselman, G., 2000. Slope based filtering of laser altimetry data. In: International Archives of Photogrammetry and Remote Sensing, vol. 33, part B3/2, pp. 935-942.

Ground Estimation of Laser Radar Data using Active Shape Models

Abstract

In this paper a method of ground estimation using laser radar data is presented. The algorithm uses an active shape model. A surface with physical properties, elasticity and stiffness, is unleashed in the potential field calculated from the data set. The method can be likened with a sticky rubber membrane being fastened on the ground surface.

The algorithm is robust and is working on different types of landscapes, rough areas, forest or areas with buildings.

The development of the algorithm were performed as a master thesis work at FOI in Linköping during 1999 (Elmqvist, 2000).

1 Introduction, Active Shape Models

Active shape models are something in between the fields of image processing and computer graphics. A deformable model is influenced by an image to be transformed into a certain shape. In image processing the models are used to find edges and lines in images and referred to as active contours. Due to their nature the active contours are suited to find continuous edges or lines in the images.

When dealing with contours in two dimensional images the active contour is commonly mentioned as a snake (Kass et al, 1988).

The shape of the active contour is the solution that minimize an energy function. The energy function consists material behavior like elasticity and rigidity of the snake. It is also a function of the attractor image derived from features in the image.

In this algorithm for ground estimation the active shape model can be likened with a sticky rubber cloth being pushed up from beneath. The cloth sticks to the lowest points, forming a continuous surface.

1.1 Active Contour Spline in a Two Dimensional Image

To describe the principle, the case when the model is a spline is chosen.

The snake's position in the image I is given in a parametric form

$$v(s) = (x(s), y(s)) , s \in [0, 1]$$

The energy function can be written as

$$E(v) = \int_0^1 (E_{\text{int}}(v(s)) + E_{\text{im}}(v(s)) + E_{\text{ext}}(v(s))) ds$$

E_{int} is the internal energy of the snake, this gives the spline its smoothness. The internal energy is derived from the elasticity and rigidity of the snake

$$E_{\text{int}}(v(s)) = w_e (v'(s))^2 + w_r (v''(s))^2$$

where the first term is the elasticity and the second is the rigidity. If $w_e \neq 0, w_r = 0$ the snake has no rigidity and it behaves like a rubber band, if $w_r \neq 0$ rigidity is added to the snake, preventing it from forming corners.

E_{im} is the attractor image. The attractor image is computed from the image I . If the attractor image

$$E_{\text{im}} = -I(x, y)$$

i.e. the energy is the negative image intensity, the snake will be attracted to light lines in the image. If we want to detect edges in the image we can set

$$E_{\text{im}} = -|\nabla I(x, y)|^2$$

Then the snake is attracted to contours in the image with large gradient.

E_{ext} comes from the external constraint forces. If the snake is forming a closed loop and $-E_{\text{ext}}$ is the area inside the loop, then the snake will act as an inflated balloon.

2 Ground Estimation

Because of the data set used when developing the algorithm and as a simplification the data was resampled into a regular grid. In the data set there were 10 to 20 measurements per square meter and the data was resampled in a grid with nine samples per square meter. There are no obstacles to modify the algorithm to work on raw laser radar data built up in a tin.

The active model in the ground estimation algorithm is discrete and built up by node points. Then the energy function can be written as a sum

$$E(v) = \sum (E_{\text{int}}(v(k)) + E_{\text{im}}(v(k)) + E_{\text{ext}}(v(k)))$$

The model is a grid the same size as the resampled data set. A node in the model is only allowed to move along the Z-axis during the minimization of the energy function.

The image energy, E_{im} , is a function of the distance between the node in the model and the measured data. E_{im} is a Gauss function, strong with short range. This makes the model behave like a magnet attaching to close points and being unaffected by objects further away.

Often one problem with active shape models is the start state of the model. In this case when fitting a model to the ground surface, this is no problem. There are no measured points from below the ground and the start state of the surface is simply a plane below the lowest point in the data set.

In the first round minimizing the energy function a small negative gravitation force is added with the potential energy E_{ext} . Due to the short range of the E_{im} function the model needs some initial guidance to attach to the data. In the final round E_{ext} is excluded.

2.1 Results

The laser radar equipment used for the measurements is the TopEye™ system. The data set used in the following examples were taken in 1998 by Saab Survey Systems AB.

The algorithm has shown itself robust and runs well with the same settings in the physical parameters in all tested areas.

The first example contains a building in a forrest area, Figure 2.1. It is 100m in a square and has large amount of data, totally 200.000 measured points and 29 percent of them have hit the ground.

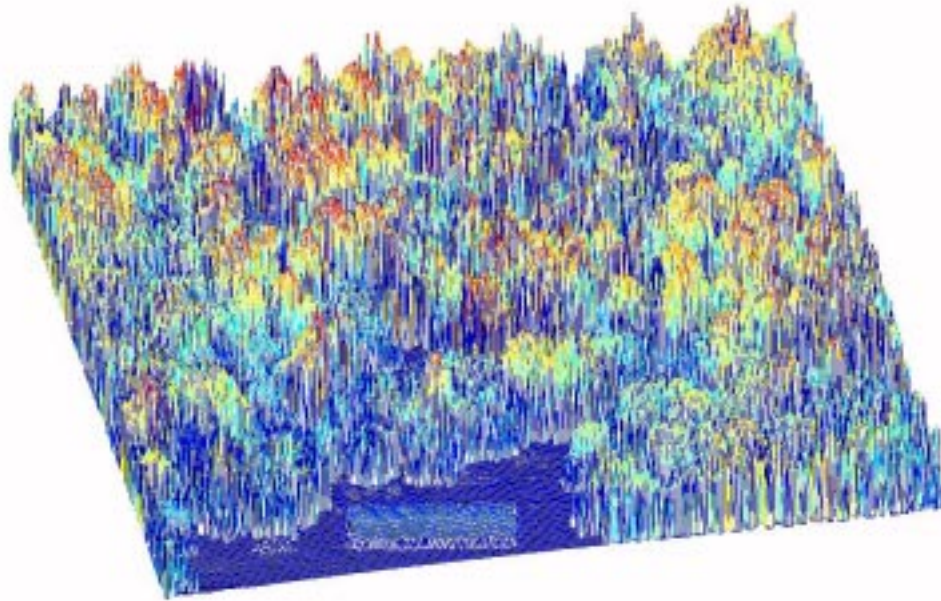


Figure 2.1The raw data image from a forrest area with a building down left.

In Figure 2.2 the ground estimation is seen. The short range of the attractor force has made the ground estimation flat under the building. The ditches that stand out in the

image are about 0.5 to 0.1 m deep.

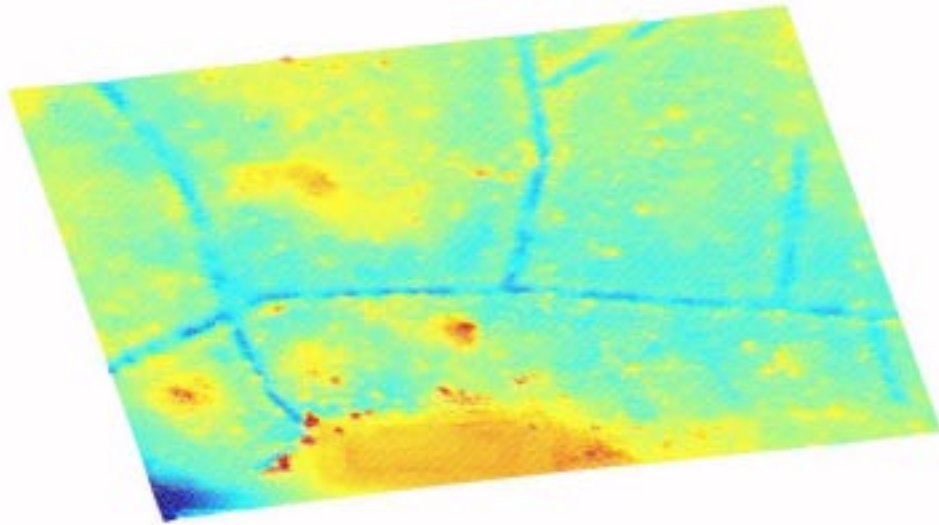


Figure 2.2The estimated ground. The building is flattened and the ditches stand out from beneath the trees.

In Figure 2.3 the raw data is plotted with negative Z-axis. Here one can see the large amount of data points from the ground forming a smooth ground surface.

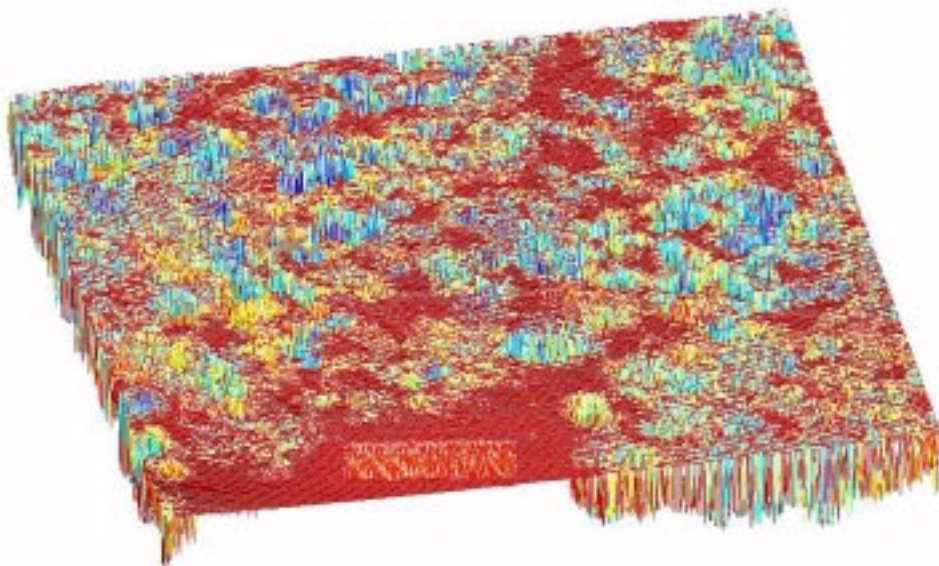


Figure 2.3The negative raw data image of the building. As one can see from this image there are lots of data from the ground. Except from under the building there are no large connected areas without data from the ground.

The next example is from a road with a walking tunnel, Figure 2.4 and 2.5. In the

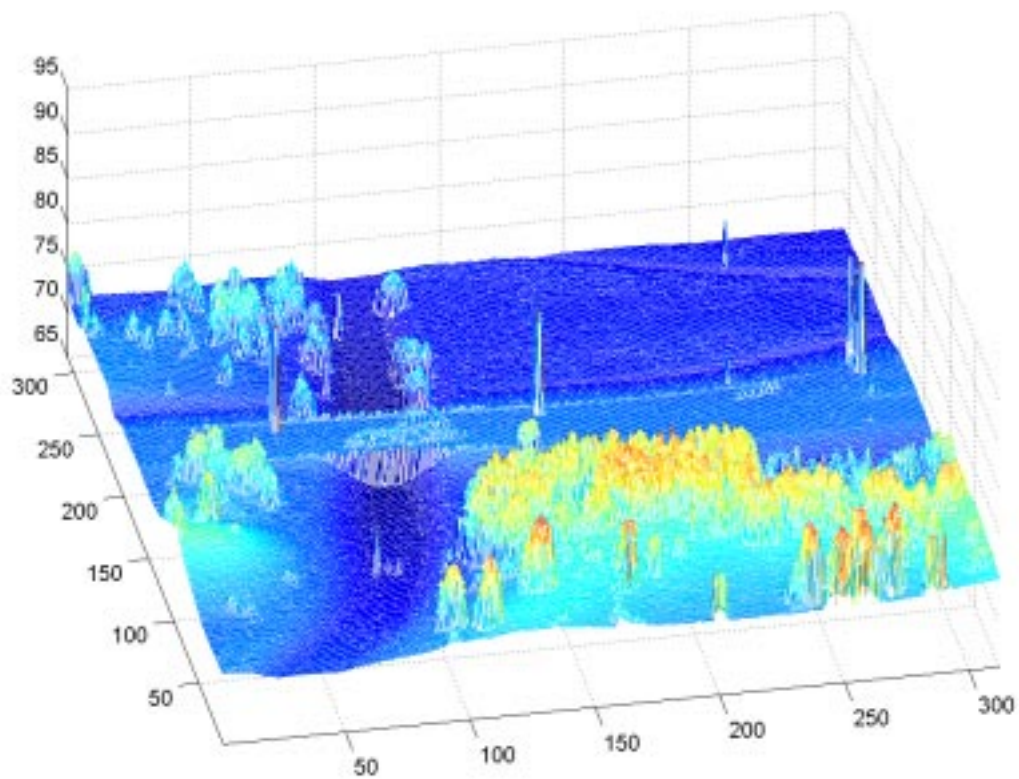


Figure 2.4The raw data image showing a road with street lamps and a tunnel. Down right in the image there are small pine trees.

ground estimate one can note that the physical properties of the model allows the surface to stretch in a steep slope on the sides of the tunnel. In Figure 2.6 a single sweep from the laser radar is showed plotted along with the corresponding section in the ground estimate.

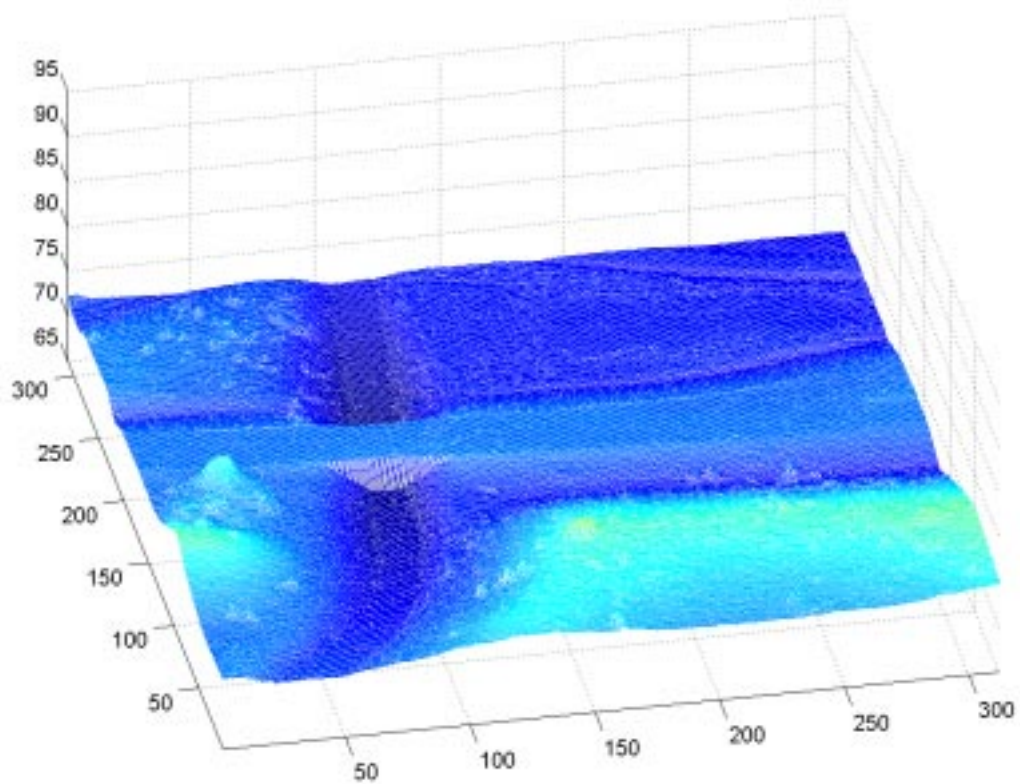


Figure 2.5The estimated ground of the road and tunnel. The little peak left of the tunnel is a boulder.

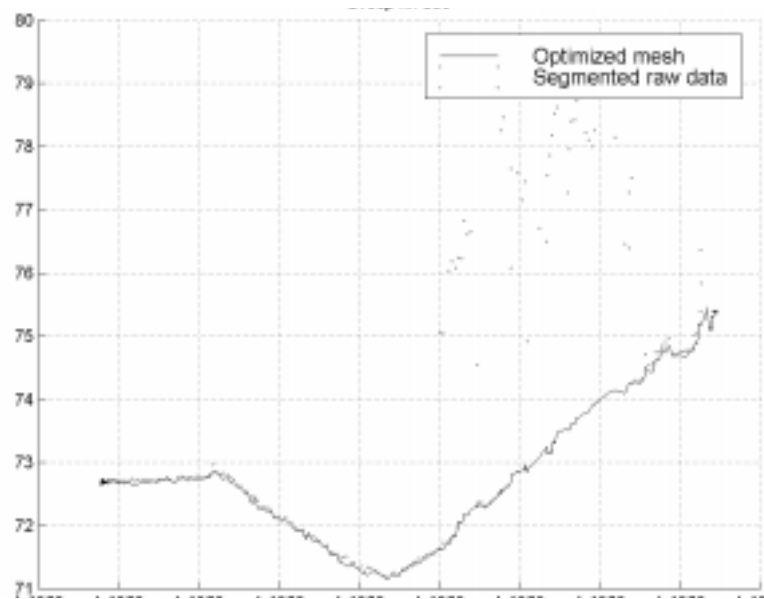


Figure 2.6A A single laser radar sweep from the road and tunnel data set. It is from the left, the roadway, a ditch and a slope with trees. The dots are the laser data points and the line is a section of the estimated ground surface.

References

- [1] Michael Kass, Andrew Witkin and Demetri Terzopoulos,
"Snakes: Active Contour Models", *International Journal of Computer Vision*,
1:321-331,1988
- [2] L.D. Cohen, "On Active Contour Models and Balloons",
Computer Vision, Graphics, and Image Processing, 53 211-218, 1991
- [3] Magnus Elmqvist, "Automatic Ground Modeling using Laser Radar Data",
Master thesis, LiTH-ISY-EX-3061,2000

REGION-BASED INFORMATION EXTRACTION FROM LASER SCANNING DATA AND OPTICAL IMAGERY

Jochen Schiewe

University of Vechta

Research Centre for Geoinformatics and Remote Sensing

e-mail: jschiewe@iuw.uni-vechta.de

Abstract: In the context of multi-sensor data modelling an improvement for the integration of elevation and image data using a region-based, multi-scale approach is presented which can be applied for the normalization of a Digital Surface Model as well as for the extraction of object types. The method consisting of a region-based segmentation of inputted multi-sensoral data and a follow-up classification using a fuzzy-logic approach is described. Empirical tests showing the applicability of the general approach are given.

1 Introduction

The current status in spatial data handling can be characterized in such a way that tremendous efforts have been made to deliver more data in shorter times by using new sensors and the benefits of the internet, while on the other hand a couple of important automatical data processing methods are neither reliable enough nor operational yet.

This general statement is also valid for acquiring and processing Digital Elevation Models. On one hand, important developments like radar-interferometric sensors (e.g., the Shuttle Radar Topographic Mission) or laser scanners (e.g., the operational systems *TopoSys* or *ALTM*) have become available to the market. On the other hand, important tasks along the data processing chain like the automatical blunder detection, the normalization of Digital Surface Models (DSMs) or the extraction of object types using elevation information very often do not lead to satisfying and reliable results as obtained with human operators.

One reason for these drawbacks is that the full information potential which a human or automatical processing system needs for interpretation purposes is not given if only one data source is considered. For instance, laser scanning methods produce “blind data”, i.e. no semantical or image information is associated with the elevation values - in contrast to optical sensors, whereas laser scanners are much better suited for capturing and processing heights, especially in wooded or urban areas. Hence, an integrated processing of different data sources should be considered. As a next step, ACKERMANN (1999) foresees multi-sensor-systems that will represent a new development stage in the field of photogrammetry and remote sensing.

In this context, this paper wants to contribute to an improvement for the integration of multi-sensoral data using a region-based, multi-scale approach for extracting information about the terrain surface or about object types. Using two different data sets (see chapter 2) the key aspects of the region-based idea - the segmentation (using the commercial software *eCognition*) and the classification (using a fuzzy-logic approach) - will be presented in chapter 3.

2 Data sets

Both laserscanning data sets in use (figure 1) are captured with the *TopoSys*-Sensor (TOPOSYS, 2001). The original measurements have been transformed into a regular 1-m-grid after eliminating blunders and data gaps in a pre-processing step. Both the positional and the vertical accuracy of the sensor is estimated to be about 0.1 to 0.2 m.

The data set **Stuttgart** covers a part of the old city showing rather low terrain undulations as well as various buildings of different sizes. This data set is courtesy of the OEEPE project on "Laser Data Acquisition". Additionally, a digital orthoimage (pan-chromatic, horizontal grid width of 0.25 m) and vector data containing cadastral information (from the digital German Real Estate Map, ALK) are available.

The data set **Denmark** covers a hilly area showing wooded as well as built-up areas. No additional optical imagery is available here.

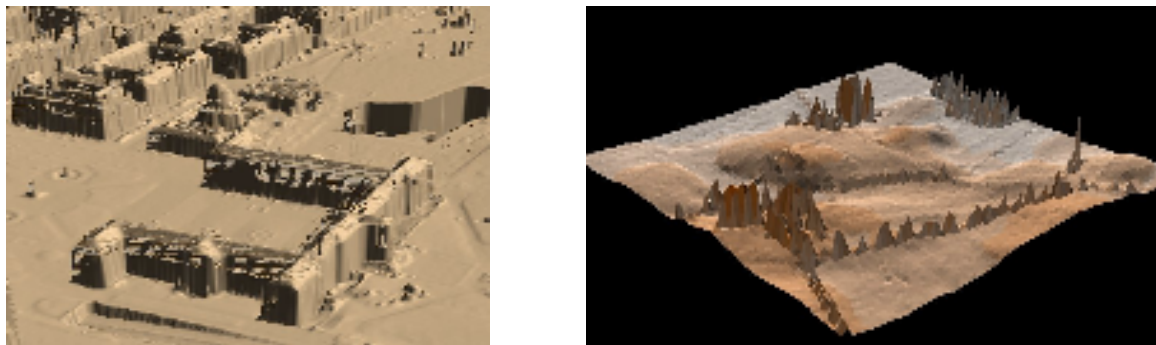


Figure 1: Sections of laserscanning data sets Stuttgart (left; 200 m • 400 m) and Denmark (right; 700 m • 700 m)

3 Methodology and examples

3.1 Overview

Core of our method is a region-based, multi-scale approach for extracting information from elevation and/or image data. The procedure as illustrated in figure 2 can be used both for extracting the terrain surface from a Digital Surface Model (DSM) and for extracting object types. It can be divided into two major parts: Firstly, the segmentation of inputted multi-sensoral data (using a commercially available software product) which produces geometrical regions without any semantics (section 3.2). In analogy to a visual interpretation the segmentation can be performed at various scales in order to obtain the most significant representation of every single terrain feature or object.

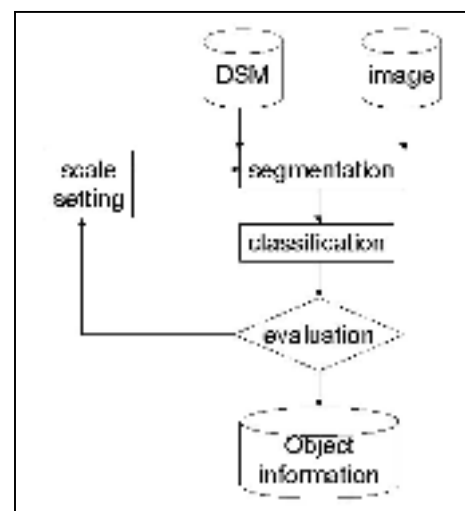


Figure 2: General work flow

Secondly, a classification of these segments using a fuzzy-logic approach (section 3.3) is performed which in the case of extracting the terrain surface identifies those regions which shall be reduced and those which already describe the terrain, resp., and in the other case directly determines desired object types.

3.2 Segmentation

The reasons for applying a region-based in contrast to an edge-based segmentation method are the tolerance against noise, the existence of closed borders as well as the homogeneity of attributes within the acquired segments. We use the commercial software product *eCognition* (DEFINIENS, 2001) which allows a multi-scale and hierarchical processing (BAATZ & SCHÄPE, 2000).

The goals of our investigations are a proper choice of inputted data sources and derived homogeneity criteria in order to meet quality measures in terms of

- *geometry*, i.e. the accurate positions of segment outlines, as well as
- *semantics*, i.e. the membership of one and only one class (which will be determined later on) to a segment.

In a first step we will concentrate on the case of deriving the terrain surface using elevation data only. While absolute elevation values do not consider an undulated terrain surface we follow the hypothesis that regions which have to be normalized, i.e. reduced in height (especially buildings and wooded areas) are characterized by strong gradients of altitude (commonly but not precisely named "slope"). In our case we summarize the gradient - actually being a vector of derivatives of altitude - in such a way that we compute its mean within a 3x3-window.

The surface representation through an interpolated discrete point distribution leads to the facts, that

- not only the exact horizontal position of object borders (like walls) can not be determined exactly (figure 3, top),
- neither one does not obtain sharp peaks and pits within the altitude gradient graph in order to locate precise borders (figure 3, middle).

Considering the first problem, one could assume the most probable position of the segment outline (e.g., a wall) to be in the middle of the gradient extremes. However, for the purpose of extracting the actual terrain surface, this assumption can lead to undesired errors because it is possible that some elements between the middle and the base points could not be reduced. On the other hand, the declaration of these regions as being candidates for a reduction although they already represent the terrain surface is not a problem. Hence, our definition of the outline to be extracted will be based upon the base heights within the altitude profile.

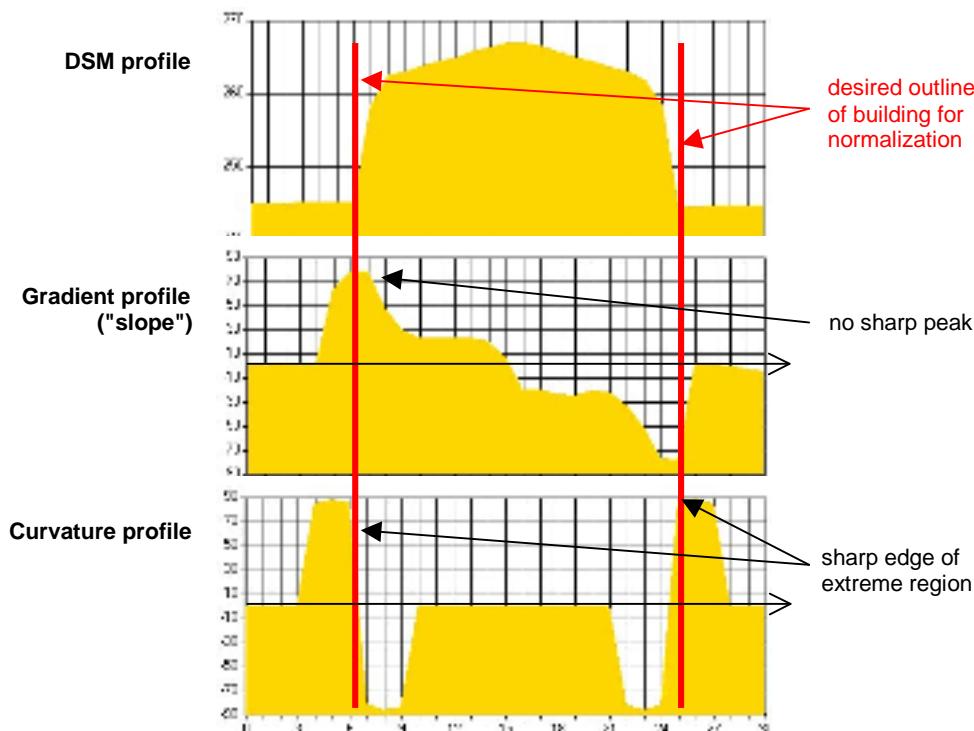


Figure 3: Characterization of building outline in laserscanning data set

Based on this "safe" definition and considering the second problem of having no sharp edges in the representation of gradients, the surface curvature represents these outlines through sharp edges which leads to a more precise description after the segmentation - under the assumption that such an edge is actually visible within an individual pixel and is not mixed by surrounding values. In this case the segmentation algorithm in use is able to yield a significant progress in terms of more accurate segment border lines, as figure 4 demonstrates.

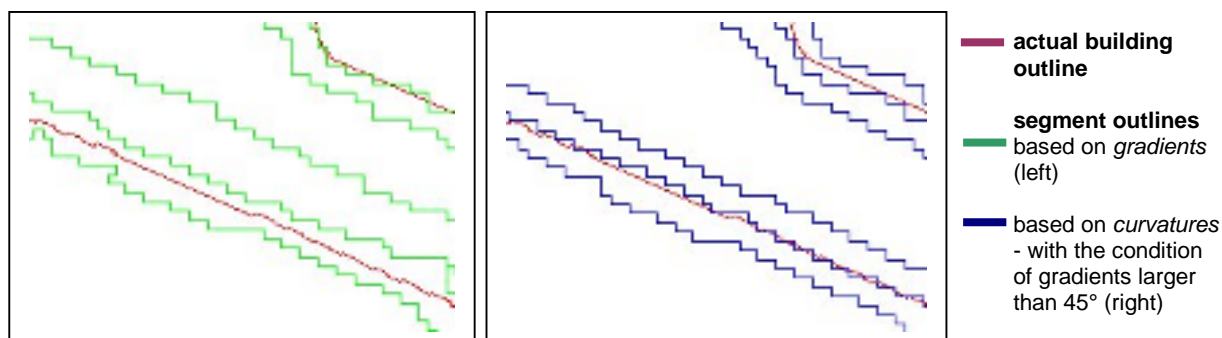


Figure 4: Comparison of actual building and (not smoothed) segmentation outlines (30 m • 15 m; test site Stuttgart)

Extending the complexity presented so far by additionally introducing pan-chromatic image data we obtain worse segmentation results due to irregular and inaccurate border lines. Beside

the fact that spectral and not geometrical features are taken into consideration, this effect is mainly due to a strong affection of image data by noise and shadows as well as to an imperfect geo-referencing. However, if the goal would not be the derivation of the terrain surface or the quality of inputted elevation data would be rather limited, optical image data would be able to improve the segmentation process significantly.

3.3 Classification

The segmentation step as presented in section 3.2 yields regions which have no semantical meaning so far. This assignment is performed in the classification step described in the following.

The reason for applying a fuzzy classification approach is that the limited resolutions and accuracies as well as the possibility of contradictory information coming from different data sources or derived information should be modelled properly. Here, the introduction of fuzzy sets and partial memberships, resp., is a meaningful modelling method.

As input for the classification we can use the *observations* $x_{S,I}$ for every extracted segment ($S=1,\dots,s$) and every indicator in use ($I=1,\dots,i$). The choice of indicators is depending on the application and will be discussed later. The next step is the *fuzzification*, i.e. the definition of the membership function $\mu_{S,I}(x)$ of a property (e.g., region to be reduced; object type) related to a segment based on the observations. Because a generic determination of these function seems to be impossible we apply tolerance intervals from logical considerations and a linear function in order to describe the range of partial memberships. Finally, the desired decision is based on a weighted summation of the obtained single membership values.

The choice of indicators depends on the current application. Our experiments show that for the normalization of a DSM based on inputted elevation data only the mean as well as the maximum altitude gradient within a segment are meaningful parameters. Here, the mean value characterizes such regions that do not show up crisp edges, but high variations in their interior (like wooded areas), whereas the maximum value very well identifies regions with opposite properties (like buildings). A more detailed description of the following fuzzification and the decision making process is given in SCHIEWE (2001). A post-processing step deals with island segments which are segments that are completely surrounded by regions of large gradients, but which are showing rather low gradients (like a roof segment surrounded by wall segments).

Empirical tests for the Denmark test site have shown no errors of first type (omission errors), while the number of errors of second type (commission errors) is below 2% of the entire number of segments. Critical regions are small clearings within wooded areas. Figure 5 demonstrates the performance of the entire process.

Applying the segmentation and the following classification not only at one, but at multiple scales, reduces the number of commission errors. However, this scaling process must not be performed as far as possible because the number of omission errors would increase and in the extreme case one would end up with an undesired point-wise classification.



Figure 5: Given DSM (250 m • 250 m; left), results of segmentation (middle) and classification (extracted regions that have to be reduced are in black; right)

For the application of extracting object types from elevation and image data - especially separating buildings from wooded areas - we have found that the normalized DSM altitude, the density of altitude gradients, the aspect, the Normalized Difference Vegetation Index (NDVI) and the spectral texture (especially in pan-chromatic imagery) are meaningful indicators for the classification step (SCHIEWE, 2000).

4 Summary and outlook

We have presented a region-based method which is able to extract the terrain surface from a given Digital Surface Model (i.e., to perform a normalization) and to determine object types. It consists of a segmentation at multiple scales and a classification based on a fuzzy-logic approach. Empirical tests have shown the successful applicability of this approach. However, the quality of results obviously depends on the quality of inputted data - a corresponding, negative example using a DSM acquired through automatic matching is given in SCHIEWE (2001).

Future work will concentrate on a more detailed examination of segmentation algorithms, ending up with the introduction of more than one method in order to meet the requirements of the specific application. Also the multi-scale aspect will be investigated in more detail.

In general, it can be stated that the presented solutions for DSM normalization and object extraction, resp., can not be seen separately. In fact, the traditional linear processing chain - starting with the blunder detection within a DSM, then performing the normalization, and ending up with the object extraction - has to be changed to a linked net of methods which allows an iterative, eventually also backward oriented work flow. For instance, the hypothesis of a certain object type (e.g., a building) for a given segment is also a valuable information for an improvement within the normalization process.

Finally, it can be stated that - in analogy to visual interpretations - a combined analysis of all available data sources will scoop the full potential of remotely sensed data. In this context, the simultaneous acquisition of electro-optical imagery and laserscanning data in the near future can actually open a new development stage in the field of photogrammetry and remote sensing.

5 Acknowledgements

We thank the following institutions for making available the test data for this study: The laserscanning and the cadastral data for the test site Stuttgart is courtesy of the OEEPE-project on "Laser Data Acquisition". The digital orthoimage was provided through the State Survey of Baden-Württemberg (www.lv-bw.de/LVShop2/index.asp). The data set Denmark is courtesy of *TopoSys*.

6 References

- ACKERMANN, F. (1999): Airborne laser scanning – present status and future expectations. *ISPRS Journal of Photogrammetry & Remote Sensing* (54): 64-67.
- BAATZ, M. & SCHÄPE, A. (2000): Multiresolutional segmentation - an optimization approach for high quality multi-scale image segmentation. In: Strobl, J., Blaschke, T. & Griesebner (Ed.): *Angewandte Geographische Informationsverarbeitung XII*: 12-23.
- DEFINIENS (2001): www.definiens.de
- SCHIEWE, J. (2000): Improving the integration of Digital Surface Models. *International Archives of Photogrammetry and Remote Sensing*. 32(B3): 807-813.
- SCHIEWE, J. (2001): Ein regionen-basiertes Verfahren zur Extraktion der Geländeoberfläche aus Digitalen Oberflächen-Modellen. *Photogrammetrie - Fernerkundung - Geoinformation*. in print.
- TOPOSYS (2001): www.toposys.com

LASERSCANNING FOR ANALYSIS OF DAMAGES CAUSED BY EARTHQUAKE HAZARDS

Eberhard Steinle, John Kiema, Johannes Leebmann and Hans-Peter Bähr

Institute for Photogrammetry and Remote Sensing (IPF), University of Karlsruhe

Englerstraße 7, 76131 Karlsruhe, Germany

{steinle / kiema / leebmann / baehr}@ipf.uni-karlsruhe.de

KEY WORDS: laserscanning, disaster management, man-made objects, change detection, damages, roads, obstacles

ABSTRACT

The University of Karlsruhe hosts a major collaborative research center that deals with the topic of strong earthquakes (CRC 461). The objective of this project is to provide measures for addressing earthquake caused disasters. Within this framework, one aim is focused on disaster management. This paper demonstrates that the analysis of post-event height data can be a basic component in the derivation of information to meet these challenges. In addition, data acquired by laserscanning systems is an integral part of this system, since it provides a versatile and fast possibility for height data acquisition. This is particularly important because most of these tasks are time critical.

The data is processed in order to extract and to reconstruct man-made objects. In a first application, this is accomplished with the help of a pre-event data set, the detection of changes, and with the use of additional knowledge, as well as their rating according to the detected damages. In a second application, this is realised through the detection of blocked roads, as well as the search for alternative passages for rescue vehicles.

1 INTRODUCTION

In the past few years, many strong earthquakes around the whole world (for example in Turkey, Greece, Taiwan, El Salvador and India) resulting in immense loss in life and destruction of infrastructure have been recorded. Each case has been quite different from the other, although there have been some common characteristics. One of them is that in general, the situation after the event was not clear, nobody knew what happened exactly, where it happened and how many people were affected (see e.g. [Comfort, 2000]). Unfortunately, however, this information is basic for any rescue measures because the available resources must be speedily adapted to single building sites in order to be effective and to rescue as many people as possible. Another problem is that the information comes within hours after the catastrophe. Since this can originate from many different sources, like rescue teams, inhabitants or the international press, it can differ or even conflict each other. Furthermore, it is not always possible to rate the information according to their reliability. Against this background, there exists a strong demand for objective, comprehensive and fast methods for information acquisition.

This has progressively been recognized by people dealing with catastrophe management (e.g. [Hecker et. al., 2000]) and different attempts have been made in the recent past. Research in this area follows mainly two directions. On the one hand, the fusion of all available data that can be regarded as more or less reliable, and acquired before the catastrophe, but suitable for helpful drawbacks. Alternatively, the development of specific acquisition and analysis methods in order to gain information. As an example for the first method, the work done by [Casciati et al., 1997] can be mentioned. This combines GIS data, space- and airborne imagery. Examples for the use of a specific sensor to obtain the needed information are [Hasegawa et. al, 1999], using aerial imagery taken with high-definition television (HDTV) cameras and [Matsuoka & Yamazaki, 1999] using different satellite-based sensors (e.g. Landsat and ERS).

In this paper, a synopsis of the work is presented done within projects of the collaborative research center 461 ("Strong earthquakes: A challenge for geosciences and civil engineering" [CRC 461, 2001]) which uses laserscanning derived

data as a main component. At first, a method to extract and model buildings from a digital height data set is outlined. The resulting building models can be used to detect changes by comparing these to models acquired before the earthquake. These changes can then be interpreted by using additional knowledge about typical damage patterns.

In a second application, streets are checked if they are blocked by obstacles. This means that the street network has to be known a priori e.g. by using data stored in a GIS. The analysis is carried out by applying segmentation algorithms to a digital surface model (DSM).

In the case of blocked roads the search for alternative paths to reach damaged buildings become necessary. This can be done by using spectral and height data to find paths and applying passability checks for the available vehicles. This will be shown as a third usage of laserscanning data.

2 LASERSCANNING

The height data used in the following applications was acquired by the TopoSys system. This is a sensor using pulsed laser light for the determination of distances between the measured points and the referring system position. This adopts the runtime measurement principle and is mostly flown in airplanes. Differential, kinematic GPS and INS sensors are used to define the airplane position with high precision. For the used TopoSys I generation, the system parameters were given by the company as shown in Table 1. A special characteristic of this sensor is the relatively high measurement point density with more than 4 points per m².

Sensor type	Pulse modulated Laser Radar	Field of view	+/- 7°
Range	< 1000 m	Number of pixels per scan	127
Scanning principle	Fibre optic line scanner	Swath width (at 1000 m flight height)	250 m
Transmitter	Solid state at 1.5 µm	Accuracy of a single distance measurement	< 0.3 m
Measurement principle	Run-time measurement	Resolution of a distance measurement	< 0.1 m
Scan frequency	300 Hz (adjustable)	Laser classification	class 1 by EN 60825 (eye-safe)

Table 1: Performance parameters of the TopoSys I sensor system [Lohr & Eibert, 1995]

The results presented later on in this paper were produced based on two digital surface models with 1 x 1m grid size (DSM) computed from both the first as well as from the last pulse mode laserscanning data set, depending on the specific application. Both data sets contain the inner city area of Karlsruhe. This is essentially an urban area characterized by large differences in the shape and sizes of buildings and streets.

3 INFORMATION EXTRACTION

After a catastrophic event, the rescue measures have to be initiated as fast as possible, because the losses in lives and values increase very fast with time. This means that the information derivation has to be also very fast. Laserscanning of high point density as provided by firms such as TopoSys can of course, not deliver height data of large cities within minutes. Compared with other sensors providing comparably dense point distribution like airborne cameras or optical sensors installed on satellites (e.g. IKONOS [Gerlach, 2000]) which are capable of acquiring strips with a width of some kilometers, the typical strip width of within 100 – 300m means a significantly longer flight time to cover larger areas. Nevertheless, laserscanning seems to be more suitable for the tasks of a fast information collector because the acquired data can be processed and analyzed much faster than data from other sensors so that in the end, the *information*

is faster available. This is on the one hand due to the fact that all the data is directly received in digital form and therefore suitable for automatic processing.

On the other hand, heights and not spectral features are collected. When searching for damages in man-made objects, it is necessary to model their after-event status geometrically and interpret it. To do this automatically is not trivial, whether using spectral or height data. But the automatic extraction of geometric features from spectral data suffers from potentially more disturbing influences like shadowed regions. Often correlation is used to extract geometric primitives from spectral image pairs. In the case of collapsed buildings, this can be extremely critical because the remaining structure can show a highly inhomogenous spectral behaviour. Since inhomogeneity is used to establish e.g. edges, the likelihood of misassignments can increase significantly. This is avoided by using laserscanning because the pointwise measurement leads directly to point coordinates in 3D.

Another problem can occur when there are bad weather conditions or the catastrophe happens at night. Spectral data acquisition is then normally not possible. Since laserscanning systems are active sensors, this means they produce the measurement signal themselves, and they can be used in such scenarios. Because of these reasons the methods described in the following sections use laserscanning as a basic component.

3.1 BUILDINGS

The main focus after an earthquake is on the buildings in the affected region. This is because people could eventually be trapped in damaged buildings. Depending on when it happened, i.e. at what time of the day, residential houses or public buildings e.g. schools, factories, shops and office buildings are more critical.

To detect damages in buildings, the buildings have at first to be recognized in the used data sets, extracted from these and modelled according to their geometry. Afterwards they can be compared to a pre-event presentation of the same. This means a model generated preferably before the disaster or one computed from pre-event data sets after the disaster. By comparing the above, changes can be determined. With the use of expert knowledge on typical damage patterns these can be rated according to their damage type and grade, i.e. interpreted accordingly. This information can then be used by the disaster management to set priorities in rescue measures and to allocate the rescue resources in a more objective and optimal way.

In the following, a method is presented based mainly on the already described first pulse laserscanning derived DSM. As this data set has a resolution of not more than 1 meter, it means that in terms of building damages some sort of generalization will be done implicitly. For example, the resolution is too coarse to enable the detection of small cracks or small building tilts. With the chosen method it is also impossible to detect changes at very small building parts as chimneys or small balconys. Nevertheless, this data set is acceptable when regarding this method as a tool for the rescue measures where the described undetectable changes are in general, not relevant despite the building cracks. But they can hardly be recognized by using any method based on remote sensing data and need therefore be added by investigation from the ground.

3.1.1 AUTOMATIC MODELLING OF BUILDINGS

Many attempts for an automatic building reconstruction from all sorts of remote sensing data have been made in the past (see [Förstner, 1999]). Most of these use geometric constraints for the reconstruction process, such as parallelism or right corner criteria. This is not only critical with some special roof shapes, but even more when considering destroyed buildings. In the following, an attempt is made to avoid such criteria. Nevertheless, one assumption has remained, namely that a building can be modelled by planar surfaces. Of course, this is not true in every case but it leads in principal, to a kind of generalization of the shape, e.g. a dome is approximated as a kind of pyramid. Since the resolution of any detected damages will be rather coarse, the changes caused by this generalization are not significant.

In Figure 1 the process of the building recognition and reconstruction is illustrated. The method is described in detail in [Vögtle & Steinle, 2000]. In this attempt, a true orthophoto was used in addition to the DSM. Thinking of data acquisition and fast analysis in case of disasters this might seem to be a contradiction. However, since the newest generation of laserscanning systems are more and more complemented with other sensors this is not. For example, in the case of the TopoSys II sensor ([Lohr, 1999]) the system is complemented with a spectral line scanner. On the contrary, one will procure spectral data with direct georeference and acquired simultaneously with the laserscanning data, such that a common analysis of both data sets will be uncritical.

At the beginning objects not being buildings are found by trying to "interpret" all the objects located above the ground. Interpretation is meant here not on a higher semantic level, but implied in the use of building models. Buildings are assumed to exhibit a low normalized difference vegetation index value (NDVI, see [Vögtle & Schilling, 1997]). Hence, they can be separated from vegetation based on spectral features. Another characteristic is that they have a significant

height above ground. This is checked by producing a terrain free DSM, a so-called dDSM, by ground filtering algorithms and extraction of the obtained digital terrain model (DTM) from the DSM, and analysis of the heights of the remaining objects.

Using these criteria, objects regarded as being probably buildings are extracted. A shape analysis is then carried out, using e.g. rectangular lines, parallel lines, number of points per area, area etc. as indicators to separate further the building from non-building objects and finally extract the objects that seem to be buildings, here referred to as "building hypothesis".

Of course, the building recognition procedure can fail in case of damaged buildings if they do not fulfill the above mentioned criteria any more. It is planned to use additional data acquired before the disaster for explicitly derived the building hypotheses. For instance, this can be gained by using the described procedure with a data set acquired for the pre-event status. Another possibility could be to use the attempt given by [Centeno et. al., 1999], where maps in combination with a laserscanning derived DSM are used to extract building contours automatically.

Within the areas of the building hypotheses a plane segmentation is carried out. The principle of the algorithm is to install a small seed plane, e.g. of 3x3 pixel, that build up a plane, i.e. the derivations between them and a equalized plane installed between them are sufficient low. Starting from this plane, the neighbouring pixels are examined according to their possible membership of the plane. This is done in a similar way as in the beginning. Thus, a new plane is computed of all points and the derivations are analysed to decide on the membership (see [Quint & Landes, 1996]). In this way the single surfaces of the building roof are established. They are used to find the building edges and corners by intersection of at first the planes and afterwards the detected edges. The geometrical primitives are then connected to CAD conform representation of the buildings. An example of a reconstructed building gained with that method is given in Figure 2.

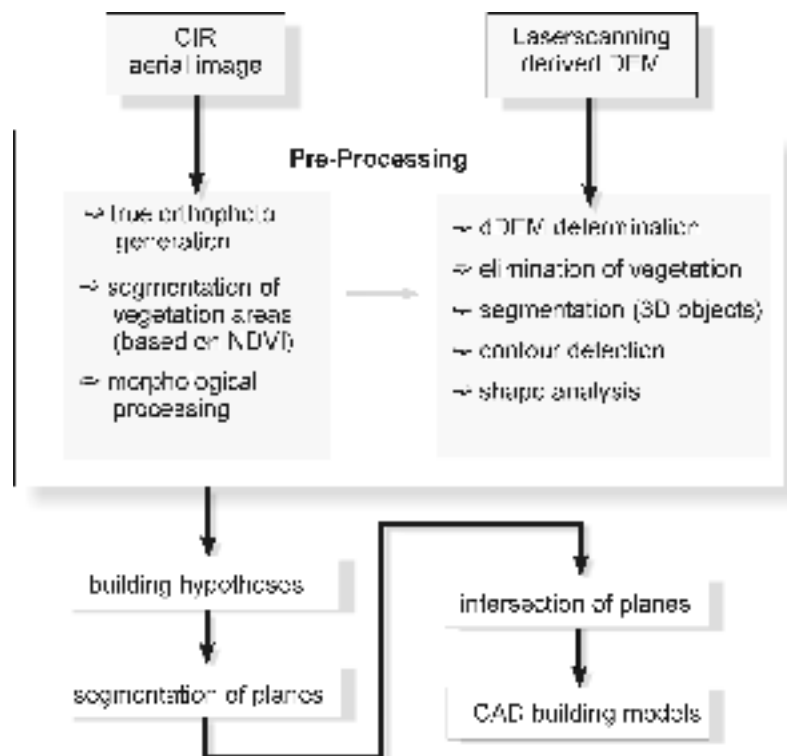


Figure 1: Principle of the building recognition and reconstruction process

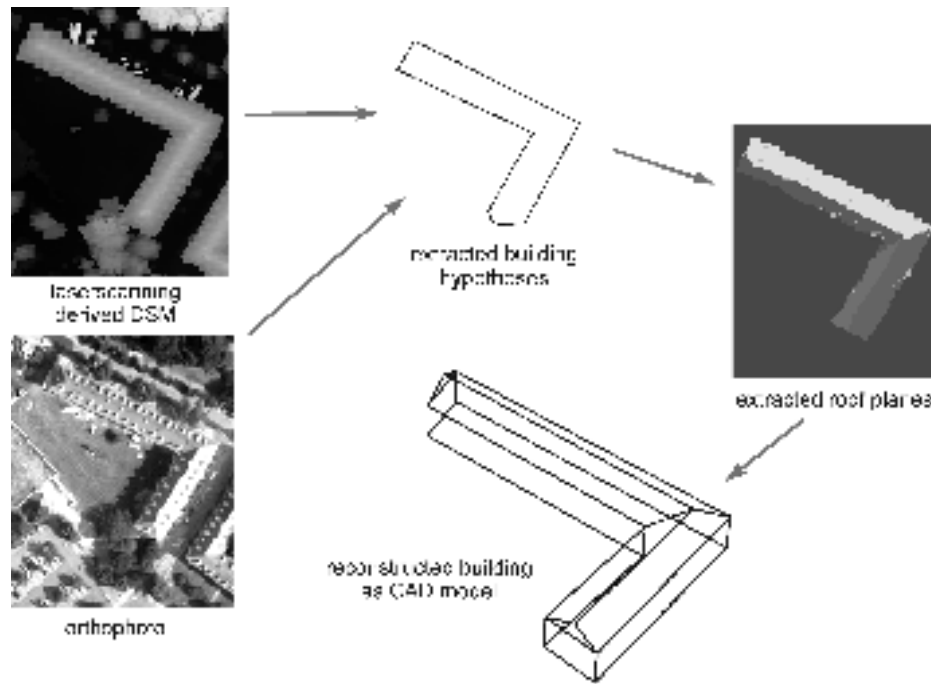


Figure 2: Example for the building recognition and reconstruction process

3.1.2 CHANGE AND DAMAGE DETECTION

Since the following has not yet been realized, these are first concepts that definitely need to be evaluated in the future. To detect changes in buildings two models are necessary, one derived from the pre- and one from the post-event status. The computation of the pre-event model can be done before the event with regard to the seismic risk of a urban region and is therefore time uncritical. This means that the model need not necessarily be gained by using the above mentioned methods. It can be interpreted by other methods as well, e.g. by using photogrammetry. However, what must be assured is a comparable resolution and use of at least equal accuracy of the model in order to be able to interpret occurring differences.

As in this application, not only changes but *damages* are in the focus. The change detection process has to be adopted accordingly. This means that "changes" means derivation of specific features of the both models. The most important one for rescue activities is the volumina change ([Markus et. al., 2000]), since conclusions about the stability and probability of finding in the damaged parts locked people alive can be drawn out of it. Other features refer to the surface planes, e.g. changes in orientation, size, shape or missing of planes.

To interpret the changes as damages additional knowledge is used. Damages at buildings are generally described based on damage classes. This may differ from country to country. A proposal for a summarization and internationally usable damage catalogue is given by [Markus et. al., 2000] (see Table 2).

Symbol	Damage pattern	Symbol	Damage pattern
	plane with angular voids		multi layer collapse
	pancake collapse		overturn collapse
	rubble heap / debris		outside debris, debris out of building borders
	high rise collapse patterns, first symbol is an additional attribute which can be used with the other symbols		

Table 2: Building damage patterns ([Markus et. al., 2000])

The changes will be related to one of the above damage patterns. For each single case, a combination of different damage patterns is possible. To give an example, a "pancake collapse" damage will be detected by interpreting the roof geometry to be almost unchanged, but significantly deeper at all corner points, as is seen in Figure 3. This is due to the fact that a whole floor can collapse uniformly, what happens e.g. with so-called "soft floors" characterized by too few or poor bearing elements, e.g. weak pillars.

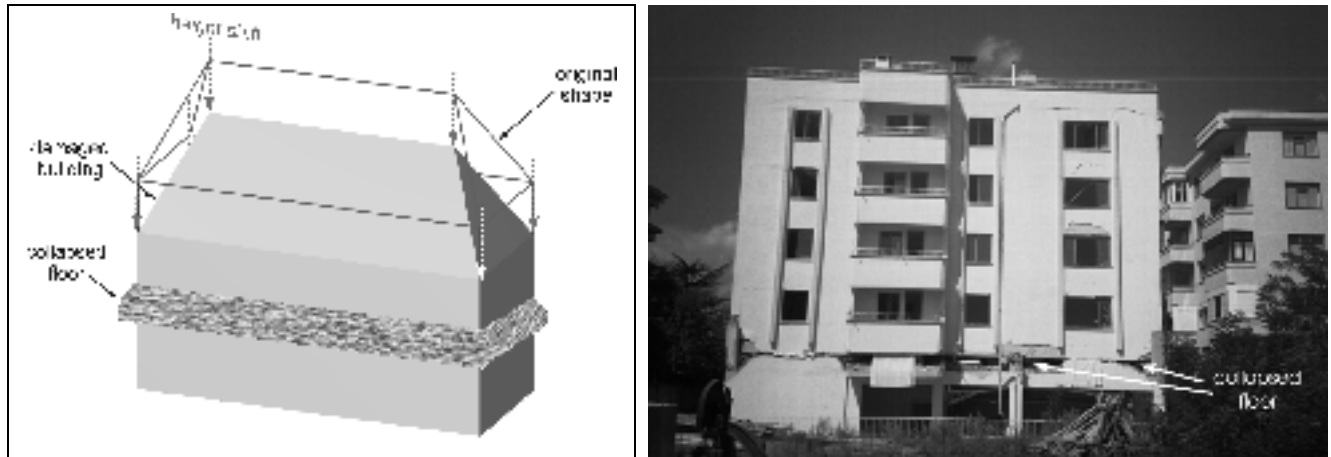


Figure 3: "Pancake collapse" damage, a whole floor collapsed; roof geometry rested almost unchanged, but building was significant shifted in height; left side: principle, right side: real example [Birgoren & Beyen, 2000]

3.2 ROADS

Roads play an important role for any disaster management. They are the life lines through which people can be provided with help in any form, e.g. support for recovery or medical help for injured persons. Their status after a catastrophe determines the accessibility of regions and therefore influences how much time will pass until help can arrive. These are two basic questions when planning the rescue activities, e.g. with a computer aided dispatch system. Such systems use a graph-based representation of street networks to navigate the resources. The used graph is generally built up based on maps or GIS information. Unfortunately, after a catastrophe this acquisition is not suitable since the street network could have been significantly destroyed. In the following chapters methods to acquire information about the actual status of the network will be given. The results can be used to built up a new graph for a computer aided dispatch system.

The principle process can be subdivided into two steps: In the first step, obstacles in the streets are detected. In this level the obstacles are represented as polygons in a two dimensional space. In the second step channels through these polygons are searched (see [Leebmann and Kiema, 2000]). These channels can be understood to represent the edges of the new graph.

A method to analyse the road status after an earthquake will be shown in the next section. Therefore eventual obstacles on the existing roads must be detected. This is done using a height analysis. With the knowledge about the barriers, the usability of the roads can be rated. If regions become inaccessible through the existing road network a search for alternative lanes, e.g. a lane through meadows will be done. This investigation is done without the usage of geometrical a priori knowledge. The only knowledge used is the information of the trafficability of different ground. These grounds are found by classification of spectral data and height information (see section 3.2.2).

The different grounds are represented as non overlapping polygons covering the whole campaign area. Nevertheless, this knowledge representation is not adequate for any planning of rescue measures. For this reason a shortest path search is applied to construct channels on which the resources can move most efficiently. Details of this are described in section 3.2.3.

3.2.1 DETECTION OF OBSTACLES ON ROADS

To detect obstacles on lanes the street network has to be known a priori, i.e. the status before the catastrophe. This information is generally available in one or the other form, e.g. by using existing GIS, maps or orthophotos. Since for this application only the 2D shape of the street borders must be known, it is much easier to create the pre-event data set as in the case of buildings where 3D representations must be available (see section 3.1). An example for the obstacle detection in which the street network was manually digitized in a orthophoto (see Figure 4) is discussed in this section. Although, the data does not show a damaged area nevertheless, "obstacles" like cars can be found even there.



Figure 4: Orthophoto with manually digitized street parts (white lines)

Obstacles on roads are objects, that differ in the height significantly from the street level. To give an example, a heap of stones is an obstacle in this context, whereas a plank is not. This is why a spectral analysis of the streets would not give meaningful results, even if it is of course, possible to detect objects being not part of the road. Therefore a DSM is analysed, preferably one computed from a last pulse laserscanning data set. This is because roads can be hidden by trees if using airborne sensors. In case of last pulse registration during a laserscanning flight, this effect is minimized since the laser light can often pass through the treetop, at least for broad-leaved trees (see [Steinle & Vögtle, 2000]). An example for such a data set is given in Figure 5. This represents the same region shown in Figure 4.

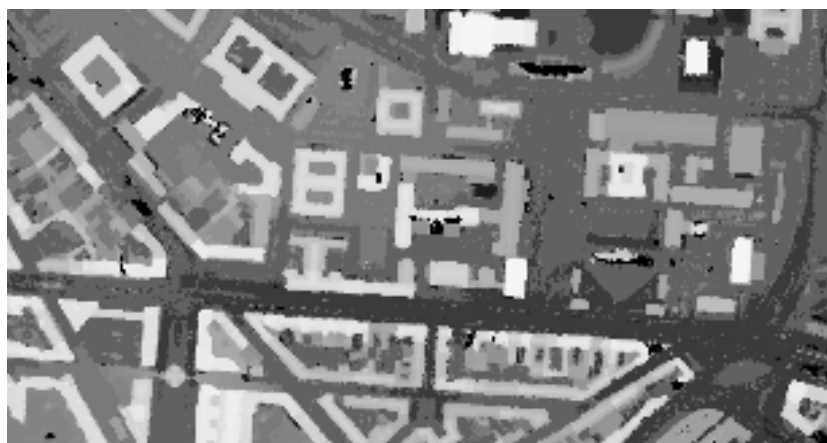


Figure 5: DSM computed from a last pulse laserscanning data set; intensity corresponds to elevation (brighter points are higher)

The obstacle detection is carried out by using the height plane segmentation algorithm also used for the roof plane segmentation in the building reconstruction process (see chapter 3.1.1). During this segmentation process the roads will be segmented in large parts and obstacles will occur as small "disturbing" elements on the larger planes. The result of the segmentation for the previous shown data set is given in Figure 6.

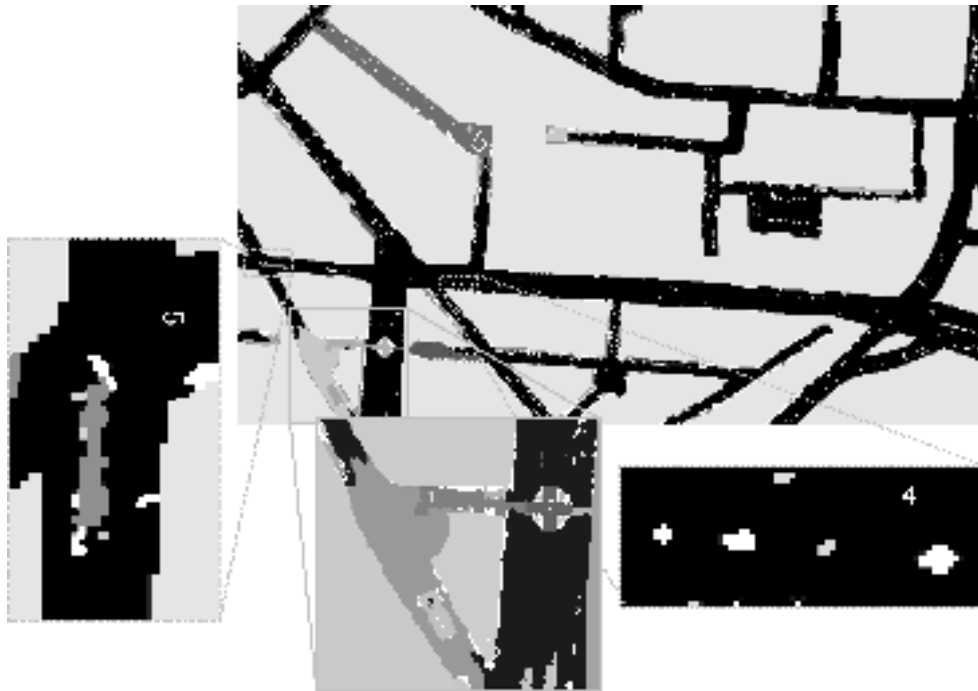


Figure 6: Obstacles (bright) on roads (dark);
 examples: ramp (1), roofage (2), bridge (3), cars (4), tram car (5);
 road with different slope (6)

In this example, the roads appear as dark areas and the obstacles as bright objects on the roads. Obviously, large parts of the street network were segmented as a single plane, indicated by the black colour. This is due to the fact that the terrain in this area is generally flat and by extension, the streets as well. Nevertheless, there are some exceptions, e.g. in the upper left corner of the image. Here a large part of a road was segmented into an extra plane (indicated by number 6), because it has a different slope. The same happened at a ramp to a bridge (indicated by the number 1).

Some obstacles were found on the roads, too. They are of different kinds, e.g. they are vehicles like cars (4) or tram cars (5). But also "immobile" objects exist, like bridges ((1) + (3)) or roofages (2). The last mentioned obstacle group does not stand on a real road, it is just a pedestrian zone. Since the roads were digitized from an orthophoto, such zones can possibly be included in the estimated street network.

It is obvious that with the described method it can not be guaranteed that the detected obstacles are real barriers. Numbers 1 and 3 belong to a bridge, the street underlying is of course passable. The bridge has a tower in the middle (3) which blocks the road space. But since the road consists of two different lanes running under the ramps (one is indicated with number 1), it is not a barrier. Such information can be collected e.g. through maps or knowledge of the site, and these objects should be treated in the same way as buildings, this means analysed according to possible damage. In such a case, the object will probably block the road. Other obstacles like cars are more difficult to handle. Of course, they do not normally block the usage of a road. One idea could be to recognize them as cars by using a "car model". Unfortunately, this will not work solely based on the used height data set since cars are generally not appropriately represented in it. It means that they do not occur always in the same way (see (4)), e.g. the size and shape highly depend on the measurement point distribution which is more or less random, since they are quite small compared to the image resolution. But an additional data set, e.g. a spectral one, acquired at the same time with the laserscanning data, could probably help to solve this problem by facilitating the analysis of several different features.

3.2.2 SEARCH SPACES FOR ALTERNATIVE LANES

Streets are not the only passable areas for vehicles. Depending on the kind of vehicle, other paths e.g. through meadows, gardens or fields might be used if the streets of an area are blocked. The search for alternative passages results therefore in a search of these grounds combined with path search algorithms.

In general, past experiences with digital imagery have demonstrated the limitation of using the spectral signature as the only image information in the separation of artificial objects. This is especially in the case of urban environments where ordinarily a diverse array of man-made objects have to be reckoned with. This happens e.g. where building roofs are

characterised by spectral reflectances similar to those exhibited by roads. This occurs often when both roads and the roofs are built from the same material or from material that exhibit similar spectral reflectance characteristics. In such cases, which occur rather often, it is not possible to distinguish between these two object features if only the spectral information is to be relied on (see [Kiema, 2000]) .

One possible way to overcome the above problem is to incorporate the object height information. This may be introduced, for example, through laserscanning derived DTM/DSMs. To facilitate the differentiation of the trafficable and non-trafficable areas, it is also important to extend the object feature base. This should seek to exploit not just the spectral but indeed also, the spatial characteristics of different objects. Against this background, this section focuses on a bottom-up, data driven approach that integrates both spectral and height image information to develop a semi-automatic approach for the extraction of trafficable areas.

In this study, the orthophoto already mentioned in section 3.1.1 is used (see Figure 7). A DSM obtained from the first pulse laser scanning measurements is then fused to the orthophoto through the additional channel concept described in [Haala & Walter, 1999].



Figure 7: Used orthophoto

The following object classes are defined: *Buildings*, *Trees*, *Grass*, *Roads*, *Pavements*, *Special*. The class *Special* is introduced in order to take care of the many miscellaneous object features of limited spatial dimension like cars, water-fountains etc. Training data is selected using manual digitisation and a conventional maximum likelihood classification is performed. The classes *Roads*, *Pavements* and *Grass* are then combined and a binary image is generated to highlight „feasible traffic lines“ as shown in Figure 8. Within the confines of this paper the above three object classes are defined as constituting potential candidates for „feasible traffic lines“.



Figure 8: Binary image highlighting potential candidates for feasible roads



Figure 9: Enhanced depiction of feasible roads

In order to reduce noise in the classified image, a dilation is carried out using a 3 x 3 mask (1 1 1;1 2 1;1 1 1). The various road features are then linked through the use of connected components and a subsequent filtering with an appropriate threshold, pre-selected from the average widths of roads in the test area. The binarised result is then dilated twice using the mask (1 1 1;1 1 1;1 1 1) resulting in Figure 9.

3.2.3 SHORTEST PATH ANALYSIS

Shortest path algorithms aim at finding a connection between two points under certain boundary conditions. "Shortest" must not necessarily mean the shortest geometrical distance. It can also be substituted by the least time needed for a travel or most economic way, e.g. lowest travelling costs. In this application, however, it will be understood as the fastest connection between the position of a tool needed for rescue measures and a "campaign area", i.e. an area where a damage occurred .

From an abstract point of view the geodesic line in the two dimensional space is searched. The geodesic line is a minimum of all path integrals over the length of the covered distance. In our case it is not possible to compute the integral directly because of the discontinuous polygonal space. For that reason this space is discretized into a finite number of discrete lines. The geodesic line is found by a discrete solution of this problem.

In case of simple obstacles that can not be passed, the minimum of all discretized integrals can be represented as a graph searching problem using the so called visibility graph (see [O'Rourke, 1998]). The visibility graph is constructed in the following manner: all nodes of the boundary polygons of the obstacles are used as nodes. This polygons can be gained e.g. based on the results of the alternative lane search, described in the previous chapter. A Delaunay net can be used to find the outer borders of the "non-trafficable" areas (compare [Vögtle & Schilling, 1997]).

All pairs of nodes that can "see" each other (the line of sight is not interrupted by an obstacle) are inserted as edges of the graph. The shortest path can now be determined for example with the method of Dijkstra (also described in [O'Rourke, 1998]).



Figure 10: Delaunay net derived obstacles borders (solid light grey lines) and results of some shortest path searches (black dashed line)

In **Figure 10**, this concept is demonstrated using buildings and trees as obstacles that cannot be manoeuvred through at all. The black dashed line represents the geodesic line in a plane with obstacles. This shortest path is now determined without using predefined channels, that means a priori street information.

4 CONCLUSION

In this paper, some applications for information extraction using laserscanning derived height data as a basic component are given. They have been developed with the focus on fast information derivation after severe catastrophes like strong earthquakes. This is because the lack of information is by far the biggest problem in such a crisis and influences the effectiveness of the rescue measures negatively. Hence, the more information is available for the planning of the rescue measures, the higher can be the effectiveness. The motivation for using laserscanning was at first based on its ability to deliver in quite a short time dense information about larger areas, in this case height information. The measurement values are digital and can be purified to a very high degree automatically (what also means fast), a essential point in such time critical applications. Another advantage is the greater robustness against bad weather and lighting conditions, compared to other air- or spaceborne sensors. The higher robustness makes it possible to use laserscanning in most cases, e.g. even at night, and it is therefore suitable to be a fully integrated part of a disaster management system.

Despite of advantages it has been recognized that laserscanning offers new possibilities. When using other sensors, the height component generally has to be computed for each point in a quite sumptuary way. Automation for example with photogrammetrical stereo image analysis is not that trivial. This is why up to now no similar dense height data sets can be derived from other methods as is possible with laserscanning within a short time. In addition, the "third dimension" increases the interpretability of changes of man-made objects significantly and makes it possible to rate them into damage classes. This is important information in order to facilitate an appropriate rescue measure operation.

The applications described in this paper, show that not only building damages can be determined by comparing pre- and a-posteriori geometrical models, but also the status of roads can be proofed, i.e. by detecting obstacles in streets. Up to now, these can not be interpreted accordingly to be a "true barrier" as building debris or to be mobile objects which will block a road only temporarily, like cars. Further investigations still need to be carried out in this field.

Another new application is the detection of trafficable ways from post-event data. This can potentially shorten the time for initiation of rescue measures at the campaign areas since the accessibility can be estimated and the fastest ways to reach a region can be found, even on alternative paths if necessary.

To summarize the above, laserscanning is not only a tool that can be used as good as any other in a case of disaster, but rather a sensor to get information that can not be acquired by other means.

5 REFERENCES

- Birgoren, G. and Beyen, K., 2000:** "*General Building Damage in Duzce-Bolu*". Photographs published online in Internet, URL: <http://www.koeri.boun.edu.tr/earthqk/duzce.htm> [Cited 2001-02-06].
- Casciati, F., Gamba, P., Giorgi, F., Marazzi, A. and Mecocci, A., 1997:** "*A Flexible Environment for Earthquake Rapid Damage Detection and Assessment*". In: Proceedings of IGARSS '97: "Remote Sensing - A Scientific Vision for Sustainable Development.", IEEE International, Volume: 1, 1997, pp. 113 – 115.
- Centeno, J. S., Kishi, R. T. and Bähr, H.-P., 1999:** "*Recognition of Buildings Using Scanned Maps and Laser Scanner Altitude Data*". In: PFG, Journal of the DGPF, Vol. 1/1999, E. Schweizerbart'sche Verlagsbuchhandlung, Stuttgart, Germany, 1999, pp. 19 - 27.
- Comfort, Louise K., 2000:** "*Information Technology and Efficiency in Disaster Response: The Marmara, Turkey Earthquake, 17 August 1999*". In: Quick Response Report # 130, Natural Hazards Center at the University of Colorado, Boulder, USA. Published online in Internet, URL: <http://www.colorado.edu/IBS/hazards/qr/qr130/qr130.html> [Cited 2001-02-01].
- CRC 461, 2001:** *Collaborative Research Center 461: " A Challenge for Geosciences and Civil Engineering"*. Online in Internet: <http://www-sfb461.physik.uni-karlsruhe.de> [Cited 2001-02-01].
- Förstner, W., 1999:** "*3D-City Models: Automatic and Semiautomatic Acquisition Methods*". In: Fritsch, D. and Spiller, R. (eds.): Photogrammetric Week '99. Published by Wichmann, Karlsruhe, Germany, 1999.
- Haala, N. and Walter, V., 1999:** "*Automatic Classification of Urban Environments for Database Revision using Lidar and Colour Aerial Imagery*". In: International Archives of Photogrammetry and Remote Sensing, Vol. 32, Part 3/1, 1999, pp. 76-82.
- Hasegawa, H., Yamazaki, F., Matsuoka, M. and Sekimoto, I., 1999:** "*Determination of Building Damage due to the 1995 Hyogoken-Nanbu Earthquake using Aerial HDTV Images*". In: Proceedings of Second Conference on the Applications of Remote Sensing and GIS for Disaster Management, The George Washington University, CD-ROM, 1999.
- Hecker, Edward J., Irwin, William, Cottrell, David and Bruzewicz, Andrew, 2000:** "*Strategies for Improving Response and Recovery in the Future*". In: Natural Hazards Review, Vol. 1, No. 3, August 2000.
- Kiema, J.B.K., 2000:** "*Wavelet Compression and Data Fusion: An investigation into the Automatic Classification of Urban Environments using Colour Photography and Laser Scanning data*". In: Proceedings of the 15th International Conference on Pattern Recognition, Barcelona, Spain, 2000. Published by the IEEE Computer Society. Vol. 3, 2000, pp. 89-93.
- Leebmann, J. and Kiema, J.B.K., 2000:** "*Knowledge Representation in Technical Information Systems for Earthquake Loss Mitigation*". In: Proceedings of Euro conference on global change and Catastrophe Risk Management: "Earthquake Risks in Europe ". Published on CD-ROM; Laxenburg, Austria, 2000.

- Lohr, U., 1999:** "*High Resolution Laser Scanning, not only for 3D-City Models*". In: Fritsch, D. and Spiller, R. (eds.): Photogrammetric Week '99. Published by Wichmann, Karlsruhe, Germany, 1999.
- Lohr, U. and Eibert, M., 1995:** "*The TopoSys Laser Scanner-System*". In: Fritsch, D. and Hobbie, D. (eds.): Photogrammetric Week '95. Published by Wichmann, Heidelberg, Germany, 1995.
- Markus, M., Fiedrich, F., Gehbauer, F. and Hirschberger, S., 2000:** "*Strong Earthquakes, Rapid Damage Assessment and Rescue Planning*". In: Kowalski, K.M. and Trevits, M.A. (eds.): Proc. of the 7th Annual Conference of the International Emergency Management Society: "Contingency, Emergency, Crisis, and Disaster Management: Emergency Management in the Third Millennium", Orlando, Florida, May 1999; published in 2000, pp. 369-378.
- Matsuoka, M. and Yamazaki, F., 1999:** "*Characteristics of Satellite Images of Damaged Areas due to the 1995 Kobe Earthquake*". In: Proceedings of Second Conference on the Applications of Remote Sensing and GIS for Disaster Management, The George Washington University, CD-ROM, 1999.
- O'Rourke, J., 1998:** "*Computational geometry in C*", 2nd ed. Published by Cambridge University Press, 1998.
- Quint, F., Landes, S., 1996:** "*Colour aerial image segmentation using a Bayesian homogeneity predicate and map knowledge*". In: International Archives of Photogrammetry and Remote Sensing (IAPRS), Vol. XXXI, Part B3, Vienna, Austria, 1996, pp. 663-668.
- Steinle, E. and Vögtle, T., 2000:** "*Effects of different laser scanning modes on the results of building recognition and reconstruction*". In: IAPRS, Vol. XXXIII, Part B3, Amsterdam, The Netherlands, 2000, pp. 858-865.
- Vögtle, T. and Schilling, K.-J., 1997:** "*An approach for the extraction of settlement areas*". In: Grün, A., Baltasvias, E.P.: "Automatic Extraction of Man-Made Objects from Aerial and Space Images (II)", Proceedings of the Centro Stefano Franscini (Ascona), Birkhäuser Verlag, Basel, 1997, pp. 333-342.
- Vögtle, T. and Steinle, E., 2000:** "*3D Modelling of Buildings using Laser scanning and Spectral Information*". In: IAPRS, Vol. XXXIII, Part B3, Amsterdam, The Netherlands, 2000, pp. 927-934.

Decision support system for flood risk analysis for the River Thames, United Kingdom

Sanders, R. and Tabuchi, S.

This paper can not be published as an OEEPE paper as it was taken out of another publication. However, the paper can be found in PE&RS Journal, American Society for Photogrammetry and Remote Sensing:

Sanders, R and Tabuchi, S. (2000). Decision support system for flood risk analysis for the River Thames, United Kingdom. Photographic Engineering&Remote Sensing. 66 (10). pp. 1185 - 1193.

SURVEYING OF ZONES AT RISK OF LANDSLIDE BY LASER SCANNING. REPEATABILITY AND ACCURACY ANALISYS.

maurizio Barbarella & carmine Fazio

DISTART - University of Bologna. maurizio.barbarella@mail.ing.unibo.it
carmine.fazio@mail.ing.unibo.it

Abstract

The aim of this work is to study the potentiality of Laser scanning to carry out detailed surveying of zones at risk of landslide characterized by gully of steep slope.

By using adjacent strips characterized by a large overlapping, it has been possible to evaluate the internal compatibility, on the intersection area, among them. It has been defined a procedure that has allowed to work on the whole strips, solving the problem related to the huge amount of acquired data. There have been quantized the difference of altitude in the overlapping zone, in such a way to obtain the raster for a first rough visual control. Having made this preliminary control there have been examined reduced zones of relevant interest. There were individuated artefacts on narrow gully near the strip boundaries, probably due to problems related to the sensor position. The laser data corresponding to these zones have large internal discrepancies.

Besides the relative discrepancies on the overlapping zones, absolute discrepancies have been estimated comparing the laser data to the ground control points surveyed with consolidated techniques. In order to carry out this calculations there have been chosen several test zones characterized by the morphological type and by the presence of elements of anthropical origin, as for instance drainage canal, houses, etc.

1. Introduction

Within the framework of the Italian National Research Project financed by the Italian Ministry of the University project, the University of Bologna, the University of Cagliari and the Naval Institute of Naples realized a campaign of measure in order to investigate the potentiality of laser scanner to carry out surveying of landslide slopes.



Figure 1 - Landslide of Bracigliano (Italy).

For this goal a detailed surveying carried out over zones at risk of landslide characterised by gully of steep slope. The check area covers the landslide slope close to Bracigliano (Italy) (Figure 1). The analysis of the data is reported in this paper.

The initial project foresaw two laser flights: a high one, characterized by a flying height of 195 meters and a low one characterized by a flying height of 105 meters. Because of reception problems of the GPS signal it has not been possible to complete the project. Instead only one flight without instrumental guide took place. The laser beam used is a TopEye system, with a frequency of sampling of 7000 Hz setup on helicopter. Both, first and last pulse echoes were recorded. The flying height was about 100 m and the maximum scanner angle of 40°. The data set consists of 8 strips, which have big overlapping zones. The width of each strip is about 70m with a density of 15 points per square meter.

To verify the accuracy there have been used ground control points (*GCP*) measured by GPS methodology integrated with classical methodology. The classical methodology has been used to survey the points within the forest area and on the walls of the gully. For this, it has been used a special total station that works also without the target-reflector.

The co-ordinates of the ground control points have been calculated in the GPS reference system, since it is the reference frame used for the laser surveying. Figure 3 shows an extract of the laser strips of the area surveyed with terrestrial methodology.

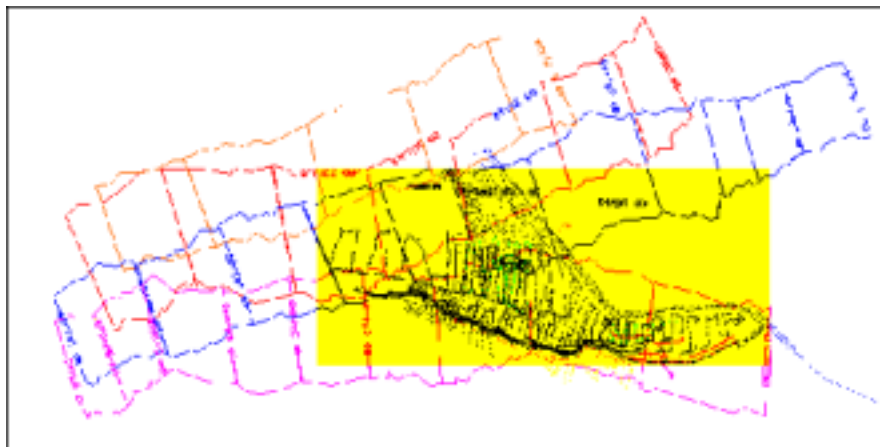


Figure 2 - Strips on the control zone.

2. Control internal congruence of the strips

On the overlapping zones there have been performed some tests to verify the congruence between the strips (internal congruence). The height discrepancy among the points belonging to the overlapping zones has been considered to calculate the internal congruence.

For a systematic study of these differences it is necessary to work on entire strips. This would mean to work with an amount of data of the order of the million, so it would take too long to perform numeric controls.

Thus in order to speed up the routine, a procedure that foresees a visual control to individuate possible anomalous zones where to concentrate has been followed.

The steps of this procedure can be summarized as:

- Individuation of the overlapping zones;
- Sampling of the points belonging to these zones;
- Interpolation of the data in order to obtain a regular grid (grid spacing 1 m);

- Computation of the difference grid;
- Quantization of the difference grid at 24 bits in order to get a colored raster;
- Choice of reduced zones to perform numerical controls.

This numerical control consist in calculating the height differences by a dense grid. For this purpose there have been realized the following operations:

- Interpolation of the points belonging to one of the strips (i.e. "a") on a regular grid (grid spacing 25 cm) using the Kriging algorithm;
- Calculation of the height residual values of the points belonging to the overlapping strip (i.e. "b").

The software used in order to realize this control were two: the TerraScan to obtain the colored raster and the Surfer v.7 to perform the numerical control.

2.1 Overlapping zone between strips "a" with "b"

After having individuate the overlapping zone of these two strips it has been obtained the raster of the height differences (Figure 4). It becomes evident from the analysis of the raster that the differences in quota remain constant almost everywhere except on the zone inside the red rectangle. In Figure 5, it is shown a zoom of the interested zone.

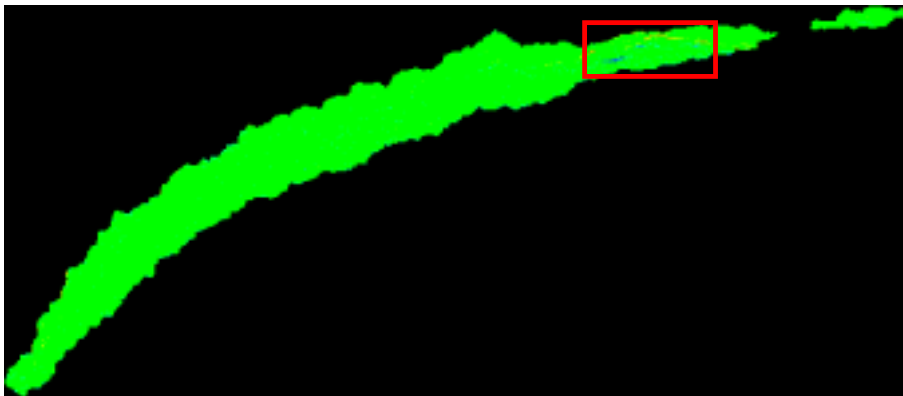


Figure 3 - Rasterisation of the differences in quota on the overlapping zone between strips 1 and 5.

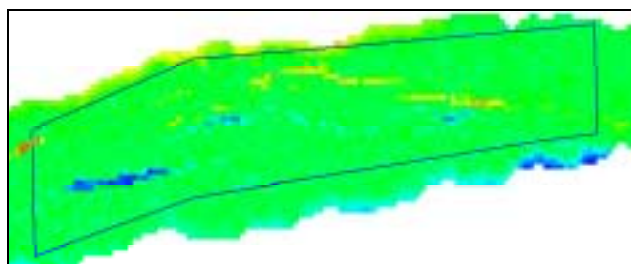


Figure 4 - Zoom of the interested zone

From the Figure it can be observed that both, the blue pixels and the orange ones follow a certain order, as if they were lying on a pattern.

For a most accurate control on this zone there have been calculated the residual values. For this purpose there have been resampled the data inside the polygon (see figure 4). The grid size was of 25 cm and the Kriging algorithm was the one used. The statistics of the height differences are shown in Table 1. In Figure 6 it is shown the 3-D model of the differences.

From the Table it is observed that the average of these differences is -18 cm, the standard deviation is 66 cm, and the maximum values is just higher than 5 m. Further controls have been made on the contour lines. These are visualized on the same layer (see Figure 6).

Zone inside the polygon	
Check points	7379
Mean (m)	-0.18
Standard Deviation (m)	0.66
Max (m)	5.17
Min (m)	-4.66

Table 1 - Statistics relative to height differences.

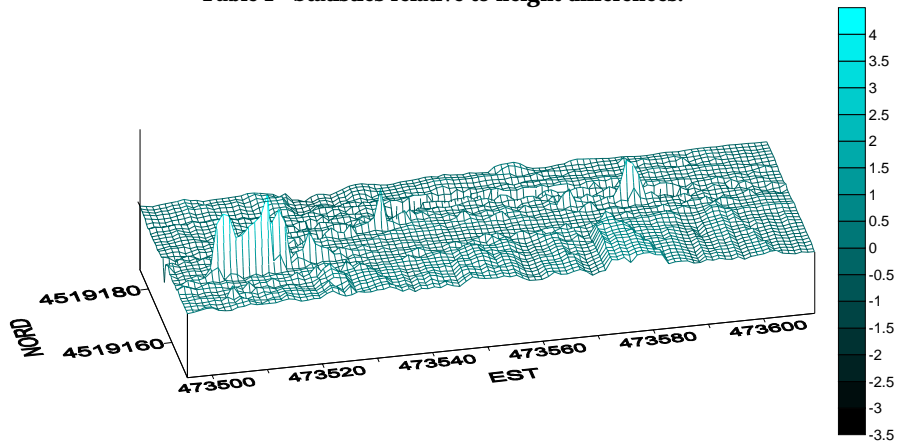


Figure 5 - 3-D model of the height differences in meters.

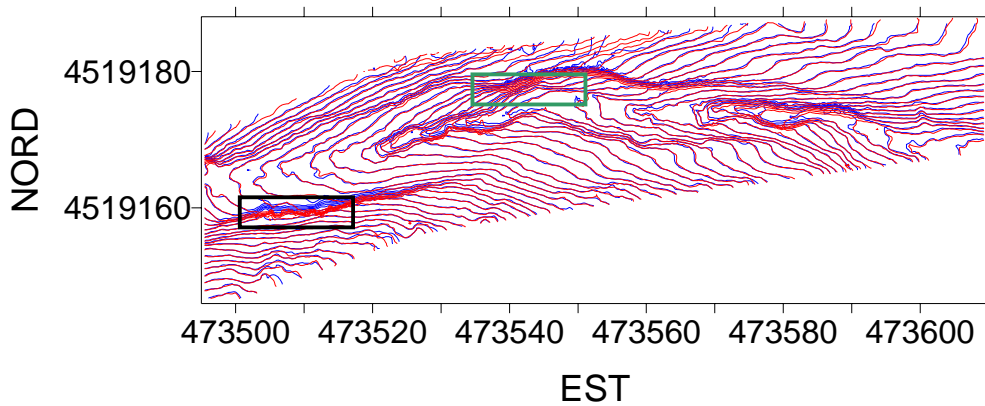


Figure 6 - Contour lines. The red ones belong to strip 1, the blue ones to strip 5.

From the Figure it is observed that the data covers a very narrow gully and it is evident that where the pixels follow a regular structure (see raster) the contour lines are very close. A zoom of the green patch is shown in Figure 7 and of the black patch in Figure 8.

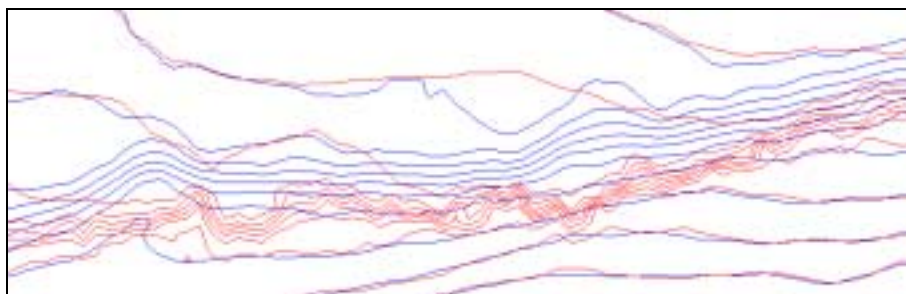


Figure 7 - Detail of contour lines of the patch on the north wall of the gully.

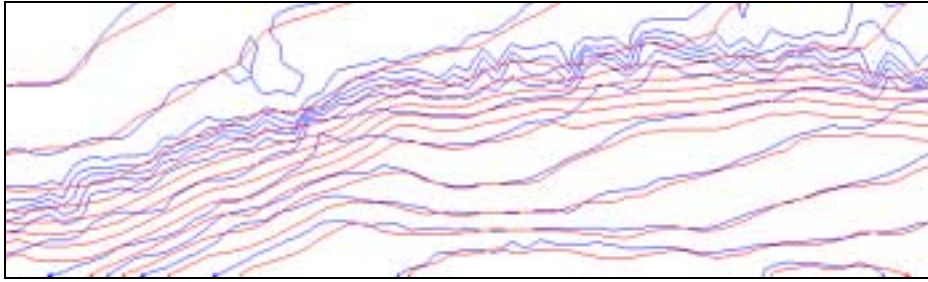


Figure 8 - Detail of contour lines of the patch on the south wall of the gully.

Analyzing the two patches it is observed that there are artefacts on the two opposite sides of the gully. While on the north wall (Figure 7) the artefacts (see red contour lines) are generated with the laser data belonging to the strip 1, on the south wall (Figure 8) the artefacts (see blue contour lines) are generated with the laser data belonging to the strip 5. These artefacts are related to the sensor position, since the narrow gully, where the artefacts were found, are located close to the respective strip boundaries. In order to explain this phenomena it is shown (Figure 9) a simple sketch that relates the sensor position with the target object to earth.

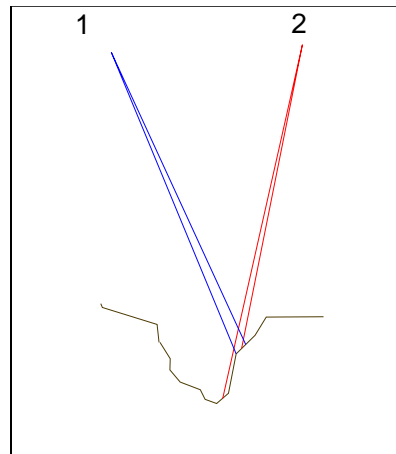


Figure 9 - Influence of the sensor position on the object resolution.

From the sketch it is observed that performing the laser surveying of the right side of the gully with the sensor in position "2" one faces two problems: the first one called "shade effect" caused by the presence of morphological prominences that obscure the zones situated on lower levels; the second one linked to the increase of the footprint size, that depends on the terrain slope and on the instantaneous scan angle (Baltavias 1999). Analogously if the sensor is positioned at 1 the same problems occur on the left side of the gully.

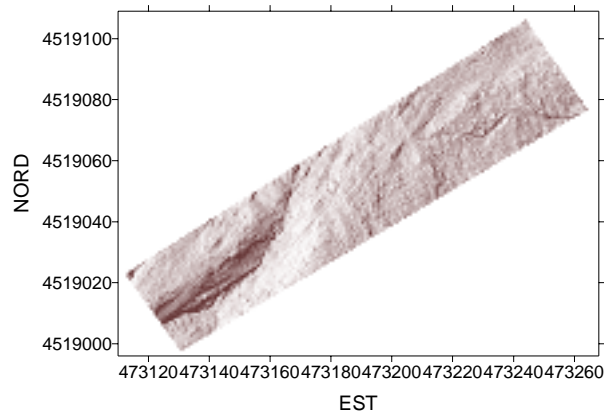


Figure 10 - Surface obtained with Lambertian reflection of a test zone.

Latter several congruence tests have been performed on other sampled zones where anomalies had not been found during the first visual control. On these zones the congruence tests gave good

results. In Figure 10 it is shown one of these zones. In table 2 it is reported the statistics of the height differences. Here it can be observed that the average of the height differences is -1 cm with a standard deviation of 6 cm. The maximum absolute value of the height differences is not higher than 85 cm.

Other standard zone	
Check points	63609
Mean (m)	-0.01
Standard Deviation (m)	0.06
Max (m)	0.85
Min (m)	-0.60

Table 2 - Statistics of the height differences

3. Control external congruence (Accuracy)

In order to verify the accuracy there have been used 7983 *GCPs* measured by GPS methodology integrated with classical methodology. Since the accuracy of the laser point depends also on the footprint size and on the morphological characteristic of the target, the control zone has been divided in homogeneous zones characterized by the morphology and by the presence of vegetation.

The punctual comparison is not practicable thus it has been preferred to interpolate the laser data on a regular grid in order to get a laser surface, and then calculate the height residual values by using the *GCPs*.

The interpolator and the grid size influences the residual value. There, three algorithms implemented into Surfer v.7, were been investigated: the Natural Neighbor, the Triangulation with Linear Interpolation and the Kriging. Between these it has been chosen the Kriging algorithm, because it is considered more robust to elaborate these laser data points. The grid size has been chosen of 25 cm according to the dense laser point. However there have been carried out several tests on reduced zones starting from a grid spacing of 1 meter up to 10 centimeters, and for each grid size there have been calculate the residual values on the original mass points. The results confirm that this was a good choice, since the average of the residual value is minimum.

3.1 Accuracy tests on several zones

The check area containing the *GCPs* was subdivided into smaller zones and the statistics of the residual were computed for each group. The criteria used in order to subdivide the check area in according to the morphology, the presence of anthropical element and the presence of vegetation. It is reported below the test zones:

- Flat zone;
- Zone characterized by medium slope (about 50 %);
- Gully;
- Edge gully;
- Forest zone;
- Drainage canal.

In Figure 11 it is shown the map of the test zones.

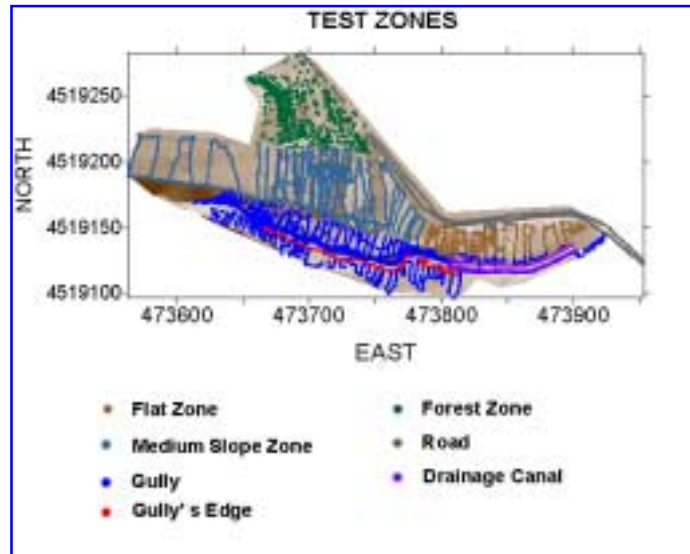


Figure 11 - Map of the test zones.

Before performing the tests on each zone, it has been carried out a global test on the whole check area reported in Table 3. In Figure 13 it is shown the distribution of height differences.

accuracy	
Check points	7973
Mean (m)	0.06
Standard Deviation (m)	0.28
Max (m)	2.23
Min (m)	-2.46

Table 3 - Statistics of height residual (whole check area).

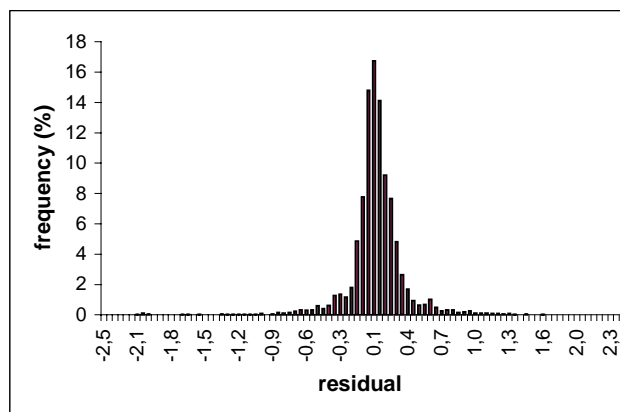


Figure 12 - Histogram of height residual (whole check area).

From the Table it is observed that the residual mean value of the ground control points respect to the grid obtained with data laser are of 6 centimeters with a standard deviation of 28 centimeters. Almost all the residual are inferior in absolute value to 0.7 meters (see histogram).

Afterwards the external congruence test have been performed on each test zone. The results obtained are reported below.

Accuracy (cm)			
Zone	GCP	Mean	Std Dev
Check area	7973	6	28
Flat zone	724	0	12
Zone with slopes (about 50%)	548	9	14
Gully	4663	4	43
Forest zone	172	0	7
Gully Edge	183	6	15
Drainage canal	775	17	21

Table 4 - Results accuracy test

It can be observed from the table that the forest zones and the flat zone are characterized by minimum residual values. The maximum difference of 17 cm is found on the points belonging to the drainage canal, however the maximum standard deviation is obtained on the gully (43 cm).

In what follows it is reported into detailed two of the zones, between the most meaningful: the gully important from the view point morphological and the forest zone important for the study of the last echo. The grid size and the algorithm used are those mentioned above.

3.1.1 Gully

On the gully 4663 ground control points have been surveyed. The gully sides were surveyed with the total station without the reflector as target. Table 5 shows the results obtained comparing the GCP with the grid laser data. In Figure 14 it is shown the distribution of the height residual.

Gully	
GCP	4663
Mean (m)	0.04
Standard Deviation (m)	0.43
Max (m)	4.59
Min (m)	-4.28

Table 5 - Statistics of the height differences.

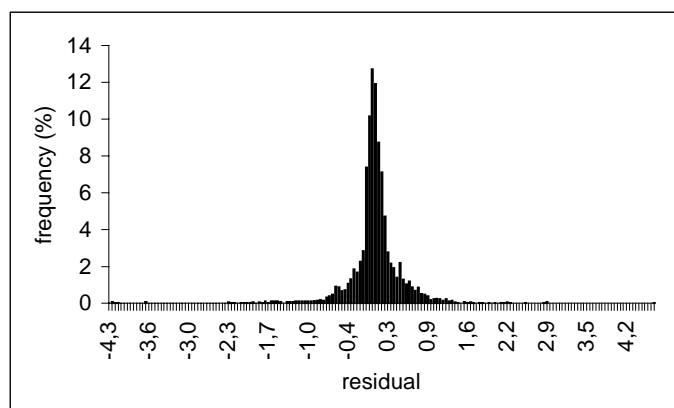


Figure 13 - Histogram of the height differences

It can be observed from the table that the mean values of the residuals is 4 cm with a standard deviation of 40 cm. This big standard deviation value is due to the presence of residual higher than

4 meters. The presence of this big discrepancies located on the practically vertical side of the gully could be cause by error due not only to the laser methodology but also to the terrestrial methodology.

3.1.2 Forest zone

This zone is characterized by terraces with high and dense vegetation. In this zone 172 *GCPs* have been surveyed by classical methodology. Furthermore other 151 points belonging to the trunks of the trees have been surveyed in order to get supplementary controls. To compare the data in this zone it has been made a preliminary accurate editing on the laser data.

Table 6 shows the results obtained from this comparison. In Figure 15 it is shown the distribution of the height residuals.

Forest zone	
Check points	172
Mean (m)	0
Standard Deviation (m)	0.07
Max (m)	0.25
Min (m)	-0.32

Table 6 - Statistics of the height differences.

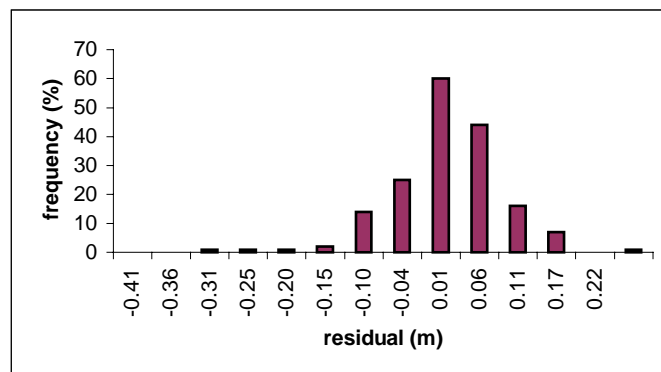


Figure 14 - Histogram of the height differences

It can be observe from the table that the mean value of the residual is practically zero. The standard deviation is 7 centimeters and the maximum absolute residual value is just higher than 0.30 cm.

These results somehow are surprising, one could suspect that the accuracy of the laser tecnology is not influenced by the presence of vegetation.

4. Conclusion

In this field the use of the laser scanner on helicopter allowed to obtain accurate DTM. The experiment has been done on a landslide slope characterized by morphological complexity. There are narrow gullies with steep slope, a drainage canal and the area near the edges of the gully is covered by dense vegetation. The high density of sampling (at least 15 points per square meter) permitted the detailed reconstruction of this morphological elements.

The control of the internal congruence between overlapping strips shows that the two DTMs coincide, because the height discrepancies are minimum. Instead in the particularly difficult zones, for example narrow gullies, there have been found out big differences. These discrepancies are

linked to the sensor position since the narrow gullies, where the bigger height differences were found, are located close to the boundary strip.

The comparison with the terrestrial surveying, in order to get external discrepancies, has given good results. In the flat zones with or without presence of vegetation there are practically no discrepancies. Here the standard deviation is of 10 cm. Instead in the rough zones, for instance gully and drainage canal, the average differences reach 17 cm with a standard deviation of 40 cm.

References

Ackermann F., 1999. Airborne laser scanning present status and future expectations. *ISPRS Journal of Photogrammetry and Remote Sensing*, 54(2-3), pp. 64-67.

Baltsavias, E., 1999. Airborne laser scanning: basic relations and formulas. *ISPRS Journal of Photogrammetry and Remote Sensing*, 54(1), pp. 199-214.

Behan, A., 2000. On the Matching Accuracy of Rasterised Scanning Laser Altimeter Data. 19th ISPRS Congress, Amsterdam.

Favey, E., 2000. Surface modelling for alpine glacier monitoring by airborne laser Scanning and digital photogrammetry.

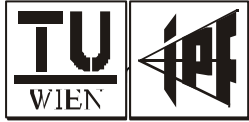
Gomes Pereira, L.M., Janssen, L.L.F., 1999. Suitability of laser data for DTM generation: a case study in the context of road planning and design. *ISPRS Journal of Photogrammetry and Remote Sensing*, No.54, pp.244-253.

Kraus K., Pfeifer N. 1998. Determination of terrain models in wooded areas with airborne laser scanner data. *ISPRS Journal of Photogrammetry & Remote Sensing*, Vol 53. n. 4, August 1998, pp. 193-203.

Maas, H.-G., 2000. Least-Squares Matching with Airborne Laserscanning Data in a TIN Structure. 19th ISPRS Congress, Amsterdam.

Petzold, B., Reiss, P. and Stössel, W., 1999. Laser scanning - surveying and mapping agencies are using a new technique for the derivation of digital terrain models. *ISPRS Journal of Photogrammetry & Remote Sensing* 54(2-3), pp. 95-104.

Saab, 2000. TopEye. <http://www.combitech.se/survey/index.html>.



Gottfried Mandlbauer
Institute of Photogrammetry and
Remote Sensing
Vienna University of Technology
Gusshausstraße 27-29

1040 Wien

Austria

Tel.: +43-1-58801-12235
Fax.: +43-1-58801-12299
e-Mail: gm@ipf.tuwien.ac.at

Herbert Brockmann
German Federal Institute of Hydrology
Department Geodesy

Kaiserin-Augusta-Anlagen 15-17

56068 Koblenz

Germany

Tel.: +49-261-1306-5214
Fax.: +49-261-1306-5280
e-Mail: brockmann@bafg.de

Vienna / Koblenz, in February 2001

Paper – OEEPE-Workshop:

**Airborne Laser-scanning and Interferometric SAR for Detailed Digital Elevation
Models**

Stockholm, 1 March to 3 March 2001

**Modelling a watercourse DTM based on airborne laser-scanner data –
using the example of the River Oder along the German/Polish Border**

1 Introduction

In July and August 1997, an extreme flood event occurred on the River Oder, inflicting vast economic damages on all the riparian states: the Czech Republic, Poland and Germany (LAUSCHKE, OPPERMANN, 1998). To be better prepared in future events of this kind and to

avert damages, numerous preventive activities have been implemented in the past few years or were initiated at least. This comprises not only constructive measures (e.g. maintenance and strengthening of flood defences) and improved disaster prevention. Moreover, advanced hydraulic models for flood-flow and low-flow forecasting or scenario simulations should be developed.

Many of these preventive actions depend on modern, highly detailed geo-data as an indispensable prerequisite. In the German point of view, priority was due in this context to the development of digital terrain models (DTMs) of the River Oder along the German/Polish border (*Grenzoder*) including the so-called Westoder.

2 The project "Watercourse DTM of the *Grenzoder*"

2.1 Background

The end-users requested two kinds of DTMs.



Fig.1: General map – DTM-W of the *Grenzoder*

Especially the water managers in the *Land Brandenburg* demanded an up-to-date DTM of 5-m grid size of the areas protected by dykes on the German territory. These specialized demands are equivalent to a standard product of the Brandenburg State Mapping Authority (*LVermA*), also for a larger area. Therefore the project area was extended to 3,075 km².

Moreover, an up-to-date DTM of the watercourse (DTM-W) was needed in any case. This DTM-W had to describe the flow-effective area of the riparian forelands as well as the riverbed. Regarding the reaches of the Westoder with a length of 17 km and the *Grenzoder* with 163 km, this meant that essentially the area between the dykes covering some 273 km² both on Polish and German territories had to be surveyed and modelled (cf. Figure 1). Main users of the DTM-W are the Brandenburg State Office for Environment (i.e. the supreme water-management authority), the Waterways and Shipping Office (*WSA*) Eberswalde (responsible for operation and maintenance of Federal

waterways), and the Federal Institute of Hydrology (*BfG* - the scientific institution of the Federal government in the fields of hydrology, water-resources management, and conservation of waters) and the respective authorities on the Polish side. The DTM-W is especially needed for the development and operation of a water-level forecasting model and the updating of data on the riparian forelands and the documentation of the state of the

groynes¹. The following paper gives a detailed description of the model development in view of the particular important requirements on the DTM.

The demand for the two DTMs led to a joint project between the *LVermA* and the *BfG*. The aim was to bundle as many sub-tasks as possible. For economic considerations the project partners agreed to use the airborne laser-scanning technique for acquisition of the terrain data (BROCKMANN, 2000).

2.2 Requirements on the watercourse DTM

The acquisition of the terrain data and the processing of these measured data before the DTM-W modelling that were commissioned to a consultancy. The partially very high requirements are summarized as follows:

- Density of measuring points: $D_P < 1$ point per 2 m x 2 m grid cell;
- Hydrological boundary conditions; i.e. airborne data acquisition:
 - at low-flow conditions;
 - in the no-growth season, if it is possible after the first frost at the ground;
 - during absence of ice or snow covers;
- Classification (filtering), i.e. separation of laser points:
 - of the riparian forelands;
 - of the flow-effective built structures;
 - of the water surface;
- Criteria for quality checks; limit for differences in elevation ($d = \text{rated value} - \text{actual value}$) with a probability of $p = 95\%$:
 - flat to slightly sloped terrain with sparse vegetation: $d = 0.20$ m;
 - flat to slightly sloped terrain with dense vegetation: $d = 0.40$ m;
 - steeply sloped terrain with sparse vegetation: $d = 0.50$ m.

The DTM-W areas of the covered terrain with ground points should be modelled at least in 2-m grid-cell size. This necessity is mainly due to the required highly resolved reproduction in the DTM-W of the riparian forelands and of the groynes in the *Grenzoder*. Out of the DTM-W, longitudinal groyne sections should be derived (cf. Figure 2). The final settings for the DTM computation should be performed only after the assessment of the data material collected in the flight missions.

The riverbed should be modelled along the river axis on the basis of echo-sounder data along cross sections measured in one epoch (cf. Figure 6.). Ground measurements of the forelands at these cross sections were not available. Because of the intensive, short-cycled

¹ Groynes are structures built transverse to the direction of flow into the river; their main purpose is acceleration of flow to minimize sediment deposits in the main channel (fairway); a secondary effect is a slight increase of the water level.

morphodynamics of the Oder riverbed, this density was considered sufficient. Since these cross sections covered the groyne fields only slightly, their description had to be made by laser-scanner data as far as possible.

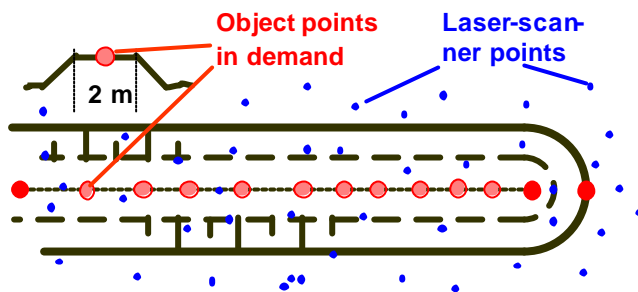


Fig.2: Groynes of the *Grenzoder* with intended laser-point density (to scale)

The DTM-W had to be modelled from the laser-scanner data of the riparian forelands, the groynes and the areas of the groyne fields fallen dry (cf. Figure 3) as well as the echo-sounder data of the riverbed in such a way that all these areas are reproduced as realistically as possible. It should be possible to derive cross sections at every location. Consequently, the Delaunay-Triangulation, which is frequently used in hydrology, could not

be used without appropriate pre-treatment of the data. The program system SCOP was chosen with the special developments (i.e. the morphistic cross-sections fitting) resulting from the *BfG* pilot project "Hydrological GIS-Saar" on the river Saar (BROCKMANN, KRAUS AND MANDLBURGER, 2001). For more details, refer to Chapter 4.1.

3 Database

3.1 Terrain Data

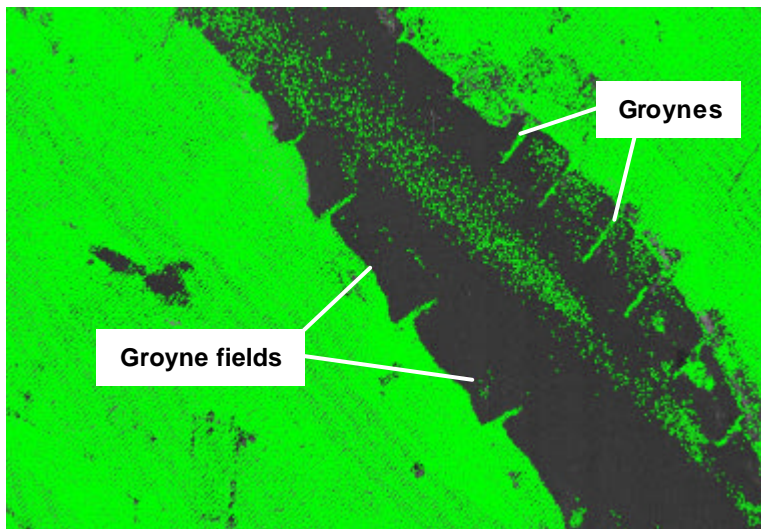


Abb. 3: Laser point density – *Grenzoder*

The terrain data were collected by the airborne laser-scanner "Optech 1020" late in November 1999 according to the requirements listed above. The actual mean laser point density after the classification (cf. Figure 3) achieved was 1 point per 2.5 m x 2.5 m. Of course one must keep in mind that the considerable lower laser-point density on the water surface (making up roughly 1/4 of the area) is included in this value, so that the above-mentioned requirement was reached.

Before the actual computation of the DTM-W, the laser points of the "solid" surfaces (land, groynes, dry-fallen areas in the groyne fields) had to be separated from those of the water surface. This should be effected possibly by an automatic routine. As - because of varying water levels - no other

measurements were available for delineating water and land surfaces, and results of water-level computations of flowing waters (in contrast to impounded rivers (BROCKMANN, KRAUS UND MANDLBURGER, 2001)) can usually not be used here, the water-land boundaries (WLBs) had to be derived from the laser-scanner data of the water surface.

3.2 *Riverbed data and other information of the waterway*

It was necessary to use here riverbed cross sections at distances of 50 m, 100 m and 200 m, that were recorded by single-beam echo-sounder at mean flow in 1998 according to the local conditions. Because these sections usually extended into the groyne fields, they were used for DTM modelling, what made the description of the wet parts of the groyne fields possible at all.

Additional basic data could be gained from orthophoto maps on the photo scales of 1 : 34,000 and 1 : 10,000, which had been taken at considerably higher water levels than those prevailing during the laser-scanner mission, as well as from necessary transformation parameters, axis points and control points of the waterway in cross-section distances.

4 **Watercourse DTM modelling**

4.1 *Fundamentals*

As mentioned in the previous chapter, the program system SCOP was used to compute a DTM-W from the available original measurements. The terrain model system SCOP was developed at Vienna (Institute of Photogrammetry and Remote Sensing - *I.P.F.*) and at Stuttgart (*INPHO GmbH*). The outstanding feature of SCOP is the interpolation method used, namely the linear prediction with a covariance function locally adapted to the data (KRAUS, 2000). This approach allows a qualified smoothing of the terrain model based on statistical analysis, what eliminates random errors in elevation measurements and also smoothes the contour lines. Another essential element of the strategy of SCOP is the integration of structural lines (e.g. breaklines, lines of framework) which are generally considered as necessary components of high-quality DTMs.

A precondition for deriving a DTM-W is the correct classification of "solid" areas (forelands, groynes, dry-fallen groyne fields) and the water surface. This means, in fact, the delineation of the WLBs. The extraction from the digital orthophoto maps was not possible, because of the different water levels during the laser-scanner mission and during the orthophoto mission. Therefore a photogrammetric identification of the shoreline, that is available at the *LVermA*, could not be used here. Consequently, the WLBs had to be derived from the available laser-scanner data, with the aim of a possibly high degree of automation. The identification of the WLBs is described in detail in the following chapter.

The successful application of the linear prediction needs a certain homogeneity in the distribution of the points of support. While this precondition is sufficiently met in the case of the laser-scanner data, the widely spaced echo-sounder cross section data need higher

density. To this end, additional sections at regular distances are computed by means of morphistic cross-sections fitting in such a way that along the river axis the shape of the initial section is successively transferred into the shape of the next section (MANDLBURGER, 2000).

4.2 Identification of water-land boundaries

It was intended to use a possibly automatic routine for the determination of the WLBs. The underlying idea was that this boundaries results from an intersection of the DTM-W with a digital model of the water surface (DWM).

For this DWM, first all laser points within a band of 30 m to the left and to the right of the river axis were determined. These points are then transferred into the coordinate system of the section (distance on the cross section, river-km, and elevation) and sorted for increasing river-km. Through averaging, one dimensional water levels representative elevation values could be determined for river reaches of 100 m each. By means of SCOP, a digital model of the water surface was then computed from these water-level data, neglecting possible sloping or upbulging of the water surface.

Now, the WLBs could be determined in a 2-step process:

- Step 1:
 - Computing a DTM from all laser points (DTM Laser; including the water surface);
 - Computing a difference model (DTM Laser minus DWM) by means of SCOP.INTERSECT;
 - Deriving the preliminary WLBs from the contour line 0.00 m, respectively 0.20 m, difference model by means of SCOP.ISOLINES.

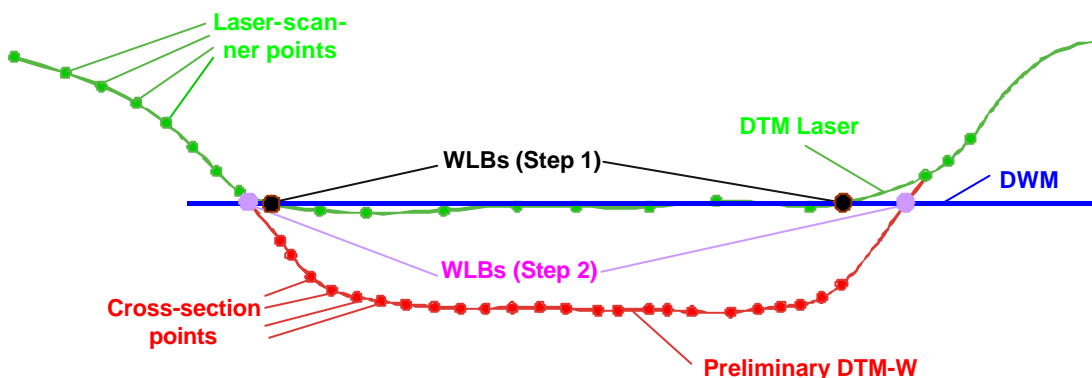


Fig. 4: Principle of deriving the WLBs

- Step 2:
 - Eliminating all laser points within the preliminary WLBs;
 - Inserting the densified cross sections within the preliminary WLBs;
 - Computing a preliminary DTM-W;
 - Computing a difference model (preliminary DTM-W minus DWM);
 - Deriving the final WLBs from the difference model.

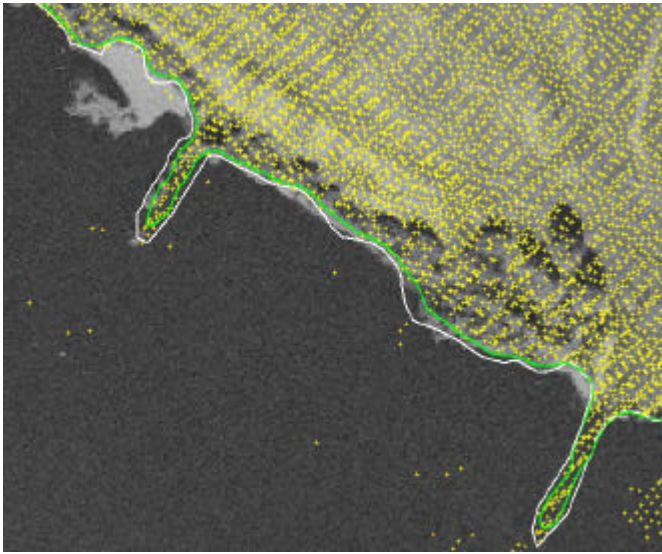


Fig. 5: Orthophoto map, original laser points (yellow), temporary (white) and final (green) WLB

WLBs were at first eliminated and substituted by the riverbed points of the echo-sounder. This improved in Step 2 the intersection conditions on the bank slopes. The intersection of the preliminary DTM-W with the DWM allowed now to define the WLBs with higher accuracy (Figure 5, green line). This final WLBs is used for the actual classification in terrain and water surfaces.

4.3 Computing the DTM-W and results

After eliminating all laser points within the WLBs and the densified echo-sounder cross sections data (cf. Figure 6), the pre-conditions were created to compute the DTM-W by means of SCOP.

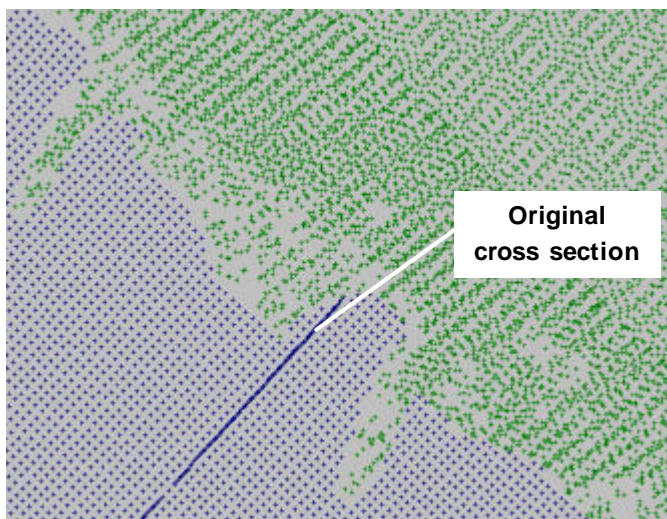


Fig. 6: Classified laser (green) and riverbed data (blue)

especially on the groynes, point densities of one point per 1 m x 1 m square occur, what justifies the use of a grid-cell size of 1,25 m for the DTM-W. For applications that need less detailedness, reduced resolutions (2.5 m, 5 m, and 10 m) may

One can see in Figures 3 and 5 that here only relatively few laser points exist on the water surface. Thus, the DTM Laser was very inaccurate on the water surface (Step 1). Moreover, drag intersections occurred in the areas of the banks in the intersection of the DTM with the DWM. The zero-elevation line of the difference model often consists of non-continuous fractures and numerous short continuous lines. Only the 20-cm elevation line (offset) forms a nearly continuous line and may be used as preliminary WLBs (white line). However, it is still very uncertain, and there is a high risk of misclassifications. For this reason, the laser points within the preliminary

An output listing for a DTM-W computation of a test area of about 7,000 m² (cf. Figure 7) shows that a grid-cell size of 1.25 m was used. This value is below the mean distance between points of about 2 m. The grid-cell size was chosen so small to ensure a sufficiently detailed description of the groyne structures. Furthermore, it was found in an examination of the data distribution pattern that

```

*****
*   DIGITALES HOEHENMODELL
*   KARTENBLATT: 3353SO
*
*   LAGE UND GROESSE
*   LINKE UNTERE ECKE      RECHTS ..... 3471652.66
*                           HOCH .....      5827692.48
*   AUSDEHNUNG
*                           RECHTS .....      2729.65
*                           HOCH .....      2515.26
*   ANGABEN ZUM DHM
*   RASTERWEITE           RECHTS .....      1.25
*                           HOCH .....      1.25
*   ANZAHL INTERPOLIERTER RECHENEINHEITEN ..... 6322
*   ANZAHL GESPEICHERTER RASTERPUNKTE ..... 2788002
*
*   ANGABEN ZUR INTERPOLATION
*   LINEARE PRAEDIKTION
*   ANZAHL GEBENER STUEZPUNKTE ..... 696944
*   MITTLERE FILTERBETRAEGE
*   MASSENKUNDE ..... 0.117
*   MAXIMALE FILTERBETRAEGE
*   MASSENKUNDE ..... 2.263
*****

```

Fig. 7: Output listing for a DTM-W computation

be derived. The mean filter value of 0.117 m indicates, on the one hand, the good quality of the laser-scanner data and, on the other hand, also that the laser-scanner data could be successfully fit together with the echo-sounder data.

Figures 8 to 10 visualize the DTM-W in the forms of contour lines, hill shading and perspective view.

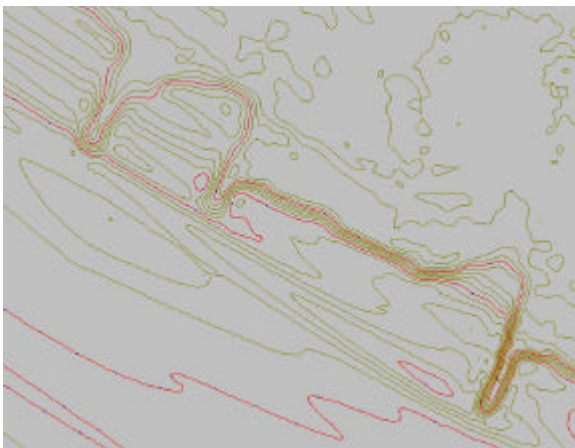


Fig. 8: Contour lines (interval = 0.5 m)

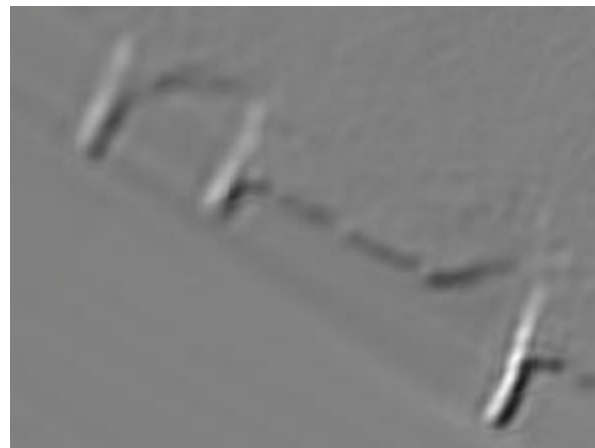


Fig. 9: Hill shading

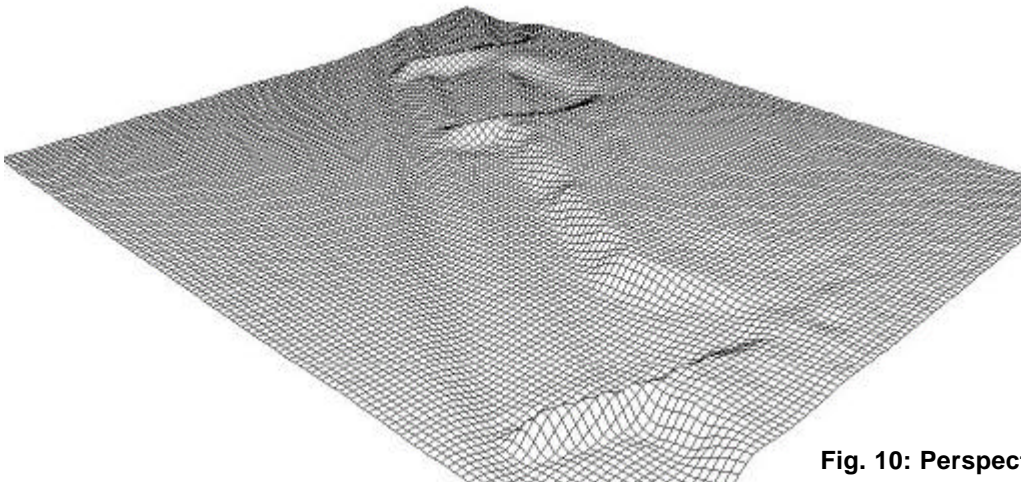


Fig. 10: Perspective view

4.4 Description of groyne structures

The WSA, one of the users of the DTM-W is particularly interested in assessing the state of groyne structures by means of this model. Here, the possibly correct depiction of the longitudinal section of the groynes is in the foreground (Figure 11).

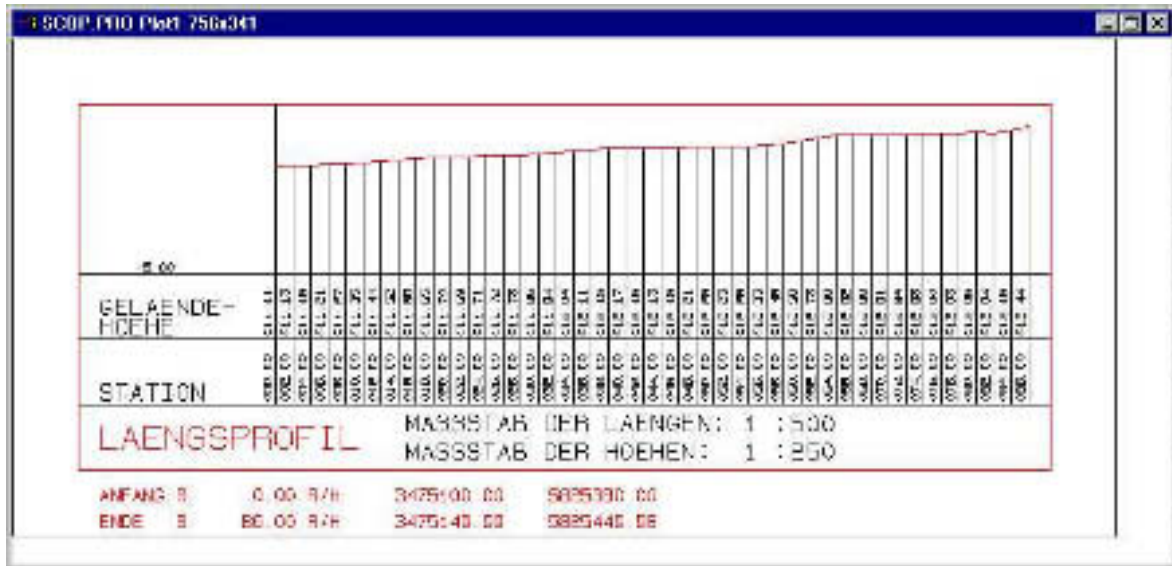


Fig. 11: Length section through a groyne

The Figures 8 to 10 visualizes that the present state of the groynes is far from the ideal, as it is shown in Figure 2. The WSA officials now have the possibility to identify and localize groynes in poor condition by means of the longitudinal sections derived from the DTM-W or from other forms of visualization.

5 Summary and outlook

Manifold tasks in hydrology, water management, hydraulic engineering and geodesy need digital terrain models of watercourses (DTM-Ws), as it is illustrated here by the River Oder. The modelling of the DTM-W was based on laser-scanner data and echo-sounder data (cross sections) of the riverbed. In order to run the DTM-W nearly automatically, methods were developed for the separation of the laser-scanner data of the terrain from those of the water surface, and for the derivation of water-land boundaries as well as for morphistic cross-section fitting in the environment of the program system SCOP.

The results of the first applications show that the expectations of the users could be satisfied. The software modules that were used on the River Oder will also be applied in the future for modelling DTMs on other Federal waterways, e.g. on the rivers Elbe and Rhine. The Federal Institute of Hydrology (*BfG*) has the opinion that the development of such methodologies is necessary also for economic reasons, especially against the

background of the new possibilities offered by laser-scanner technique, parallel recording of radiant intensity and multi-channel digital imaging for instance for orthophoto mapping.

Moreover, the *BfG* sees further chances for applications of laser-scanner technique. Through further research and development it should be possible in the future to derive roughness parameters (flow resistance) and flow-effective breaklines in sufficient resolution and exactness for use in hydraulic modelling.

References

Brockmann, H.: Einsatz flugzeuggestützter Fernerkundungstechniken zur Bearbeitung hydrologischer Fragestellungen. *Wasserwirtschaft, Zeitschrift für Wasser und Umwelt*, 90. Jahrgang, Heft 1, Januar 2000

Brockmann, H., Kraus, K. und Mandlbürger, G. (2001): Modellierung digitaler Höhen-
daten zur Bearbeitung hydrologisch/hydraulischer Fragestellungen an Wasserläufen –
Am Beispiel des Projektes „HGIS-Saar“ –. *Zeitschrift: Hydrologie und Wasserbe-
wirtschaftung*, 45. Jahrgang, Heft 3, Juni 2001 (das Erscheinen ist zum angegebenen
Zeitpunkt zugesichert)

Kraus, K.: *Photogrammetrie, Band 3: Topographische Informationssysteme*. Dümmler-
Verlag, 2000.

Lauschke, C. und Oppermann, R.: Das Sommerhochwasser 1997 in Odergebiet.
Zeitschrift für Binnenschifffahrt, Nr. 1/2, Januar 1998

Mandlbürger, G.: Verdichtung von Echolot-Querprofilen unter Berücksichtigung der
Flussmorphologie. *Österreichische Zeitschrift für Vermessung und Geoinformation*,
Heft4/2000.

LASER SCANNER DATA FOR TRUE DIGITAL ORTHOPROJECTION

Sergio DEQUAL, Andrea LINGUA, Fulvio RINAUDO

Politecnico di Torino, Italy

Dipartimento di Georisorse e Territorio

dequal@polito.it, lingua@polito.it, rinaudo@polito.it

KEY WORDS: True orthophoto, Laser scanner, Dense DTM.

ABSTRACT

The digital orthophoto is a cheap and efficient product that is suitable for representing the correct plane projection of any 3-D object. In the case where the surface that models the object is discontinuous (urban areas, architectural objects, etc.), “breaklines” and hidden areas should be taken into account, and the orthoprojection procedure therefore needs to be more sophisticated. A complete description of the hidden areas is often obtainable using multiple images (often available in a photogrammetric block), while a rigorous geometric description of the object requires the restitution of a great deal of breaklines or, as an alternative, several points, according to a dense regular grid.

In urban areas (and, similarly, in architectural and archaeological applications) the capturing of all the spatial breaklines is almost equivalent, in terms of time and cost, to a complete photogrammetric restitution. A “dense” DTM seems to be a more efficient solution: a new opportunity is offered by the laser scanning technique, that is available for aerial and terrestrial applications. The authors have studied in depth this last approach and conceived an original software, named ACCORTHO (=ACCurate ORTHOphoto), which is here described in detail: it produces rigorous digital orthophotos, using multiple images and DTM acquired by a laser scanner. A practical obtained result is shown, which refers to an aerial application: a large scale orthophoto of the urban area of Pavia.

1. INTRODUCTION

Orthophoto is an efficient and economic way of representing an object in a 2D-reference system, in the form of a “photo” of the object itself. The geometry of this particular photo is obtained by an orthogonal projection onto a plane. This particular photo is metrically correct, therefore the user can easily measure the represented object (in a known scale), exactly like in a map. This orthoprojection is very simple, if the surface of the object is continuous (smoothed), and the obtainable accuracy satisfies all kinds of applications. Unfortunately, this is not the case in urban areas. The surface that models the man-made objects (buildings, bridges, etc.) is certainly not smooth, and a regular grid (DTM) is not able to describe it properly.

Orthoprojection of these types of objects requires more sophisticated procedures.

2. RIGOROUS ORTHOPHOTO OF A DISCONTINUOUS SURFACE

Let us consider the house represented in figure 1. If the DTM describes only the ground, the projection of the point Q falls in the wrong position Q'_0 instead of being recorded in the right position Q_0 , which is also the correct orthoprojection P_0 of point P. Figure 2 shows the practical effect: the roof of the building is shifted to an incorrect position.

Now, let us consider the case where the house is described by the DTM (figure 3). Point Q is correctly represented in Q_0 but, if a traditional orthoprojection is used, point P (hidden by point Q due to the perspective effect) is lost, whereas the visible point Q is doubled (in P_0) on the resulting orthophoto.

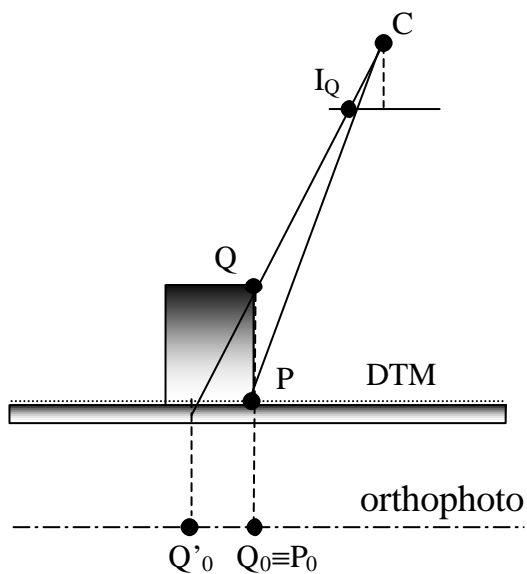


Figure 1. Orthoprojection with incorrect shape description

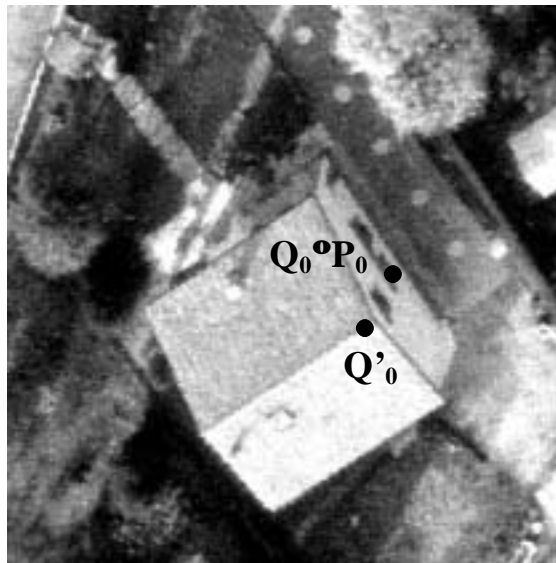


Figure 2. Practical example

This effect is shown in figure 4. Obviously, the image of the hidden area is not available in the photo (it should be taken from other photos, if available), but the double imaging generates confusion and is surely not desired.

Considering the two previously mentioned effects, it can be stated that, in order to generate an accurate and complete orthophoto of a discontinuous surface, the correct description of the surface and the availability of the images of all the details of an object are required.

If different perspective images are available, as shown in figure 5, special precautions should be taken to use the right projection ray for each point, thus avoiding double imaging. For example, point Q_0 is obtained from the image I_Q and P_0 from I_P .

3. 3D MODEL GENERATION

The detailed description of a 3D discontinuous surface can be obtained using different approaches.

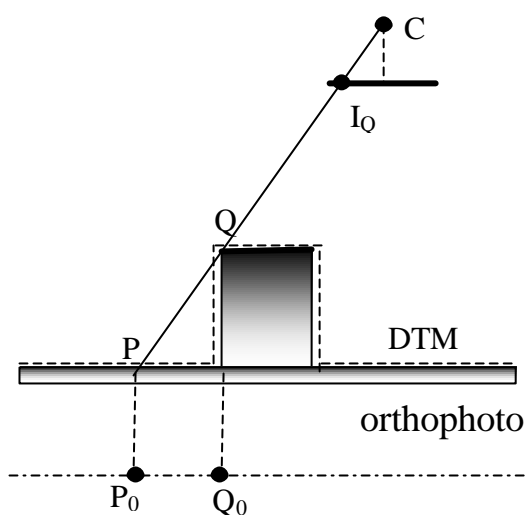


Figure 3. Orthoprojection with hidden areas

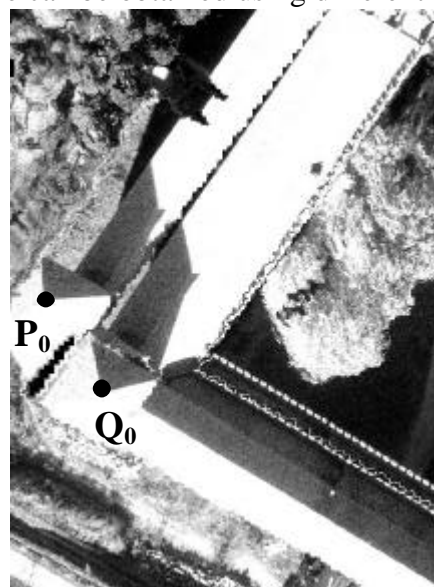


Figure 4. Practical example

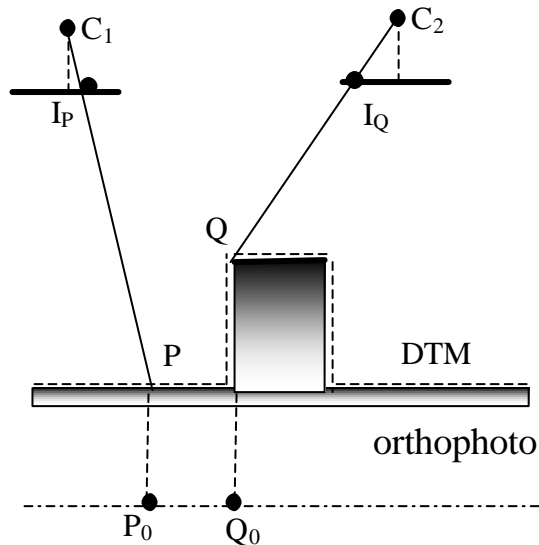


Figure 5. True orthophoto generation

to describe the building boundaries and a relational database is used to manage this sophisticated interpolating tool. The creation of a DSM cannot be automated and, furthermore, the management of such an instrument requires heavy software and a large amount of computation time.

One way of avoiding the necessity of breaklines is to use a very “dense” grid of points, where the size of the mesh ranges from 1 m to a few centimetres. The high density of the points makes the use of breaklines unnecessary.

It is possible to conceive three different procedures for measuring a dense DTM.

The first one consists of a direct manual restitution: this is unacceptable (too long and too expensive).

The second possibility is based on the use of an automatic DTM generation procedure, using matching algorithms. As known, this method gives an average of about 80% of successful results: the remaining points have to be measured manually by the operator. This average decreases dramatically in the case of urban areas. This procedure is not advisable.

A third, recent chance of generating a dense grid is offered by the use of a laser scanner. This new surveying device is able to collect thousands of points in a few seconds, with high accuracy. The laser scanner technology, based on optical-electronic devices, uses a high intensity pulse directed towards the object, and is able to measure the distance from the device itself. The two direction angles are measured at the same time and the 3D co-ordinates of the points are thus determined. A digital image can be derived from these points. Laser scanners are produced both for aerial or terrestrial applications. The grid generated by a laser scanner is irregular, the X and Y spacing depending on the distance and direction between the instruments and the measured point: it is therefore possible to choose the point density simply by changing the acquisition distance. The process is completely automatic and the DTM generation (acquisition and data processing) is easy and fast. Therefore the laser scanner device can be considered as the optimal solution for producing a dense DTM, both from the technical and economic points of view.



Figure 6. Acquired regular DTM

In order to detect outliers and gross errors, which occur especially in aerial acquisition, and to simplify the management of the data, the DTM generated by laser scanners must be pre-processed and regularised. This procedure has been implemented in an original software which allows the choice of the final grid size of the DTM [Roggero, 2001]. If the chosen grid size is close to the mean

The first possible solution tries to minimise the number of required points. This can be obtained by using a regular grid of points, integrated with a suitable number of breaklines, which are necessary to describe the discontinuities of the surface.

If one considers an urban area, however, it is clear that the restitution of all the breaklines would be almost equivalent to plotting the entire area: the breakline measurement cannot be automatic, and therefore it is expensive in terms of time and money.

A second solution consists of the definition of a DSM (Digital Surface Model) for modelling the complex urban texture. Plane triangles and quadrangles are defined as geometric primitives

distance between the acquired points, some points of the regularised DTM can be undefined. These “empty points” are not acceptable in the automatic orthophoto generation. In order to solve this problem, median filtering can be applied and residual undefined heights must be recorded by means of a traditional photogrammetric survey.

As an example, in the test area of Pavia (see fig. 6, where heights are coded by different colours) a laser scanner acquisition with approx. 15 points/m² (taking distance of 400 m) has been made. The regular DTM generated by the previously mentioned software, with a grid size of 0.5 m, shows a 26% of the points undefined. The use of median filtering reduced the amount of the undefined heights to 4%. These remaining “empty points” have been recovered by means of standard photogrammetric measures.

4. HOW TO PRODUCE A TRUE ORTHOPHOTO

Amhar and Ecker proposed an original solution for producing a true orthophoto in 1996. The procedure was designed for orthophotos in urban areas; it is based on a DSM managed by means of a relational database [Amhar, 1996]. Ground and buildings are automatically recognised onto the images and the orthophoto is generated in two separate phases: first the terrain, then the roofs. The results of these two steps are then merged in a single digital orthophoto. Hidden areas are reduced or eliminated by combining orthophotos of the same area generated from different images.

The solution proposed by the authors of this paper is quite different and more general. The input data are: a dense DTM, generated using a laser scanner device, and a series of oriented digital images, containing the area to be orthoprojected.

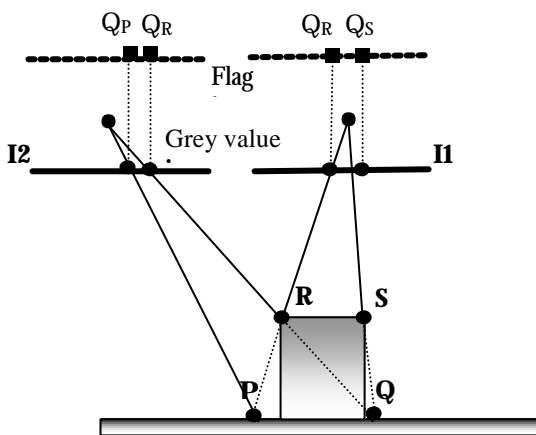


Figure 7. True orthoprojection

Let us consider, as an example, the house in figure 7. In the perspective image (considered to be a black and white image), along a projection ray, the higher point hides the lower one, therefore the procedure runs from the highest to the lowest point.

The procedure starts from point R. The best recording of the grey value of this point should be found in the image which has its “principal centre” nearest to the point itself (image I1). In order to avoid double imaging (remember fig. 4), this pixel should be inhibited: for this reason a “flag image” is created, where each pixel records the height used for the orthoprojection of the corresponding pixel on the original image. An image of point R is also present in I2 and, for the same reason, this pixel should also be

inhibited on I2, even though it will not be used (I1 is closer to R). The procedure then projects point S with the same criteria (point S is present only in I1). When the procedure comes to point P, it finds that the pixel on I1 has already been used for point R. Therefore the flag image inhibits a second use of this pixel, because the height recorded on it is higher than the height of point P. The procedure then looks for the grey value in I2. This pixel is not inhibited and the projection of point P is therefore possible. When trying to project point Q, the first attempt is to use the corresponding pixel on I1, but this pixel has already been used for point S and the “flag image” then inhibits the reading of its radiometric value. The second attempt is to use the corresponding pixel on I2, but this pixel has also been inhibited because it contains the grey value of point R. In this case, no other images are available and the orthoprojection of point Q cannot be defined: it will be represented by a conventional “white” (= 255) value.

This simple example describes all the possible cases that can occur in the orthoprojection procedure.

5. THE SOFTWARE ACCORTHO

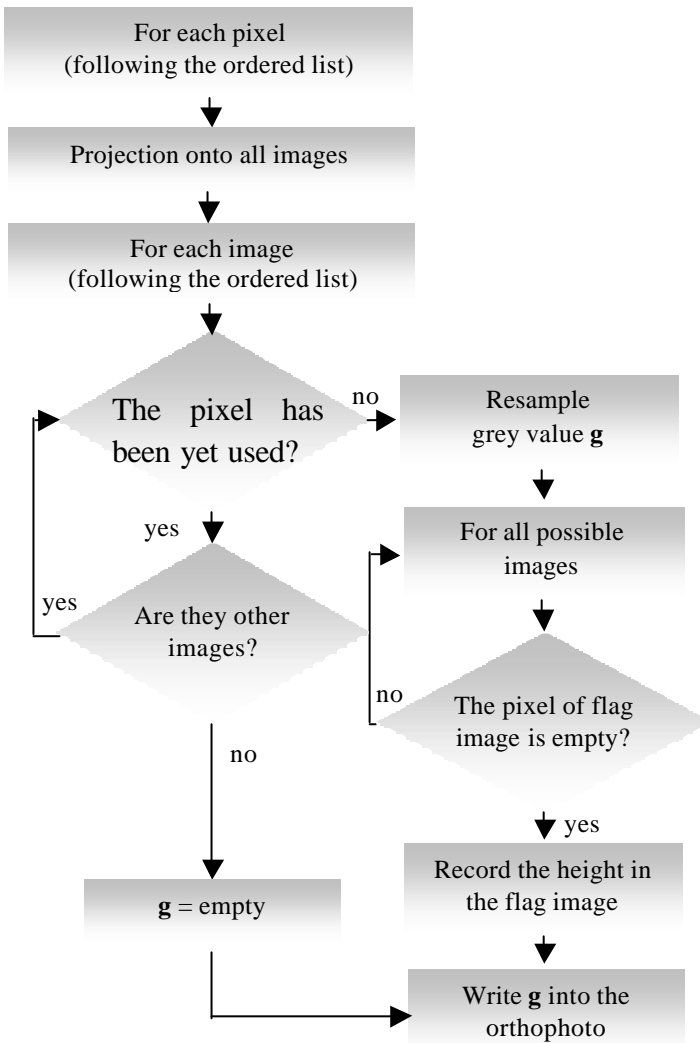


Figure 8. Flow-chart of ACCORTHO

of the six used images and a graphic index of the images used in the orthophoto generation. Figure 10 shows the orthoprojection made using traditional software (one image and a DTM describing the ground level) and the obtained true orthophoto of the test area. The superimposed

The procedure described in the previous paragraph has been implemented in a specific software named ACCORTHO (ACCurate ORTHOprojection). The input data are a regular dense grid generated from the irregular DTM, acquired using a laser scanner device and a set of oriented digital images. The software runs in two separate steps. In the first step:

- it computes the height of each pixel of the output image (the true orthophoto) and orders the pixels from the highest to the lowest;
- it extracts the portions of the images involved in the procedure;
- it prepares an index of the images, where it is possible, for each pixel, to find the grey value of the pixel. The images are ordered considering the distance between the projection centre and the pixel;
- it generates an empty “flag image” for each input image.

The second step of the procedure performs the process described in the previous paragraphs. Figure 8 shows a flow-chart of the basic functions.

The test area is contained in six different images. Figure 9 shows a raster representation of the DTM, the portions

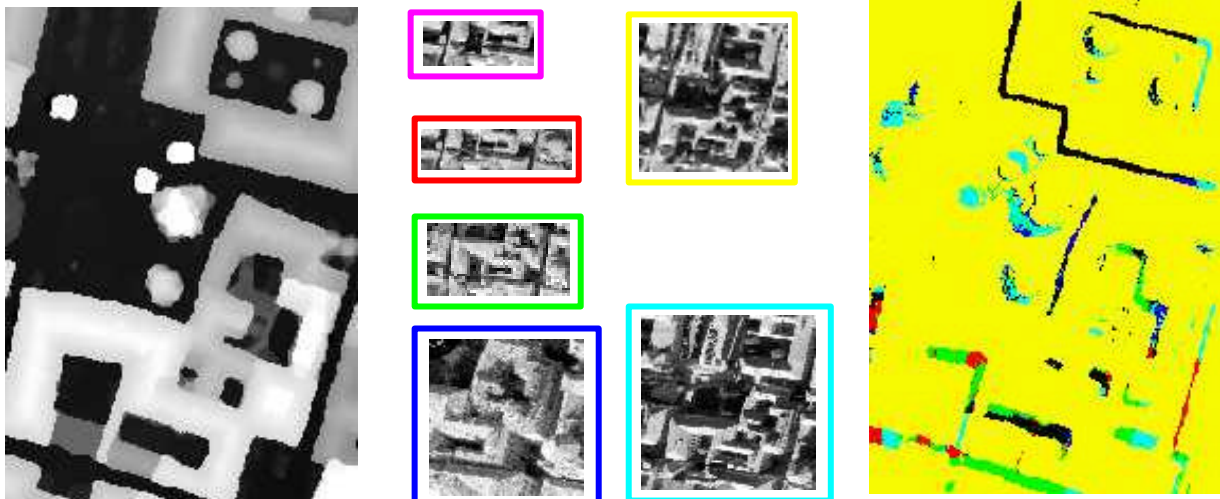


Figure 9. Input data and raster index image

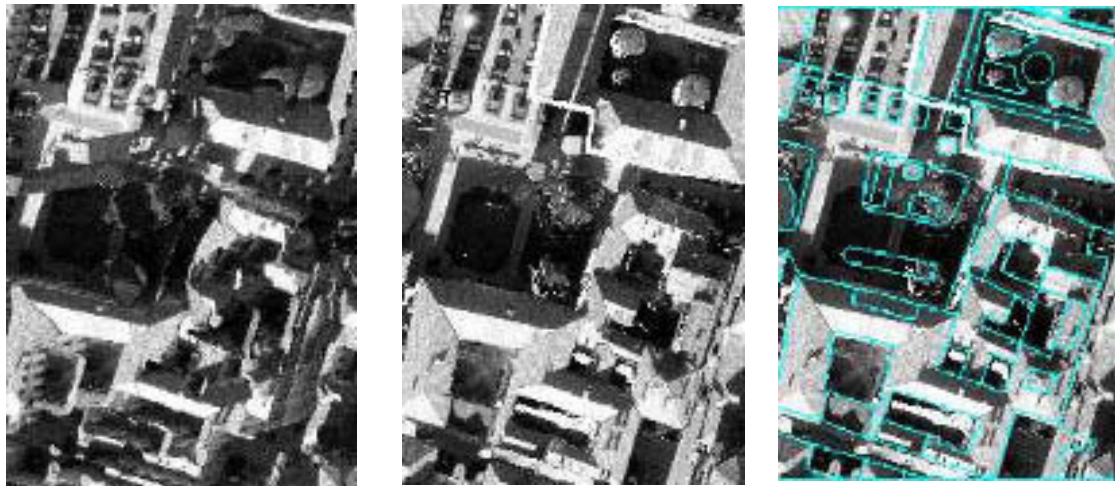


Figure 10. Traditional orthophoto (left), true orthophoto (centre) and superimposition of a digital map of the test area.

vectorial map highlights the achieved accuracy .

A PENTIUM III PC - 880 Mhz, 512 Mb RAM - requires a computation time of about 2 hours for a 50 x 60 cm² orthophoto (300 DPI).

The achieved accuracy satisfies the standard requirements for an orthophoto at 1:1000 scale.

6. CONCLUSIONS

ACCORTHO is a user friendly software that is able to produce rigorous (“true”) orthophotos of urban areas and architectural objects using a fully automatic procedure.

It is based on the use of a dense DTM, acquired using a laser scanner. The proposed procedure can be applied to any kind of discontinuous surface (urban areas, monumental and archaeological sites, industrial applications, etc.) and allows a great diffusion of the orthophoto advantages in many unexplored fields.

The proposed solution has been obtained by mixing different modern techniques: photogrammetry, laser scanner, image processing.

ACKNOWLEDGEMENT

This study is a part of the project “Digital surface modelling by laser scanning and GPS for 3D city models and digital orthophoto”, financed by the Italian Ministry for University and Scientific and Technological Research (MURST).

REFERENCES

- Amhar, F., Ecker R., 1996: An integrated solution for the problems of 3D man-made objects in digital orthophotos. International Archives of Photogrammetry and Remote Sensing, Vol. XXXI, Part B4
- Kraus, K., 1997: Photogrammetry, Volume 2, Dümmlers Verlag
- Boccoardo P., Comoglio G., 2000: New methodologies for architectural photogrammetric survey. International Archives of Photogrammetry and Remote Sensing, Vol. XXXIII, Part B5/1
- Roggero M., 2001: Dense DTM from Laser Scanner Data. OEEPE Workshop “Airborne laser scanning and interferometric SAR for detailed digital elevation models” - Stockholm

OEEPE workshop
DENSE DTM FROM LASER SCANNER DATA

Marco Roggero

Politecnico di Torino
Dipartimento Georisorse e Territorio
Tel: +39 0161 226390
email: roggero@atlantic.polito.it

1. ABSTRACT

Laser scanning represents a powerful tool to survey the territory. Its precision depends on many, partly random and partly systematic factors. Systematic errors, which are greater in planimetry than in height, are generally removed by the Companies on a calibration field. It could be interesting to look for residual systematic errors inside the data, that have not been removed, in order to improve the final result, and also for testing purposes, as there no specific Regulation concerning this at the moment. This paper proposes to find planimetric biases through correlations, that where performed on the overlapping zones of two laser strips.

2. INTRODUCTION

Systematic errors, both planimetric (more marked) and altimetric, can be found in the complex system of laser positioning. The majority of these are reduced through a calibration procedure of the system performed by the different Companies that are involved and using different modalities which, unfortunately, are not always known to the final user. The calibration operations make use of ground control point measurements, in the best cases, or of data obtained from pre-existing cartography. At this stage, the rototranslation parameters of each strip are calculated. This operation is performed on all the strips during the calibration flights but only on some strips in the production flights; usually the other strips are rotated and translated, identifying control points that are in common with the transversal strips.

It could be interesting to carry out research into the presence of unremoved residual bias inside the data. This research could be carried out “externally”, comparing the data with ground control points. It could also be performed “internally” if the strips have a sufficient overlapping. A reasonable hypothesis on the entity of these *biases* could also be performed by analysing all the possible reasons for the errors in the system in detail (GPS, INS and scanner laser). This work deals with the intrinsic comparison of the data, which offers the advantage of allowing an estimation of the precision constrained by measuring ground control points.

3. RELATIONAL ARCHIVE OF THE DATA

The quantity of data involved, some thousands of tri-dimensional coordinates, make it necessary to build up the instruments that are necessary for the management. The first operation that was carried out was that of the construction of a relational archive that permits direct access to the raw data. The second operation concerns the validation of the data and the setting up of a regular spaced digital surface model (DTM). The gridding step of this DTM was chosen in function of the ground point density so that there were at least 6-8 points for each element, this being the minimum necessary to identify the *outliers* and *gross errors*. This operation permits the management of the DTM with the same commercial software that was created for the digital management of images of large dimensions, with great time and cost advantages.

Given the remarkable quantity of raw data, the sequential reading is excessively long, and it is therefore necessary to change the raw data files into direct access files. The archiving inside a grid (DTM) that is directly accessible and in which one wishes to read all the raw data, requires that the position of the data is already known, that is, that a pointer system exists which, after a first sequential reading of the set of all the data, memorises their position inside the file.

Each datum is classified on the basis of the grid criterion and its position inside the file is memorised in an index. The relational archive of the data is made up of three files:

- **Frequency file**: this contains the number of data in each element of the grid (frequency or density of sampling).

- **Cumulated frequency file**: this contains the cumulated frequency values
- **Pointer index**: this contains the positions (pointers) of the data in the raw data file ordered by line and column and has the purpose of allowing direct access to trace these data.

The DTM_Laser package that has been developed in the present study for the generation of a DTM, starting from the scattered points, has two characteristics:

- reduced DTM calculation times, as it makes use of a quick interpolation method;
- it permits, even after the interpolation, to access to the original data directly;

The DTM_Laser package constructs the relational archiving files and, at a later stage, uses these files to generate the DTM.

3.1. DATA CLASSIFICATION PARAMETERS

The parameters used in the classification of the raw data for the construction of the relational archive are here defined.

3.1.1. Gridding step

This step is determined in function of the mean ground point density, their planimetric distribution and the application purposes of the DTM. By decreasing the gridding step one obtains an increase in the definition of the model, but also its dimensions and the necessary calculation times also increase; the number of empty elements also increases while the reliability of the classification of the height values decreases, as will be seen in the following section. As the distribution of the measurements is not uniform, it is necessary to refer not to the mean density but to values close to the minimum in order to avoid measurements being missing in many DTM elements. It is necessary to find a compromise solution and there are no general rules as the sampling density and the distribution of the points vary in function of many factors (parameters referring to scanning, flight height terrain morphology, overlapping between the strips etc.).

3.1.2. Classification of the height measurements

The height measurements that belong to the same DTM element are classified on the basis of their distribution with respects the median in: *robust measurements*, *outliers* and *gross errors*. The median was chosen as the discriminant parameter, so as to avoid the classification reference from being influenced by any possible gross errors. Two modulus intervals r and R (with $r < R$) were determined centred on the median \tilde{m} , in order to classify:

- **the robust measurements**: the values within the $|\tilde{q} - x| = r$ interval;
- **the outliers**: the values within the $|\tilde{q} - x| = R$ interval, but external to the $|\tilde{q} - x| = r$ interval;
- **the gross errors**: the values external to the R radius. These are the gross errors that for various reasons could be mixed with the *robust measurements*. The reasons behind these errors are not yet clear;

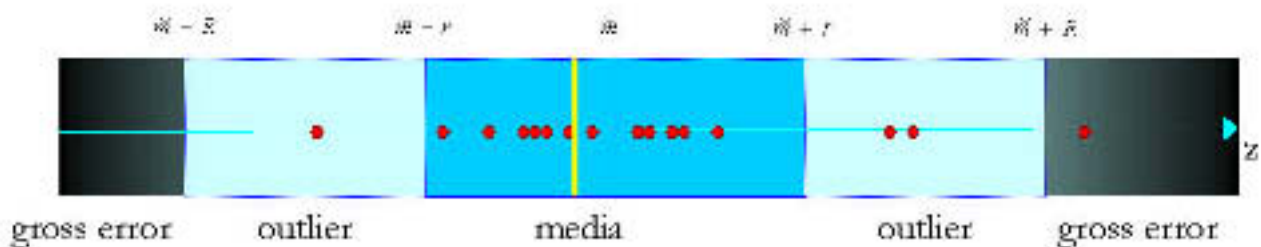


Fig 1 - Classification of the measurements with respects to the median.

The r and R parameters should take into consideration the morphology of the terrain and the type of area the measurements refer to (countryside, wooded areas or intensely built up areas), and the difficulty of making an a priore choice. It is better to first make some attempts on a test area, then choose the values of the parameters that give the best results. On the whole greater values should be adopted for both parameters for built up areas. There are however different reasons for this: for r

80÷100 cm was chosen for the majority of cases, this means that those points that belong to objects that have a higher Dh have been classified, therefore building and fence perimeters, for example, have been included. The choice of r also depends on degree of detail that one wishes to obtain when extracting the borders; R instead should be larger than the maximum difference in height between two contiguous measured points (in the case where it occurs on a tower or buildings). The drawbacks of this system concerns the individual elements of the grid; as a consequence the classification has no significance if even one single measurement is found on the inside of a grid element. In some data sets there are many gross errors which are to a great extent eliminated but not completely; the case has occurred of a single datum that is a gross error or of several data, all gross errors, in the same grid element. The classification with respects to the median cannot recognise these errors, which are therefore classified as robust measurements; the problem was resolved by later applying a median filter to the DTM matrix.

4. CONSTRUCTION OF THE RELATIONAL ARCHIVE

The DTM_Laser package sequentially reads the raw file to construct the data archive. When this stage has finished, it is possible to read the data directly. Some of the variables used are here defined:

- **matrix pointer:** each element in a matrix can be univocally identified by a pointer. The relational archive uses height matrix pointers (DTM), frequencies and cumulated frequency pointers;
- **raw data file pointers:** these correspond to the number of records in which a determined measurement is written.

For each datum read from the sequential file, the algorithm performs three operations:

- calculation of the matrix pointer of the heights, frequencies and cumulated frequencies;
- memorisation of the heights matrix pointers and those of the raw data file in a two column vector and with a number of rows equal to the data. The vector, as it is written by reading the raw data in a sequential manner, is ordered in an increasing way in function of the file pointers;
- updating the frequency and cumulated frequency value in the respective files. The frequency and the cumulated frequency files have the same number of elements as the grid.

At this point, having finished the sequential reading, the pointer vectors are ordered in function of the matrix pointers and the column of the data file pointers is saved in a file called *index*.

5. GENERATION OF THE DTM

The values of the height matrix (DTM) are calculated in sequence, from the first element of the matrix and proceeding by row. It is also possible to calculate any element, without having to proceed in a sequential manner; in other words, the DTM construction system and the archiving system allow direct access to the data, whether raw or averaged. This is particularly useful, as it permits going back to original data, for example for filter applications, classification of points, cluster analysis and the recognition of the borders or objects.

The value of a grid element is calculated by the algorithm as follows:

- reading of the frequency (f) and the cumulated frequency (f_c) corresponding to the element that has to be calculated. The cumulated frequency acts as the index file pointer;
- reading of the data file pointers in the index file f , from the $f_c \cdot f$ record to the f_c record;
- reading of the f measurements in the data file, in the records indicated by the pointers;
- calculating the median of the measurements and classify them as *robust measurements*, *outliers* or gross errors;
- calculating the height to assign to the cells as height mean, if only robust measurements are present. If outliers are present code -100 should be assigned to the cell and when there are gross errors code -200 should be assigned.

Saving the calculated height values on a file or any possible code.

After the classification of the points, the DTM contains both the height values and the codes. This intermediate product can already be used for the extraction of borders and the calculation of statistics on any possible *gross errors*. A second scanning of the DTM is then performed, to calculate an height value for those elements that have been temporarily marked by a code. Three different cases occur in the matrix scanning:

- the cell is empty or contains a previously calculated height value; this datum is simply written on a new file of analogous form;
- the cell contains code -100, therefore at least one outlier is situated within the data. The measured points are still classified in three sets: *robust measurement*, *outlier* of heights below $\bar{q} - r$ and *outlier* of heights above $\bar{q} + r$. At least two of these three sets are not empty. The height value is calculated as the mean of the most numerous set of heights and is then written on the file;
- the cell contains code -200, which signals the presence of one or more *gross errors*. The package reads the data belonging to this cell from the raw file, orders them and classifies them according to the median in four sets: *robust measurement*, *outlier* of heights below $\bar{q} - r$, *outlier* of heights above $\bar{q} + r$ and *gross error*. It does not take into consideration the data from this latter set and calculates the height value as the mean of the most numerous set of heights. The package then writes the obtained height in a file.

The output of the second scanning does not yet make up the final DTM. Empty cells can in fact still be found in which it is however possible to calculate an heights value using a mobile mean filter, or cells are present that containing gross errors that could not be removed with the applied classification criterion. In this second case, the classification of the height measurements with respects to the median had no significance as the sample was not numerous enough or was even made up of one single measurement. These problems are later corrected through the application of a median filter to the DTM.

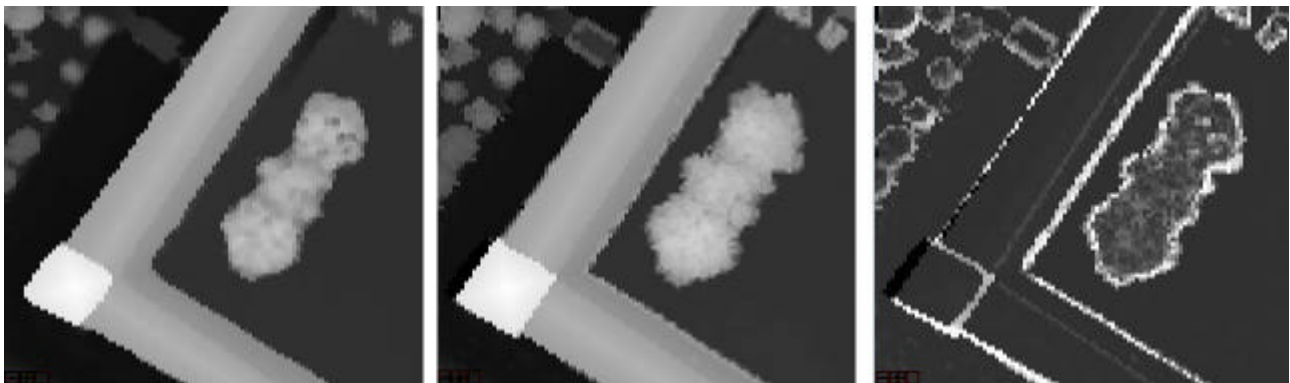


Fig. 2 – From left to right: DTM obtained with TopoSys, DTM obtained with the DTM_Laser package and the difference between the two.

6. VERIFICATION OF THE PRECISION

The differences in height between two adjacent strips are almost zero on flat surfaces, a little higher (10÷15 cm) on sloping surfaces and remarkable (even some metres) close to the perimeters of buildings. Darker shades of grey indicate greater differences in height, in correspondence to elements classified as *outliers*, that is, vegetation and borders (see fig. 3). On the perimeter of buildings the difference in height is almost equal to the height of the building itself. This result has been interpreted as the effect of a planimetric *shift* between two strips. It is also known, from considerations on the geometry of the scanning, that the planimetric error is higher than the altimetric error. Furthermore, the altimetric error, for small scanning angles, does not depend on the flight height.

The data relative to the test are the two cross-tracks obtained by TopoSys with a flight height of 400 m and sampling density of 12 points/m². The steps of the DTMs is 1 m in *x* and *y* direction.

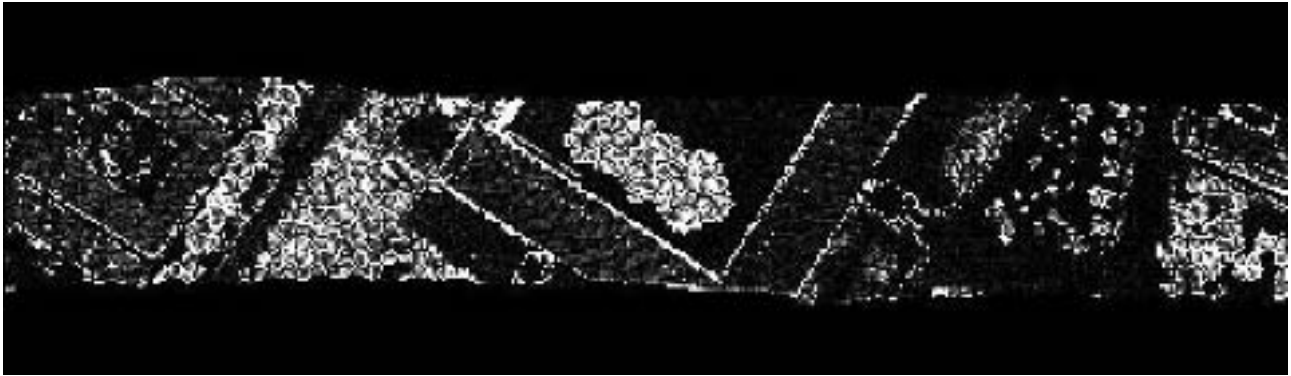


Fig 3 – Difference in height between two strips calculated in the cross-track overlapping zone.

The altimetric *shift* was considered to be zero while the planimetric *shift* was measured. This measurement is obtained by using the digital image autocorrelation algorithms. In the present case the radiometric tones are represented by the heights.

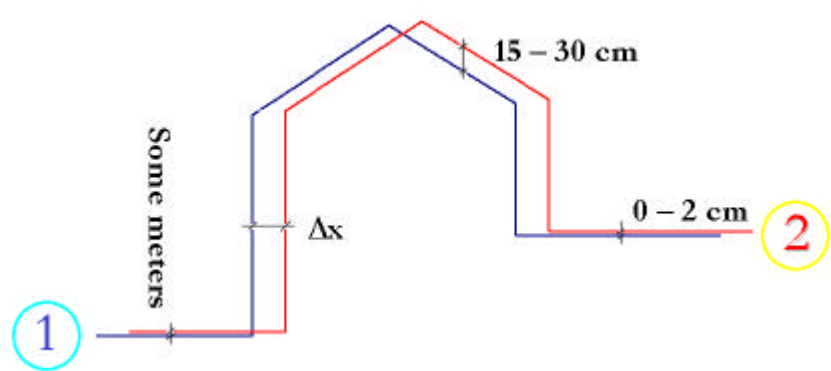


Fig 4 – Building projected in both strips, with an evident planimetric shift.

A preliminary measurement of the correlation was performed using standard autocorrelation algorithms. The values of the correlation coefficient (represented in figure 5) are normally between 0.8 and 1, but values close to zero are also found. The lower values, indicated by darker shades of grey, are close to borders because it is in fact on the inside of these lines that, in images that are different from the same area, the greatest differences occur. The automatic calculation of the correlations is made difficult not only by the presence of noise but also by the fact that intermediate pixels exist close to the borders.



Fig 5 – Values of the autocorrelation coefficient, represented in grey scale.

Once the shift has been found with pixel approximation (maximum values of 2 pixel are found), the calculation is extended to the least squares matching algorithm.

In digital photogrammetry the position of the two series of grey q_1 and q_2 are connected by means of the relation:

$$\mathbf{n} + q_2(\mathbf{x}) = b \cdot q_1(\mathbf{x} + x) + c \quad [1]$$

With this hypothesis it is acknowledged that the target and search areas differ not only in position but also as far as the height values are concerned. In reality, for physical reasons, it is not reasonable to think that there is a scale factor between the heights of the two strips. It would be more logical to acknowledge a constant c shift, for the basic hypothesis (planimetric errors are being searched for) and for those of precision (the planimetric accuracy is lower than the altimetric one) it has deliberately been neglected. Equation (1) can be re-written as:

$$\mathbf{n} = q_1'(\mathbf{x}) \cdot x - [q_2(\mathbf{x}) - q_1(\mathbf{x})] \quad [2]$$

where the casual components v appear.

The positioning precision increases with the discontinuity of the height, that is, on the borders (fig. 5). This increase in precision can be estimated by the inverse matrix of the normal system. The precision increases if the dimension of the target matrix increases, provided other borders take over; close to the borders a RMS of $2 \div 3$ cm was found for shift values of $30 \div 40$ cm.

From the calculation of the *subpixel* correlation, the (Dx, Dy) shifts are found in the x and y coordinates and the relative RMS (see fig. 6 – 7). The raster representation of the *shifts* does not allow one to draw conclusions on the presence of *biases*, in that the results which are affected by accidental errors induced by the noise that is present in the DTMs of the two strips, make the image difficult to read.



Fig 6 – Raster image of the Dy values (Dy>0 in light grey, Dy<0 in dark grey, undefined Dy in black).

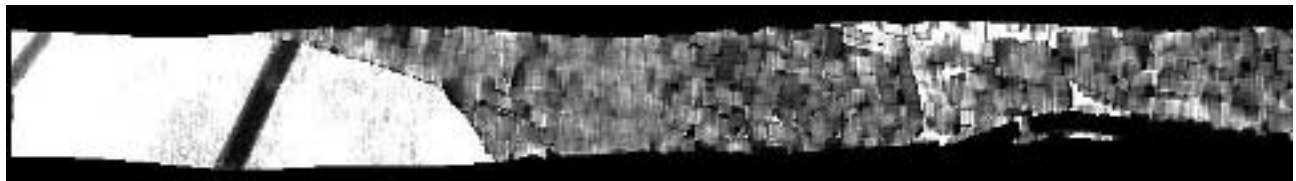


Fig 7 – RMS of Dy (the highest values can be found in the area of terrain without buildings on the left of the image).

By applying the mobile mean and median operator to the images that represent this shift, an archive as been obtained that has been refined of noise in the two strips.



Fig 8 – Values of Dy refined of noise.

The obtained result is still not satisfactory as the calculated shift values present high RMS in some zones of the image. In order to exclude the Dy with high RMS, a mask was applied to the results of figure 8 and the image in figure 9 was obtained.



Fig 9 – Values of Dy with RMS lower than 15 cm.

The final results leads to the following considerations:

- The built up areas are the most suitable sampling areas to carry out correlation measurements as the presence of frequent borders minimises the RMS; the values obtained on areas without buildings are of little significance and have been excluded from the analysis of the results.
- In the sample area both positive and negative shifts can be found. In the central area of the image in particular a sequence of “bands” of values with opposite signs can be seen. It can only be hypothesised that these have been caused by systematic errors in the measuring of the roll angle by the inertial system.

Further tests were carried out on couples of TopoSys strips acquired from a flight height of 850 m. The histograms of the values of Dx and Dy follow the Gauss distribution and their mean value is far from zero. In this case modulus shifts of 40 ± 60 cm can be found, which are however still lower than the pixel dimension (1 m). These errors can be compared with those found by studying all the possible sources of error and their influence on the 3D positioning (Baltsavias) is shown in fig. 10.

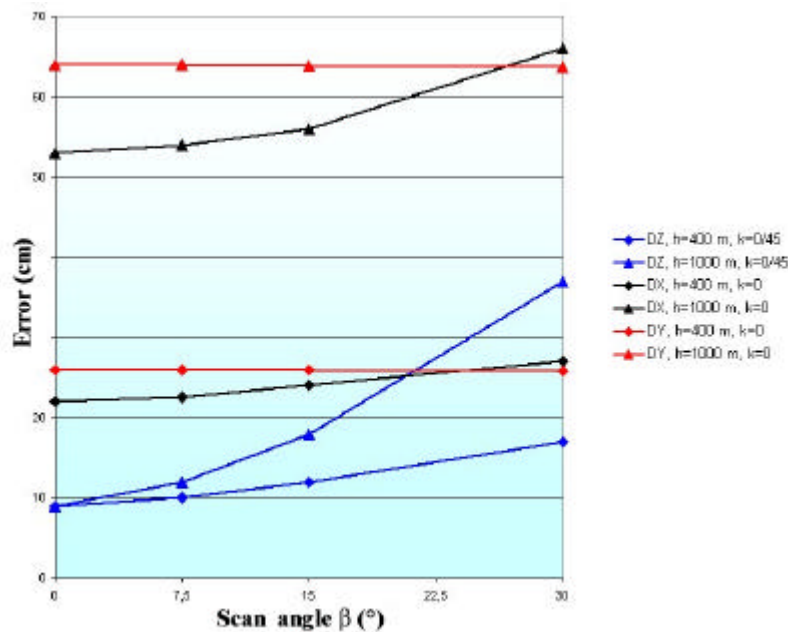


Fig 10 – Errors in the measured coordinates in relation to the flight height, scanning and drift angle (E.P.Baltsavias, 1999).

7. CONCLUSIONS

The calculation of the correlation between adjacent strips could be used in the calibration and testing stage of laser flights. The here proposed method, apart from being totally automatic, offers the advantage of being independent of the measurement of ground support points. At present however no officially recognised standard or testing regulation exist for laser flights; what can be proposed however is to respect the planimetric and altimetric values relative to the equivalent scale of the cartography or of the orthophoto for which the flight is performed.

8. ACKNOWLEDGEMENT

This study is a part of the project "Digital surface modelling by laser scanning and GPS for 3D city models and digital orthophoto", financed by the Ministry for University and Scientific and Technological Research (MURST).

9. BIBLIOGRAPHY

AA. VV. (1999)- *Airborne laser scanning*, ISPRS Journal of Photogrammetry & Remote Sensing, Vol. 54.

Baltsavias E. P. (1999) – *Airborne laser scanning: basic relations and formulas*, in ISPRS Journal of Photogrammetry & Remote Sensing, Vol. 54, pagg. 199 – 214.

Casella V., Galetto R., Spalla A. (2000) - *Il progetto di ricerca Cofin98 sull'impiego del laser a scansione* in bollettino SIFET n° 2, pagg. 13-26.

Roggero M. (2000) - *Scansione laser da piattaforma aerea, trattamento e analisi dei dati*, Tesi di Laurea: Politecnico di Torino II Facoltà di Ingegneria, Vercelli. Luglio 2000.

Topographical Survey using Laserscanning at the State Surveying & Mapping Authority of Bavaria

by Peter Reiss, Munich, Germany

Introduction

In 1994 the first discussions about laser scanning as a new method for the derivation of digital terrain models had been started among the Surveying and Mapping Agencies (SMA's) of the Federal States of Germany [Hoss (1996); Petzold & Knabenschuh (1999); Reiche, Schönemeier & Washausen (1997)]. A user group was formed in 1996 and several tests were carried out and evaluated. Since the results were very promising, a standard procedure for verification and handling of the data was developed and published for use by other interested SMA's. The presentation shows general results of this report as well as the implementation at the "Bayerisches Landesvermessungsamt" (BLVA; i.e. *State Surveying & Mapping Authority of Bavaria* aka *Bavarian Land Survey Office*).

Situation in Bavaria

The state of Bavaria is the largest of all 16 Federal States of Germany; it covers an area of 70,550 km². At the end of the 1950's photogrammetry was introduced for the mapping of the mountainous areas in the Bavarian Alps and later on for the other parts as well during the 1960's. Very flat terrain in the open fields as well as housing areas and woods still had to be completed using terrestrial survey (tacheometry). As a result of the transition from analogue to analytical photogrammetry from 1990 on map compilation changed from graphical methods to object-coded data collection with contours in digital form being the main result together with digital terrain data as a by-product and possible input for a high quality DTM. But still one third of the state area then was covered only by contours going back as far as 1872-1918; therefor the throughput had to be increased considerably.

A first test using laser scanner data was carried out in 1996; since 1997/98 a combined method is in operational use with

- laser scanning as the main input

supported by

- digital photogrammetry (checking / editing of the laser data),
- analytical photogrammetry (additional compilation of features / geomorphological structures) and
- terrestrial tacheometry (densely wooded areas).

While in the past the primary product were contours compiled at stereoplotters with DTM data as a by-product now the DTM derived from laserscanning (enhanced by photogrammetry and tacheometry) is the main result with contours being computed as a follow-up from the DTM.

Planning, requirements

The planning / contracting phase for a project using laser scanning for topographical survey includes

- definition of the project area (preferably of long rectangular shape)

- preparation of maps for the contractor
- supply of coordinates (project boundaries, GPS-reference stations, geoid undulations)
- definition of one or more check areas for the contractor (to check transformation from WGS84 to local; not to be used for adjusting the orientation in height)
- definition of several check areas for the SMA (for an initial overall check of orientation / transformation of the delivered mass points and – as far as applicable - individual strips)

Laserscanner flight, photo flight, preparatory field work

Laserscanner flights for the BLVA usually have been carried out so far under the following conditions

- flying height approx. 900 m
- strip width approx. 650 m
- side lap approx. 250 m
- resulting point density approx. 1.5 m (in the beginning starting from about 4.5 m)

(one recent project using a flying height of about 2.3 km resulting in a broader strip width and side lap is not finished yet).

Additional photo flights are characterized as follows

- image scale 1 : 14 000
- color film (diapositive)
- signalized control points (coordinated using terrestrial DGPS)

Necessary field work supporting laserscanner and photo flight resp. consists of

- signalization and measurement of control points
- survey of check areas (plane areas with little or no vegetation – usually soccer fields; approx. grid of about 50 m x 50 m with 10 m spacing)

Checks (acceptance of data)

Besides a report, plots (flight plan) and GPS-coordinates (of flight lines) several files of laser data are supplied by the contractor (who up to now is also responsible for the filtering process):

- file of registered points classified as ground points
- file of points classified as vegetation / buildings
- file of highest points (to define a raw surface model; optional)
- file of height differences (to define relative height of vegetation; optional)

A first check concerning accuracy and reliability consists of the comparison of the laser scanner measurements against the check areas. The laser data are accepted if the height difference from comparison to the grid surface is within |0.3 m| for 95 % of the laser points classified as ground points.

Further initial checks concern coverage and point density (point plots), outliers (contours and / or shaded reliefs derived from a very dense DTM-grid based on the delivered laser data).

Data processing (evaluation, editing, additional data collection)

To enhance the results received from laser data geomorphological structures are compiled at analytical stereoplotters. Typical features are banks of streams and lakes, natural or artificial breaklines (especially at dams), ridge lines, valley lines, edges of cuts and fills as well as local extrema (saddle points, hills and hollows).

Later on the data are checked and edited in detail at digital photogrammetric workstations which give a stereoscopic 3D-view (of the laser data plus the additional features) superimposed upon the stereomodels from the image flight.

Areas that are not covered (or not covered completely) have to be filled by field survey parties using tacheometry. This mainly concerns young and dense coniferous forest areas. Until last year the field survey delivered only a graphical product which had to be digitized; meanwhile registration in the field has been made possible which gives a complete digital data flow.

Concluding remarks

Since the introduction of laser scanning as the primary input for topographical survey the percentage of areas that have to be completed outdoors through a terrestrial survey went down from approx. 40% to less than 10% (Bavaria has large parts covered by forests mainly consisting of conifers). Traditional photogrammetric stereo-Compilation has been reduced as well. This led to an increase in throughput of factor 4-5 so far which does not mark the end (primarily because the advantage of a complete data flow from outdoor work to office did not show in those figures yet).

Further details can be found in [Petzold, Reiss & Stössel (1999); Reiss (2001)].

References

Hoss, H. (1996):

DTM Derivation with Laser Scanner Data; Geomatics Information Magazine (GIM), no. 10/1996, pp. 28 - 31

Petzold, B.; Knabenschuh, M. (1999):

Data post-processing of Laser Scan data for countywide DTM production; in: Fritsch/Spiller (Eds.): Photogrammetric Week '99, pp. 233-240, Heidelberg

Petzold, B.; Reiss, P.; Stössel, W. (1999):

Laser scanning – surveying and mapping agencies are using a new technique for the derivation of digital terrain models; ISPRS Journal of Photogrammetry and Remote Sensing, vol. 54, nos. 2-3, pp. 95-104

Reiche, A., Schönemeier, P., Washausen, M.(1997):

Der Einsatz des Laserscanner-Verfahrens beim Aufbau des ATKIS-DGM; Nachrichten aus der Niedersächsischen Vermessungs- und Katasterverwaltung, 2. Vierteljahr 1997, pp. 68-87 (in German)

Reiss, P. (2001):

Neue Verfahren zur Gewinnung von Geobasisinformationen aus der Sicht der Landesvermessung - Teil 2: Einsatz von Laserscanning und Digitaler Photogrammetrie für die Topographische Geländeaufnahme; Mitteilungs-blatt des DVW-Bayern 53, pp. 55-73 (in German)

Operational Production of DTMs Using ScaLARS

Karl-Heinz Thiel, Aloysius Wehr

Institute of Navigation
University Stuttgart
Geschwister-Scholl-Str. 24D
70174 Stuttgart
Germany

e-mail: thiel@nav.uni-stuttgart.de
wehr@nav.uni-stuttgart.de

Abstract - Summary

This paper reports about the production of a Digital Terrain Model (DTM) for an area of about 1300 km² using data from the airborne laser scanner ScaLARS (Scanning Laser Altitude and Reflectance Sensor) as contractual work. In order to perform this task, an operational processing chain had to be established. Based on the development of our own laser scanner system ScaLARS some software tools already were available for testing and generating small sized Digital Elevation Models (DEMs). These modules were adapted and supplemented by additional algorithms to provide an operational and complete processing chain for DTM production. Of large interest were solutions with a high degree on automatic computations. This means software modules not only have to run as batch jobs but also must have a flexible validation tool to eliminate remaining errors.

First this paper shortly presents the laser system ScaLARS and gives an overview over the processing chain with some typical results.

1. Introduction

In the surveying project in Thuringia ScaLARS was used operational first time for extended areas. The surveyed area covers more than 1300 km² and shows many different topographical features as e.g. low mountain range, forests, farmland, cities and industrial areas. The customer, the Landesvermessungsamt of Thuringia required a DTM, where the laser measurements were separated in points reflected from ground and those which were no ground points, like measurements on roofs of buildings, trees, etc. Due to the large amount of data the Institute of Navigation established a processing chain which comprises a number of batch routines which assure an efficient data processing with respect to time and manpower. The stringent requirements of the customer to distinguish between ground and non ground points made it necessary to develop new efficient algorithms, which need minor manual interaction, and a flexible validation tool to eliminate remaining errors.

In Figure 1-1 the main steps for DTM generation are compiled. The complete processing chain can be subdivided in five parts:

- flight planning
- survey (flights)
- sequential processing of navigation and laser data with calibration
- rastering process, classification and validation
- delivery and archiving

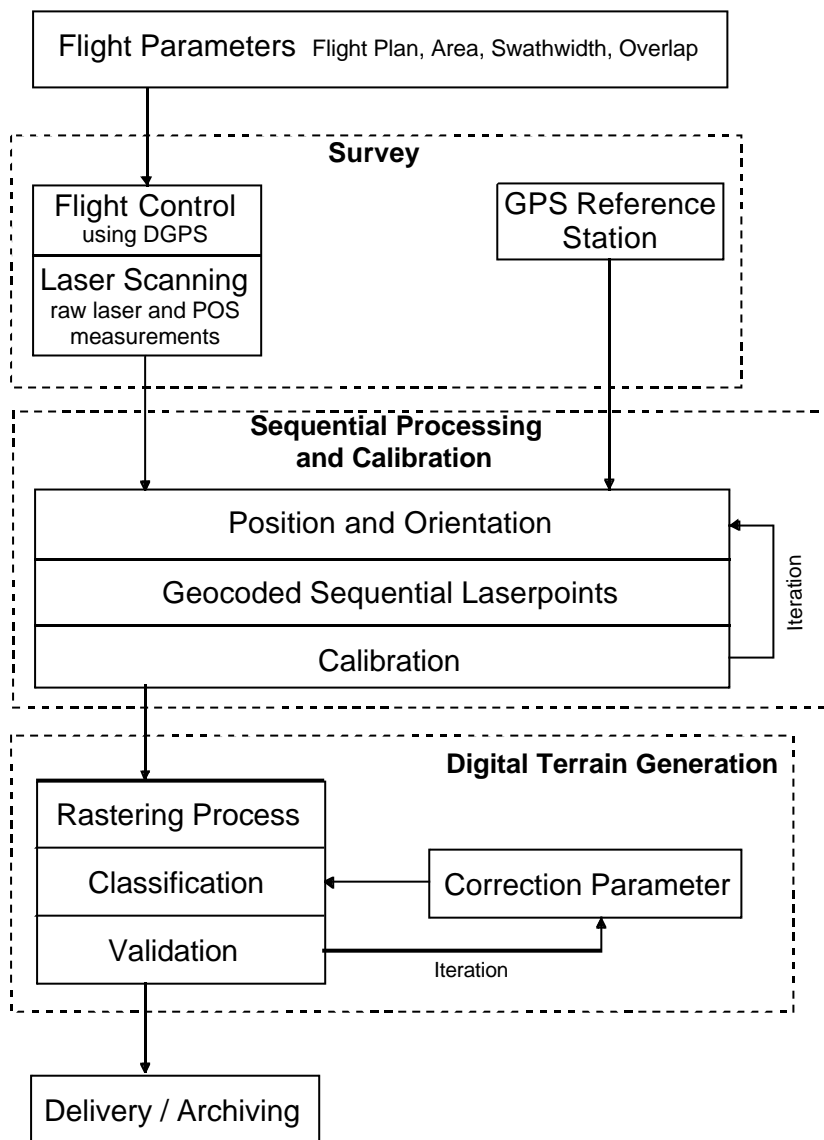


Figure 1-1: Operational Processing Chain

determined better than a hundredth of a degree. For this purpose the redundant information of the Palmer scanning pattern can be exploited for calibration as will be shown later. According to Figure 1-1 this task is carried out iteratively in "Sequential Processing and Calibration". Studying the expenditure of work of the total processing chain it came out that the demand of manpower was especially high for calibration and validation. Here main emphasis was given to reduce the necessary time afford by sophisticated programming and proper defined procedures. Special flight procedures can drastically ease the calibration; e.g. flying across a very smooth surface, like a runway. Validation effort is also minimized, if the signal-to-noise ratio of the laser measurement is high which means that the flight height should be within specification of the surveying system. Also flights should be done during winter season, where almost no leaves could be found on the trees and the probability is high that the laser light will mainly be reflected from ground.

Before the different tasks of Figure 1-1 will be discussed in detail the functioning of the ScaLARS is explained.

In the Thuringia project the Institute of Navigation was a subcontractor and responsible for laser scanning and data processing. Flight planning and inflight operations were carried out by the main contractor, who owned the airplane and will not be discussed here. The laser and navigation data were available for a preview directly after the flight. The laser measurement can be looked through for a first inspection immediately after flight with a special software routine.

Before any DTM can be computed the laser scanner data must be calibrated. This means ScaLARS's position and orientation relative to Position and Orientation System (POS) must be determined. The lateral displacements are not so critical, because they are independent of the flight altitude, but the orientation angles must be

2. Laser Scanner ScaLARS

The main difference to other commercial laser altimeter systems can be seen in the continuous-wave phase measurement for ranging, the scanning mechanism and the high resolution for the intensity measurement.

Ranging is done by measuring multifrequency phase differences. A continuous laser beam emitted by a high power laser diode is amplitude modulated by the sum of two sinusoidal signals of different frequencies. The phase delay between emitted and received modulation signals caused by the time of flight of the light from the sensor to the surface and back is according to (2-1) proportional to the distance R between the sensor and the surface.

$$\phi = 2 \cdot R \frac{\omega}{c} \quad (2-1)$$

where $\omega = 2\pi \cdot f_{\text{Mod}}$

f_{Mod} : modulation frequency

c: speed of light

In addition the intensity I is detected and measured by synchronous demodulation with a 13 bit resolution. For each measurement point on earth the slant range, the intensity and the

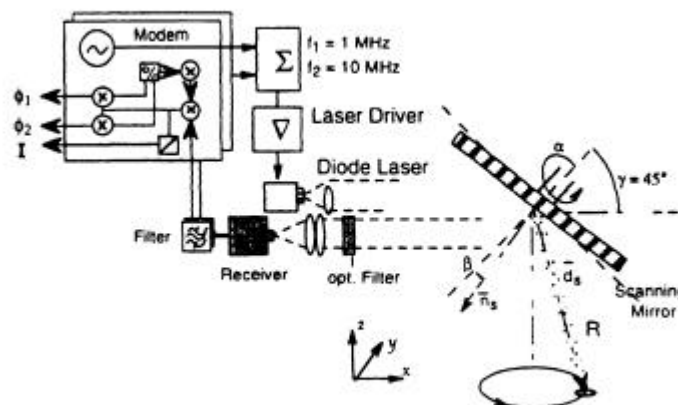


Figure 2-1: Block Diagram of ScaLARS

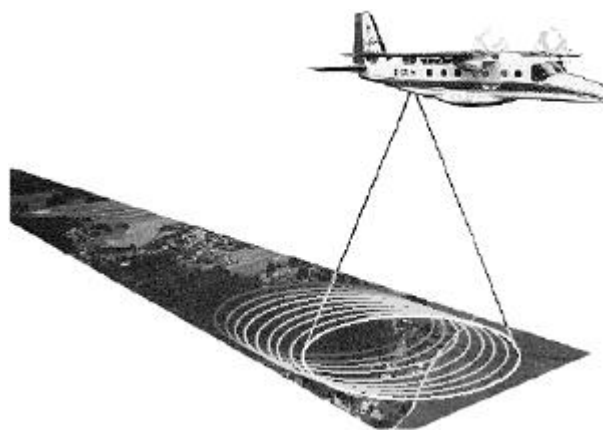


Figure 2-2: Scanning Pattern

Table 2-1: Technical Data of ScaLARS

laser source	CW laser diode
detector	Si avalanche photodiode (APD)
average emitted opt. radiation	0.8 W
laser wavelength	810 nm
beam divergence (IFOV)	1 mrad
max. slant range at 20% reflectivity	750 m
sample spot diameter at flying height h = 650 m	0.65 m
ranging frequencies (modulation)	1 MHz, 10 MHz
standard deviation (slant range)	0.04 m – 0.17 m
sample rate	7.5 kHz
dynamic range	50 dB
scanrate adjustable	max. 20 Hz
FOV: in flight direction across flight direction	± 9.7 deg / ± 13.4 deg ± 13.6 deg / ± 19.0 deg
swath width at (h = 700 m / ± 13.6 deg) (h = 650 m / ± 19.0 deg)	338 m 448 m
max. distance between adjacent samples in flight direction at 60 m/s across flight direction at h = 650 m	≤ 3 m ≤ 2.4 m
intensity measurement	13 bit

instantaneous scanning angle are stored. If the instantaneous position and orientation of the laser scanner is known the measurement point can be geocoded by straight forward transformations. In Table 2-1 the technical data of ScaLARS are compiled. Figure 2-1 shows the principle setup and Figure 2-2 illustrates how the scanning pattern propagates during flight. ScaLARS is explained in detail in [1,2].

3. Sequential processing of navigation and laser data and Calibration

Navigation data comprises POS-measurements by an inertial measurement unit (IMU), GPS, GPS-reference and possible additional data. Accurate POS-data for each laser measurement is calculated with help of Applanix postprocessing software. In a first step a differential and kinematic GPS carrier solution is created. This result is combined with the IMU-data in a Kalman filter with the following max. errors:

Position	0.05 – 0.3 m
Pitch and roll	0.005 degree
Heading	0.008 degree.

The accuracy achieved with this navigation system is stable and precise enough to estimate the geographic location of the reflecting spot. The laser scanner data exhibit only the slant range between laser scanner and the illuminated point on Earth and the instantaneous direction. The slant range vector \underline{s}_L can be described by this information in a laser scanner coordinate system L. To obtain the elevation of the laser measurement point on Earth the position and the orientation of the laser scanner in respect to an earth fixed coordinate system must be known. The laser measurement point \underline{r}_{s_WGS} in the earth fixed coordinate system WGS84 can be calculated straight forward by:

$$\underline{r}_{s_WGS} = \underline{r}_{GPS_WGS} + (---)_{WGS_I} \left[\underline{p}_{L_I} + \underline{p}_{GPS_I} + (---)_{I_L} \underline{s}_L \right] \quad (3-1)$$

\underline{p}_{GPS_WGS} is the position determined by differential GPS (DGPS) described in the coordinate system WGS84. \underline{p}_{L_I} is the displacement vector between the inertial measurement unit (IMU) and the laser scanner both mounted in the airplane. \underline{p}_{GPS_I} is the translation vector between GPS-receiving antenna and IMU. Both displacement vectors are described in the IMU coordinate system. The vectors \underline{p}_{L_I} and \underline{p}_{GPS_I} have to be surveyed before flight. They can be determined with required accuracy by conventional means. The transform matrix $(_)_{WGS-I}$ contains the orientation angles yaw, pitch and roll. These angles are measured continuously during flight by IMU. This matrix carries out the coordinate transformation from the coordinate system of IMU into WGS84. Matrix $(_)_{I-L}$ transforms the slant range vector measured in the coordinate system of the laser scanner into the IMU coordinate system. $(_)_{I-L}$ contains the Euler angles describing the orientation of the laser scanner with respect to IMU. Only a coarse estimation of the mounting angles can be done before the flight. They are accurately determined off-line after the mission. The displacement vectors are not so critical for the final measurement result, because they are independent of the flying height and can be measured quite accurate. The orientation angles are most critical, because they are multiplied by the slant range. The computation of elevation points on Earth is only straight forward, if the orientation is measured by IMU with an accuracy better than 0.01 degrees and the position accuracy is about 10 dm. This means, the mounting angles should be calibrated with an accuracy better than 0.01 degrees.

Before automatic sequential processing process is started, the calibration parameters for pitch angle, heading angle and roll angle offsets must be determined. Due to the high required angular accuracy the calibration is carried out by using sequentially processed laser data of selected calibration areas. These parameters can only be computed by iteration (s. Figure 2-1), which will be explained in chapters 3.1 -3.3.

The calibration procedures make use of the special geometric features of the Palmer scan. Due to the propagation of the ellipse with time caused by the movement of the airplane, one can subdivide the pattern into a forward looking and a backward looking part (s. Figure 2-2). After a certain time the backward looking part scans almost the same groundpoints as the forward part of the ellipse. Having correct calibration parameters there do not exist a difference in elevation and position of the measured groundpoints. Assuming precise measurements any observed deviation is caused by wrong position and/or orientation parameters. This effect is exploited in the following calibration procedures.

3.1 Calibration of Pitch Angle Offset

A pitch angle offset $d\nu$ shifts the scanning pattern either in flight direction or backward, lifting one side and lowering the opposite at the center line. According to Figure 3.1-1 this offset leads to an elevation error dH . dH can be determined with a high sensitivity if the forward and backward scans are evaluated for the same ground points in flat terrain. If d is the diameter of the ellipse in flight direction, the offset pitch angle $d\nu$ is calculated by

$$d\nu = \arcsin\left(\frac{dH}{d}\right) \quad (3.1-1)$$

In order to achieve 0.01 degree accuracy dH has to be estimated with less than 5cm from laser data. This can only be reached by taking mean values at smooth surfaces in the middle of the swath ($d \approx 250m$).

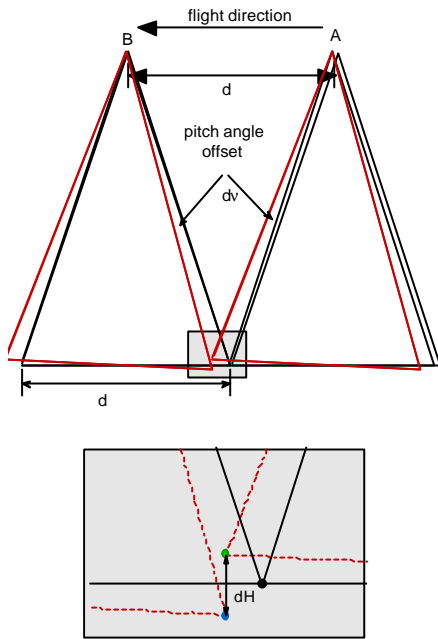


Figure 3.1-1: Elevation Error due to Pitch Angle Offset

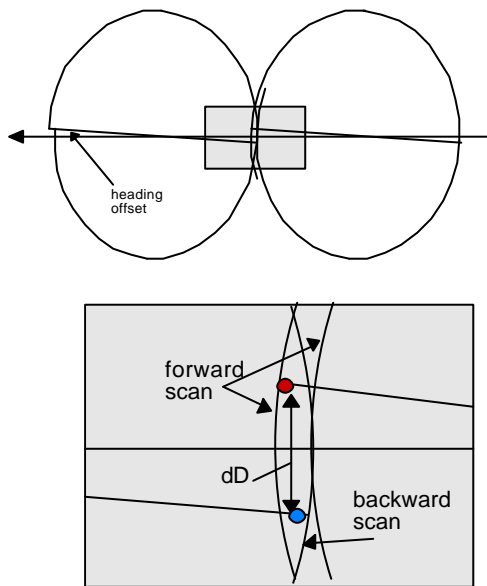


Figure 3.2-1: Heading Angel Offset

For an accuracy of 0.01 degree, dD_R has to be found with an accuracy of less than 0.3m at a flight height of 750m. Beside the intensity information also height information with characteristic features, like buildings, can be used.

Calibration is done in several iteration steps (s. Figure 1-1), because the estimation of dH , dD und dD_R does not allow an accurate separation of the error contribution from roll, pitch and heading for these unknown values. The stability of the calibration is checked with data from different flights to guarantee that the system works stable, which means, that the calibration values can be used for the total campaign and overlapping stripes can be combined without a sort of block adjustment.

3.2 Calibration of Heading Angle Offset

Figure 3.2-1 depicts the geometric configuration to determine heading angle offsets. An error in heading causes a twist between backward and forward scans. This can be directly observed by the intensity image evaluated separately for the forward and the backward scan. The heading offset $d\alpha$ identified in Figure x can be calculated by

$$d\alpha = \frac{dD}{2b} \quad (3.2-1)$$

if dD is the observed displacement at the nadir line and b is the semi-minor axis of the ellipse. To keep the horizontal error less than 0.3 m, dD has to derived from the intensity image with the same accuracy.

3.3 Calibration of Roll Angle Offset

The roll angle offsets can be optimally calibrated by flying two overlapping stripes in opposite flight directions. In this case the tilt of both stripes is a direct measure for the roll offset, if flat terrain is surveyed. However, a more advanced and generally applicable method was developed on the basis of the intensity information. In case of a correct roll angle offset objects like houses or house corners, which can be identified easily in the intensity laser data, must be found at exactly the same position in the overlapping area. With a roll angle offset is a displacement dD_R is observed in the intensity laser images. With regard to the center point between the displaced laser points the roll offset $d\beta$ can be determined by

$$d\beta = \arcsin\left(\frac{dD_R}{2 \cdot R}\right) \quad (3.3-1)$$

if R is the slant range measured by the laser.

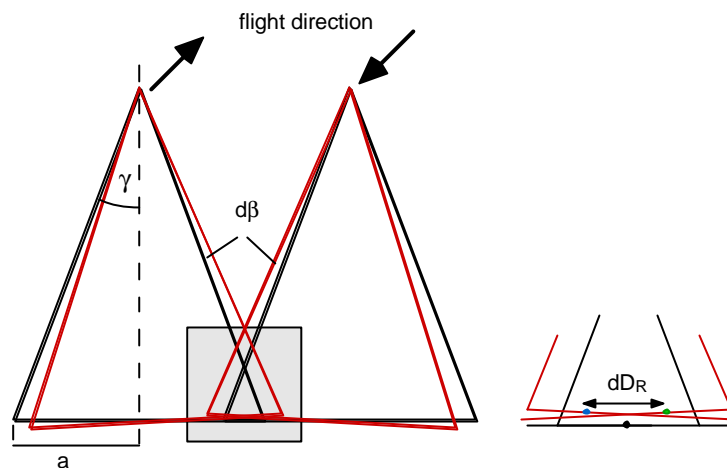


Figure 3.3-1: Roll Angle Offset and Resulting Displacement

After the sequential processing of all flight stripes this laser data is merged together and a transformation into regular grid is carried out. In combination with this step the transformation from WGS84 coordinate system to a specific map projection is done. For this project the complete area was subdivided in parts with 2,5km by 2.5km with a pixel size of 5m by 5m.

4. Classification and validation

For classification the use of a polynomial method revealed for almost all areas very good results. With help of a special search routine the most probable ground points were chosen within a 5m by 5m pixel. One pixel can show different height values, depending on the

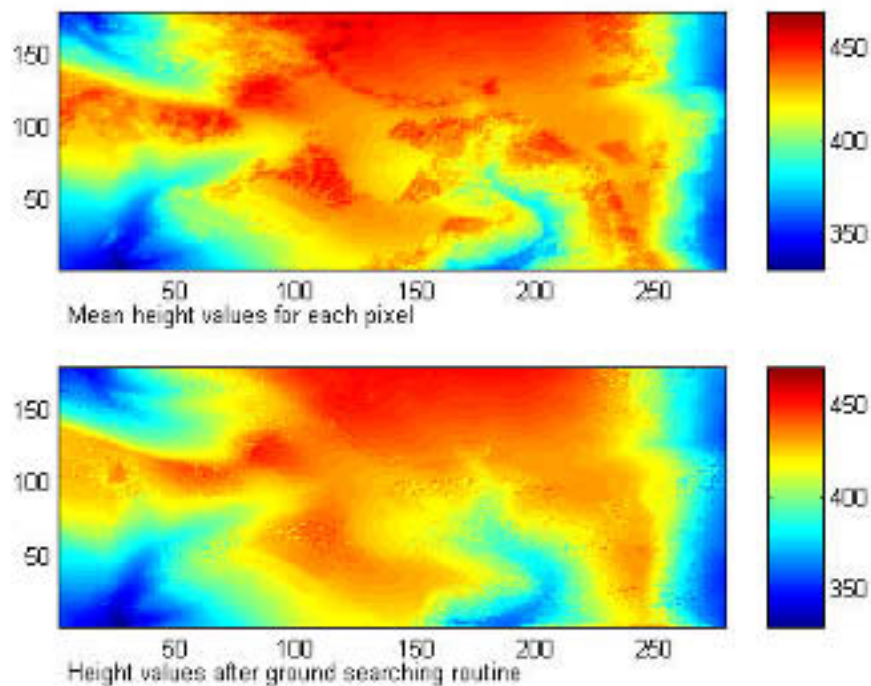


Figure 4-1: Mean Height Values for a Small Area and Resulting Values after Search Routine for Possible Ground Representatives

position of the laser spot within the pixel, for example if a building covers only a part of the pixel. A priori knowledge from a first sequential classification during laser/navigation computation as well as the relationship to neighboring pixels and a rough classification mask with three classes (open, urban, forested) were used to generate a single representative ground value for each pixel. Empty pixels, mainly resulting from rivers and seas where no return signal was available, were given a height value by using bilinear interpolation in order to provide complete data sets for computational reasons. This data reduction forms the basis for a first estimation of ground representing height values and these are taken as an input to the curve fitting algorithm. The difference between both data sets can be seen in Figure 4-1. This routine provides more ground points and helps to find a reference DTM for further processing.

Length and degree of the polynomial will be estimated with respect to the surface roughness of the laser measurements in the analyzed area. This variability allows for a better representation of natural features, like small and narrow valleys, edges, etc. and to find enough ground points in forested areas to offer good results (s. Figure 4-2 and Figure 4-3). The continuous monitoring of the distribution of the laser measurement with respect to a polynomial fitted curve gives a clear indication, either open or covered areas are processed. In forested and urban areas the polynomial will be forced down to the ground measurements in consecutive steps, using the measurement distribution for these data. Since the maximum and minimum length of the polynomial is limited (75m to 250m) and also the highest degree is 6, this algorithm is able to follow almost all terrain features and only reveals problems, if not enough ground point could be found within the extension of the polynomial. Also the distribution of the ground points along the polynomial is essential and is checked, because gaps, especially at the endings, may cause large errors in the fitting process.

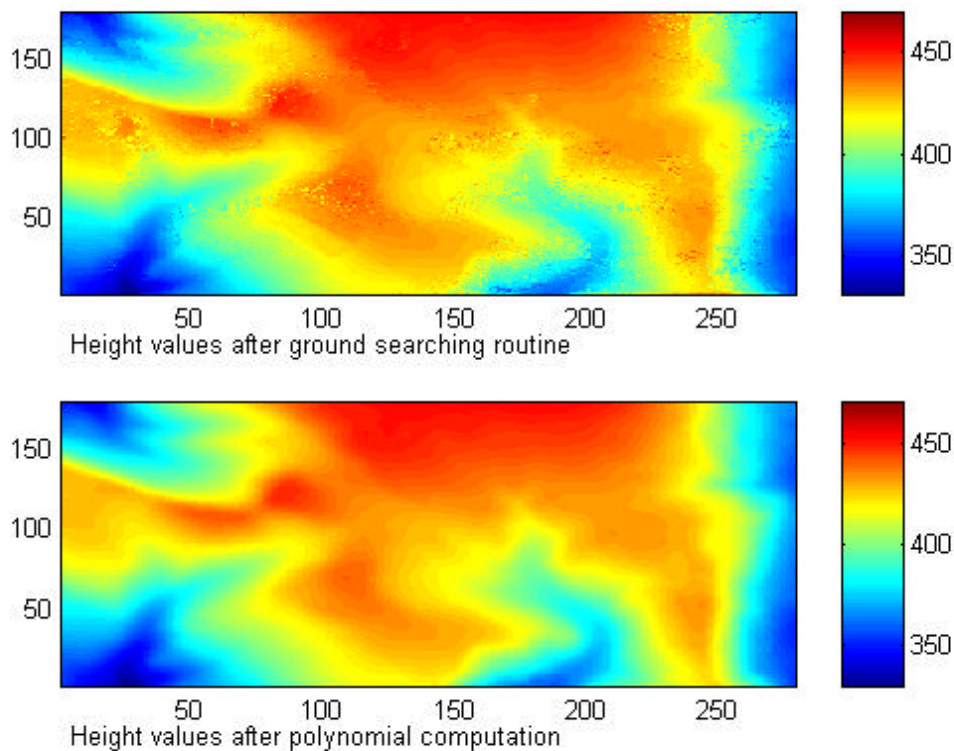


Figure 4-2: Reference DTM after Polynomial Computation Using Values Based on Searching Routine (upper picture)

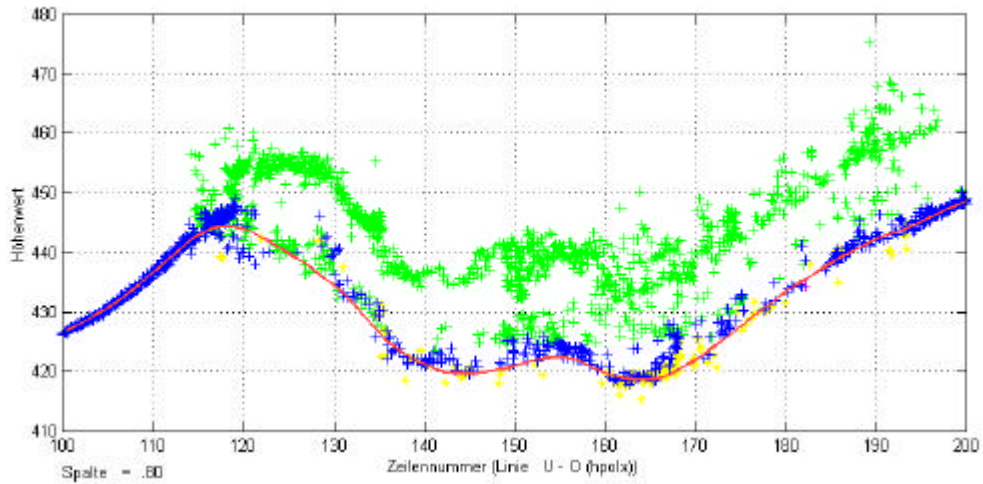


Figure 4-3: Row 80 of the Above Figures Showing Line 100 to 200. (All laser measurement are shown, colors are representing our sequential classification, the line represents the automatic polynomial calculation)

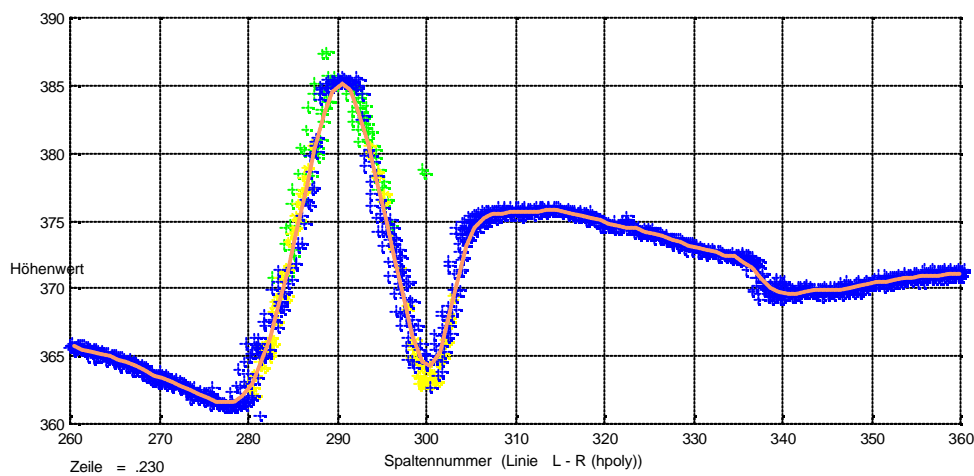
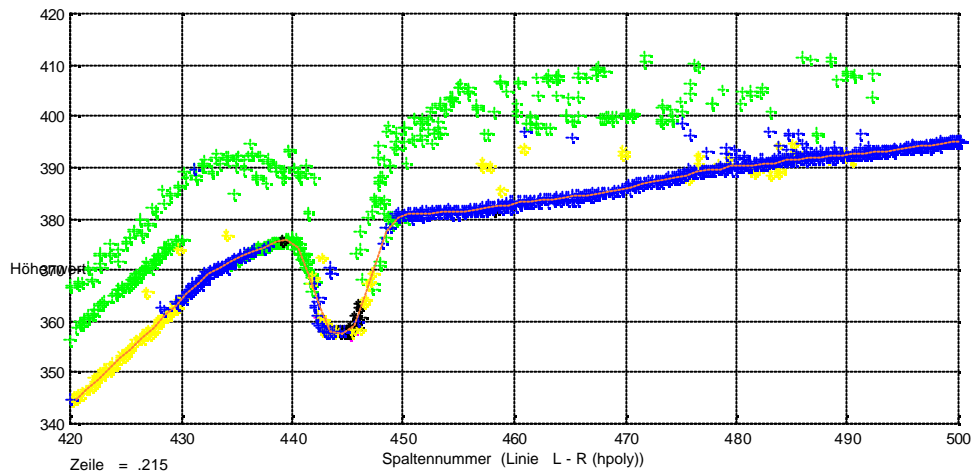


Figure 4-4: Classification Capabilities for Reproduction of Narrow Passes in Forest Areas (upper diagram) and of Embankments (lower diagram)

After this automatic classification run an interactive validation of the estimated terrain heights is performed. The measurement data and the classification results for lines and rows can be visualized, to inspect the conformity of both parts. If the classification result is not correct in critical areas – large buildings, very dense coniferous forest – probable ground point can be marked manually and will now be used in the polynomial calculation with high priority to fix the classification result around these values.

This error removal can be performed for a marked area with exactly the same routines as before, where the interactive corrections will be used as further data.. The manual corrections could be done line by line or row by row, taking each line/row or only every n^{th} line/row. In order to keep the manual interactions as small as possible these points were connected with help of a spline function. These corrected values were now taken to chose only measurement points within given limits for a new polynomial estimation. The limits could be adapted to a specific topography, thus allowing to preserve critical features like embankment, heaps, narrow passes and pits. In Figure 4-4 this capability is demonstrated for narrow pass on a forested area and for embankment in severe environment.

After the validation, which includes the corrections, this classification result corresponds to a Digital Terrain Model (DTM) where all objects, by definition no ground points, will be removed. With help of this reference DTM it is possible to differentiate between laser measurements which result from reflection from ground and those from buildings, trees, etc..

In order to guarantee an as good as possible classification result, a second final interactive inspection was carried out, where the validation is done on lines and rows different from the first operation. As a good practicable distance 5 lines or 25 m between lines/rows was used. Thus the maximum distance between inspected lines/rows was 15m, taking both inspections into account.

5. Archiving and delivery

The last step is the data output for the client and the internal archiving of relevant data. Output medium and output data was defined by our client. The internal archiving was done on CD, where also intermediate results were stored for further investigations and to be in a position to reprocess data, if necessary.

6. Conclusions

The presented processing chain was applied successfully for an area of 1300 km². Sample test show that the calibration parameters were stable during the whole survey. The classification procedures worked well even in critical areas e.g. cities and dense forests. The most manpower was used for validation. Validation can only be done manually by visual inspection of the data. A typical final DTM in 3D-projection is presented in Figure 6-1. Certain features like e.g. railway tracks can be identified clearly.

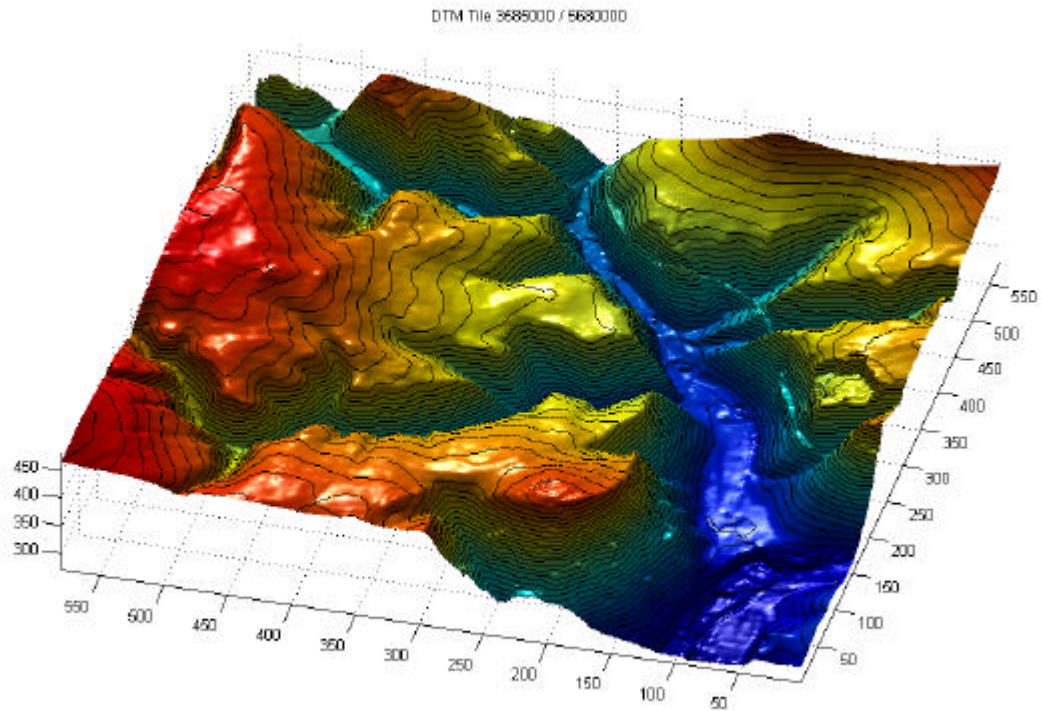


Figure 6-1: Final DTM in 3D-projection

7. References

- [1] Chr. Hug, A. Wehr
"Topographische Geländeaufnahme mit ScaLARS", GIS, 2/99, Jahrgang 12, Vol. 12, April 1999, Hüthig Verlag.
- [2] K.-H. Thiel, A. Wehr
"Advanced Processing Capabilities with Imaging Laser Altimeter ScaLARS", Proc. of SPIE Conference on Laser Radar Technology and Applications IV, Orlando, Florida, SPIE Vol. 3707, April 1999.

Airborne laserscanning versus airborne InSAR — a quality comparison of DEM's

Regine BRÜGELMANN, Remko de LANGE

Ministry of Transport, Public Works and Water Management, The Netherlands

Survey Department

Section of Remote Sensing and Photogrammetry

r.brugelmann@mdi.rws.minvenw.nl, r.dlange@mdi.rws.minvenw.nl

KEY WORDS: DTM/DEM/DSM, laserscanning, InSAR, accuracy

ABSTRACT

In this paper the results of a comparison of height data acquired from different sensors will be presented. The available datasets are a $1\text{ m} \times 1\text{ m}$ InSAR DEM, a DEM acquired with helicopter born laseraltimetry with a point density of 10-16 points/ m^2 and terrestrial measured profiles along dikes (GPS and tachymetry). In order to assess the quality of the two DEM's, they have been compared with the terrestrial reference data as well as with each other. The achieved height precision of the 1 m radar DEM is a systematic shift of 7 cm with a standard deviation of 37 cm . However, the position of the terrestrial reference points was not optimal for the radar DEM assessment. The precision of the laser DEM turned out to be quite impressive with a mean deviation of 3 cm and a standard deviation of 4 cm .

1 INTRODUCTION

Airborne laserscanning and airborne interferometric SAR are two recently developed technologies for the acquisition of high resolution and high precision digital elevation models (DEM's). With a grid spacing of one to several meters and a vertical accuracy of a few centimeters up to several decimeters, they have become a true alternative for DEM generation with classical photogrammetric and terrestrial methods.

The Dutch Survey Department of the Ministry of Transport, Public Works and Water Management (Meetkundige Dienst, Rijkswaterstaat) has extended experience with laser altimetry projects. As one of the first countries it will be provided with a new dense digital terrain model acquired by laser altimetry (Wouters and Bollweg, 1998). The entire surface of The Netherlands is expected to be covered with laserdata in 2001. The point density of the new DEM is one point per 16 m^2 , except for forest regions where the point density may be one point per 36 m^2 . For the acquisition and filtering task, the Survey Department contracted several companies. The quality of the delivered laserdata is thoroughly checked by the Survey Department (Crombaghs et al., 2000). The guaranteed height quality of the laserdata is a maximal systematic error of 5 cm and a maximal standard deviation of 15 cm . From the irregularly distributed laserpoints regular grids with grid spacings of 5 m , 25 m and 100 m are derived and delivered to customers such as local water management organisations. Beside the creation of a new national DEM, the Survey Department did some projects to analyse the quality of laserdata (Huising and Gomes Pereira, 1998). In addition, further applications of laserdata and therefrom derived features were investigated, such as road planning and design (Gomes Pereira and Janssen, 1999), determination of waterlevels (Bollweg, 1999), extraction of beach profiles (Vaessen et al., 1998) and extraction of breaklines (Gomes Pereira and Wicherson, 1999), (Brügelmann, 2000).

Beside gathering experience in laseraltimetry projects, the Survey Department also did some investigations on the potential of InSAR for the acquisition of high precision DEM's. A first test was performed with the airborne E-SAR of DLR in XTI-mode at X-band VV-polarization in 1997 (Huising et al., 1999), (Greidanus et al., 1999). Test areas were two islands in the Dutch Waddensea: Terschelling and Ameland. Improvement of the radar technique as well as possibly cost saving aspects and more independence from weather conditions with respect to laseraltimetry, motivated the Survey Department to perform a new test with airborne InSAR in 2000. This new test was flown by the German company Aerosensing with the AeS-1. There are promising publications over experiments in the Waddensea with the AeS-1. There a height standard deviation of 5 cm was achieved on flat sandbanks with a grid spacing of 2.5 m (Wimmer et al., 1999). The new study was held in a $5 \times 20\text{ km}^2$ testarea in The Netherlands. From this area laserdata as well as terrestrial data is available. In the following, these datasets will be introduced (section 2) and the performed experiments and achieved results will be described (section 3).

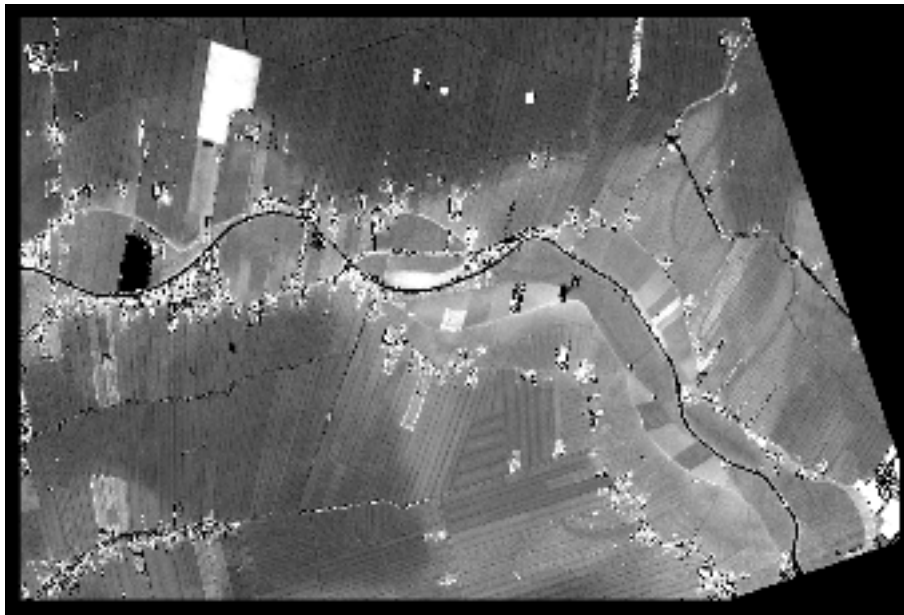


Figure 1: Radar DEM of $5.4 \text{ km} \times 3.6 \text{ km}$ testarea

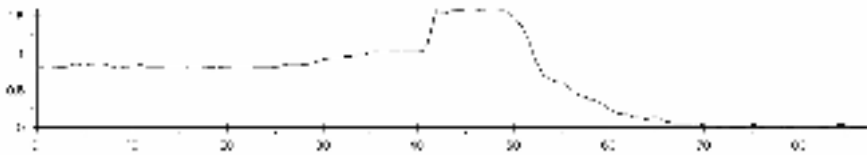


Figure 2: Profile of typical dike [meters]

2 DATA

The rectangle testarea which has been recorded with the AeS-1 lies along the river "Hollandsche IJssel" west of the city Utrecht between the towns of Haasdrecht and IJsselstein/De Meern. However, only a small part of the whole $5 \times 20 \text{ km}^2$ radar-DEM has been chosen for closer quality analysis. This subarea shown in fig. 1 comprises about $5.4 \times 3.6 \text{ km}^2$. The reason for this spatial restriction were problems concerning the handling of the huge amount of data, especially of the dense laser data.

The testarea consists of mostly flat terrain with meadows separated by narrow parallel ditches. Furthermore, the testarea comprises some small villages and isolated farms, but almost no forests and only a few trees. The larger black area on the left side represents water and the larger white field a dumping site. In west-eastern direction the course of the river Hollandsche IJssel can be distinguished by the curved black line of no-data pixels with dikes along both sides of the river. The height of the dikes, which form almost the only relief of this region, is about $0.80 \text{ m} - 2 \text{ m}$ with respect to the height of the surrounding terrain. The profile in fig. 2 shows the dimensions of a typical dike. In the following three subsections, the three datasets, that is the radar DEM, the laser data and terrestrial data, will be described.

2.1 InSAR data

The InSAR flight was carried out with the system AeS-1, designed and manufactured by the German company Aerosensing. It is operational since October 1996. The AeS-1 is a full interferometric synthetic aperture system (X-band, two antenna radar) with a ground resolution up to $0.5 \text{ m} \times 0.5 \text{ m}$. A detailed description of the system and the data processing chain can be found in (Schwäbisch and Moreira, 2000) and (Wimmer et al., 1999). Tab. 1 gives an overview of the main system and flight parameters of the AeS-1 SAR.

The data acquisition was carried out with a geometric resolution of 0.5 m . To cover the $5 \text{ km} \times 20 \text{ km}$ area with a 75% overlap 9 tracks with a length of 21 km and a width of 2 km were necessary. Totally 13 strips were recorded, inclusive the two reference tracks (one in NS- and the other in EW-direction). The 75% strip overlap results in three or maximal four each other overlapping DEM's. That means that for each gridcell minimal three terrain heights are available which were averaged to get the cell height. In the first place, Aerosensing had to deliver a 2.5 m -grid but finally we got even a 1 m -grid. The reason for this was that the quality of the initially delivered 2.5 m -grid was not satisfactory because of the use of a too large filtersize (10 m) during processing by Aerosensing. Within this $10 \text{ m} \times 10 \text{ m}$ area the heights — weighted

carrier frequency	9.55 GHz
radar wavelength	3.139 <i>m</i>
radar repetition frequency	12468.82 Hz
bandwidth	400 MHz
polarization	HH
peak power	2.5 kW
puls repetition frequency (PRF)	up to 16 kHz
incidence angle (mid range)	45°
swath width	2 <i>km</i>
InSAR basislength	2.51 <i>m</i>
mean flight height	3200 <i>m</i>
aircraft velocity	117.38 <i>m/sec</i>
strip overlap	75%
range pixel spacing	0.37 <i>m</i>
azimuth resolution of SLC image	0.4 <i>m</i>
azimuth pixel spacing	2.41 <i>m</i>
original ground resolution	0.5 <i>m</i>
delivered DEM pixel size	1 <i>m</i> (2.5 <i>m</i>)

Table 1: System parameters of X-Band AeS-1 SAR for testflight

by the reflectivity of the target — have been averaged. For the 1 *m*-grid a much smaller filtersize has been chosen (1.4 *m* × 1.4 *m*). The presented investigations by the Survey Department have been done with this 1 *m* DEM which describes the terrain more precisely because of less averaging of terrain heights. (The 2.5 *m*-grid results from averaging the heights of about six 1 *m*-gridcells.)

The data acquisition took place on July 6, 2000, that is during the full leaves on vegetation period. The flight conditions were good but turbulent. The flight hours added to approximately 16 hours plus 6 hours for mobilization and demobilization. The data were processed by Aerosensing and delivered to the Survey Department as geocoded 1 *m*-DEM. During the flight 16 corner reflectors were installed. Their coordinates were measured with GPS. The corner reflectors were used for geocoding and quality control purposes.

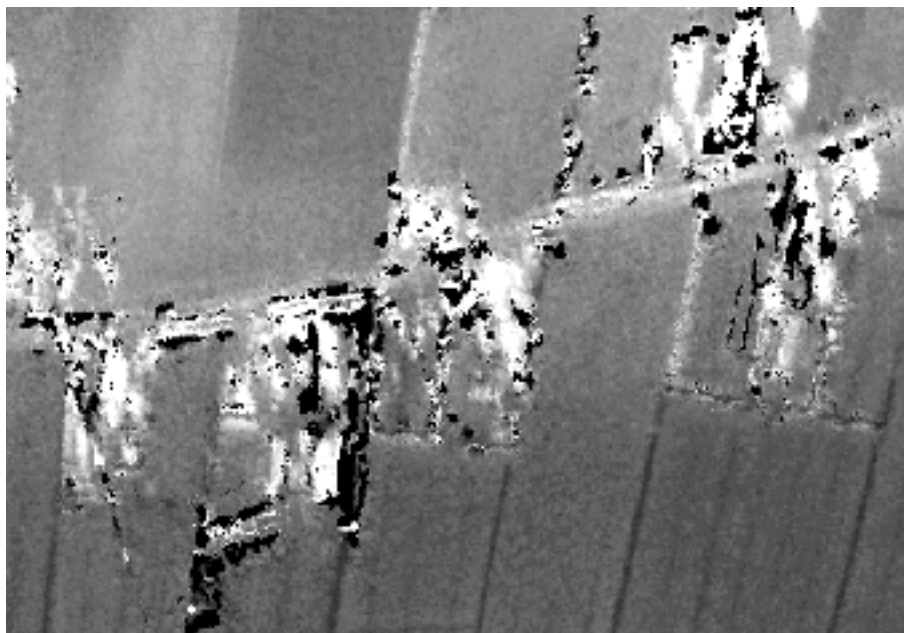


Figure 3: No-data pixels (black) in InSAR DEM in the neighbourhood of buildings and trees

Concerning the initially delivered 2.5 m-DEM, Aerosensing did some quality checks with the corner reflectors. The height differences between the heights of 8 corner reflectors and the corresponding heights in the radar-DEM were calculated. The height differences ranges from -6 cm up to +11 cm with a standard deviation of 5.8 cm. A second quality control was done by calculating the height differences of two each other overlapping tracks along a 22 km long profile in flight direction. Each meter a height difference was computed. The differences showed a standard deviation of 10.7 cm, resulting in a standard deviation of $10.7 \text{ cm}/\sqrt{2} = 7.57 \text{ cm}$ of a single track. As each height point of the final DEM is covered three times, the resulting standard deviation of the 2.5 m-DEM is estimated to be around 4.37 cm.

The investigated subarea (see fig. 1) comprises 19.7 million 1 m gridcells. Subtracting the upper and lower right corner areas where no data have been acquired results in 17.7 million gridcells. From these gridcells about 2.8% contain no data due to missing reflections, e.g. on water or behind obstacles (buildings). Another reason for no-data pixels is a bad coherence, e.g. caused by moving objects (e.g. trees on windy days). The quality of coherence is been checked during processing by Aerosensing. For each pixel a quality measure is available which determines the precision and reliability of the calculated height. Depending on the chosen threshold more or less no-data pixels will be obtained. Fig. 3 shows a subarea of the radar DEM with some no-data pixels (black) in the neighbourhood of buildings with some trees around. The flight direction corresponds approximately with the direction of the road in the centre of the figure.

2.2 Laserdata

It is important to mention that the laserdata is *not* part of the standard laserdata forming the new national DEM but has especially been acquired for monitoring purposes concerning the dikes in the district of the local water management organisation. This has been done with a much higher point density than for the national DEM. It was around 10-16 points/m². The laserscanning flight has been performed with the FLI-MAP system (Fast Laser Imaging and Mapping Airborne Platform) from Fugro-Inpark B.V. (The Netherlands). This is a helicopter born system which is primarily designed for monitoring roads, rail-roads and power-lines. Therefore, only the first returning laser pulse is recorded. The height of the aircraft as well as the swath width was about 70 m. Per second about 11000 points have been acquired. Tabel 2 shows an overview of system and flight parameters. For a further description of the FLI-MAP system see (Reed, 1997) and (Baltsavias, 1999).

Since the laserdata has been acquired for monitoring the dikes, the laserdata strips follow the river course with its smaller dikes lying directly along the water, and the larger dikes lying further away from the river course on both sides of the river. Thus, there are three, each other hardly overlapping, strips with laserdata covering only a small part of the radar DEM (about 10%) on which the analysis will focus (see fig. 4). Unfortunately, the new national DEM can not be used as reference DEM because it is not yet available in this area. Altogether, there are 1.6 million radar gridcells covered with laserdata, that is 25 million laser points.

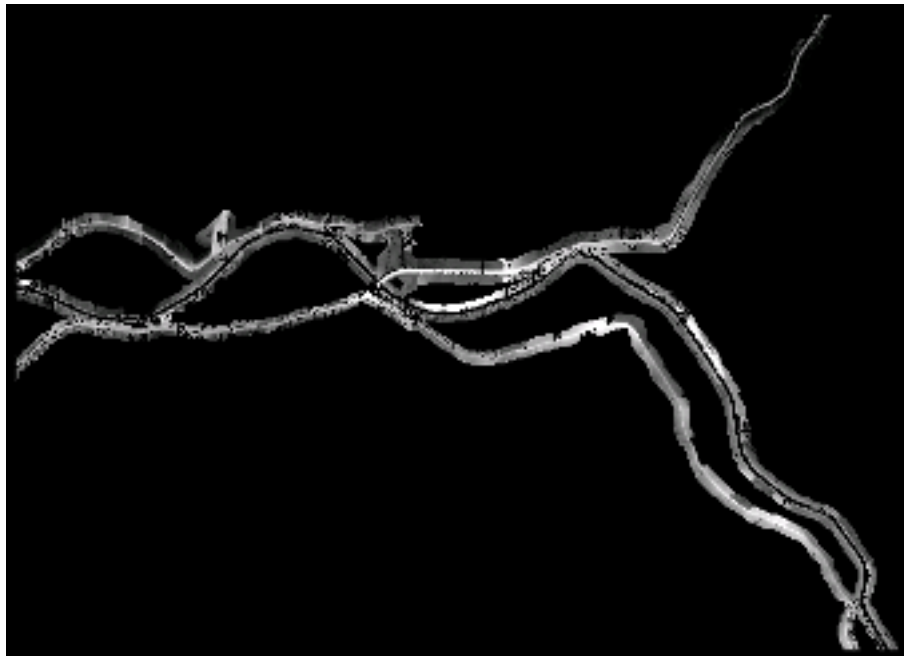


Figure 4: Laser DEM of 5.4 km × 3.6 km testarea

puls repetition frequency (PRF)	11600 Hz
scan frequency	58 Hz
scan steps	5.236 mrad (200 pixels in 60°)
beam divergence	2 mrad
wavelength	904 nm
mean flight height	70 m
swath width	70 m
aircraft velocity	20 m/sec (70 km/hour)
scan angle	60°
strip overlap	about 50%
point density	10-16 points per m ²
range resolution	1.5 cm

Table 2: System parameters of FLI-MAP for testflight

The flight has been done in october 1999, also in the full leaves on period but 8 months earlier than the InSAR flight. The local water management organisation which was the purchaser of the laserscanning flight, demanded a height precision of 5 cm mean deviation and 5 cm standard deviation on hard topography, e.g. roads, and short gras. The delivered laserdata has been filtered by Fugro-Inpark. That means that all points lying on buildings, bushes and trees have been eliminated resulting in no-data pixels in the laser DEM. These no-data areas in the laserdata can be used to determine a set of optimal terrestrial points for the precision assessment of the radar DEM. This can be done by excluding terrestrial points lying on vegetation (see section 3.1). These points are not suitable for the comparison with the radar DEM because the radar signal measures the top of a tree while the reference point lies on the ground. This results in large height deviations which do not represent the real precision of the DEM. In addition, the returned radar signal of points lying near buildings will be disturbed by reflections from vertical walls acting as corner reflectors. These points also can be eliminated using laserdata as additional information source.

2.3 Terrestrial data

The terrestrial points have been acquired for the local water management organisation for control purposes concerning the FLI-MAP data because monitoring the condition of river dikes with dense laser data was a pilot project. Therefore, the terrestrial point data have been acquired along the dikes (see fig. 5 and 6). This has been done with tachymetry and a dynamic GPS system. The latter has been performed by riding with an all terrain vehicle on the top of the dikes and permanently acquiring GPS data. Not all of these many points were delivered to the local water management organisation. The distance between the now available points is about 25 m. Thus, the terrestrial reference data representing

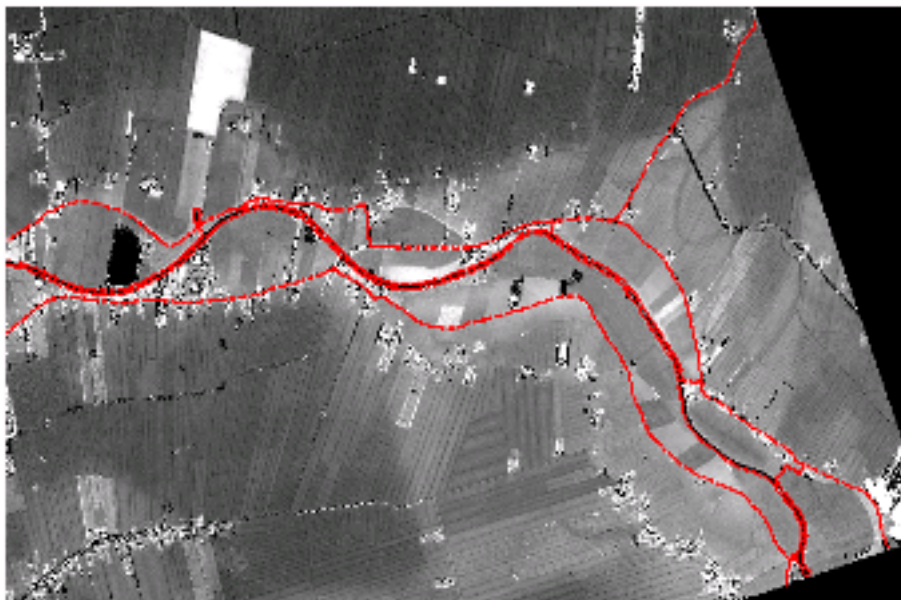


Figure 5: Radar DEM with terrestrial measured reference points (red dots)

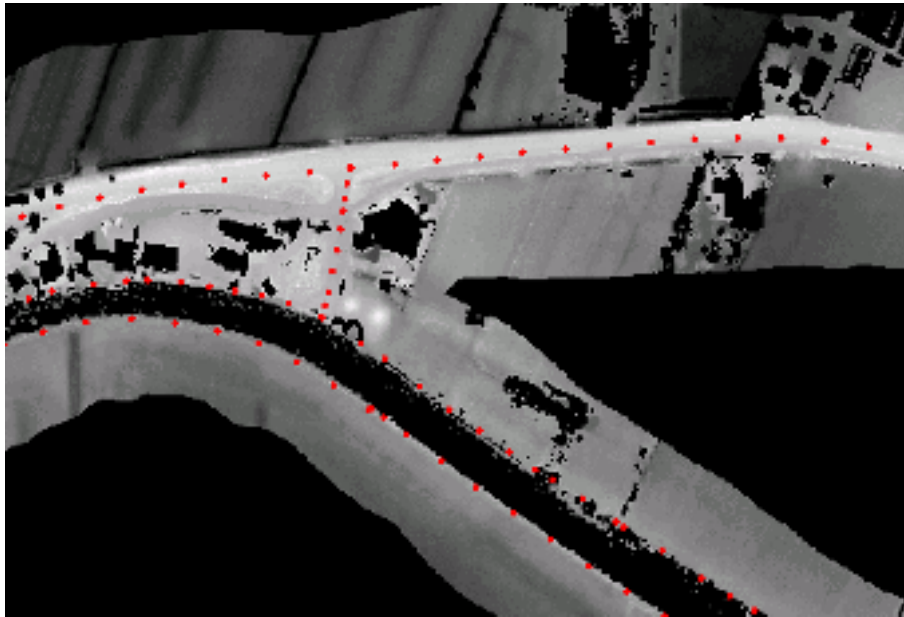


Figure 6: Position of terrestrial points along dikes (above) and river banks (below) in the laser DEM

length-profiles along the dikes, is rather dense in direction of the dikes. But the spreading over the whole DEM area is certainly not optimal for an assessment of DEM's. The whole area comprises in total about 1300 terrestrial points which have been measured during the summer of 1999. The height precision is about 1-2 *cm*. From all terrestrial points some subsets have been derived in order to exclude less suitable points, e.g. points lying near buildings or under trees, from the DEM assessment. These subsets will be described together with the concerned experiments in the following section.

3 EXPERIMENTS AND RESULTS

To assess the height quality of the radar en laser DEM, height differences have been analyzed. These differences have been calculated between:

1. InSAR DEM and terrestrial point data,
2. laser point data and terrestrial point data,
3. InSAR DEM and laser DEM.

The height differences have been investigated by means of histograms and mean and standard deviations. The following subsections describe the performed tests and results.

3.1 InSAR DEM versus terrestrial point data

In a first experiment we compared all available terrestrial points with the radar DEM. For each terrestrial point the height of the corresponding 1 *m* gridcell has been subtracted from the height of this point (measured by GPS or tachymety). This resulted in a mean deviation of 0.48 *m* and a standard deviation of 1.42 *m* (see tab. 3). These quite large deviations are ranging from about -3 *m* up to 17 *m*. But it turned out that not all terrestrial points are suitable in the same degree. Some are lying under trees or in the neighbourhood of buildings, trees or other objects. In this case, the radar is reflected on the top of the trees instead of from the ground. Or the final height is disturbed due to averaging of heights resulting from vegetation top *and* ground. Also the terrestrial points lying at the river bank are supposed to be unreliable. From water

terrestrial dataset	$n_{terr. points}$	$\overline{\Delta h} [m]$	$\sigma_{\Delta h} [m]$	$min_{\Delta h} [m]$	$max_{\Delta h} [m]$
all points	1345	0.48	1.42	-3.56	17.16
all points -5% outliers	1277	0.35	0.85	-0.78	4.63
subset	456	0.12	0.75	-3.44	8.23
subset -5% outliers	434	0.07	0.37	-0.59	1.66

Table 3: Results of 'radar DEM versus terrestrial data' (nearest neighbour method)

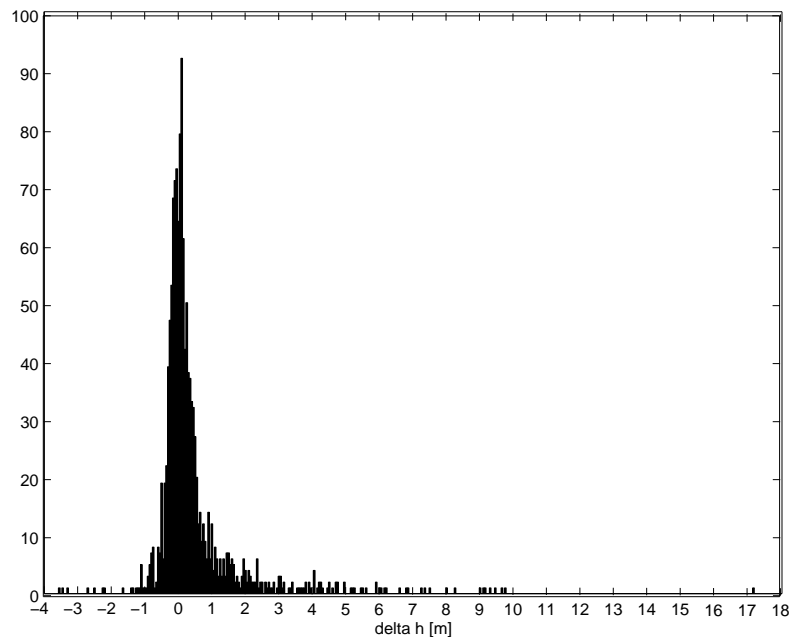


Figure 7: Histogram of $\overline{\Delta h}$ [m] between radar DEM and terrestrial data (interval = 5 cm)

surfaces no radar signal will be reflected. The heights of points situated near the water might be disturbed due to averaging of heights from an area larger than the final pixel size of 1 m. Thus, a more reliable subset of terrestrial points has been created. This has been done in the following way:

1. All terrestrial points situated on the river banks have been sorted out. Only points lying on the larger (winter-) dikes further away from the river course are retained.
2. In addition, the information inherent in the *filtered* laser DEM has been used to eliminate terrestrial points lying under trees or in the near neighbourhood of trees, buildings and other objects which do not belong to the ground. This has been done by eliminating not only all terrestrial points which are lying in no-data areas (= filtered vegetation) but also by rejecting reference points lying in dilated no-data areas (mathematical morphology operator 'dilation' with a 5×5 structure element). Fig. 8 shows such a case of points situated near trees or bushes which have been filtered in the laser data. In the radar DEM, the height of the left point certainly will be disturbed by the bush or tree and therefore this point has been eliminated.

In the following we will refer to the about 500 remaining points as 'subset'. For this subset the systematic height error with respect to the radar DEM is $\overline{\Delta h} = 12 \text{ cm}$ with $\sigma_{\Delta h} = 75 \text{ cm}$ (see tab. 3). After eliminating 5% outliers these values improve to $\overline{\Delta h} = 7 \text{ cm}$ with $\sigma_{\Delta h} = 37 \text{ cm}$ concerning the 1 m radar DEM.

Since we were originally interested in the precision of a 2.5 m grid instead of in the precision of a 1 m grid, the standard deviation has been propagated to a 2.5 m grid which yields $\sigma_{\Delta h, 2.5m} = 1/2.5 \cdot \sigma_{\Delta h, 1m} = 14.8 \text{ cm}$. But this value must be treated with caution because probably existing correlations have been neglected. Resampling of the 1m grid to a 2.5m grid and afterwards computing the differences between radar DEM and terrestrial data would be another possibility but had not yet been done.

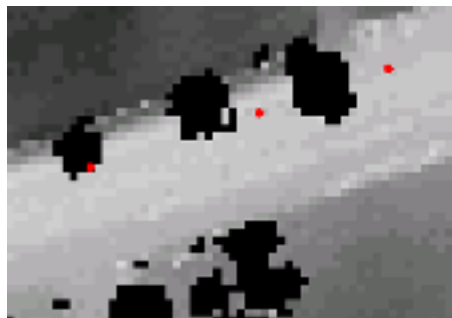


Figure 8: Terrestrial points lying near trees (black pixels = filtered laser data)

The reasons for these not entirely satisfactory results are not totally clear. Perhaps there are still too much terrestrial points where the corresponding radar heights are disturbed by obstacles (trees etc.) with respect to the sidelooking radar. Also the situation of the terrestrial reference points on top of the dikes might not be optimal for assessing the radar DEM. Perhaps averaging of heights from the dike top and lower situated terrain at the dike flanks causes such large deviations. But on the other hand the flat top of the dike is with its 10 m quite broad with respect to the pixelsize of 1 m of the radar DEM (see fig. 2).

To analyse the large height deviations, we zoomed into a dike area where height-deviations larger than 50 cm have been found (see fig. 9). On the left, the radar DEM is shown and on the right side the corresponding laser DEM. The red dots indicate the position of the terrestrial reference points. Black pixels represent no-data areas. The two profiles across the dike have been taken through the third point from the right. The figures illustrate that the shape of the dike is reproduced much better in the laser DEM than in the radar DEM. Obviously, strange effects are happening concerning the shape of the dike in the radar DEM, above all on the right side where the dike direction corresponds appropriately with the flight direction.

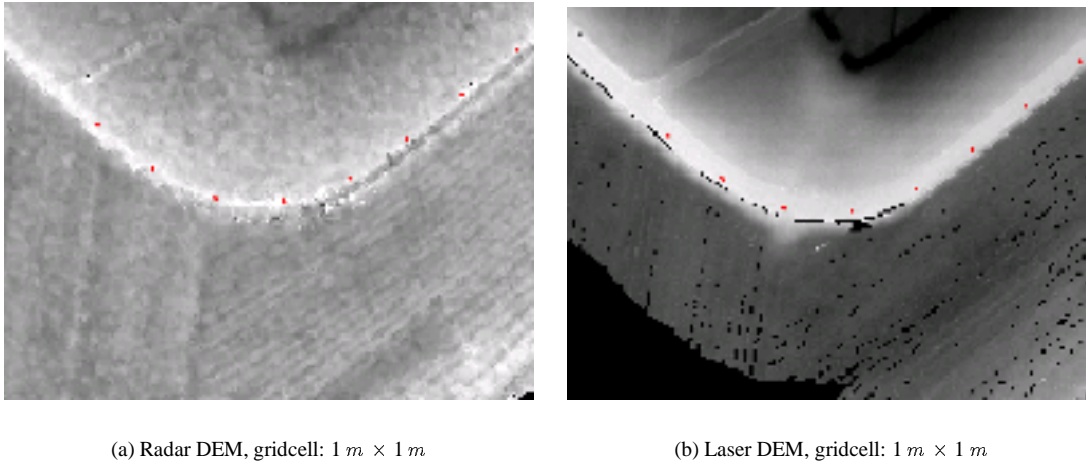


Figure 9: dike

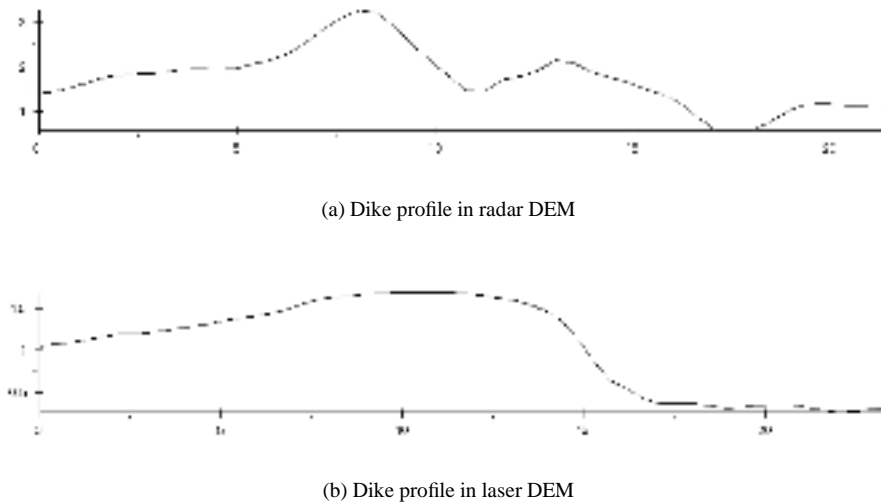


Figure 10: Profiles

3.2 Laser point data versus terrestrial point data

Concerning the analysis of the laser data, we started in the same manner as with the radar DEM assessment, that is with *all* available terrestrial points. Around every terrestrial point a 'footprint' of 1 m diameter has been taken and all laser points lying within this footprint (about 16 points) have been averaged, weighted by their distance to the center point. This yields a mean deviation of $\overline{\Delta h} = 6\text{ cm}$ with a standard deviation of $\sigma_{\Delta h} = 12\text{ cm}$ (see tab. 4). Also some smaller footprints have been applied, ranging from 30 cm to 10 cm . The latter corresponds with the nearest neighbour method because only one laser point is left in this small footprint. Tab. 4 shows that the results do not differ much from the results got with

the 1 m footprint. The conclusion of this is, that the terrain in the near neighbourhood of the terrestrial points is quite flat and that the precision of a single laserpoint is comparable to the precision of the 16 averaged heights of the laserpoints. That means, that the precision of already a *single* laserpoint is rather good. The histogram of all height deviations (see fig. 11) which resembles quite well a Gaussian distribution, shows that there are less outliers than with the radar DEM comparison. Therefore, only 1% outliers has been eliminated yielding a mean deviation of $\overline{\Delta h} = 6 \text{ cm}$ with a standard deviation of $\sigma_{\Delta h} = 10 \text{ cm}$ (see tab. 4). This fairly improves by restricting the height comparison on the same subset of terrestrial reference points as with the radar DEM assessment. The final, really impressive results then are $\overline{\Delta h} = 3 \text{ cm}$ with $\sigma_{\Delta h} = 4 \text{ cm}$.

terrestrial dataset	$n_{terr. \text{ points}}$	\bar{n}_{fpp}	$\overline{\Delta h} [m]$	$\sigma_{\Delta h} [m]$	$min_{\Delta h} [m]$	$max_{\Delta h} [m]$
all points (fp = 1 m)	1266	16	0.056	0.124	-1.0	0.95
points with fp = 0.3 m	1073	1.9	0.056	0.130	-1.0	1.3
points with fp = 0.2 m	675	1.3	0.055	0.123	-1.0	0.44
points with fp = 0.1 m	207	1.1	0.058	0.117	-0.14	0.23
all points -1% outliers	1254	16	0.056	0.097	-0.35	0.59
subset (fp = 1 m)	530	16	0.027	0.060	-1.00	0.25
subset -1% outliers	526	16	0.028	0.037	-0.08	0.20

Table 4: Results of 'laser DEM versus terrestrial data' (fp = "footprint", \bar{n}_{fpp} = mean number of laserpoints per footprint)

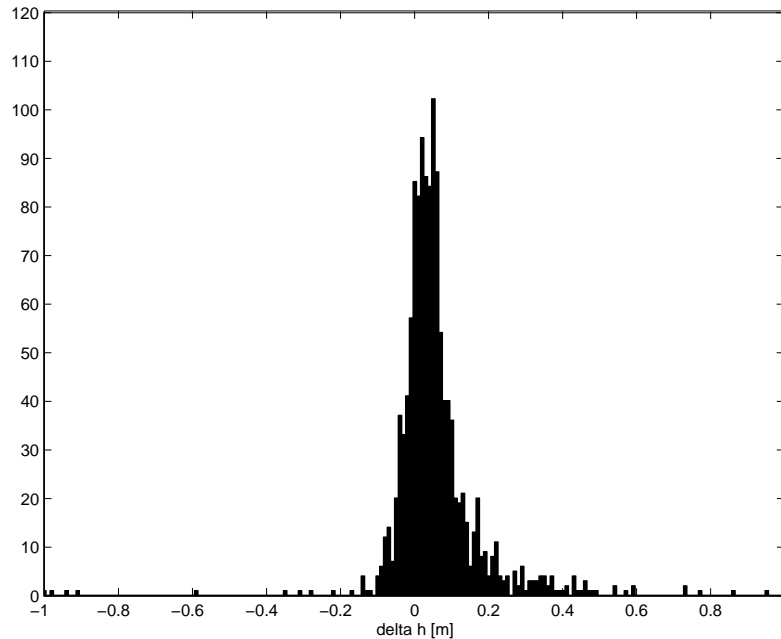


Figure 11: Histogram of $\overline{\Delta h} [m]$ between laser and terrestrial data (fp = 1 m, histogram interval = 1 cm)

3.3 InSAR DEM versus laser DEM

Finally, height differences between radar DEM and laser DEM have been calculated — even if an interpretation of the results might be difficult as each of the DEM's is erroneous. Thus, the height comparison is spread over a much larger area than the comparison with the terrestrial measured profiles. The amount of analysed points is gigantic: 1.2 millions. The height comparison has exclusively been done for the more reliable subset of the overall dataset (see section 3.1) and for two different footprint dimensions: 1 m and 10 cm. The 1 m footprint case complies with a co-located laser grid (with respect to the radar grid) whereas the 10 cm footprint case corresponds with the nearest neighbour method. The results of the two different footprint cases do not differ much from each other (see tab. 5). This property has already appeared concerning the laser data assessment with terrestrial reference data (see section 3.2). The systematic shift is about -10 cm and the standard deviation is about 60 cm. The negative shift denotes that the radar DEM is lying on average above the laser DEM. This has been expected because the chance that — supposed there is vegetation — the almost vertical and much more denser laser signals reach the ground is greater than with the sidelooking radar signal. The standard deviation of

height differences is quite large. But it must be kept in mind that also all height differences caused by different vegetation (grass) heights due to seasonal differences are contained (laser flight in july, radar flight in october) . This effect shall be illustrated in the following example.

The variations of the radar and laser height data in flat areas have been investigated for two small areas (meadows) which are supposed to be rather flat. Tab. 6 shows the results. Subareas 1a and 1b refer to the same meadow. For these subareas a vertical shift of about 15 cm can be stated. Here the radar DEM heights are lower than the laserdata heights. This somewhat unexpected behaviour can be explained by different grass heights at the two different data acquisition point of times (or a systematic error in one or both systems). In subarea 2 this effect does not appear: the heights measured by radar and laser coincide. But there is a clear difference in amount of height variation. The standard deviation of laser heights is about 5 cm whereas the standard deviation of radar heights is about 15 cm. The larger variation of radar heights can also be seen in fig. 9.

footprint	$n_{radar\ points}$	$\overline{\Delta h}$ [m]	$\sigma_{\Delta h}$ [m]
1 m	1.235.730	-0.105	0.60
0.1 m	146.309	-0.132	0.68

Table 5: Results of 'laser DEM – radar DEM' concerning the subset

subarea	radar DEM			laser point data		
	n_{points}	mean height \bar{h} [m]	σ_h [m]	n_{points}	mean height \bar{h} [m]	σ_h [m]
1a	256	0.33	0.15	1799	0.49	0.05
1b	990	0.27	0.15	7833	0.42	0.06
2	306	0.52	0.13	2110	0.52	0.05

Table 6: Variations of laser and radar DEM in flat subareas

4 CONCLUSIONS

In this paper the results of a comparison of height data acquired from different sensors has been presented. The available datasets were a 1 m × 1 m InSAR DEM, a DEM acquired with helicopter born laseraltimetry with a point density of 10-16 points/m² and terrestrial measured profiles along dikes (GPS and tachymetry). In order to assess the quality of the two DEM's, they have been compared with the terrestrial reference data as well as with each other.

The achieved height precision of the 1 m radar DEM is a systematic shift of 7 cm with a standard deviation of 37 cm. These values apply under the restriction that the position of the terrestrial reference points was not optimal for the assessment of the radar DEM. Reference points situated in open field with absolutely no disturbing vegetation around might yield better results (see Waddensea test of Aerosensing (Wimmer et al., 1999)). However, the results are better than those found by (Kleusberg and Klaedtke, 1999) which compared an InSAR DEM with trigonometric points in open terrain and got a standard deviation of 1.3 m. But on the other hand, the results of our test comply well with the results of (Sties et al., 2000) whose InSAR DEM investigation yields standard deviations ranging from 20 cm to 60 cm for bare soils.

The precision of the radar DEM can be improved by taking a stricter coherence threshold during processing to eliminate less reliable points from the DEM. However, this way the final DEM will contain more no-data gridcells. Perhaps another possibility to improve the results is to average the different available heights per pixel in a more intelligent manner, e.g. by taking the lowest height per pixel which is comparable to laserdata processing. Another conclusion is that the acquisition of objects such as dikes are not satisfactory with radar. The shape of the dike body obviously was changed too much in the radar DEM.

The precision of the laser DEM is quite impressive with a mean deviation of 3 cm and a standard deviation of 4 cm. This is even better than what can be obtained by the airborne laseraltimetry systems used for the production of the new dutch national DEM. But the differences concerning price are also very large. The same applies for the comparison of the radar and the laser DEM's in this paper. The latter is more precise but also much more expensive.

ACKNOWLEDGMENTS

The laser altimetry and terrestrial data was kindly provided by Hoogheemraadschap 'De Stichtse Rijnlanden' (local water management organisation).

REFERENCES

- Baltsavias, E. P., 1999. Airborne laser scanning: Existing systems and firms and other resources. *ISPRS Journal of Photogrammetry & Remote Sensing* 54(2-3), pp. 164–198.
- Bollweg, A., 1999. Water management of the river Rhine — water level from laser altimetry. *GIM International*, 13(11), pp. 30 – 33.
- Brügelmann, R., 2000. Automatic breakline detection from airborne laser range data. *International Archives of Photogrammetry and Remote Sensing*, Vol. XXXIII, Part 3A, Amsterdam, pp. 109–116.
- Crombaghs, M., Brügelmann, R. and de Min, E., 2000. On the adjustment of overlapping strips of laseraltimeter height data. *International Archives of Photogrammetry and Remote Sensing*, Vol. XXXIII, Part 3A, Amsterdam, pp. 230–237.
- Gomes Pereira, L. and Janssen, L., 1999. Suitability of laser data for DTM generation: A case study in the context of road planning and design. *ISPRS Journal of Photogrammetry & Remote Sensing* 54, pp. 244–253.
- Gomes Pereira, L. and Wicherson, R., 1999. Suitability of laser data for deriving geographical information - a case study in the context of management of fluvial zones. *ISPRS Journal of Photogrammetry & Remote Sensing* 54(2-3), pp. 105–114.
- Greidanus, H., Huising, E., Platschorre, Y., van Bree, R., van Halsema, D. and Vaessen, E., 1999. Coastal DEMs with cross-track interferometry. *Proceedings IGARS '99, 28 June-2 July 1999, Hamburg, Germany*.
- Huising, E. and Gomes Pereira, L., 1998. Errors and accuracy estimates of laser data acquired by various laser scanning systems for topographic applications. *ISPRS Journal of Photogrammetry & Remote Sensing* 53, pp. 245–261.
- Huising, E., Dierikx, Y., Vaessen, E., Vogelzang, J., Greidanus, H., Bree, R. V., Aardoom, J. and Huurneman, G., 1999. Airborne and spaceborne SAR interferometry. Report BCRS-99-16, Netherlands Remote Sensing Board, Delft, The Netherlands.
- Kleusberg, A. and Klaedtke, H.-G., 1999. Accuracy assessment of a digital height model derived from airborne synthetic aperture radar measurements. In: D. Fritsch and R. Spiller (eds), *Photogrammetric Week '99*, Wichmann, Heidelberg, pp. 139–143.
- Reed, M., 1997. Fugro FLI-MAP system. *EARSel Newsletter, Special Issue: Laser Scanning* pp. 18–21.
- Schwäbisch, M. and Moreira, J., 2000. The high-resolution interferometric SAR AeS-1 - conceptual design, data processing and range of applications (in German). *PFG (Photogrammetrie, Fernerkundung, Geoinformation)* (4), pp. 237–246.
- Sties, M., Krüger, S., Mercer, J. and Schnick, S., 2000. Comparison of digital elevation data from airborne laser and interferometric SAR systems. *International Archives of Photogrammetry and Remote Sensing*, Vol. XXXIII, Part B3, Amsterdam, pp. 866–873.
- Vaessen, E., Platschorre, Y., Huising, E. and Gomes Pereira, L., 1998. Extraction of beach profiles by using laser altimetry (in Dutch). Survey Department Rijkswaterstaat, Delft, p. 33.
- Wimmer, C., Siegmund, R. and Moreira, J., 1999. Derivation and validation of high precision topography models in the waddensea with airborne SAR-interferometry. *Proceedings IGARS '99, 28 June - 2 July 1999, Hamburg, Germany*.
- Wouters, W. and Bollweg, A., 1998. AHN: Actual height model of The Netherlands - a detailed elevation model using airborne laser altimetry. *GeoInformatics*, vol. 1, september 1998.

A comparison of airborne IfSAR and LIDAR data over the Vaihingen test site¹

Ian Dowman and Peggy Fischer
University College London

Abstract

This paper describes some comparisons which have been made between digital elevation models (DEMs) generated from LIDAR data in interferometric SAR data (IfSAR) over a test area in Southern Germany. The data was provided through the OEEPE for the purpose of evaluating the data. The paper describes the characteristics of the test site and the data, and the preprocessing carried out. The work described includes direct comparisons of the whole of the IfSAR and LIDAR data, of sections of the area showing similar characteristics, and between the DEMs and a grid of ground check points. The conclusions confirm a number of expectations on the nature and accuracy of LIDAR and IfSAR data and give an indication of the accuracy in this type of terrain.

1. Introduction

Digital elevation models (DEMs) derived from sensors on airborne platforms, such as Interferometric SAR (IfSAR) and LIDAR, have become more widely used in recent years because of the ability to determine the position and orientation of the platform with GPS and INS technology. LIDAR, in particular has received a lot of attention from production organisations and research establishments because of its high precision and the minimum processing required. IfSAR on the other hand has received less attention although it offers wide coverage at an economical price. OEEPE (The European Organisation for Experimental Photogrammetric Research) has set up two working groups to study data from these two sensors, and has distributed data sets for organisations to use to study the data. This paper reports on a comparison of the precision and accuracy of data over the Vaihingen test site in Southern Germany.

2. Background

The characteristics of IfSAR and LIDAR are well known. A special issue of the ISPRS Journal of Photogrammetry and Remote Sensing (Volume 54:2-3, July 1999) describes the LIDAR technology and processing and Gens and van Genderen (1996) describes airborne IfSAR. LIDAR is normally flown from platforms in the range of 500 -1000m. It will penetrate through vegetation and if first and last pulses can be recorded the height of the canopy can be determined. IfSAR is normally flown at a much higher altitude and has coarser horizontal resolution and lower vertical precision. IfSAR records signals reflected from the top of a canopy, although the penetration varies according to the radar frequency. LIDAR DEMs are normally delivered as X, Y, Z point data and IfSAR DEMs as gridded data

In March 2000 OEEPE held a workshop on airborne IfSAR and in March 2001 it held a joint workshop on IfSAR and LIDAR. Some conclusions arose from these workshops which can be

¹ This paper was presented at the OEEPE workshop on 'Airborne Laserscanning and Interferometric SAR from Detailed Digital Elevation Models' held in Stockholm, 1 - 3 March 2001, and at the ISPRS Workshop 'Three dimensional mapping from InSAR and LIDAR' held in Banff, 12 -14 July 2001.

tested by analysis of the Vaihingen data. Presentations at the meeting quoted a range of accuracies, these are summarised in table 1.

Data (Organisation)	Project	Results		Comment	
		Mean	Std dev		
IfSAR (Intermap)	Baden Wurtenburg	Bald earth	-0.47m	0.28m	Forest results shows effect of volume scattering
		Cropland	0.66m	0.34 m	
		Forest	21.04m	2.16m	
IfSAR (Aerosensing)	Venezuela	5m		3.0m	Large area mapping
IfSAR (Aerosensing)	Bremerhaven			0.05m	Tidal flats validated with theodolite measurements
LIDAR (FLI- MAP)	Netherlands	0.28m		0.037m	Flat polder area with dykes.
IfSAR (Aerosensing)	Netherlands	0.35m		0.85m	Flat polder area with dykes.

Table 2. Accuracy of airborne IfSAR and LIDAR quoted at workshops.

It is generally recognised that both technologies work well and can generate products which meet user requirements. It is also recognised that:

- Airborne LIDAR and IfSAR is a reliable and cost effective way of acquiring data for DEMs, and that LIDAR is more precise but more expensive.
- Accuracy can be selected to suit the application. This ranges from 5cm to several metres.
- Accuracy is dependent on the type of terrain and land cover and the DEM produced will be of the surface features.
- In IfSAR DEMs gaps may occur in hilly terrain where Radar shadow occurs, or phase unwrapping was not possible because of coherence problems. Multiple passes can overcome this problem. In LIDAR gaps will occur in built up areas due to occlusions. Multipath effects can occur with both systems.

3. Data description

3.1 Vaihingen Test site

The Vaihingen Test site is in Baden Wurtenburg, Southern Germany. It covers an area of about 1.2 x 2.2 km including urban, agriculture, woodland, water and quarry features. Elevation values within the area range from about 203 to 326 m.

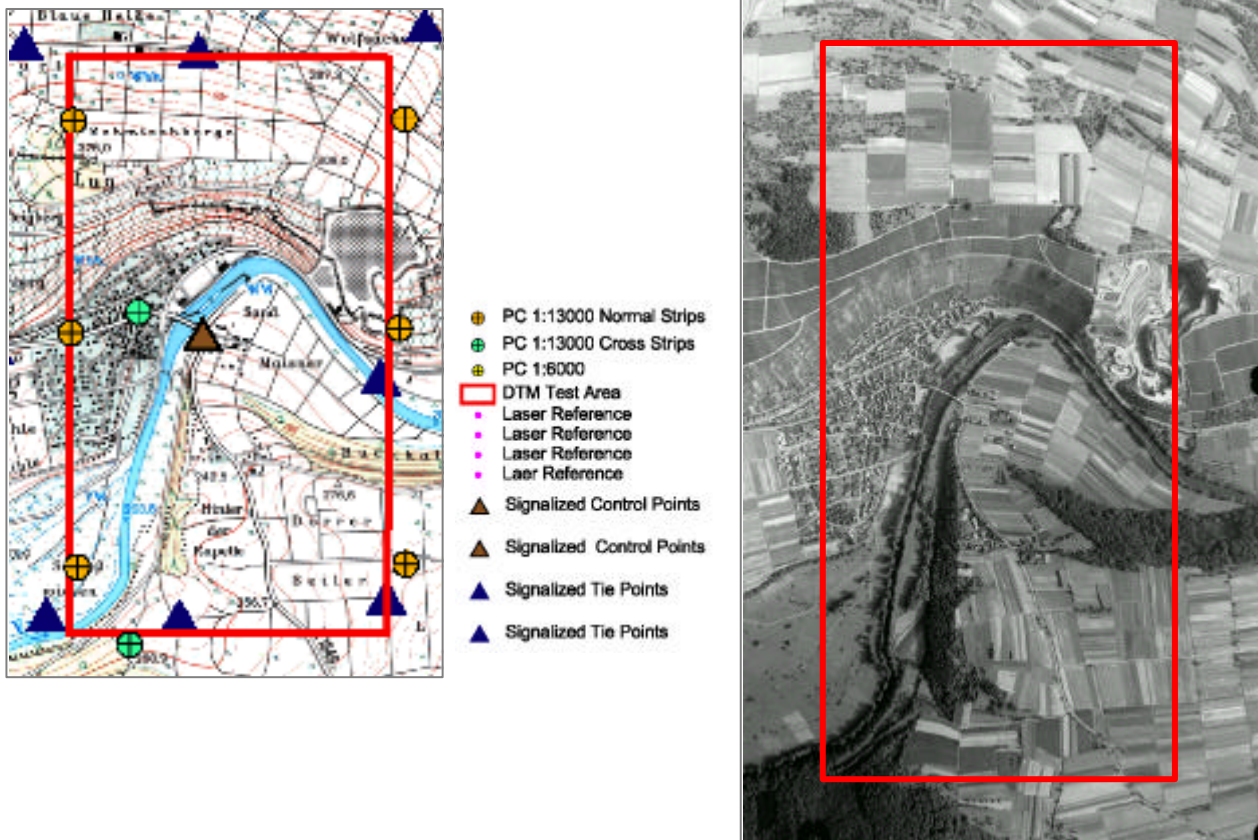


Figure 1. A map and aerial photograph of the Vaihingen test site.

3.2 IfSAR data

The data was acquired in August 1998 by Intermap Technologies Inc. and was recorded by the Star-3i interferometric SAR system. The IfSAR data provided on a CD-ROM consists of two elevation files: 'vaihingen_dem_fsurface.bil' and 'vaihingen_dem_fsurface.raw.bil'. Both elevation files are identical except that in the fsurface.raw.bil file missing data are shown as 10,000 values, whilst an interpolation program was used to infill the missing data to generate the 'fsurface.bil' file. It was decided to make use of the 'fsurface.bil' rather than to use the 'raw' version within the data comparison. It is understood from Intermap that large errors do not usually occur in the IfSAR DEM because of the processing used. For a better understanding within the data processing steps the fsurface.bil file was renamed ISAR smooth DEM. The characteristics of the data are given in figure 2.

The grid size of the elevation data is approximately 2.5 meter, but the horizontal 'resolution' is about 7.5 meters owing to upstream filtering operations - thus independent samples are separated by about 10 meters.

3.3 LIDAR data

The laser data was collected on the 1st of April 2000 and processed by FOTONOR AS from Norway. Data is stored in ASCII files containing XYZ values. Each ASCII file represents one strip of LIDAR point data. This means that for each single strip the data CD includes one ASCII file representing the first pulse and one file representing the last pulse. Overall the test site Vaihingen is covered by 10 complete strips that are recorded on the CD, but only the 6 corresponding to the IfSAR data were used. Small gaps, approximately 0-110m wide, exist between neighbouring strips.

Coordinate system and datum:

- UTM Zone 32 - WGS-84
- Coordinates are center of pixel

NW: 493252.500 5421797.500
SW: 493252.500 5419000.000
NE: 495400.000 5421797.500
SE: 495400.000 5419000.000

Image Dimensions:

1120 Rows
860 Columns

Data format:

32bit float data in MSB 2.5m pixels



Figure 2. Characteristics and a hill shaded visualisation of the Vaihingen IfSAR smooth data.

The co-ordinate system and datum of the LIDAR point data is UTM, Zone 32. The data were recorded from 700m altitude with a X spacing of 2 meter and a y-spacing of 2 meter. The LIDAR point data (6 strips that cover the extension of the IfSAR smooth DEM) consist of nearly 1 million points both for the first and for the last pulse.

3.4 Reference data:

The reference data is represented by 103 GPS-points (X, Y, Zvalues) and were provided by the Institute for Photogrammetry at Stuttgart University. The height values were acquired from aerial photographs on a Planicom C 100 using the original images and controlled using digitised 7.5 micron images on an Intergraph Image Station. The GPS points are available as Gauss-Krueger co-ordinates as well as UTM, zone 32 and local WGS 84 Horizontal System.

All data processing was carried out in UTM zone 32.

4. Data processing

4.1 Data Import

The IfSAR smooth DEM on the CD was available as a .bil file (uncompressed band interleaved by line multiband image). By creating an ASCII header file (.hdr) in Notepad that described the structure of the data (e.g. columns, rows, corner co-ordinates, cell size, nodata-value and byteorder) it was possible to display the DEM in ArcView. All necessary information was extracted from the data description included in the readme file. The option 'hillshade' (extension 3D Analyst) was used to display the DEM in a three dimensional way.

It was necessary to edit the original ASCII files of the LIDAR data (either first and last pulse data) before importing them into ArcView. ArcView needs a certain structure within the ASCII files to import the data in a correct way. On the one hand the ASCII files should be free of space characters between the different columns and also each column needs to be

separated by commas to distinguish the varying columns. Furthermore the first column within the file needs to contain a 'id-number' to make sure the points can be differentiated between each other. In the case of the LIDAR point data it means that the structure of each ASCII file, either first or last pulse, had to be changed into a strict id-number, X, Y, Z structure. The original ASCII files included a large number of space characters between the coordinates as well as headings in the beginning of the files. Besides that the commas between the X, Y and Z values were missing, however a serial id-number for each single point was already existing.

First of all Excel seemed to be very useful to carry out these changes within the files. Unfortunately it was not taken into account that Excel has a limitation of 32,000 rows to work with. However each strip of LIDAR point data consisted of about 150 000 points and any points greater than 32000 were lost by importing them into Excel. As a result of importing the LIDAR point data into Excel and afterwards into ArcView the strips appeared much smaller than the gaps between them. Therefore another software had to be used to edit the ASCII files. It was Pfe32 (Programmer's File Editor, 32-Bit-Version), a program that is able to handle a high amount of data in the LIDAR. Each modified ASCII file was imported into ArcView using the option 'Add Event Theme' and converted into a shapefile afterwards. The conversion into a shape file is essential to get access to the table containing the X,Y,Z values and thus be able to calculate statistics later on.

The ASCII file containing the GPS points (UTM co-ordinates) was treated similarly to the LIDAR point data. As the LIDAR point data the gps-file contained space characters and headings that had to be deleted. Also the commas between the X, Y, Z values were missing and had to be inserted before importing the file into ArcView. Again it was necessary to make sure that each gps-point was marked by an individual id number (already existing in the original file) using the first column of the file. Although it was possible to use Excel this time (just 103 points), again Pfe32 was used to carry out the modifications within the files. The actual import of the gps-file was undertaken in the same way as for the LIDAR data. Again the option 'Add Event theme' was used to import the ASCII file and later on the txt-file was converted into a shapefile.

4.2 Data preparation

First the LIDAR strips, either first and last pulse (now point-shapes), were superimposed with the IfSAR smooth DEM. It could be seen that the LIDAR data was overlapping the IfSAR smooth DEM at both sides (horizontal direction). Due to the fact that the non-overlapping area was not usable for the purpose of a data comparison and also because of the speed of data processing was noticeable slow (high amounts of points) the LIDAR strips were cut to match the size of the IfSAR smooth DEM.

The DEM's from the LIDAR first and last pulse point were derived using the point shapes including the LIDAR point data first and last pulse. Therefore the option 'Interpolate Grid' under the main menu 'Surface' was used. For all DEM calculations the same options came into operation. This means in detail that an output grid cell size of 2.5 m was used for all processing and also that the interpolation method IDW (Inverse Weighted interpolator) was chosen at all times. The IDW assumes that each input point has a local influence that diminishes with distance. It weights the points closer to the processing cell greater than those farther away. A specified number of neighbor points, in this case 12 points, were used to determine the output value for each location. Besides that, a power parameter of 2 was chosen as well as the option 'no barriers'. The power parameter in the IDW interpolation controls the significance of the surrounding points upon the interpolated value. A higher power results in

less influence from distant points. A choice of 'no Barriers' uses all points specified in the field number of neighbor points.

Generally two different methods were undertaken to interpolate the DEM's. All LIDAR strips that cover the IfSAR smooth DEM were merged together respectively separate for the first and for the last pulse using the extension 'Geoprocessing'. Later on the modified point shapes were used to interpolate two DEM's, one including the LIDAR point data first pulse and one including the LIDAR point data last pulse. In the end the 'hillshade' option in ArcView was used to generated a three dimensional display of each of the interpolated grids. As input parameters an azimuth value of 330 and an altitude value of 30 degrees were put used.

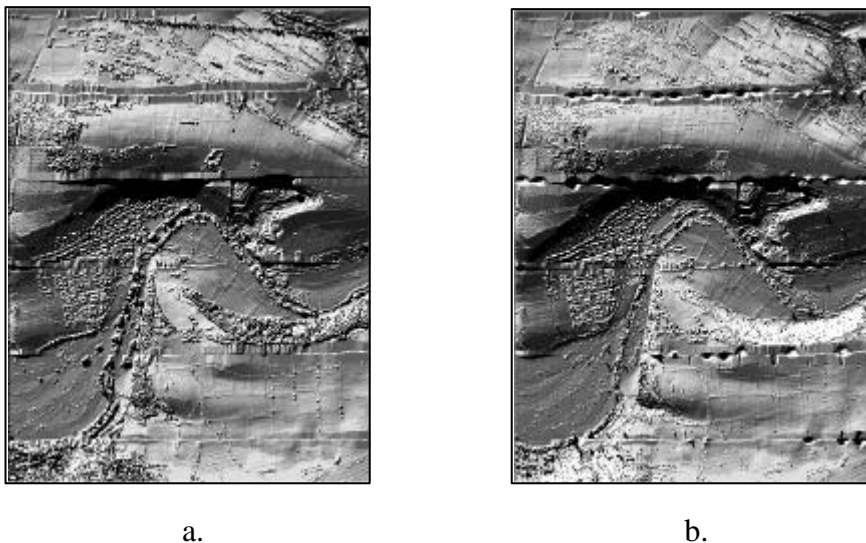


Figure 3. Gridded DEMs of the LIDAR first pulse (a) and last pulse (b) data.

5. Data comparison

5.1 Overview

The first comparison carried out was designed to determine the overall characteristics of the complete data sets. The difference values were calculated between the LIDAR point data (either first or last pulse) and the IfSAR smooth DEM. No editing had been done and some gross errors were apparent in the data. Selected strips were then compared to see how the results differed for different terrain types and land cover. Furthermore the LIDAR point data first and last pulse in one strip (strip 6) were compared with each other using the gridded data already generated within previous processing steps.

These results enabled some general conclusions to be made on the characteristics of the IfSAR and LIDAR data.

This was followed by a comparison between the reference data (gps-points) and the IfSAR smooth DEM and between the gridded LIDAR point data first and last pulse versus the gps-points. All calculations were carried out in ArcView but also ArcInfo needed to be used.

5.2 Procedure to compare LIDAR point data with gridded IfSAR data

Basically the surface value for each LIDAR point (either first or last pulse) was interpolated from the IfSAR smooth DEM using a bilinear interpolator and the interpolated height value was then stored in a new column. Because the original height values (Z co-ordinates) of the LIDAR point data were brought together with the interpolated surface values (source: IfSAR smooth DEM) in a new output file, it was now possible to determine different values between the LIDAR data and the IfSAR smooth DEM.

The ArcInfo command 'latticespot' was used to interpolate the surface values and the same procedure was carried out either for the LIDAR point data first and last pulse.

It was impossible to compare the LIDAR point data directly against each other because a LIDAR point within the first pulse data did not have automatically a identical LIDAR point (same UTM- co-ordinates) within the last pulse data. That is why gridded data had to be used to avoid errors that would have been appeared due to different locations of LIDAR points within first and last pulse. Difference values between the gridded LIDAR data were determined by using the 'Map Calculator' in ArcView.

6. Results

6.1 Comparison of LIDAR and IfSAR data

The statistics for the comparison between the IfSAR data and the LIDAR for the whole dataset are shown in table 1. and illustrated in figures 4 and 5. The small mean between the IfSAR and the first pulse LIDAR indicates that the first pulse is reflected from a similar surface to the IfSAR and the standard deviation gives a measure of the difference in penetration of the two sensors. The large range of minimum and maximum values is due to the use of unedited LIDAR data. Intermap have indicated that a minuscule number of such anomalies occur in the SAR data and that they are usually associated with some peculiarity such as the quarry, perhaps due to double bounces or otherwise. Figure 4. Shows that the biggest differences occur on the steepest slopes and over the wooded and built up areas; the difference plot highlights very clearly these features, shown in red and pink. The differences between the IfSAR and last pulse LIDAR are much greater over the wooded areas as shown in figure 5. In other areas the difference are very small.

	No of points	Mean (m)	Min (m)	Max (m)	Sigma (m)	Comment
IfSAR smooth vs LIDAR point data first pulse	969092	0.517	-64.287	55.005	4.133	Good correspondence, biggest errors in steepest slopes.
IfSAR smooth vs LIDAR point data last pulse	992958	2.253	-88.794	117.847	5.806	Large mean, due to greater penetration of LIDAR last pulse.

Table 1. Differences between IfSAR and LIDAR of the whole data set.

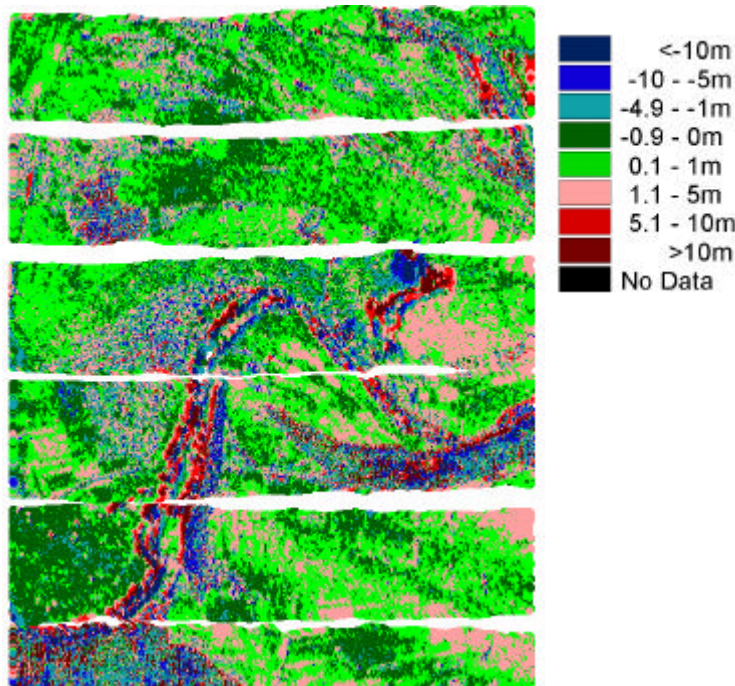


Figure 4. Difference between IfSAR And LIDAR first pulse data.

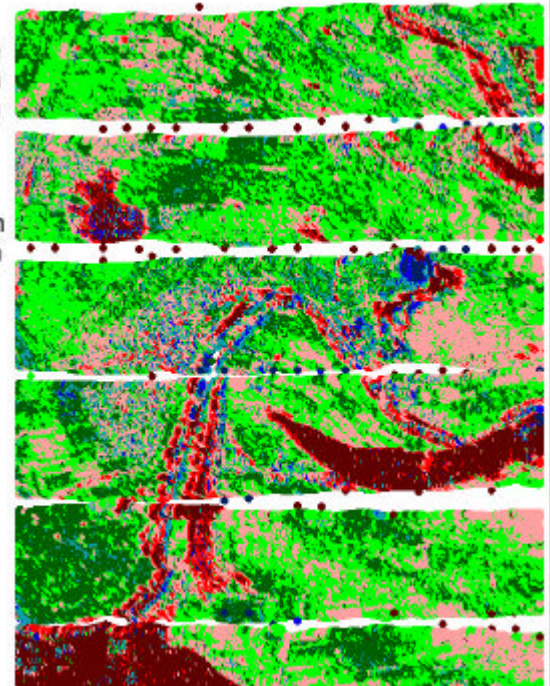


Figure 5. Difference between IfSAR And LIDAR last pulse data

Table 2 shows the same statistics for two strips. In strip 7 the mean and standard deviation are smaller because of the reduced area of building and woodland. The range of errors is also smaller indicating that steep slopes and wooded areas are more likely to produce gross errors. The differences between the first and last pulse data agree with those of the whole dataset. Strip 6 has much more variable characteristics with steep slopes, on the valley sides and in a quarry, and built up areas. There is less woodland. The mean differences are smaller, indicating the variable nature of the surface, and the standard deviations are larger, for the same reason. The difference between the first and last pulse LIDAR is smaller than expected, probably due to the smaller amount of woodland.

	No of points	Mean (m)	Min (m)	Max (m)	Sigma (m)	Comment
Strip 7						
IfSAR vs LIDAR first pulse	190307	0.421	-21.388	28.048	2.551	An area of woodland and open Country with no steep slopes. Note greater range of errors in last pulse data and difference in mean and sigma between first and last pulse.
IfSAR vs LIDAR last pulse	190562	1.608	-38.270	117.847	3.995	
Strip 6						
IfSAR vs LIDAR first pulse	165632	0.345	-64.287	55.005	4.637	An area of buildings, trees and Steep slopes. Note smaller means, larger differences and larger sigmas.
IfSAR vs LIDAR last pulse	166448	0.695	-88.794	94.145	4.464	
LIDAR first pulse vs LIDAR last pulse using gridded data	139158	0.497	-148.008	39.742	2.023	

Table 2. Difference between IfSAR and LIDAR of selected strips.

6.2 Comparison of LIDAR and IfSAR with reference data

The reference data is located in open areas on undulating terrain, with a few points on the valley side. The first point to note is that, except for the unedited LIDAR data, the mean difference is very small, less than 0.25m. For the unedited data the IfSAR has a standard deviation of 0.82m whereas the LIDAR first and last pulse has a standard deviation of over 4m. However the standard deviation of the edited data reduces to 0.7m for the first pulse data and 0.3m for the last pulse. The fact that there is such a difference between the first and last pulse data is rather surprising, given that the points are supposed to be on open ground.

	No of points	Mean (m)	Min (m)	Max (m)	Sigma (m)	Comment
Reference data vs IfSAR gridded smooth DEM	103	0.207	-1.056	3.139	0.820	Indicates performance of IfSAR over bare ground after removal of gross errors and smoothing.
Reference data vs LIDAR first pulse gridded DEM	103	0.059	-17.509	27.099	4.350	No editing carried out. Note large max and min errors.
Reference data vs LIDAR last pulse gridded DEM	103	-0.795	-33.376	10.901	4.560	No editing carried out. Note large max and min errors.
Reference data vs edited (pts with diff > 0.5 removed) LIDAR first pulse gridded DEM	97	-0.095	-1.711	4.995	0.704	Indicates performance of LIDAR over bare ground after errors removed.
Reference data vs edited (pts with diff > 0.5 removed) LIDAR last pulse gridded DEM	95	-0.240	-1.720	1.208	0.310	Indicates performance of LIDAR over bare ground after errors removed.

Table 3. Difference between IfSAR and LIDAR and ground reference data.

7. Conclusions

The tests on the OEEPE Vaihingen test site have confirmed a number of expectations on the nature and accuracy of the airborne IfSAR and LIDAR data used. The following characteristics have been determined:

- Both IfSAR and LIDAR are capable of producing the ground surface in open areas with a mean and standard deviation of less than 1m.
- IfSAR and the first pulse LIDAR response have similar characteristics and give a good representation of the features on the surface of the terrain.
- A comparison of IfSAR and LIDAR shows that they penetrate vegetation canopy to different degrees.
- The LIDAR data available for this test had a number of large errors on individual points.

A number of points are left unresolved from the work done on this data, and further work is needed:

- Editing of the LIDAR data is not satisfactory.
- More needs to be found out about the nature of the control points.
- More work needs to be done on the penetration of vegetation canopies.

The use of the Vaihingen data has allowed valuable comparisons to be made between the IfSAR and LIDAR data, but more work is required by looking at small test areas of homogeneous features, and with better global reference data.

Acknowledgements

The authors thank OEEPE, Fotonor AS and Intermap Technologies Inc for providing the data and for help in clarifying points arising in the analysis.

References

Gens R, Van Genderen J L, 1996. SAR interferometry - issues, techniques, applications. International Journal of Remote Sensing, (17(10):1803-1835.

BUILDING DETECTION AND EXCLUDING IN DIGITAL TERRAIN MODELLING

Borislav MARINOV
University of Architecture, Civil Engineering and Geodesy,
Faculty of Geodesy, BULGARIA
MarinovB_fgs@uacg.acad.bg

KEY WORDS: Segmentation, Building detection, DEM

ABSTRACT

The influence of artificial objects is very important for the processes of terrain modelling. The problems generated by the building existence in land images are formulated. The methods for building detection and restoration are proposed. Different methods for excluding the influence of buildings from terrain model are formulated. The comparison of possibilities of the different methods is made based on the used level of automation when digital photogrammetric workstations are used. The simplified semi-automatic technology for digital terrain modelling is applied to areas with middle dense of buildings.

1. INTRODUCTION

There are several aspects of disturbances that arise in the process of producing a digital terrain model for territories with human influence. The buildings create problems with conjunction of their presence in images of such territories. They create problems at stage of data acquisition, and image understanding. The problems are connected with space position of buildings, which result in viewing only part of buildings, hiding of another buildings or surrounding terrain, and shadows produced by buildings. Another problem is including the buildings in 3-D realistic model and their excluding from the terrain model when only topographic surface is presented. The problems are connected with terrain model data capturing, DEM storing and visualisation. Digital photogrammetric workstation, image processing and understanding give new possibilities for solving these problems.

Including the information about artificial objects over the defined territory is of great importance for Land information systems, for GIS analyses, for Cadastral Services, Design of Engineering projects over the defined territory.

Specific problems are connected with the type of the data sources. They depend on the type of energy sources - passive or active image capturing systems. Another problem is

the vehicle carrying the sensor. Usually to detect buildings and other artificial objects is necessary to use large-scale images. Some of them could be obtained from satellites. But more often the airborne sensors are used. They could be photcameras, scanners, CCD devices or active devices like SAR or laser scanning systems. Every one of these image sensors has its own specific features, concerning wavelength of the used electromagnetic energy and the geometry of the obtained images.

2. DETECTION OF ARTIFICIAL OBJECTS AND DATA COLLECTION

There are several groups of problems that have to be solved when artificial objects are detected. They include classification features, planar and space geometry of objects and image understanding.

The proper choice of classification features is of a great importance for detecting buildings. They could be spectral or texture characteristics of artificial or natural objects— roofs, walls, pavements, roads, trees, and grass. Obtaining the texture information induced from the observed objects in SAR images is difficult due to the speckle disturbances. This requires filtering of texture produced by speckle. Better results could be obtained by combined usage of optical and SAR images [Hellwich, O., 2000].

The second type of specific characteristics is connected with the context. It is defined by the surrounding objects like gardens, pavements and other objects. The shadow presence could be added to context too. This requires usage the data from different sources [Soergel, U., 2000]. Successful interpretation of these image aspects is based on the application of artificial intelligence methods.

Third types of features are geometrical features extracted from mono or stereo images. They include straight lines, parallel lines, square objects. The analyses of space information about registered objects, obtained from stereo images, allow producing a space model of buildings or other artificial objects. To find the corresponding border lines in stereo image in some procedures are used methods of structural matching [Wang, Y., 1996]. Some specific procedures for image understanding are based on picture grammars. They could be used to detect buildings and to produce an adequate space model [Marinov, B., 1996].

Automation of procedures for model creation is achieved by using digital photogrammetric workstations. Their usage is suitable for high-resolution images that allow achieving adequate accuracy of the created model. In situation when an operator collects terrain data it is preferable to use traditional technology of contour lines generation. The operator could measure the boundary elements of planar object and essentially the building edges.

Modern digital photogrammetric systems allow obtaining terrain data over the regular or pseudo regular grid in automatic mode. It is possible also to detect edges of buildings' walls and roofs in automatic or semi-automatic modes.

In practical situation the combination between possibilities of automatic methods and operator control at critical points is applied. This allows to achieve high speed of processing and high reliability of collected data [Kraus, K., 1997].

The parameters of automatic data collection are very important for successful terrain modelling. The main parameter is the step of interpolation grid. A smaller step increases the accuracy and particularity of model but require much time of processing. Other parameter is the allowed limit of height difference between adjacent terrain points. In urban areas there are height jumps between terrain and building roofs. If the allowed difference between adjacent points is high this ensures the accurate following of terrain and artificial objects. From the other side higher threshold of such jump does not filter correctly the errors in measuring due to the false correlation and increase the time of processing. Such parameter is defined for automatic procedure of terrain measuring by Digital Video Plotter of Leica [DVP, 1995].

The adequate combination of automatic processes and operator control allows achieving high speed and accuracy of obtained data.

3. BUILDING EXCLUDING METHOD

The method for building excluding from terrain model requires obtaining the foundation contour of objects. Different approaches could be used to generate this contour. One of them is the direct measurement of borders of founding. Usually only one or two sides of building are visible in stereo mode. The second approach is based on roof edges measurement. It is connected with another problem. The size of roof's eaves is not the same for all the sides of the building. Another problem is that the edge lines of roof do not lie in the same plane. This makes usage of roof edges too complicated.

The method of building registration and restoration is dependent on the used technology for registration and the level of automation. There are two possible approaches. The first approach uses simultaneous measuring of the terrain and the artificial objects. The separation is produced at the following stages of processing. The second approach is based on preliminary measuring of buildings. This requires operator's invention or usage of system with very high level of image understanding, which is capable to determine the artificial objects. At the stage of collecting the data for terrain the areas of buildings are excluding from the process of data collection.

The semi-automatic mode for building excluding uses the following steps:

1. Measuring of random set of point over the pseudo regular grid of terrain and building points.
2. Measuring of roof edges.
3. Correction of roof size due to the eaves to obtain wall offsets. At this step are possible different approaches to measure the eaves and the corresponding offset of walls – measuring on field, or stereo measuring from one side of the building and making of suggestion for equal size of eaves at the different sides of the building.

4. Projection of building contour over the terrain. Usually it is necessary to project the roof contour on the one plane. The second step is moving the contour to lie onto the terrain. The more convenient approach is to project the building contour on the terrain. This requires availability of appropriate software to calculate such projection.

5. Moving the points lying on building roofs to the terrain.

6. Generation of a terrain model from terrain points, break lines, lines from building founding and artificial points inside the buildings. The internal points are necessary to produce more reliable model of the terrain.

Another approach requires producing of pseudo-realistic model of the terrain and the buildings. Generation of such model requires generation of simplified model of the buildings [Läbe, T., 1996]. The level of simplification depends on the required accuracy and the amount of data. Depending on the accuracy it is possible to take into account the eaves or does not estimate them. The possibilities of terrain modelling system depend on the used mathematical model of the surface and the algorithms for its realisation. Its complexity and flexibility are in contradiction with the amount of stored data and the time of processing.

The variants of processing depend on the possibilities of digital photogrammetric workstation and digital terrain modelling program.

The simplest program creates the copy of the planar contour of the roof's edges at mean height of terrain. More accurate results could be obtained by using of terrain modelling and linear object design like InRoads of Intergraph [InRoads, 1995]. Usage of this system allows projecting the building contour over the terrain model. To utilise this solution is necessary to measure points in the vicinity of building foots. It is suitable to measure border lines near to buildings like pavements, flower gardens and so on.

The process of photorealistic model creation follows the several steps:

1. Generation of terrain model without buildings.
2. Creation of space model of eaves.
3. Conversion of contour from space to planar.
4. Projection of building contour over the terrain model.
5. Generation of skeleton 3-D model of buildings with accuracy corresponding to the highest accuracy of the required hard copy of the model.
6. Moving the roof points to the elevation inside the building contours. This process creates fictitious points inside the building boundaries to stabilise DEM.
7. Generation of set of terrain models – model without buildings. 3-D modelling of terrain and existing buildings.

The higher level of automation could be reached if the methods of artificial intelligence are involved wider. They allow to determine the buildings and to solve the process of automatic building excluding without operator intervention.

4. EXPERIMENTAL RESULTS

The simplified variant of the suggested method is applied to test images with photo scale 1:2500. The photos are made with Wild camera RC20. Digital images are obtained by scanning with resolution of 600 dpi. Grid raster for terrain modelling is 10m. The produced terrain models without buildings and with buildings are shown below. Finally the complex model is produced that could be used for 3-D modelling of territory.

Figure 1 shows the part of the terrain model without building influence.

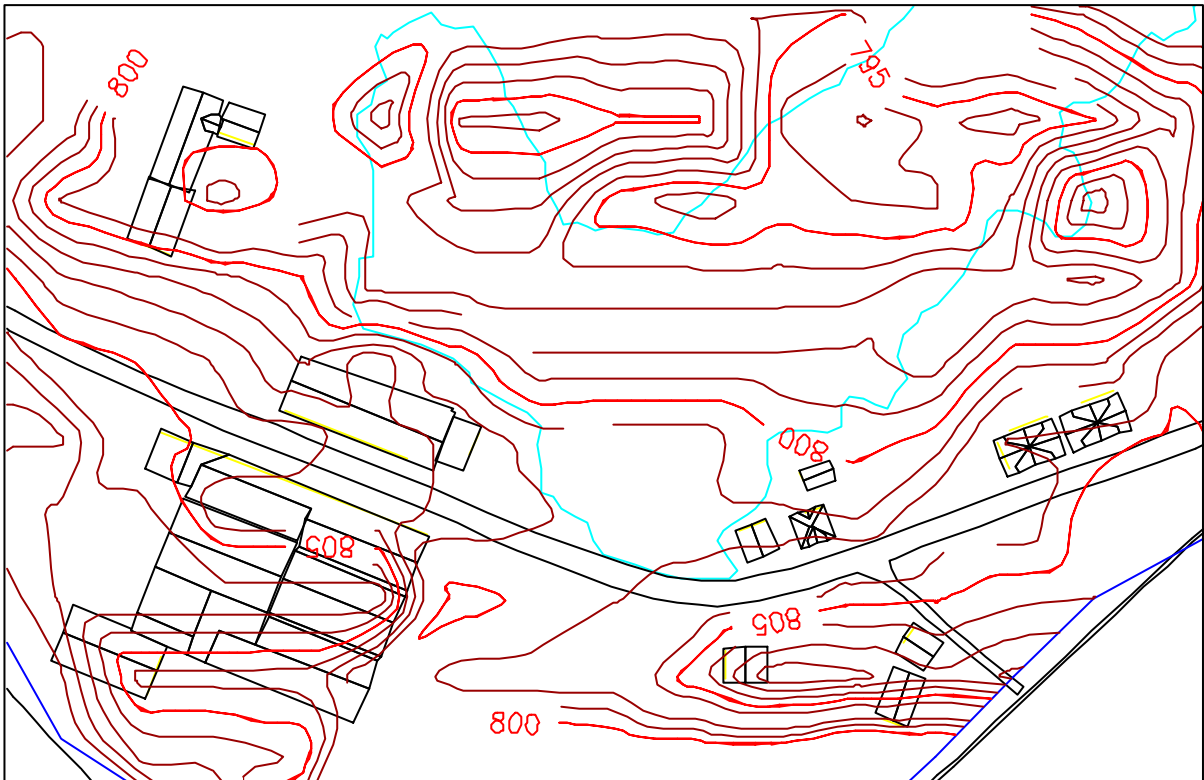


Figure 1. Orthogonal map of the terrain without buildings.

Terrain model of the same area with excluded building areas is shown on figure 2 and its isometric image is shown on figure 3.

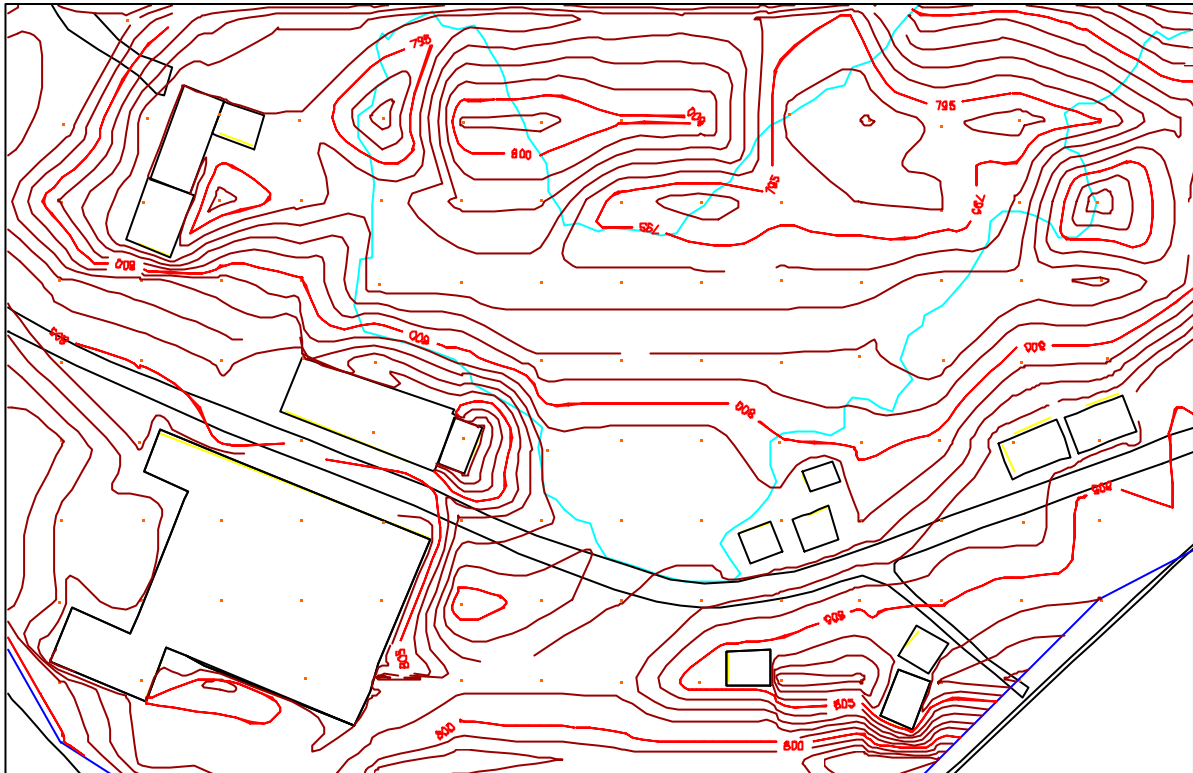


Figure 2. Orthogonal map of the territory with excluded building areas.

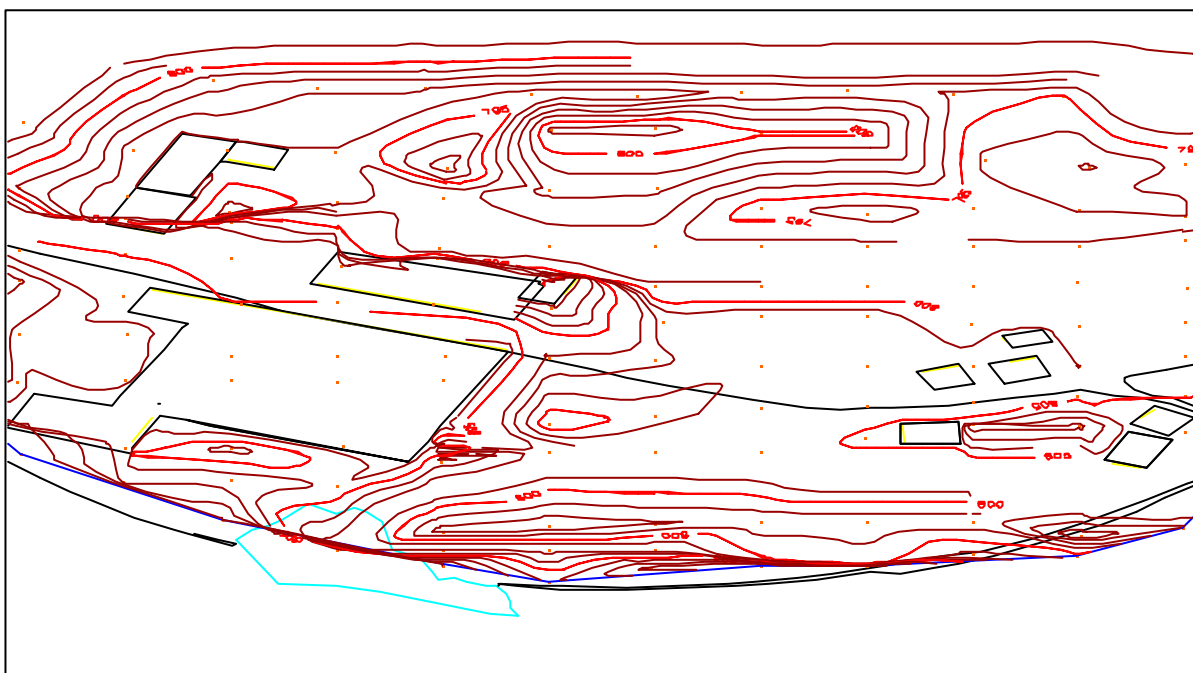


Figure 3. Isometric view of the terrain with excluded building areas.

The next step of processing forms terrain model that includes the boundaries of buildings. The model includes building roofs and footing contours. Its orthogonal view is shown on figure 4.

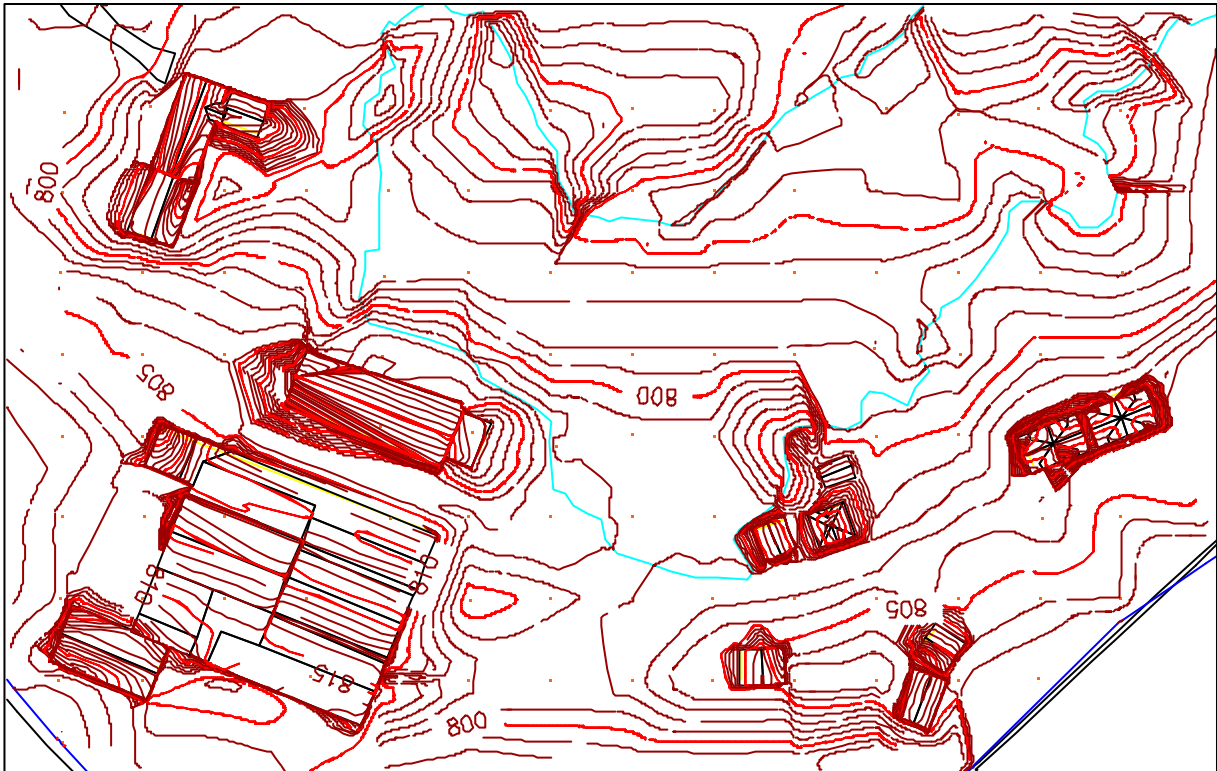


Figure 4. Orthogonal view of terrain with included buildings.

The isometric view of the same area is shown on figure 5.

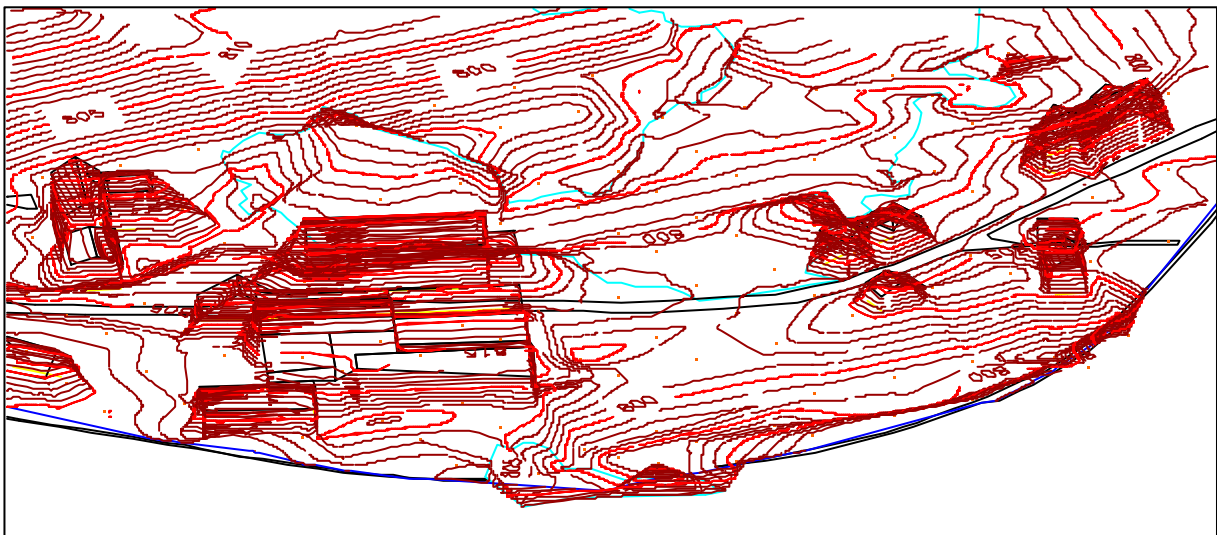


Figure 5. Isometric view of the model with buildings.

The obtained results show the necessity of full building description and usage of adequate terrain modelling software.

5. DISCUSSIONS AND CONCLUSIONS

The experimenting of the above method show the necessity of analysis of image. In semi automatic mode this tends to work with intensive operator's participation. In such mode the hard errors could appear and the velocity of processing decrease significantly.

The usage of "clever" systems with involving the methods of artificial intelligence will give better results. Such system have to combine the features of digital photogrammetry and image processing and recognition that will allow working with small part of operator invention or in fully automatic mode.

The analyses of procedures for building exclusions shows that for creating of adequate model the process of image understanding and producing of correct vector model of artificial objects is of great importance. Its successful solution is impossible without using the artificial intelligence methods.

REFERENCES

1. *DVP - User's Guide - vers. 3.5*, Leica (DVP GEOMATIC Systems Inc.), 1995.
2. Hellwich, O., M. Günzl, C. Wiedemann, Fusion of Optical Imagery and SAR/INSAR Data for Object Extraction, *IAPRS XIX Congress of ISPRS*, vol. XXXIII, part B3, Amsterdam, 2000, pp.389-396.
3. *InRoads*, Tutorial, Intergraph, Huntsville, Intergraph Corporation, 1995, pp 240.
4. Kraus K., with contributions by J. Jansa, H. Kager, *Photogrammetry*, vol.2: Advanced Methods and Applications, Bonn, "Ferd. Dümmler Verlag", 1997, pp. 466.
5. Marinov B. D., Processing of Protruding Objects in Digital Images of Urban Areas, *IAPRS XVIII Congress of ISPRS*, vol. XXXI, part B3, Vienna, 1996, pp.497-502.
6. Läbe, T., K. Ellenbeck, 3-D Wire Frame Models as Ground Control Points for the Automatic Exterior Orientation, *IAPRS XVIII Congress of ISPRS*, vol. XXXI, part B2, Vienna, 1996, pp.218-223.
7. Soergel, U., U. Thoennesen, H. Gross, U. Stilla, Segmentation of Interferometric SAR Data for Building Detection, *IAPRS XIX Congress of ISPRS*, vol. XXXIII, part B1, Amsterdam, 2000, pp.328-335.
8. Wang, Y., Structural Matching and Its Applications for Photogrammetric Automation, *IAPRS XVIII Congress of ISPRS*, vol. XXXI, part B3, Vienna, 1996, pp.918-923.

LIST OF THE OEEPE PUBLICATIONS

State – March 2001

Official publications

- 1 *Trombetti, C.*: „Activité de la Commission A de l'OEEPE de 1960 à 1964“ – *Cunietti, M.*: „Activité de la Commission B de l'OEEPE pendant la période septembre 1960 – janvier 1964“ – *Förstner, R.*: „Rapport sur les travaux et les résultats de la Commission C de l'OEEPE (1960–1964)“ – *Neumaier, K.*: „Rapport de la Commission E pour Lisbonne“ – *Weele, A. J. v. d.*: „Report of Commission F.“ – Frankfurt a. M. 1964, 50 pages with 7 tables and 9 annexes.
- 2 *Neumaier, K.*: „Essais d'interprétation de »Bedford« et de »Waterbury«. Rapport commun établi par les Centres de la Commission E de l'OEEPE ayant participé aux tests“ – „The Interpretation Tests of »Bedford« and »Waterbury«. Common Report Established by all Participating Centres of Commission E of OEEPE“ – „Essais de restitution »Bloc Suisse«. Rapport commun établi par les Centres de la Commission E de l'OEEPE ayant participé aux tests“ – „Test »Schweizer Block«. Joint Report of all Centres of Commission E of OEEPE.“ – Frankfurt a. M. 1966, 60 pages with 44 annexes.
- 3 *Cunietti, M.*: „Emploi des blocs de bandes pour la cartographie à grande échelle – Résultats des recherches expérimentales organisées par la Commission B de l'O.E.E.P.E. au cours de la période 1959–1966“ – „Use of Strips Connected to Blocks for Large Scale Mapping – Results of Experimental Research Organized by Commission B of the O.E.E.P.E. from 1959 through 1966.“ – Frankfurt a. M. 1968, 157 pages with 50 figures and 24 tables.
- 4 *Förstner, R.*: „Sur la précision de mesures photogrammétriques de coordonnées en terrain montagneux. Rapport sur les résultats de l'essai de Reichenbach de la Commission C de l'OEEPE“ – „The Accuracy of Photogrammetric Co-ordinate Measurements in Mountainous Terrain. Report on the Results of the Reichenbach Test Commission C of the OEEPE.“ – Frankfurt a. M. 1968, Part I: 145 pages with 9 figures; Part II: 23 pages with 65 tables.
- 5 *Trombetti, C.*: „Les recherches expérimentales exécutées sur de longues bandes par la Commission A de l'OEEPE.“ – Frankfurt a. M. 1972, 41 pages with 1 figure, 2 tables, 96 annexes and 19 plates.
- 6 *Neumaier, K.*: „Essai d'interprétation. Rapports des Centres de la Commission E de l'OEEPE.“ – Frankfurt a. M. 1972, 38 pages with 12 tables and 5 annexes.
- 7 *Wiser, P.*: „Etude expérimentale de l'aérotiangulation semi-analytique. Rapport sur l'essai »Gramastetten«.“ – Frankfurt a. M. 1972, 36 pages with 6 figures and 8 tables.
- 8 „Proceedings of the OEEPE Symposium on Experimental Research on Accuracy of Aerial Triangulation (Results of Oberschwaben Tests)“ *Ackermann, F.*: „On Statistical Investigation into the Accuracy of Aerial Triangulation. The Test Project Oberschwaben“ – „Recherches statistiques sur la précision de l'aérotiangulation. Le champ d'essai Oberschwaben“ – *Belzner, H.*: „The Planning. Establishing and Flying of the Test Field Oberschwaben“ – *Stark, E.*: Testblock Oberschwaben, Programme I. Results of Strip Adjustments“ – *Ackermann, F.*: „Testblock Oberschwaben, Program I. Results of Block-Adjustment by Independent Models“ – *Ebner, H.*: Comparison of Different Methods of Block Adjustment“ – *Wiser, P.*: „Propositions pour le traitement des erreurs non-accidentelles“ – *Camps, F.*: „Résultats obtenus dans le cadre du projet Oberschwaben 2A“ – *Cunietti, M.*;

- Vanossi, A.*: „Etude statistique expérimentale des erreurs d'enchaînement des photogrammes“ – *Kupfer, G.*: „Image Geometry as Obtained from Rheidt Test Area Photography“ – *Förstner, R.*: „The Signal-Field of Baustetten. A Short Report“ – *Visser, J.; Leberl, F.; Kure, J.*: „OEEPE Oberschwaben Reseau Investigations“ – *Bauer, H.*: „Compensation of Systematic Errors by Analytical Block Adjustment with Common Image Deformation Parameters.“ – Frankfurt a. M. 1973, 350 pages with 119 figures, 68 tables and 1 annex.
- 9 *Beck, W.*: „The Production of Topographic Maps at 1 : 10,000 by Photogrammetric Methods. – With statistical evaluations, reproductions, style sheet and sample fragments by Landesvermessungsamt Baden-Württemberg Stuttgart.“ – Frankfurt a. M. 1976, 89 pages with 10 figures, 20 tables and 20 annexes.
- 10 „Résultats complémentaires de l'essai d'«Oberriet» of the Commission C de l'OEEPE – Further Results of the Photogrammetric Tests of «Oberriet» of the Commission C of the OEEPE“
Hárry, H.: „Mesure de points de terrain non signalisés dans le champ d'essai d'«Oberriet» – Measurements of Non-Signalized Points in the Test Field «Oberriet» (Abstract)“ – *Stickler, A.; Waldhäusl, P.*: „Restitution graphique des points et des lignes non signalisés et leur comparaison avec des résultats de mesures sur le terrain dans le champ d'essai d'«Oberriet» – Graphical Plotting of Non-Signalized Points and Lines, and Comparison with Terrestrial Surveys in the Test Field «Oberriet»“ – *Förstner, R.*: „Résultats complémentaires des transformations de coordonnées de l'essai d'«Oberriet» de la Commission C de l'OEEPE – Further Results from Co-ordinate Transformations of the Test «Oberriet» of the Commission C of the OEEPE“ – *Schürer, K.*: „Comparaison des distances d'«Oberriet» – Comparison of Distances of «Oberriet» (Abstract).“ – Frankfurt a. M. 1975, 158 pages with 22 figures and 26 tables.
- 11 „25 années de l'OEEPE“
Verlaine, R.: „25 années d'activité de l'OEEPE“ – „25 Years of OEEPE (Summary)“ – *Baarda, W.*: „Mathematical Models.“ – Frankfurt a. M. 1979, 104 pages with 22 figures.
- 12 *Spiess, E.*: „Revision of 1 : 25,000 Topographic Maps by Photogrammetric Methods.“ – Frankfurt a. M. 1985, 228 pages with 102 figures and 30 tables.
- 13 *Timmerman, J.; Roos, P. A.; Schürer, K.; Förstner, R.*: On the Accuracy of Photogrammetric Measurements of Buildings – Report on the Results of the Test “Dordrecht”, Carried out by Commission C of the OEEPE. – Frankfurt a. M. 1982, 144 pages with 14 figures and 36 tables.
- 14 *Thompson C. N.*: Test of Digitising Methods. – Frankfurt a. M. 1984, 120 pages with 38 figures and 18 tables.
- 15 *Jaakkola, M.; Brindöpke, W.; Kölbl, O.; Noukka, P.*: Optimal Emulsions for Large-Scale Mapping – Test of “Steinwedel” – Commission C of the OEEPE 1981–84. – Frankfurt a. M. 1985, 102 pages with 53 figures.
- 16 *Waldhäusl, P.*: Results of the Vienna Test of OEEPE Commission C. – *Kölbl, O.*: Photogrammetric Versus Terrestrial Town Survey. – Frankfurt a. M. 1986, 57 pages with 16 figures, 10 tables and 7 annexes.
- 17 *Commission E of the OEEPE*: Influences of Reproduction Techniques on the Identification of Topographic Details on Orthophotomaps. – Frankfurt a. M. 1986, 138 pages with 51 figures, 25 tables and 6 appendices.
- 18 *Förstner, W.*: Final Report on the Joint Test on Gross Error Detection of OEEPE and ISP WG III/1. – Frankfurt a. M. 1986, 97 pages with 27 tables and 20 figures.
- 19 *Dowman, I. J.; Ducher, G.*: Spacelab Metric Camera Experiment – Test of Image Accuracy. – Frankfurt a. M. 1987, 112 pages with 13 figures, 25 tables and 7 appendices.

- 20 *Eichhorn, G.*: Summary of Replies to Questionnaire on Land Information Systems – Commission V – Land Information Systems. – Frankfurt a. M. 1988, 129 pages with 49 tables and 1 annex.
- 21 *Kölbl, O.*: Proceedings of the Workshop on Cadastral Renovation – Ecole polytechnique fédérale, Lausanne, 9–11 September, 1987. – Frankfurt a. M. 1988, 337 pages with figures, tables and appendices.
- 22 *Rollin, J.; Dowman, I. J.*: Map Compilation and Revision in Developing Areas – Test of Large Format Camera Imagery. – Frankfurt a. M. 1988, 35 pages with 3 figures, 9 tables and 3 appendices.
- 23 *Drummond, J.* (ed.): Automatic Digitizing – A Report Submitted by a Working Group of Commission D (Photogrammetry and Cartography). – Frankfurt a. M. 1990, 224 pages with 85 figures, 6 tables and 6 appendices.
- 24 *Ahokas, E.; Jaakkola, J.; Sotkas, P.*: Interpretability of SPOT data for General Mapping. – Frankfurt a. M. 1990, 120 pages with 11 figures, 7 tables and 10 appendices.
- 25 *Ducher, G.*: Test on Orthophoto and Stereo-Orthophoto Accuracy. – Frankfurt a. M. 1991, 227 pages with 16 figures and 44 tables.
- 26 *Dowman, I. J.* (ed.): Test of Triangulation of SPOT Data – Frankfurt a. M. 1991, 206 pages with 67 figures, 52 tables and 3 appendices.
- 27 *Newby, P. R. T.; Thompson, C. N.* (ed.): Proceedings of the ISPRS and OEEPE Joint Workshop on Updating Digital Data by Photogrammetric Methods. – Frankfurt a. M. 1992, 278 pages with 79 figures, 10 tables and 2 appendices.
- 28 *Koen, L. A.; Kölbl, O.* (ed.): Proceedings of the OEEPE-Workshop on Data Quality in Land Information Systems, Apeldoorn, Netherlands, 4–6 September 1991. – Frankfurt a. M. 1992, 243 pages with 62 figures, 14 tables and 2 appendices.
- 29 *Burman, H.; Torlegård, K.*: Empirical Results of GPS – Supported Block Triangulation. – Frankfurt a. M. 1994, 86 pages with 5 figures, 3 tables and 8 appendices.
- 30 *Gray, S.* (ed.): Updating of Complex Topographic Databases. – Frankfurt a. M. 1995, 133 pages with 2 figures and 12 appendices.
- 31 *Jaakola, J.; Sarjakoski, T.*: Experimental Test on Digital Aerial Triangulation. – Frankfurt a. M. 1996, 155 pages with 24 figures, 7 tables and 2 appendices.
- 32 *Dowman, I.*: The OEEPE GEOSAR Test of Geocoding ERS-1 SAR Data. – Frankfurt a. M. 1996, 126 pages with 5 figures, 2 tables and 2 appendices.
- 33 *Kölbl, O.*: Proceedings of the OEEPE-Workshop on Application of Digital Photogrammetric Workstations. – Frankfurt a. M. 1996, 453 pages with numerous figures and tables.
- 34 *Blau, E.; Boochs, F.; Schulz, B.-S.*: Digital Landscape Model for Europe (DLME). – Frankfurt a. M. 1997, 72 pages with 21 figures, 9 tables, 4 diagrams and 15 appendices.
- 35 *Fuchs, C.; Gülch, E.; Förstner, W.*: OEEPE Survey on 3D-City Models.
Heipke, C.; Eder, K.: Performance of Tie-Point Extraction in Automatic Aerial Triangulation. – Frankfurt a. M. 1998, 185 pages with 42 figures, 27 tables and 15 appendices.
- 36 *Kirby, R. P.*: Revision Measurement of Large Scale Topographic Data.
Höhle, J.: Automatic Orientation of Aerial Images on Database Information.
Dequal, S.; Koen, L. A.; Rinaudo, F.: Comparison of National Guidelines for Technical and Cadastral Mapping in Europe (“Ferrara Test”) – Frankfurt a. M. 1999, 273 pages with 26 figures, 42 tables, 7 special contributions and 9 appendices.

- 37 *Koelbl, O.* (ed.): Proceedings of the OEEPE – Workshop on Automation in Digital Photogrammetric Production. – Frankfurt a. M. 1999, 475 pages with numerous figures and tables.
- 38 *Gower, R.*: Workshop on National Mapping Agencies and the Internet
Flotron, A.; Koelbl, O.: Precision Terrain Model for Civil Engineering. – Frankfurt a. M. 2000, 140 pages with numerous figures, tables and a CD.
- 39 *Ruas, A.*: Automatic Generalisation Project: Learning Process from Interactive Generalisation. – Frankfurt a. M. 2001, 98 pages with 43 figures, 46 tables and 1 appendix.

The publications can be ordered using the electronic orderform of the OEEPE website

www.oeepe.org

or directly from

Bundesamt für Kartographie und Geodäsie
Abt. Geoinformationswesen

Richard-Strauss-Allee 11
D-60598 Frankfurt am Main